Structural Guidelines for Stabilization of α-Helical Coiled Coils via PEG Stapling

Qiang Xiao, Zachary B. Jones, Samantha C. Hatfield, Dallin S. Ashton, Nicholas A. Dalley, Cody D. Dyer, Judah L. Evangelista, and Joshua L. Price*

Electronic Supplementary Information

1. Structures of coiled-coil and affibody variants

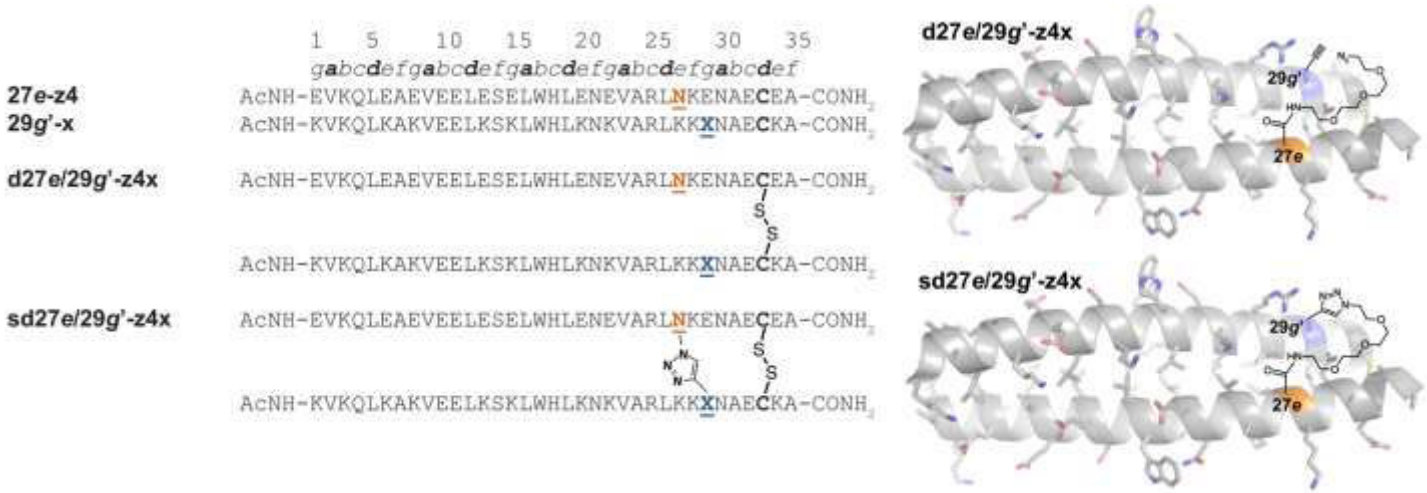

Figure S1. Sequences of (A) acidic monomer **27*e*-z4**, basic monomer **29*g*'-x**, disulfide-bound coiled-coil heterodimer **d27*e*/29*g*'-z4x**, and its stapled counterpart **sd27*e*/29*g*'-z4x**. **X** represents propargyl glycine; **N** represents an azido-terminated PEG-modified Asn residue. Also shown are the structures of the side chains of **X** and **N** and their stapled counterpart superimposed on the ribbon diagram of parent disulfide-bonded heterodimer **A/B** (PDB ID: 1KD9). Side chains are shown as sticks; position 27*e* is highlighted in orange, whereas position 29*g*' is highlighted in blue. Variants **d27*e*/29*g*'-z4x** and **sd27*e*/29*g*'-z4x** are from reference [1]. The PEG oligomer(s) within each variant have the number of ethylene oxide units indicated in the structural drawings and in the compound names.

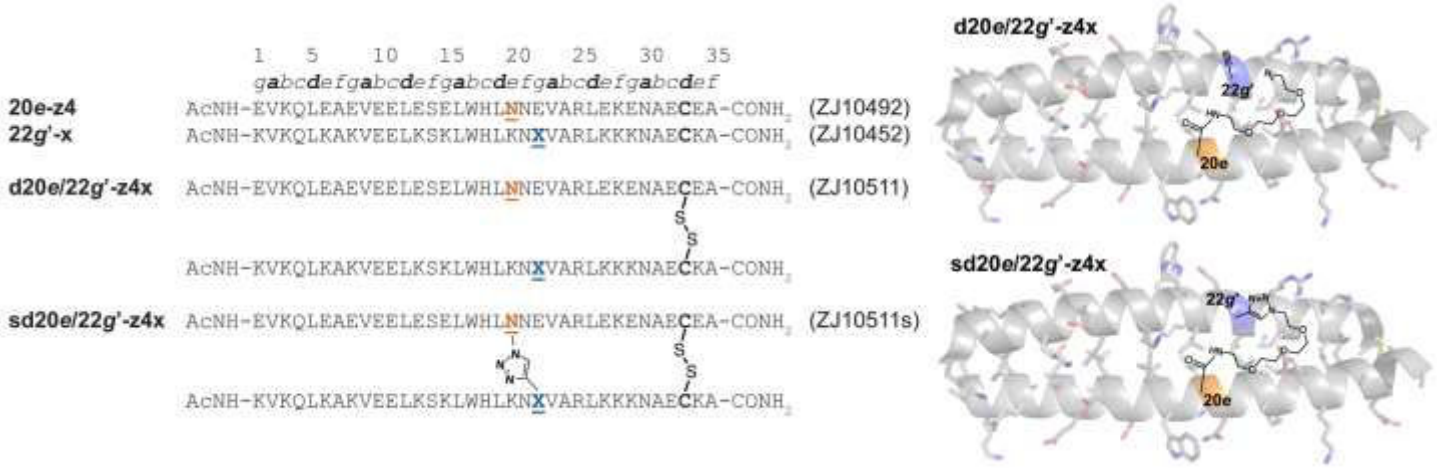

Figure S2. Sequences of (A) acidic monomer **20*e*-z4**, basic monomer **22*g*'-x**, disulfide-bound coiled-coil heterodimer **d20*e*/22*g*'-z4x**, and its stapled counterpart **sd20*e*/22*g*'-z4x**. **X** represents propargyl glycine; **N** represents an azido-terminated PEG-modified Asn residue. Also shown are the structures of the side chains of **X** and **N** and their stapled counterpart superimposed on the ribbon diagram of parent disulfide-bonded heterodimer **A/B** (PDB ID: 1KD9). Side chains are shown as sticks; position 20*e* is highlighted in orange, whereas position 22*g*' is highlighted in blue. The PEG oligomer(s) within each variant have the number of ethylene oxide units indicated in the structural drawings and in the compound names. Numbers in parentheses indicate notebook numbers associated with each compound.

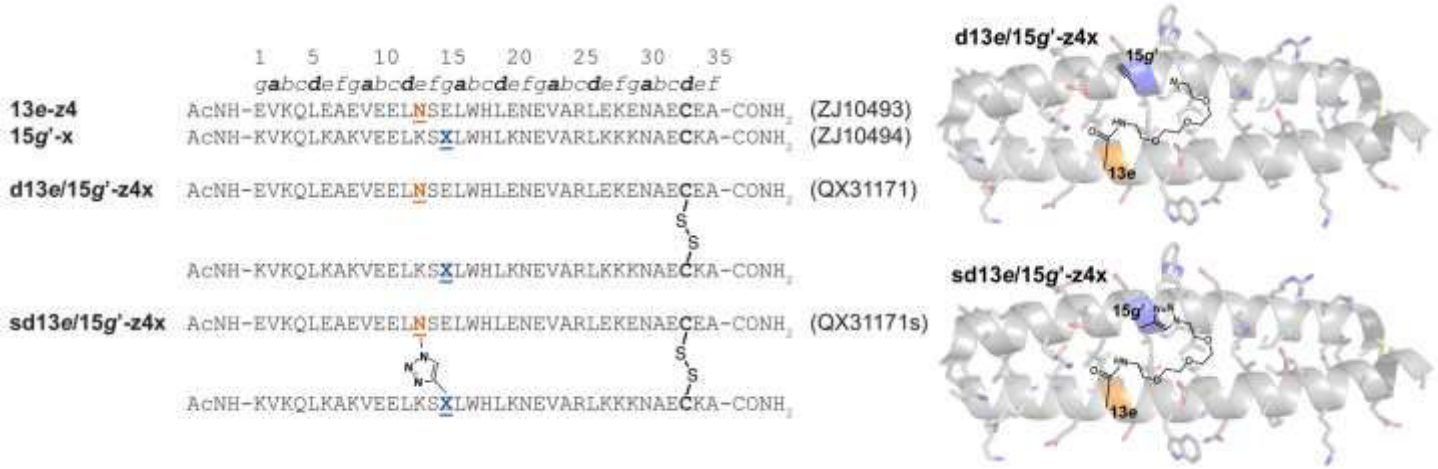

Figure S3. Sequences of (A) acidic monomer **13*e*-z4**, basic monomer **15*g*'-x**, disulfide-bound coiled-coil heterodimer **d13*e*/15*g*'-z4x**, and its stapled counterpart **sd13*e*/15*g*'-z4x**. **X** represents propargyl glycine; **N** represents an azido-terminated PEG-modified Asn residue. Also shown are the structures of the side chains of **X** and **N** and their stapled counterpart superimposed on the ribbon diagram of parent disulfide-bonded heterodimer **A/B** (PDB ID: 1KD9). Side chains are shown as sticks; position 13*e* is highlighted in orange, whereas position 15*g*' is highlighted in blue. The PEG oligomer(s) within each variant have the number of ethylene oxide units indicated in the structural drawings and in the compound names. Numbers in parentheses indicate notebook numbers associated with each compound.

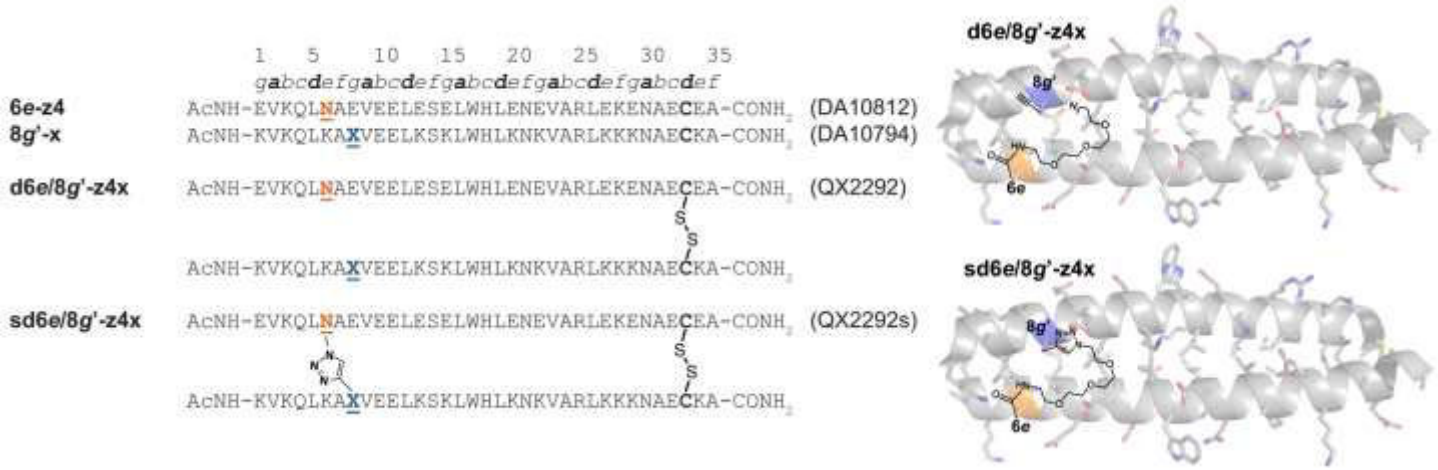

Figure S4. Sequences of (A) acidic monomer **6*e*-z4**, basic monomer **8*g*'-x**, disulfide-bound coiled-coil heterodimer **d6*e*/8*g*'-z4x**, and its stapled counterpart **sd6*e*/8*g*'-z4x**. **X** represents propargyl glycine; **N** represents an azido-terminated PEG-modified Asn residue. Also shown are the structures of the side chains of **X** and **N** and their stapled counterpart superimposed on the ribbon diagram of parent disulfide-bonded heterodimer **A/B** (PDB ID: 1KD9). Side chains are shown as sticks; position 6*e* is highlighted in orange, whereas position 8*g*' is highlighted in blue. The PEG oligomer(s) within each variant have the number of ethylene oxide units indicated in the structural drawings and in the compound names. Numbers in parentheses indicate notebook numbers associated with each compound.

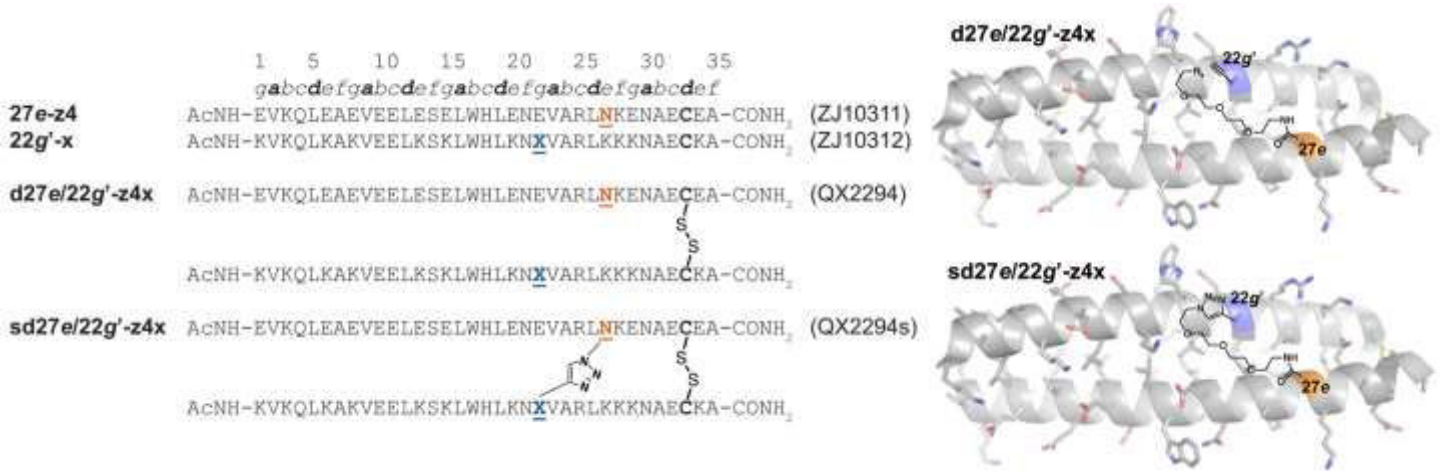

Figure S5. Sequences of (A) acidic monomer **27*e*-z4**, basic monomer **22*g*'-x**, disulfide-bound coiled-coil heterodimer **d27*e*/22*g*'-z4x**, and its stapled counterpart **sd27*e*/22*g*'-z4x**. **X** represents propargyl glycine; **N** represents an azido-terminated PEG-modified Asn residue. Also shown are the structures of the side chains of **X** and **N** and their stapled counterpart superimposed on the ribbon diagram of parent disulfide-bonded heterodimer **A/B** (PDB ID: 1KD9). Side chains are shown as sticks; position 27*e* is highlighted in orange, whereas position 22*g*' is highlighted in blue. The PEG oligomer(s) within each variant have the number of ethylene oxide units indicated in the structural drawings and in the compound names. Numbers in parentheses indicate notebook numbers associated with each compound.

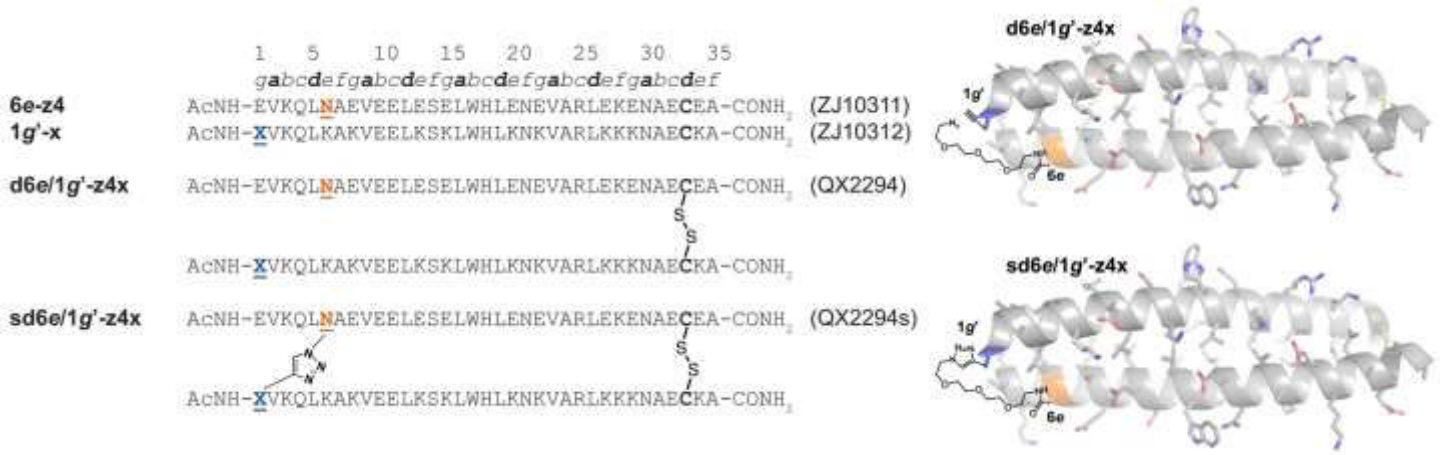

Figure S6. Sequences of (A) acidic monomer **6*e*-z4**, basic monomer **1*g*'-x**, disulfide-bound coiled-coil heterodimer **d6*e*/1*g*'-z4x**, and its stapled counterpart **sd6*e*/1*g*'-z4x**. **X** represents propargyl glycine; **N** represents an azido-terminated PEG-modified Asn residue. Also shown are the structures of the side chains of **X** and **N** and their stapled counterpart superimposed on the ribbon diagram of parent disulfide-bonded heterodimer **A/B** (PDB ID: 1KD9). Side chains are shown as sticks; position 6*e* is highlighted in orange, whereas position 1*g*' is highlighted in blue. The PEG oligomer(s) within each variant have the number of ethylene oxide units indicated in the structural drawings and in the compound names. Numbers in parentheses indicate notebook numbers associated with each compound.

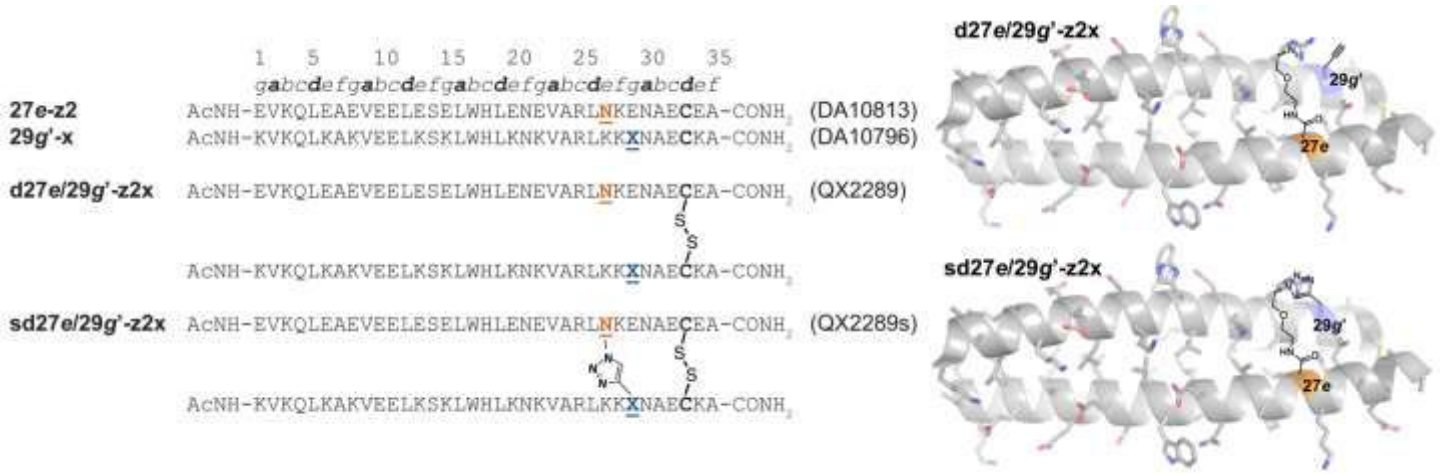

Figure S7. Sequences of (A) acidic monomer **27*e*-z2**, basic monomer **29*g*'-x**, disulfide-bound coiled-coil heterodimer **d27*e*/29*g*'-z2x**, and its stapled counterpart **sd27*e*/29*g*'-z2x**. **X** represents propargyl glycine; **N** represents an azido-terminated PEG-modified Asn residue. Also shown are the structures of the side chains of **X** and **N** and their stapled counterpart superimposed on the ribbon diagram of parent disulfide-bonded heterodimer **A/B** (PDB ID: 1KD9). Side chains are shown as sticks; position 27*e* is highlighted in orange, whereas position 29*g*' is highlighted in blue. The PEG oligomer(s) within each variant have the number of ethylene oxide units indicated in the structural drawings and in the compound names. Numbers in parentheses indicate notebook numbers associated with each compound.

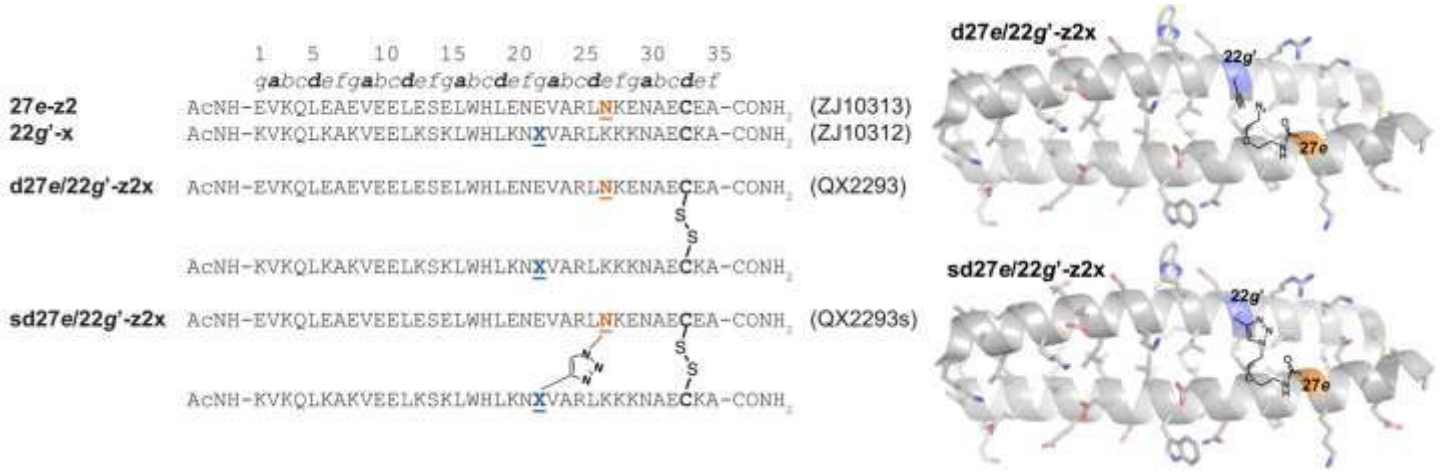

Figure S8. Sequences of (A) acidic monomer **27*e*-z2**, basic monomer **22*g*'-x**, disulfide-bound coiled-coil heterodimer **d27*e*/22*g*'-z2x**, and its stapled counterpart **sd27*e*/22*g*'-z2x**. **X** represents propargyl glycine; **N** represents an azido-terminated PEG-modified Asn residue. Also shown are the structures of the side chains of **X** and **N** and their stapled counterpart superimposed on the ribbon diagram of parent disulfide-bonded heterodimer **A/B** (PDB ID: 1KD9). Side chains are shown as sticks; position 27*e* is highlighted in orange, whereas position 22*g*' is highlighted in blue. The PEG oligomer(s) within each variant have the number of ethylene oxide units indicated in the structural drawings and in the compound names. Numbers in parentheses indicate notebook numbers associated with each compound.

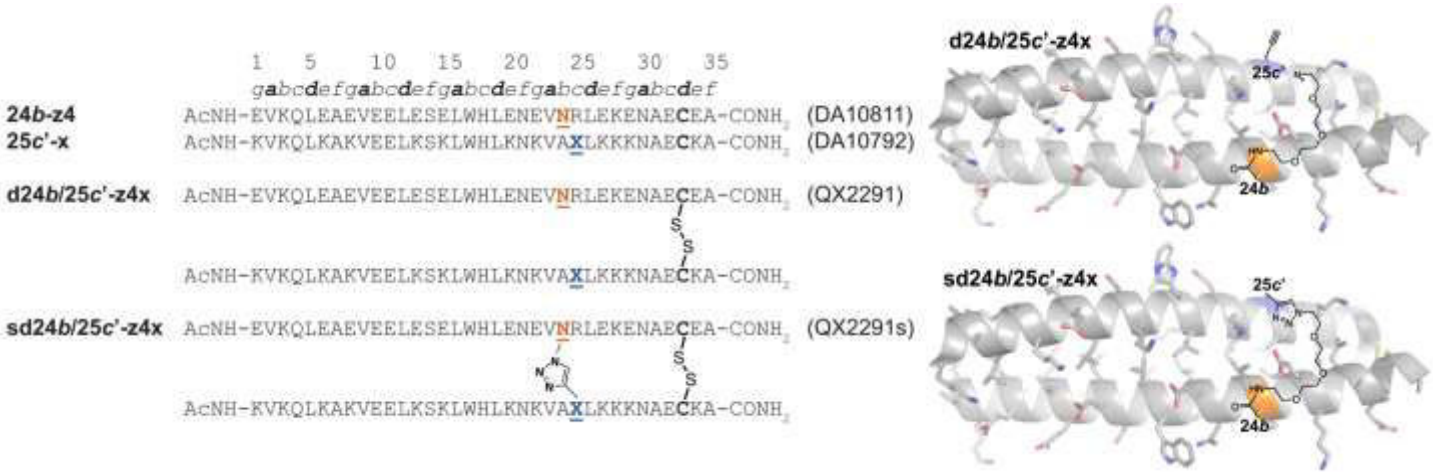

Figure S9. Sequences of (A) acidic monomer **24*b*-z4**, basic monomer **25*c*'-x**, disulfide-bound coiled-coil heterodimer **d24*b*/25*c*'-z4x**, and its stapled counterpart **sd24*b*/25*c*'-z4x**. **X** represents propargyl glycine; **N** represents an azido-terminated PEG-modified Asn residue. Also shown are the structures of the side chains of **X** and **N** and their stapled counterpart superimposed on the ribbon diagram of parent disulfide-bonded heterodimer **A/B** (PDB ID: 1KD9). Side chains are shown as sticks; position 27*e* is highlighted in orange, whereas position 29*g*' is highlighted in blue. The PEG oligomer(s) within each variant have the number of ethylene oxide units indicated in the structural drawings and in the compound names. Numbers in parentheses indicate notebook numbers associated with each compound.

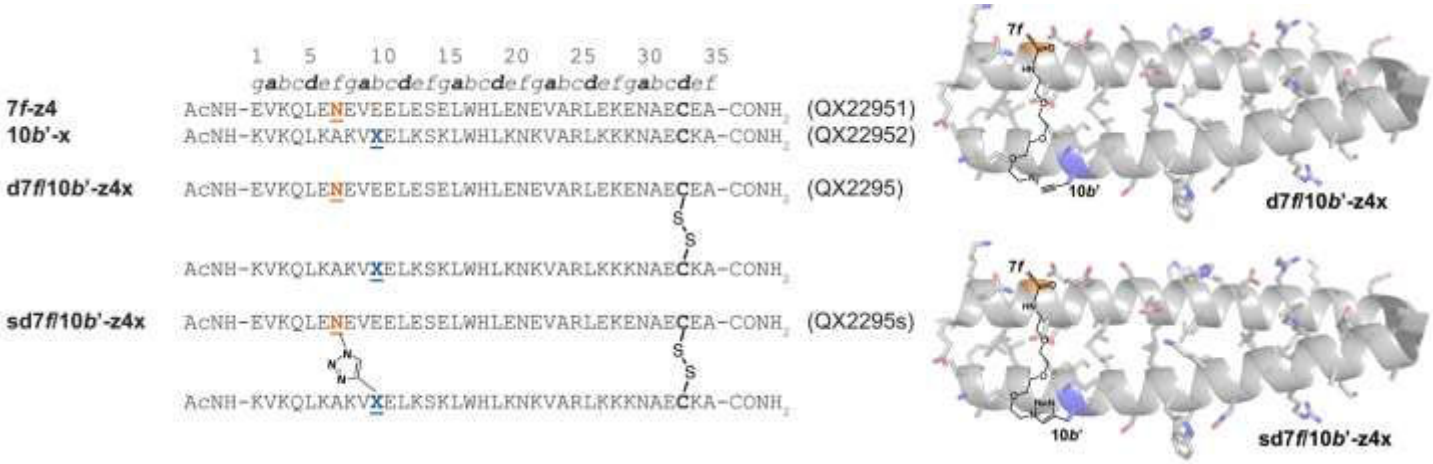

Figure S10. Sequences of (A) acidic monomer **7*f*-z4**, basic monomer **10*b*'-x**, disulfide-bound coiled-coil heterodimer **d7*f*/10*b*'-z4x**, and its stapled counterpart **sd7*f*/10*b*'-z4x**. **X** represents propargyl glycine; **N** represents an azido-terminated PEG-modified Asn residue. Also shown are the structures of the side chains of **X** and **N** and their stapled counterpart superimposed on the ribbon diagram of parent disulfide-bonded heterodimer **A/B** (PDB ID: 1KD9). Side chains are shown as sticks; position 7*f* is highlighted in orange, whereas position 10*b*' is highlighted in blue. The PEG oligomer(s) within each variant have the number of ethylene oxide units indicated in the structural drawings and in the compound names. Numbers in parentheses indicate notebook numbers associated with each compound.

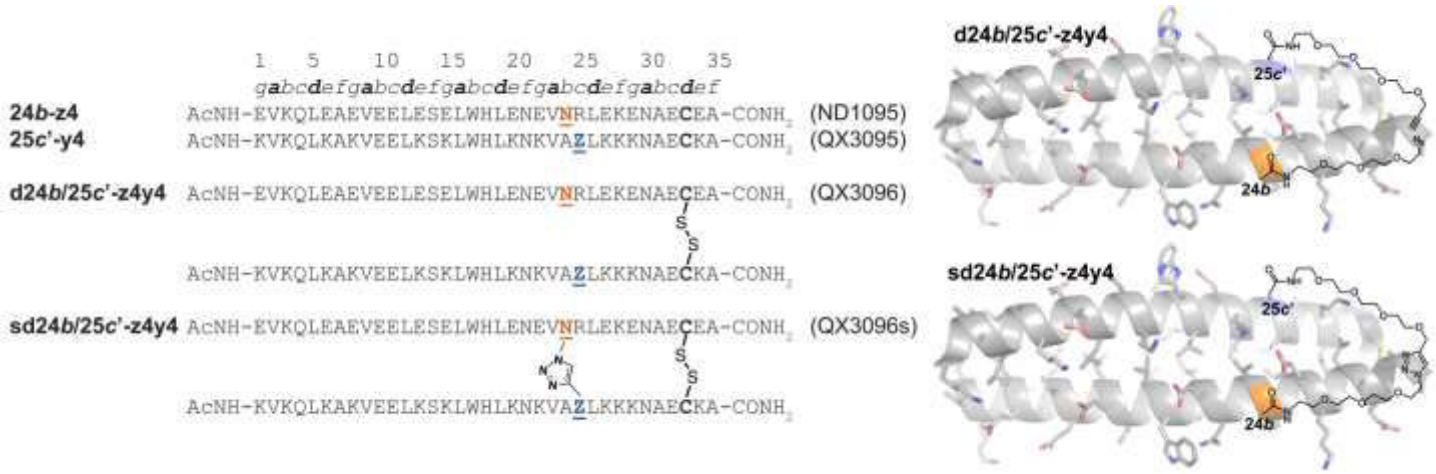

Figure S11. Sequences of (A) acidic monomer **24*b*-z4**, basic monomer **25*c*'-y4**, disulfide-bound coiled-coil heterodimer **d24*b*/25*c*'-z4y4**, and its stapled counterpart **d24*b*/25*c*'-z4y4**. **Z** represents an alkyne-terminated PEG-modified Asn residue; **N** represents an azido-terminated PEG-modified Asn residue. Also shown are the structures of the side chains of **Z** and **N** and their stapled counterpart superimposed on the ribbon diagram of parent disulfide-bonded heterodimer **A/B** (PDB ID: 1KD9). Side chains are shown as sticks; position 24*b* is highlighted in orange, whereas position 25*c*' is highlighted in blue. The PEG oligomer(s) within each variant have the number of ethylene oxide units indicated in the structural drawings and in the compound names. Numbers in parentheses indicate notebook numbers associated with each compound.

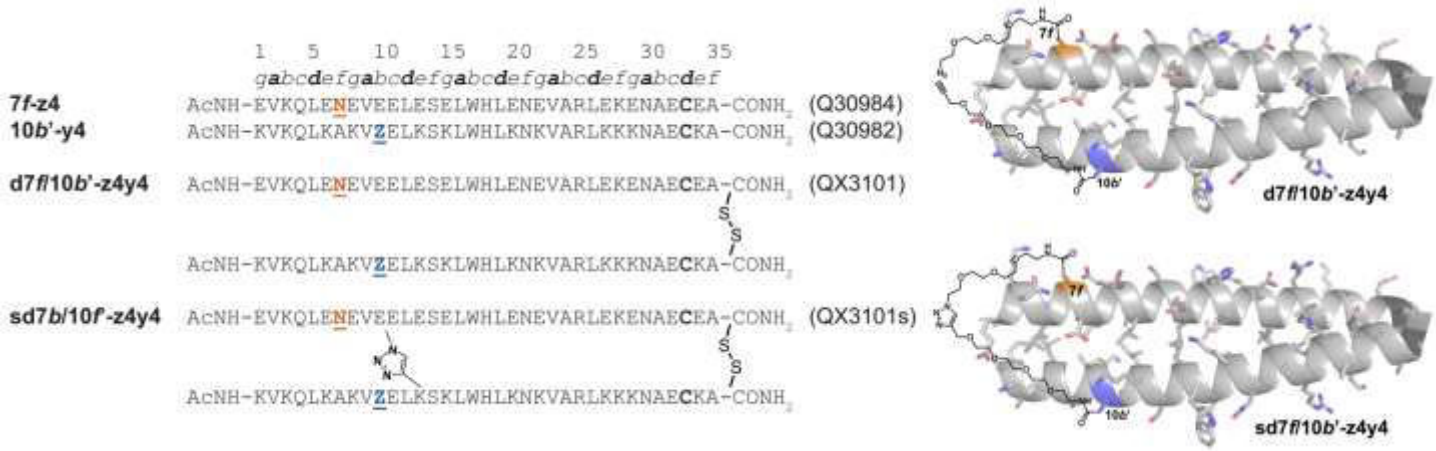

Figure S12. Sequences of (A) acidic monomer **7*f*-z4**, basic monomer **10*b*'-y4**, disulfide-bound coiled-coil heterodimer **d7f/10*b*'-z4y4**, and its stapled counterpart **d7f/10*b*'-z4y4**. **Z** represents an alkyne-terminated PEG-modified Asn residue; **N** represents an azido-terminated PEG-modified Asn residue. Also shown are the structures of the side chains of **Z** and **N** and their stapled counterpart superimposed on the ribbon diagram of parent disulfide-bonded heterodimer **A/B** (PDB ID: 1KD9). Side chains are shown as sticks; position 7*f* is highlighted in orange, whereas position 10*b*' is highlighted in blue. The PEG oligomer(s) within each variant have the number of ethylene oxide units indicated in the structural drawings and in the compound names. Numbers in parentheses indicate notebook numbers associated with each compound.

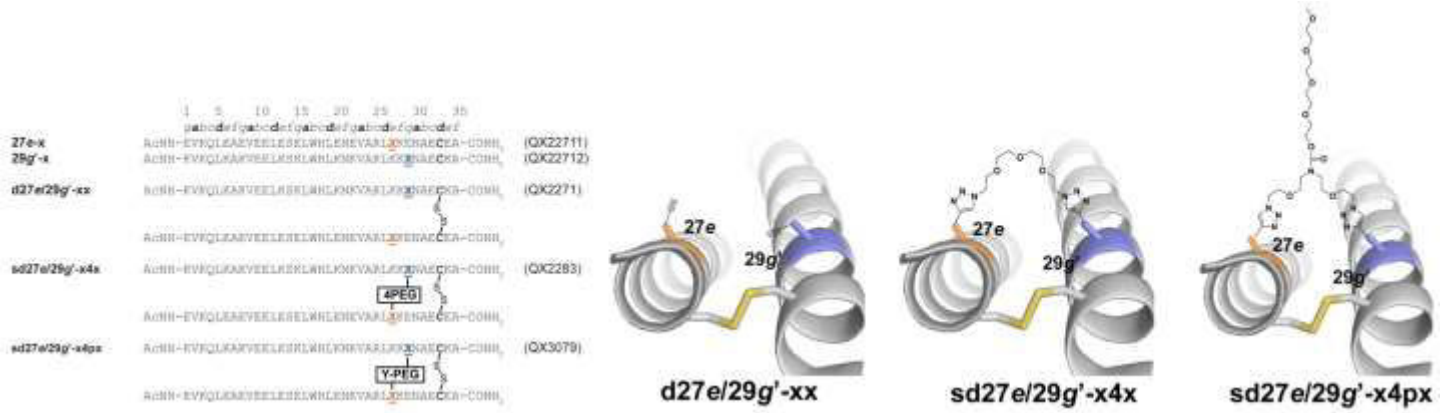

Figure S13. Sequences of disulfide-bound coiled-coil heterodimer **d27*e*/29*g*'-xx**; its bis-triazole-stapled counterpart **sd27*e*/29*g*'-x4x**; branched PEG bis-triazole-stapled counterpart **sd27*e*/29*g*'-x4px**; and their component cysteine-containing acidic and basic monomers. **X** represents propargyl glycine; The structure of the **X** residues within each variant are shown in their non-stapled and stapled forms superimposed on the ribbon diagram of **A/B** with the residue on peptide **A** highlighted in orange and the residue on peptide **B** highlighted in blue. The PEG oligomer(s) within each variant have the number of ethylene oxide units indicated in the structural drawings and in the compound names. Numbers in parentheses indicate notebook numbers associated with each compound.

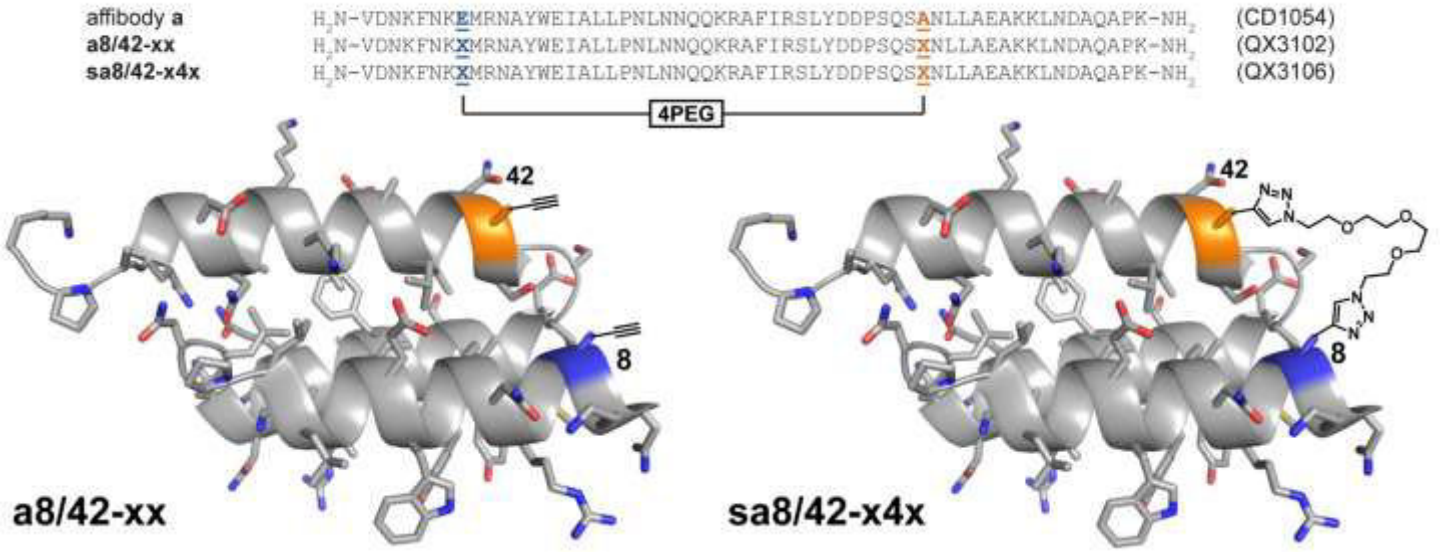

Figure S14. Sequences of native affibody **a** (PDB ID: 3MZW), non-stapled variant **a8/42-xx**; and its bis-triazole-stapled counterpart **sa8/42-x4x**. **X** represents propargyl glycine; The structure of the **X** residues within each variant are shown in their non-stapled and stapled forms superimposed on the ribbon diagram of **a** with position 8 highlighted in blue and position 42 highlighted in orange. The PEG oligomer staple has the number of ethylene oxide units indicated in the structural drawing and in the compound name. Numbers in parentheses indicate notebook numbers associated with each compound.

Modelling of z4x, z2x, z4y4, and x4x staples: We generated models for the z4x, z2x, z4y4, and x4x staples 2 in GaussView 6.0 based on the structures in main text Figure 2, but with *N*'-acetyl amino acid *N*-methyl amides on either end of the staple. We then optimized these model structure in Gaussian 16 using density functional theory (APFD) calculations with the 6-31G+d,p basis set. These optimized structures are shown below in Figure S15. We used the distance between the β-carbons on either end of each staple as an estimate of the distance that could be comfortably spanned by that staple. These distances appear in main text Table 1 and in ESI Table S2.

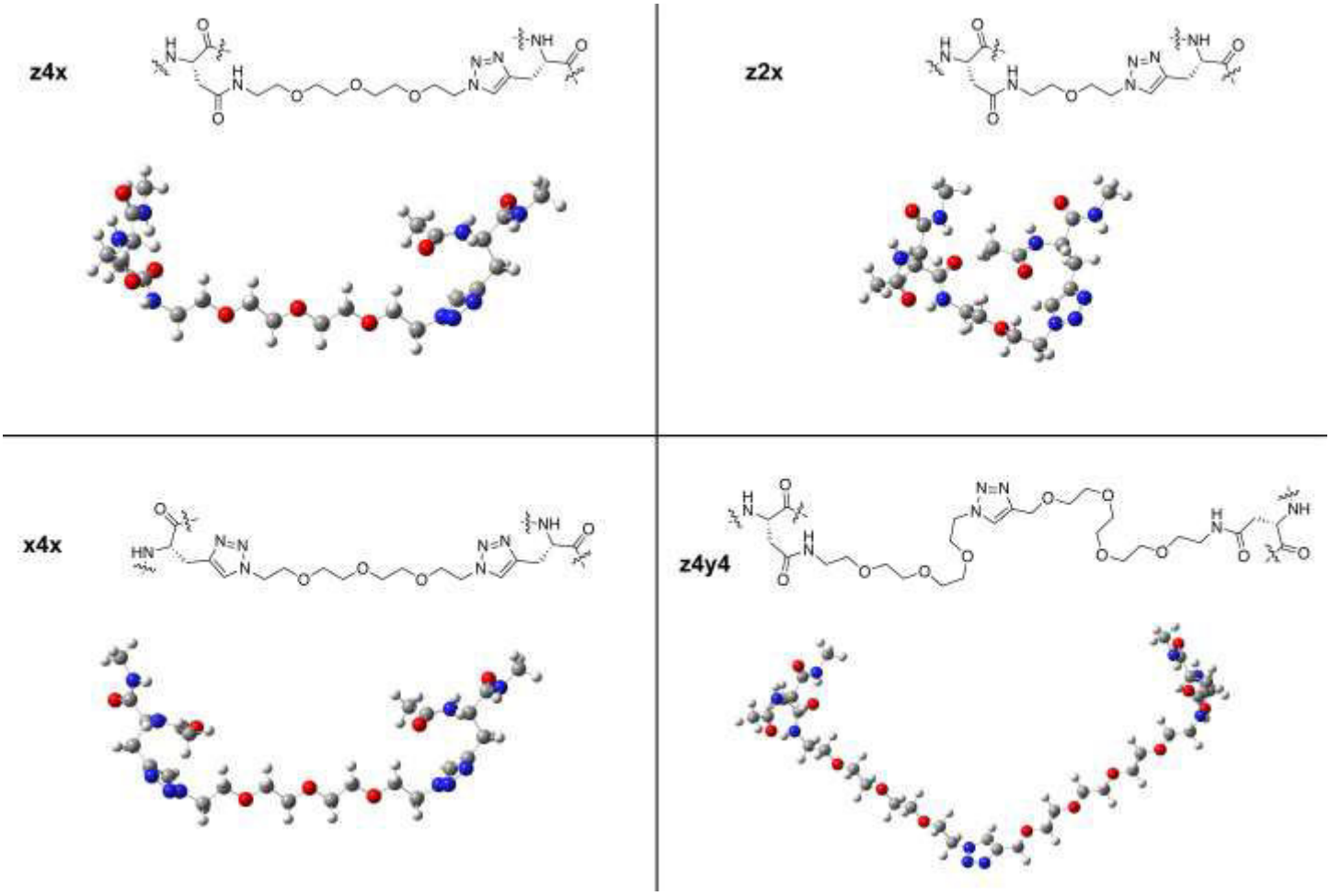

Figure S15. Drawings of staples **z4x**, **z2x**, **x4x**, and **z4y4**, along with ball-and-stick images of optimized model staples based on **z4x**, **z2x**, **x4x**, and **z4y4**. Models were built in GaussView 6.0 and optimized via DFT calculations (APFD) using the 6-31G+d,p basis set.

2. Synthesis of coiled-coil and affibody variants

Peptide Synthesis: Monomers **20*e*-z4** (ZJ10492); **22*g*'-x** (ZJ10452); **13*e*-z4** (ZJ10493); **15*g*'-x** (ZJ10494); **6*e*-z4** (DA10812, QX31101); **8*g*'-x** (DA10794); **27*e*-z4** (ZJ10311); **22*g*'-x** (ZJ10312); **1*g*'-x** (QX31102); **24*b*-z4** (DA10811, ND1095); **25*c*'-x** (DA10792); **25*c*'-y4** (QX3095); **7*f*-z4** (QX22951, QX30984); **10*b*'-x** (QX22952); **10*b*'-y4** (QX30982); **27*e*-z2** (DA10813, ZJ10313); **29*g*'-x** (DA10796, QX22712); **27*e*-x** (QX22711); and affibody variants **a** (CD1054) and **a8/42-xx** (QX3102) were prepared as C-terminal amides on Rink amide MBHA LL resin (EMD Biosciences), by microwave-assisted solid phase peptide synthesis using a standard Fmoc Nα protection strategy as described previously.[2] Fmoc-protected amino acids were purchased from Advanced Chem Tech, except for the PEGylated asparagine derivatives, which were synthesized as described previously[1] or in section **7** below. Fluorescent affibody variants **fa** (ZJ10611); **fa8/42-xx** (ZJ10612); and **fsa8/42-x4x** (ZJ1062) were synthesized in a similar process until the final amino acid following which 5(6)-Carboxyfluorescein was coupled to the peptide N-terminus through activation with standard Oxyma/DIC protocols. Peptides were cleaved from resin and purified by preparative reverse-phase high-performance liquid chromatography (HPLC) on a C18 column using a linear gradient of water in acetonitrile with 0.1% v/v trifluoroacetic acid. Peptide identity was confirmed by electrospray ionization time- of-flight mass spectrometry.

Disulfide formation in the coiled-coil heterodimer: We prepared disulfide-bonded coiled-coil heterodimers **d20*e*/22*g*'-z4x** (ZJ10511); **d13*e*/15*g*'-z4x** (QX31171); **d6*e*/8*g*'-z4x** (QX2292); **d27*e*/22*g*'-z4x** (QX2294); **d6*e*/1*g*'-z4x** (QX31172); **d24*b*/25*c*'-z4x** (QX2291); **d24*b*/25*c*'-z4y4** (QX3096); **d7*f*/10*b*'-z4x** (QX2295); **d7*f*/10*b*'-z4y4** (QX3101); **d27*e*/29*g*'-z2x** (QX2289); **d27*e*/22*g*'-z2x** (QX2293); **d27*e*/29*g*'-xx** (QX2271) by mixing their purified cysteine-containing precursors in a 1:1 ratio in an aqueous solution of ammonium bicarbonate (8 mg/mL) with exposure to air for 3 hrs. Reaction completeness was monitored by analytical HPLC. Disulfide-bonded coiled-coil heterodimers were then purified by preparative HPLC and characterized by ESI-TOF MS.

Stapling via copper-catalyzed azide/alkyne cycloaddition (CuAAC): We prepared triazole-stapled variants **sd20*e*/22*g*'-z4x** (ZJ10511s); **sd13*e*/15*g*'-z4x** (QX31171s); **sd6*e*/8*g*'-z4x** (QX2292s); **sd27*e*/22*g*'-z4x** (QX2294s); **sd6*e*/1*g*'-z4x** (QX31172s); **sd24*b*/25*c*'-z4x** (QX2291s); **sd24*b*/25*c*'-z4y4** (QX3096s); **sd7*f*/10*b*'-z4x** (QX2295s); **sd7*f*/10*b*'-z4y4** (QX3101s); **sd27*e*/29*g*'-z2x** (QX2289s); **sd27*e*/22*g*'-z2x** (QX2293s) by stirring their purified non-stapled precursors in 2:1 (v/v) water/*tert*-butanol with 10 eq. copper sulfate pentahydrate and 10 eq. sodium ascorbate at 40 Celsius degree for 2 hours. The reaction was monitored by analytical HPLC, where we observed small changes in retention time upon stapling. The triazole-stapled variants were purified via preparative HPLC.

Two-component stapling via copper-catalyzed azide/alkyne cycloaddition (CuAAC): We prepared triazole-stapled variants **sd27*e*/29*g*'-x4x** (QX2283), **sa8/42-x4x** (QX3106), **fsa8/42-x4x** (ZJ1062), and **sd27*e*/29*g*'-x4px** (QX3079) by stirring their non-stapled precursors **d27*e*/29*g*'-xx** (QX2271), **a8/42-xx** (QX3102), and **fa8/42-xx** (ZJ10612), respectively, in 2:1 (v/v) water/*tert*-butanol with 1.5 eq. of previously synthesized four-unit bis-azido PEG **4**[1] or four-unit bis-azido Y-shaped PEG **4p** (QX3075; synthesis described in section 10 below), 10 eq. copper sulfate pentahydrate and 10 eq. sodium ascorbate at 40 °C for 2 hours. The reaction was monitored by analytical HPLC, where we observed small changes in retention time upon stapling. The triazole-stapled variants were purified via preparative HPLC.

The CuAAC reaction does not change the mass of the monomeric triazole-stapled variants **sd20e/22g'-z4x** (ZJ10511s); **sd13*e*/15*g*'-z4x** (QX31171s); **sd6*e*/8*g*'-z4x** (QX2292s); **sd27*e*/22*g*'-z4x** (QX2294s); **sd6*e*/1*g*'-z4x** (QX31172s); **sd24*b*/25*c*'-z4x** (QX2291s); **sd24*b*/25*c*'-z4y4** (QX3096s); **sd7*f*/10*b*'-z4x** (QX2295s); **sd7*f*/10*b*'-z4y4** (QX3101s); **sd27*e*/29*g*'-z2x** (QX2289s); **sd27*e*/22*g*'-z2x** (QX2293s) relative to their non-stapled azide/alkyne precursors **d20*e*/22*g*'-z4x** (ZJ10511); **d13*e*/15*g*'-z4x** (QX31171); **d6*e*/8*g*'-z4x** (QX2292); **d27*e*/22*g*'-z4x** (QX2294); **d6*e*/1*g*'-z4x** (QX31172); **d24*b*/25*c*'-z4x** (QX2291); **d24*b*/25*c*'-z4y4** (QX3096); **d7*f*/10*b*'-z4x** (QX2295); **d7*f*/10*b*'-z4y4** (QX3101); **d27*e*/29*g*'-z2x** (QX2289); and **d27*e*/22*g*'-z2x** (QX2293). To confirm the completion of the CuAAC reaction, we subjected each azide-containing non-stapled variant and its triazole-stapled counterpart separately to a solution of dithiothreitol (DTT, 15 mg) in 100 μL water, followed by incubation at room temperature for 8 hours. In all cases, the unstapled variants were reduced to their corresponding monomers with DTT addition, for the triazole-stapled variants, the dimer still existed as dimer after the DTT treatment, indicating the formation of covalent linkage between monomers.

3. Mass Spectrometry Data

Mass spectra appear in Figures S16–S84; data are summarized in Table S1.

Table S1. Summary of the mass spectrum data for stapled disulfide-bonded coiled-coil heterodimers, their non-stapled counterparts, and their monomer components.

Name	Notebook Number	Molecular Formula	z	Expected [M+z·H]/z	Observed [M+z·H]/z
20*e*-z4	ZJ10492	$C_{185}H_{295}N_{51}O_{68}S$	4	1088.781	1088.770
22*g*'-x	ZJ10452	$C_{187}H_{324}N_{56}O_{46}S$	4	1031.620	1031.596
d20*e*/22*g*'-z4x	ZJ10511	$C_{372}H_{617}N_{107}O_{114}S_2$	8	1059.948	1060.066
sd20*e*/22*g*'-z4x	ZJ10511s	$C_{372}H_{617}N_{107}O_{114}S_2$	8	1059.948	1060.086
	ZJ10511s + DTT	$C_{372}H_{619}N_{107}O_{114}S_2$	8	1060.200	1060.572
13*e*-z4	ZJ10493	$C_{185}H_{295}N_{51}O_{68}S$	4	1088.781	1088.763
15*g*'-x	ZJ10494	$C_{187}H_{324}N_{56}O_{46}S$	4	1031.620	1031.601
d13*e*/15*g*'-z4x	QX31171	$C_{372}H_{617}N_{107}O_{114}S_2$	8	1059.948	1060.086
sd13*e*/15*g*'-z4x	QX31171s	$C_{372}H_{617}N_{107}O_{114}S_2$	7	1211.225	1211.195
	+ DTT	$C_{372}H_{619}N_{107}O_{114}S_2$	8	1060.200	1060.851
6*e*-z4	DA10812	$C_{185}H_{295}N_{51}O_{68}S$	4	1088.781	1088.783
8*g*'-x	DA10794	$C_{187}H_{324}N_{56}O_{46}S$	4	1031.620	1031.619
d6*e*/8*g*'-z4x	QX2292	$C_{372}H_{617}N_{107}O_{114}S_2$	8	1059.948	1059.948
sd6*e*/8*g*'-z4x	QX2292s	$C_{372}H_{617}N_{107}O_{114}S_2$	6	1415.928	1412.937
	QX2292s + DTT	$C_{372}H_{619}N_{107}O_{114}S_2$	8	1060.200	1060.074
27*e*-z4	ZJ10311	$C_{185}H_{295}N_{51}O_{68}S$	4	1088.781	1088.781
22*g*'-x	ZJ10312	$C_{187}H_{324}N_{56}O_{46}S$	4	1031.620	1031.613
d27*e*/22*g*'-z4x	QX2294	$C_{372}H_{617}N_{107}O_{114}S_2$	8	1059.948	1059.953
sd27*e*/22*g*'-z4x	QX2294s	$C_{372}H_{617}N_{107}O_{114}S_2$	8	1059.948	1059.953
	QX2294s + DTT	$C_{372}H_{619}N_{107}O_{114}S_2$	8	1060.200	1060.197
6*e*-z4	QX31101	$C_{185}H_{295}N_{51}O_{68}S$	4	1088.781	1088.789
1*g*'-x	QX31102	$C_{187}H_{324}N_{56}O_{46}S$	4	1031.620	1031.629
d6*e*/1*g*'-z4x	QX31172	$C_{372}H_{617}N_{107}O_{114}S_2$	8	1059.948	1060.088
sd6*e*/1*g*'-z4x	QX31172s	$C_{372}H_{617}N_{107}O_{114}S_2$	7	1211.225	1211.388
	+ DTT	$C_{372}H_{619}N_{107}O_{114}S_2$	7	1211.513	1211.291
27*e*-z2	DA10813	$C_{183}H_{290}N_{48}O_{67}S$	4	1066.768	1066.763
29*g*'-x	DA10796	$C_{187}H_{324}N_{56}O_{46}S$	4	1031.620	1031.622
d27*e*/29*g*'-z2x	QX2289	$C_{368}H_{609}N_{107}O_{112}S_2$	8	1048.942	1048.940
sd27*e*/29*g*'-z2x	QX2289s	$C_{368}H_{609}N_{107}O_{112}S_2$	8	1048.942	1048.942
	QX2289s + DTT	$C_{368}H_{611}N_{107}O_{112}S_2$	8	1049.194	1049.326
27*e*-z2	ZJ10313	$C_{181}H_{286}N_{51}O_{66}S$	4	1066.768	1066.769
22*g*'-x	ZJ10312	$C_{187}H_{324}N_{56}O_{46}S$	4	1031.620	1031.613
d27*e*/22*g*'-z2x	QX2293	$C_{368}H_{609}N_{107}O_{112}S_2$	8	1048.942	1048.948
sd27*e*/22*g*'-z2x	QX2293s	$C_{368}H_{609}N_{107}O_{112}S_2$	8	1048.942	1048.948
	QX2293s + DTT	$C_{368}H_{611}N_{107}O_{112}S_2$	8	1049.194	1049.067
24*b*-z4	DA10811	$C_{187}H_{297}N_{51}O_{70}S$	4	1103.282	1103.268
25*c*'-x	DA10792	$C_{187}H_{324}N_{54}O_{46}S$	4	1024.618	1024.605
d24*b*/25*c*'-z4x	QX2291	$C_{374}H_{619}N_{105}O_{116}S_2$	8	1063.698	1063.705
sd24*b*/25*c*'-z4x	QX2291s	$C_{374}H_{619}N_{105}O_{116}S_2$	8	1063.698	1063.697
	QX2291s + DTT	$C_{374}H_{621}N_{105}O_{116}S_2$	8	1063.950	1063.950
24*b*-z4	ND1095	$C_{187}H_{297}N_{51}O_{70}S$	4	1103.282	1103.268
25*c*'-y4	QX3095	$C_{197}H_{343}N_{55}O_{51}S$	4	1082.900	1082.906
d24*b*/25*c*'-z4y4	QX3096	$C_{384}H_{638}N_{106}O_{121}S_2$	8	1092.839	1093.064
sd24*b*/25*c*'-z4y4	QX3096s	$C_{384}H_{638}N_{106}O_{121}S_2$	8	1092.839	1093.072
	QX3096s + DTT	$C_{384}H_{640}N_{106}O_{121}S_2$	8	1093.091	1093.315
7*f*-z4	QX22951	$C_{187}H_{297}N_{51}O_{70}S$	4	1103.282	1103.298
10*b*'-x	QX22952	$C_{188}H_{329}N_{57}O_{44}S$	4	1031.383	1031.397
d7*f*/10*b*'-z4x	QX2295	$C_{375}H_{624}N_{108}O_{114}S_2$	8	1067.081	1067.088
sd7*f*/10*b*'-z4x	QX2295s	$C_{375}H_{624}N_{108}O_{114}S_2$	7	1219.377	1219.364
	QX2295s + DTT	$C_{375}H_{626}N_{108}O_{114}S_2$	7	1219.665	1219.807
7*f*-z4	QX30984	$C_{187}H_{297}N_{51}O_{70}S$	4	1103.282	1103.298
10*b*'-y4	QX30982	$C_{198}H_{348}N_{58}O_{49}S$	4	1089.664	1089.671
d7*f*/10*b*'-z4y4	QX3101	$C_{385}H_{643}N_{109}O_{119}S_2$	8	1096.221	1096.447
sd7*f*/10*b*'-z4y4	QX3101s	$C_{385}H_{643}N_{109}O_{119}S_2$	7	1252.680	1253.046
	QX3101s + DTT	$C_{385}H_{645}N_{109}O_{119}S_2$	8	1096.473	1096.697
27*e*-x	QX22711	$C_{178}H_{279}N_{47}O_{64}S$	4	1033.752	1033.757
29*g*-x	QX22712	$C_{187}H_{324}N_{56}O_{46}S$	4	1031.620	1031.624

d27*e*/29*g*'-xx	QX2271	$C_{365}H_{601}N_{103}O_{110}S_2$	8	1032.434	1032.442
sd27*e*/29*g*'-x4x	QX2283	$C_{373}H_{617}N_{109}O_{113}S_2$	8	1062.950	1062.953
	QX2283 + DTT	$C_{373}H_{619}N_{109}O_{113}S_2$	8	1063.202	1063.33
sd27*e*/29*g*'-x4px	QX3079	$C_{383}H_{636}N_{110}O_{118}S_2$	8	1092.090	1092.075
	QX3079 + DTT	$C_{383}H_{638}N_{110}O_{118}S_2$	8	1092.342	1092.447
(*R*)-27*e*-x	ZJ10551	$C_{178}H_{279}N_{47}O_{64}S$	4	1033.752	1033.751
(*R*,*S*)-d27*e*/29*g*'-xx	QX3118	$C_{365}H_{601}N_{103}O_{110}S_2$	8	1032.434	1032.541
(*R*,*S*)-sd27*e*/29*g*'-x4x	ZJ1056	$C_{373}H_{617}N_{109}O_{113}S_2$	8	1062.950	1063.073
	ZJ1056 + DTT	$C_{373}H_{619}N_{109}O_{113}S_2$	8	1063.202	1063.264
affibody **a**	CD1054	$C_{296}H_{471}N_{87}O_{89}S$	5	1341.103	1341.106
a8/42-xx	QX3102	$C_{298}H_{469}N_{87}O_{87}S$	5	1339.102	1339.123
sa8/42-x4x	QX3106	$C_{306}H_{485}N_{93}O_{90}S$	5	1387.927	1387.915
Fluorescent affibody **fa**	ZJ10611	$C_{317}H_{480}N_{86}O_{95}S$	5	1412.914	1412.883
fa8/42-xx	ZJ01612	$C_{319}H_{478}N_{86}O_{93}S$	5	1410.913	1410.888
fsa8/42-x4x	ZJ1062	$C_{327}H_{494}N_{92}O_{96}S$	5	1459.738	1459.705

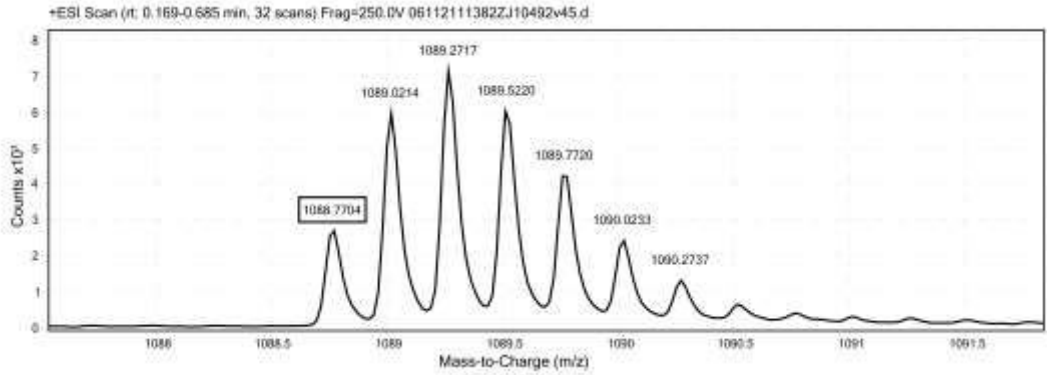

Figure S16. ESI-TOF spectrum for acidic monomer **20*e*-z4** (ZJ10492, $C_{185}H_{295}N_{51}O_{68}S$). Expected $[M+4H^+]/4$ = 1088.781 Da. Observed $[M+4H^+]/4$ = 1088.770 Da.

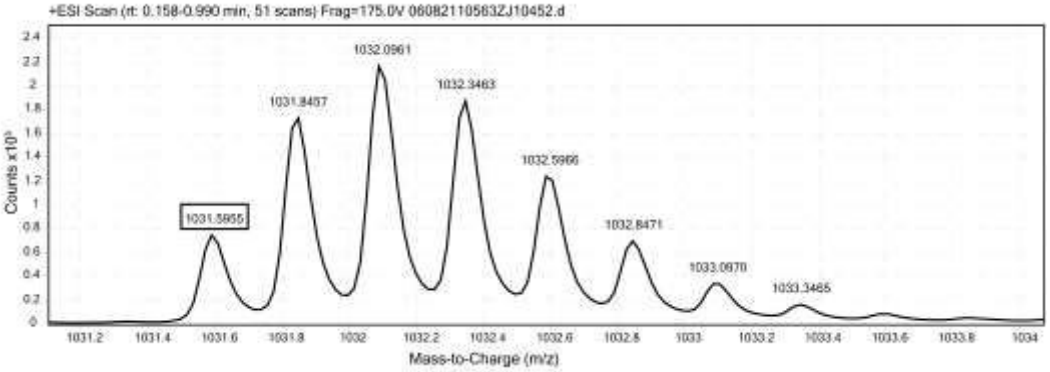

Figure S17. ESI-TOF spectrum for basic monomer **22*g*'-x** (ZJ10452, $C_{187}H_{324}N_{56}O_{46}S$). Expected $[M+4H^+]/4$ = 1031.620 Da. Observed $[M+4H^+]/4$ = 1031.596 Da.

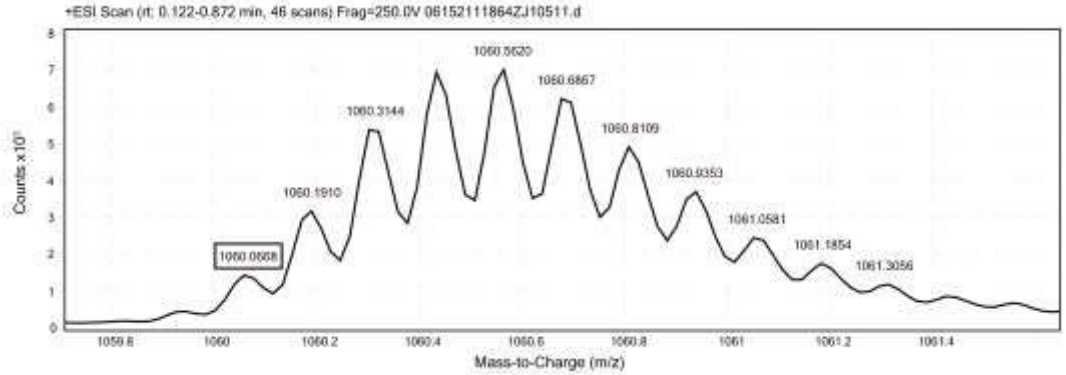

Figure S18. ESI-TOF spectrum for disulfide-bound coiled-coil variant **d20*e*/22*g*'-z4x** (ZJ10511, $C_{372}H_{617}N_{107}O_{114}S_2$). Expected $[M+8H^+]/8$ = 1059.948 Da. Observed $[M+8H^+]/4$ = 1060.067 Da.

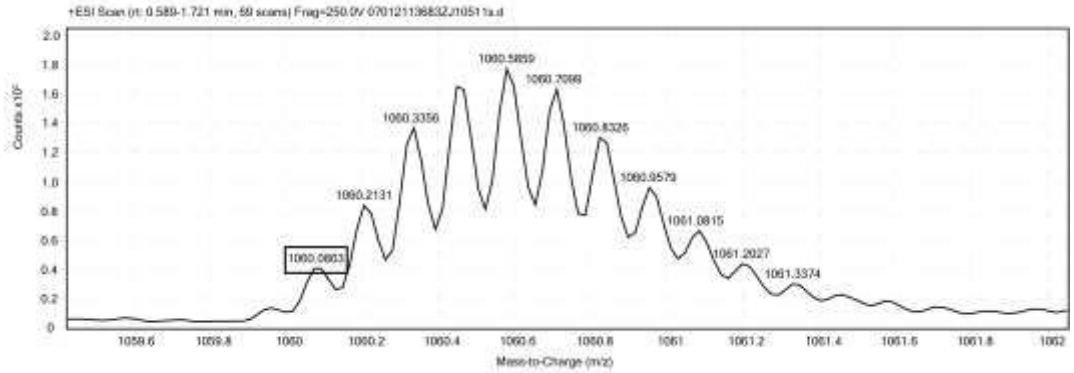

Figure S19. ESI-TOF spectrum for disulfide-bound stapled coiled-coil variant **sd20*e*/22*g*'-z4x** (ZJ10511s, $C_{372}H_{617}N_{107}O_{114}S_2$). Expected $[M+8H^+]/8$ = 1059.948 Da. Observed $[M+8H^+]/4$ = 1060.086 Da.

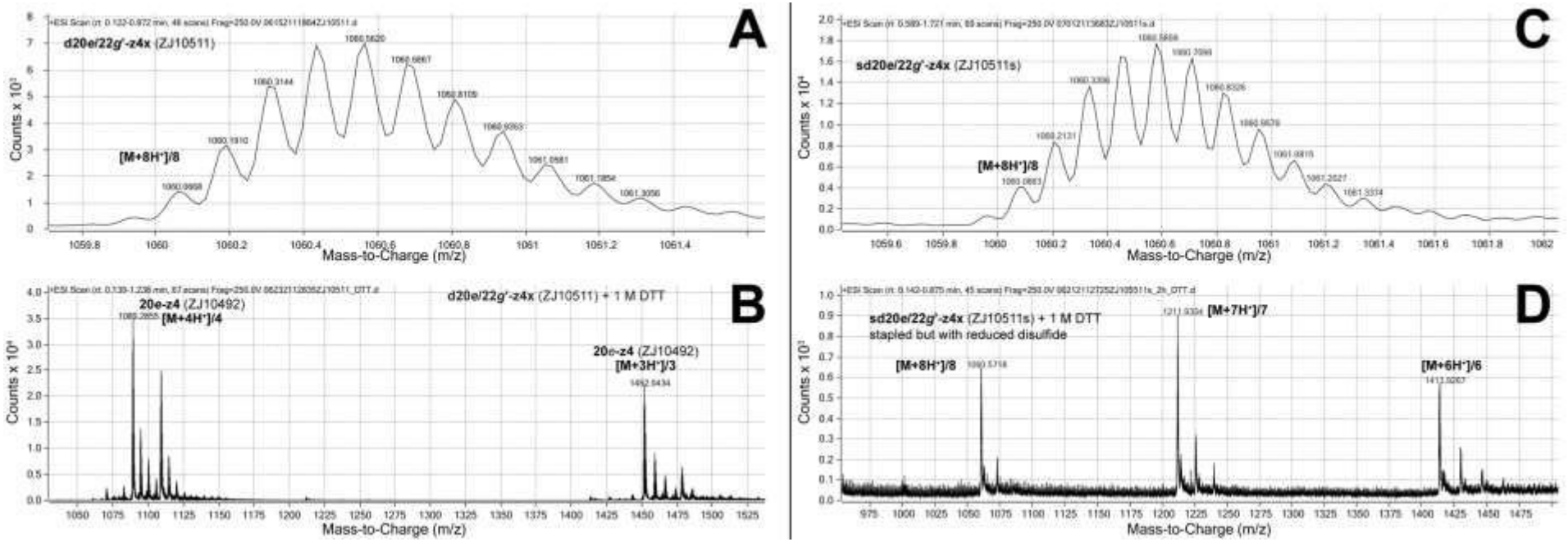

Figure S20. ESI-TOF MS data for azide-containing (A) disulfide-bound coiled-coil variant **d20*e*/22*g*'-z4x** before (ZJ10511; $C_{372}H_{617}N_{107}O_{114}S_2$; expected $[M+8H^+]/8$ = 1059.948 Da) and (B) after exposure to reducing conditions (1M DTT) for at least 8h. Following reduction, **d20*e*/22*g*'-z4x** splits into its component peptides: **20*e*-z4** (ZJ10492; $C_{185}H_{295}N_{51}O_{68}S$; expected mass $[M+4H^+]/4$ = 1088.781 Da) and **22*g*'-x** (ZJ10452; $C_{187}H_{324}N_{56}O_{46}S$; expected mass $[M+4H^+]/4$ = 1031.620 Da; does not appear in spectrum for reasons that are not clear). Also shown are ESI-TOF MS data for (C) triazole-stapled **sd20*e*/22*g*'-z4x** before (ZJ10511s; $C_{372}H_{617}N_{107}O_{114}S_2$; expected $[M+8H^+]/8$ = 1059.948 Da) and (E) after exposure to reduction conditions for at least 8h ($C_{372}H_{619}N_{107}O_{114}S_2$; expected $[M+8H^+]/8$ = 1060.073 Da after reduction of disulfide bond to cysteine residues). Note that **sd20*e*/22*g*'-z4x** remains intact even after disulfide reduction due to the triazole staple.

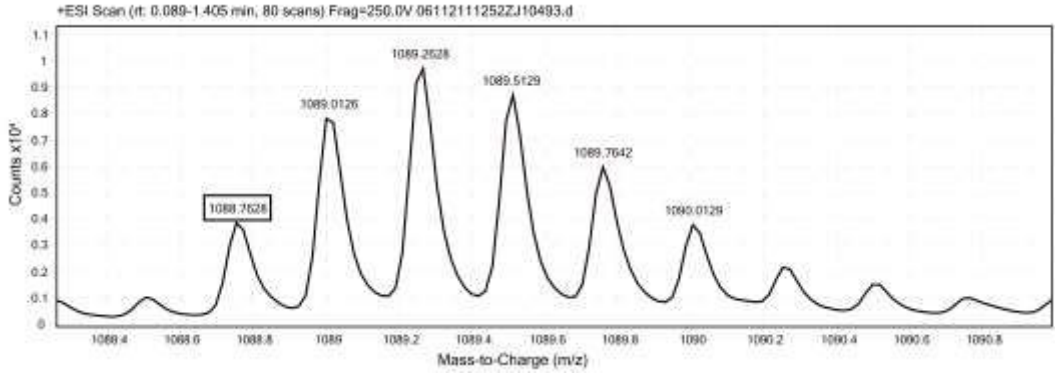

Figure S21. ESI-TOF spectrum for acidic monomer **13*e*-*z*4** (ZJ10493, $C_{185}H_{295}N_{51}O_{68}S$). Expected $[M+4H^+]/4$ = 1088.781 Da. Observed $[M+4H^+]/4$ = 1088.763 Da.

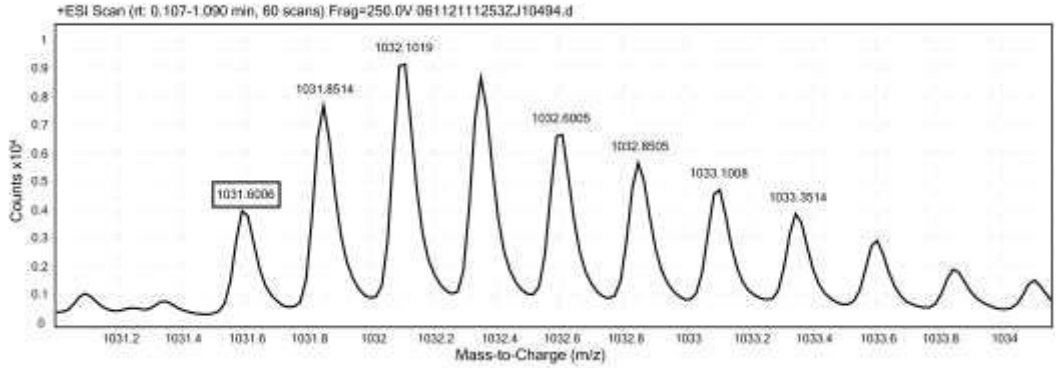

Figure S22. ESI-TOF spectrum for basic monomer **15*g*'-x** (ZJ10494, $C_{187}H_{324}N_{56}O_{46}S$). Expected $[M+4H^+]/4$ = 1031.620 Da. Observed $[M+4H^+]/4$ = 1031.601 Da.

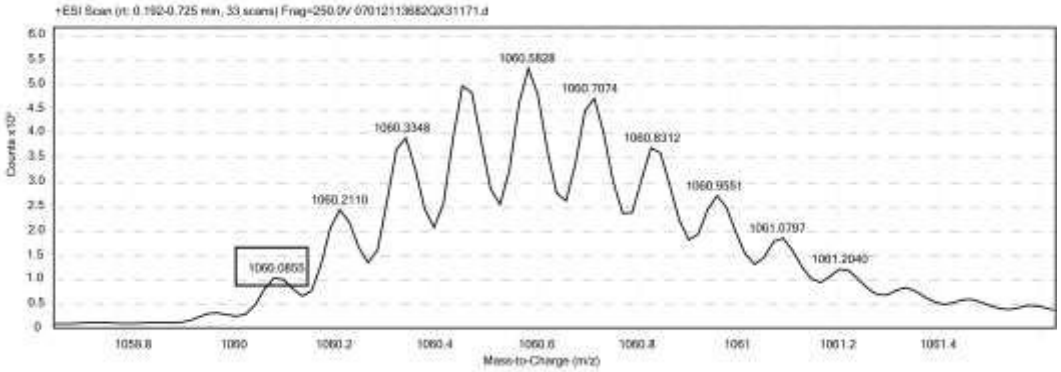

Figure S23. ESI-TOF spectrum for disulfide-bound coiled-coil variant **d13*e*/15*g*'-*z*4x** (QX31171, $C_{372}H_{617}N_{107}O_{114}S_2$). Expected $[M+8H^+]/8$ = 1059.948 Da. Observed $[M+4H^+]/4$ = 1060.086 Da.

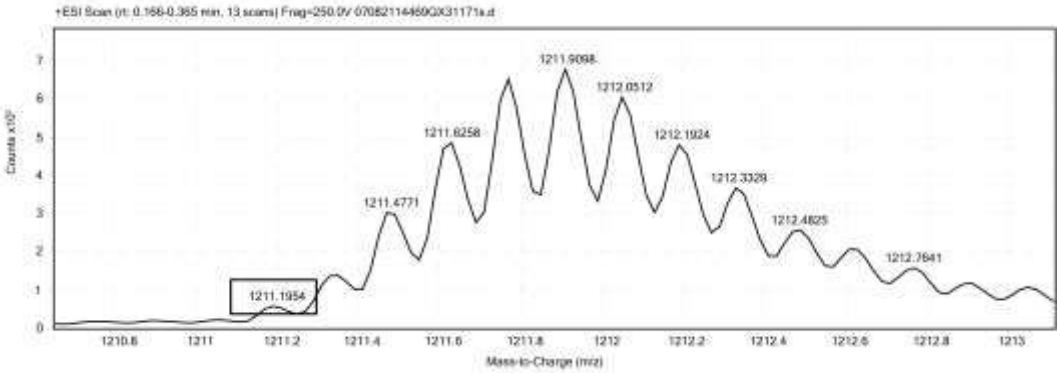

Figure S24. ESI-TOF spectrum for stapled disulfide-bound coiled-coil variant **sd13*e*/15*g*'-*z*4x** (QX31171s, $C_{372}H_{617}N_{107}O_{114}S_2$). Expected $[M+7H^+]/7$ = 1211.225 Da. Observed $[M+7H^+]/7$ = 1211.195 Da.

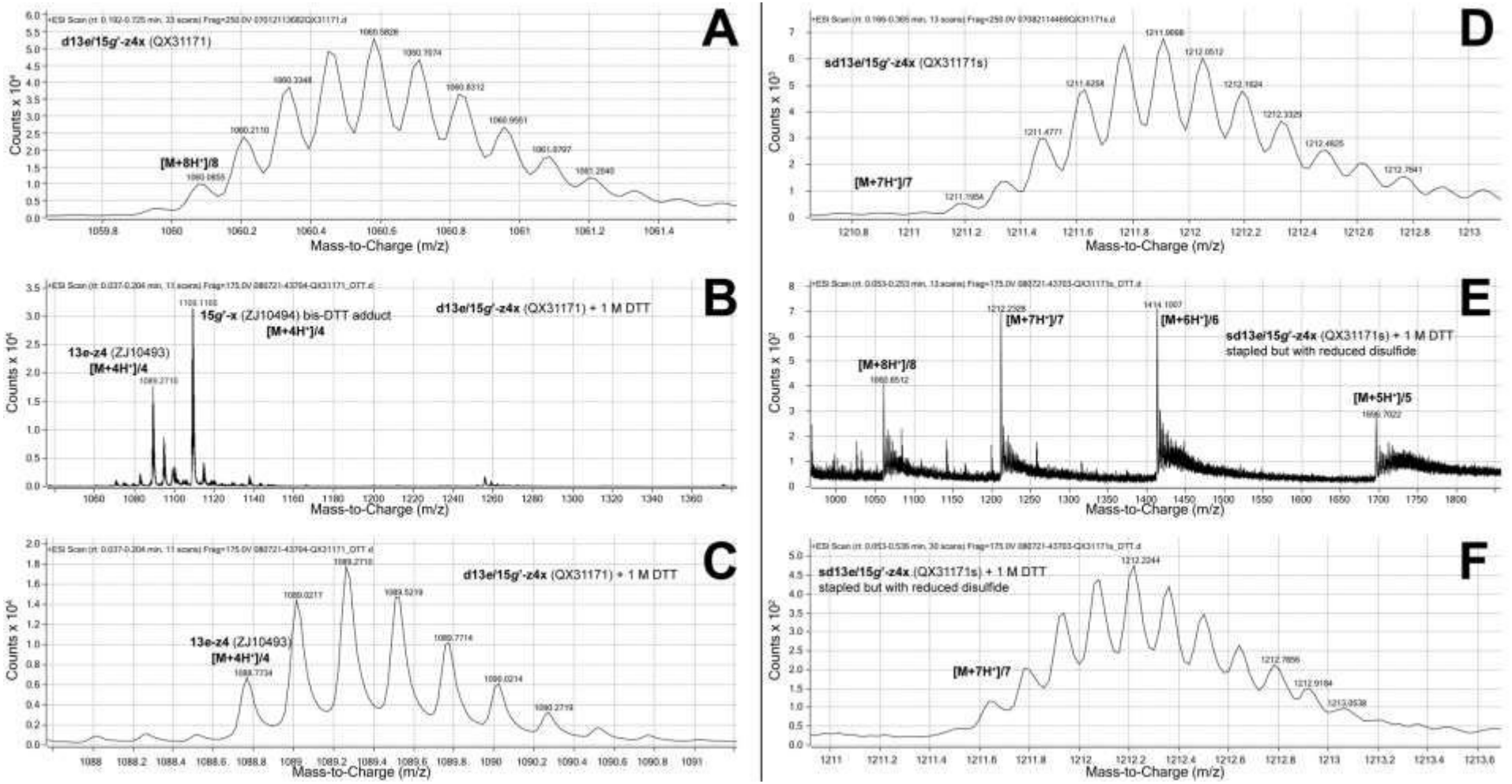

Figure S25. ESI-TOF MS data for azide-containing (A) disulfide-bound coiled-coil variant **d13*e*/15*g*'-z4x** before (QX31171; $C_{372}H_{617}N_{107}O_{114}S_2$; expected $[M+8H^+]/8$ = 1059.948 Da) and (B) after exposure to reducing conditions (1M DTT) for at least 8h. Following reduction, **d13*e*/15*g*'-z4x** splits into its component peptides: **13*e*-z4** (ZJ10493; $C_{185}H_{295}N_{51}O_{68}S$; expected mass $[M+4H^+]/4$ = 1088.781 Da) and **15*g*'-x** (ZJ10494; $C_{187}H_{324}N_{56}O_{46}S$; expected mass $[M+4H^+]/4$ = 1031.620 Da. **15*g*'-x** does not appear in spectrum for reasons that are not clear. Instead, we observe a peak with m/z = 1109.117 Da and isotopic spacing consistent with z = 4. This peak is consistent with bis-DTT adduct of **15*g*'-x** ($C_{195}H_{344}N_{56}O_{50}S_5$; expected $[M+4H^+]/4$ = 1108.626), which could be formed via tandem thiol-yne and thiol-ene reactions between the propargylglycine of **15*g*'-x** and two equivalents of DTT. Also shown are ESI-TOF MS data for (C) triazole-stapled coiled-coil variant **sd13*e*/15*g*'-z4x** before (QX31171s; $C_{372}H_{617}N_{107}O_{114}S_2$; expected $[M+7H^+]/7$ = 1211.225 Da) and (E) after exposure to reduction conditions for at least 8h ($C_{372}H_{619}N_{107}O_{114}S_2$; expected $[M+8H^+]/8$ = 1060.200 Da after reduction of disulfide bond to cysteine residues). Note that **sd13*e*/15*g*'-z4x** remains intact even after disulfide reduction due to the triazole staple.

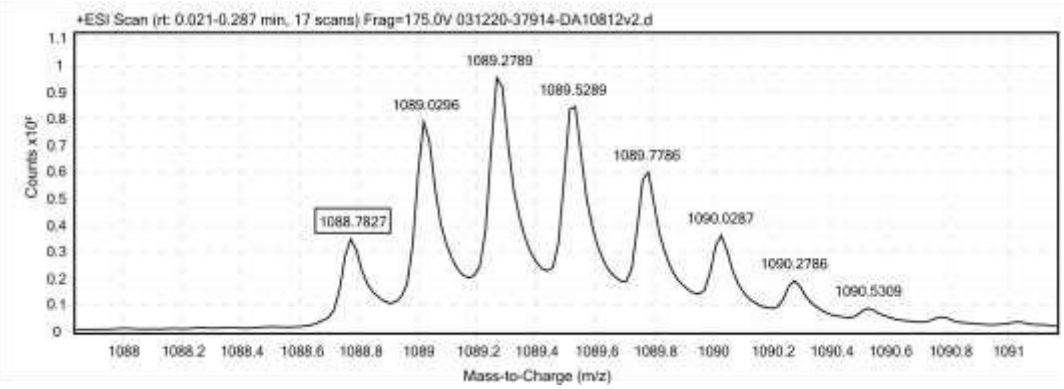

Figure S26. ESI-TOF spectrum for acidic monomer **6*e*-z4** (DA10812; $C_{185}H_{295}N_{51}O_{68}S$; expected $[M+4H^+]/4$ = 1088.781 Da. Observed $[M+4H^+]/4$ = 1088.783 Da.

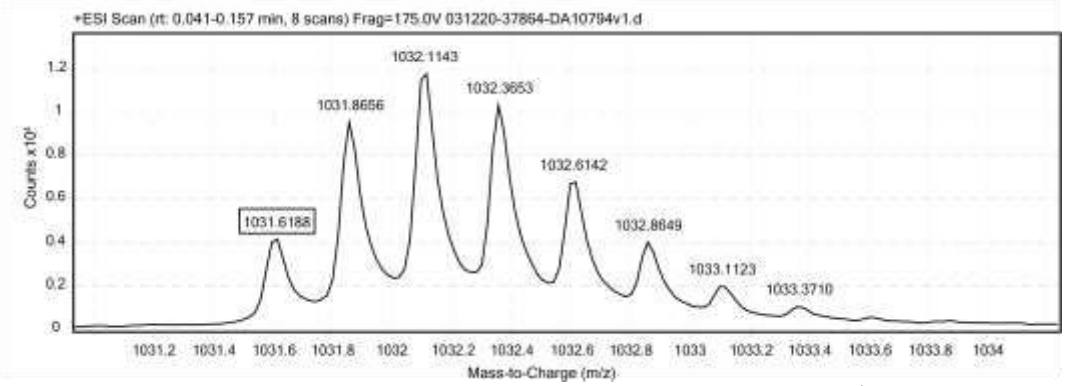

Figure S27. ESI-TOF spectrum for basic variant **8*g*'-x** (DA10794; $C_{187}H_{324}N_{56}O_{46}S$). Expected $[M+4H^+]/4$ = 1031.620 Da. Observed $[M+4H^+]/4$ = 1031.619 Da.

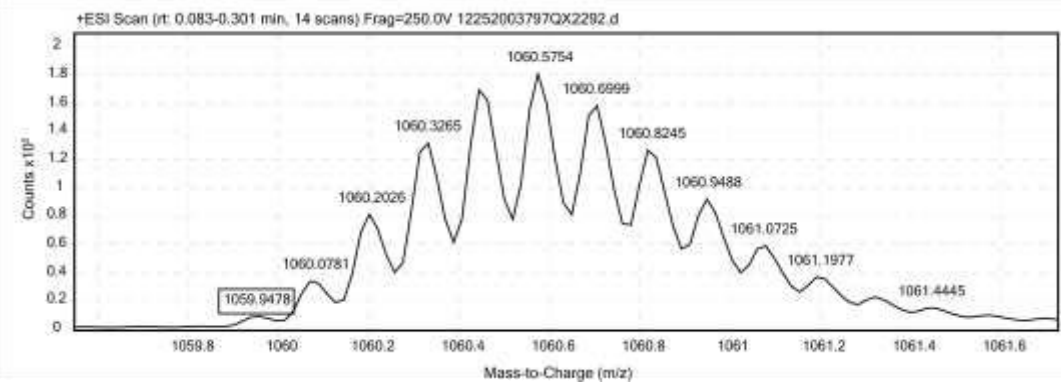

Figure S28. ESI-TOF spectrum for disulfide-bound coiled-coil variant **d6*e*/8*g*'-z4x** (QX2292; $C_{372}H_{617}N_{107}O_{114}S_2$). Expected $[M+8H^+]/8$ = 1059.948 Da. Observed $[M+8H^+]/8$ = 1059.948 Da.

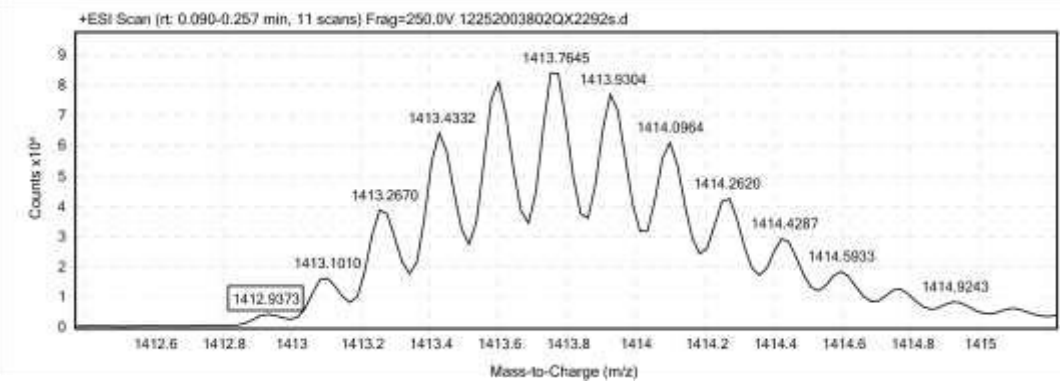

Figure S29. ESI-TOF spectrum for stapled disulfide-bound coiled-coil variant **sd6*e*/8*g*'-z4x** (QX2292s; $C_{372}H_{617}N_{107}O_{114}S_2$). Expected $[M+6H^+]/6$ = 1412.928 Da. Observed $[M+6H^+]/6$ = 1412.937 Da.

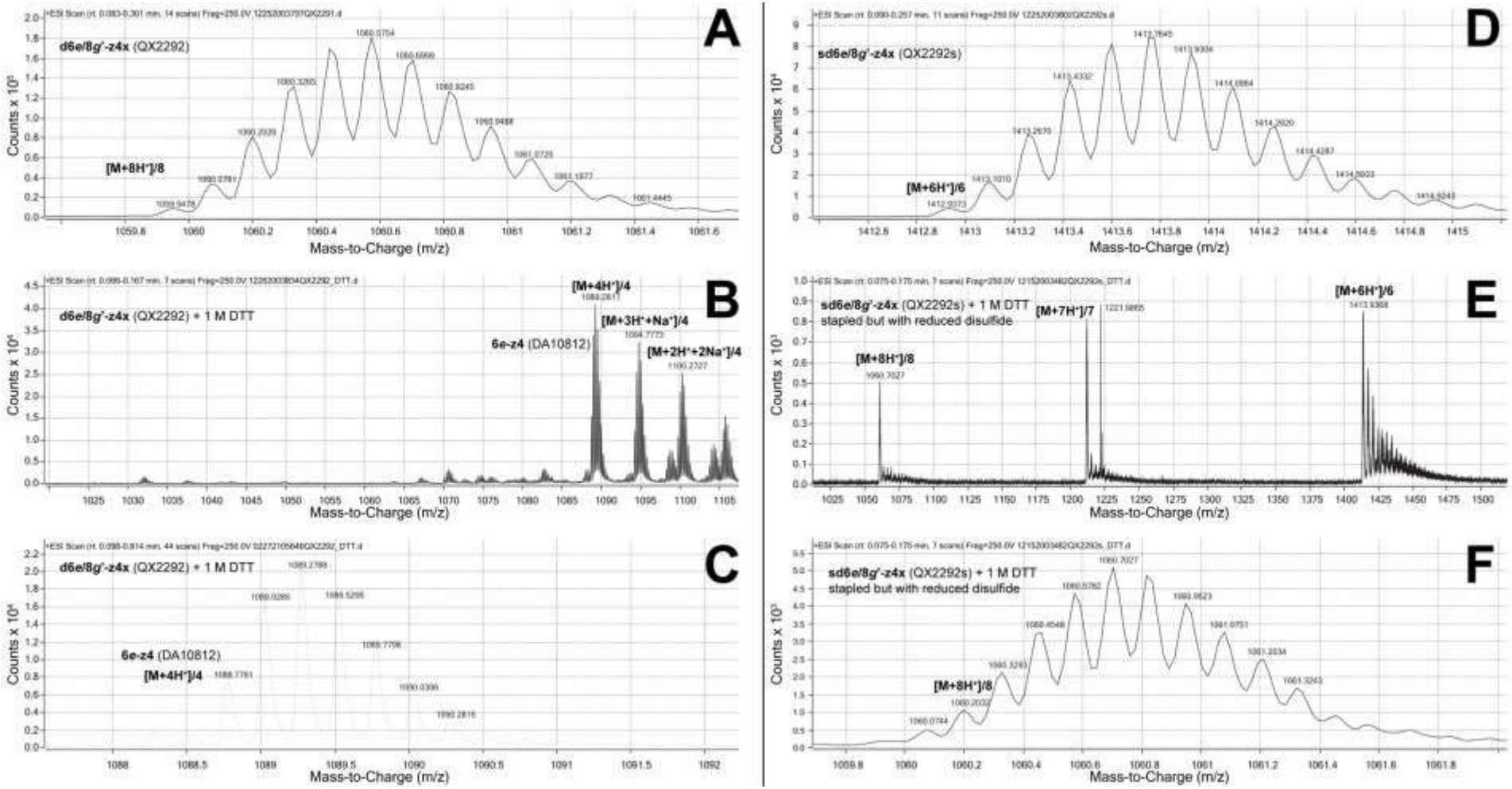

Figure S30. ESI-TOF MS data for (A) disulfide-bound coiled-coil variant **d6*e*/8*g*'-z4x** before (QX2292; $C_{372}H_{617}N_{107}O_{114}S_2$; expected $[M+8H^+]/8$ = 1059.948 Da) and (B,C) after exposure to reducing conditions (1M DTT) for at least 8h. Following reduction, **d6*e*/8*g*'-z4x** should split into its component peptides: **6*e*-z4** (DA10812; $C_{185}H_{295}N_{51}O_{68}S$; expected mass $[M+4H^+]/4$ = 1088.781) and **8*g*'-x** (DA10794; $C_{187}H_{324}N_{56}O_{46}S$; expected mass $[M+4H^+]/4$ = 1031.620 Da). Peptide **8*g*'-x** does not appear in (B,C) for reasons that are unclear. Also shown are ESI-TOF MS data for (D) triazole-stapled **sd6*e*/8*g*'-z4x** before (QX2292s; $C_{372}H_{617}N_{107}O_{114}S_2$; expected $[M+6H^+]/6$ = 1412.928 Da and (E,F) after exposure to reducing conditions (1M DTT) for at least 8h ($C_{372}H_{619}N_{107}O_{114}S_2$; expected $[M+8H^+]/8$ = 1060.200 Da after reduction of disulfide bond to free cysteine residues). Note that **sd6*e*/8*g*'-z4x** remains intact even after disulfide reduction due to the triazole staple.

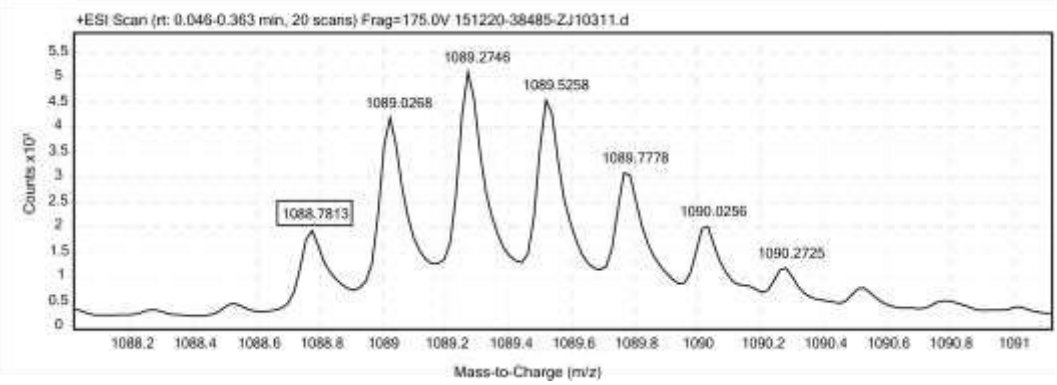

Figure S31. ESI-TOF spectrum for acidic monomer **27*e*-*z*4** (ZJ10311, $C_{185}H_{295}N_{51}O_{68}S$). Expected $[M+4H^+]/4$ = 1088.781 Da. Observed $[M+4H^+]/4$ = 1088.781 Da.

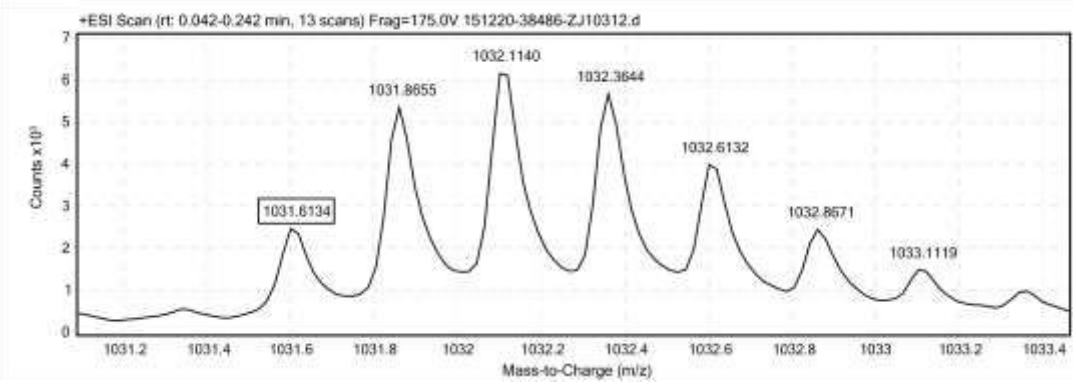

Figure S32. ESI-TOF spectrum for basic monomer **22*g*'-x** (ZJ10312, $C_{187}H_{324}N_{56}O_{46}S$). Expected $[M+4H^+]/4$ = 1031.620 Da. Observed $[M+4H^+]/4$ = 1031.613 Da.

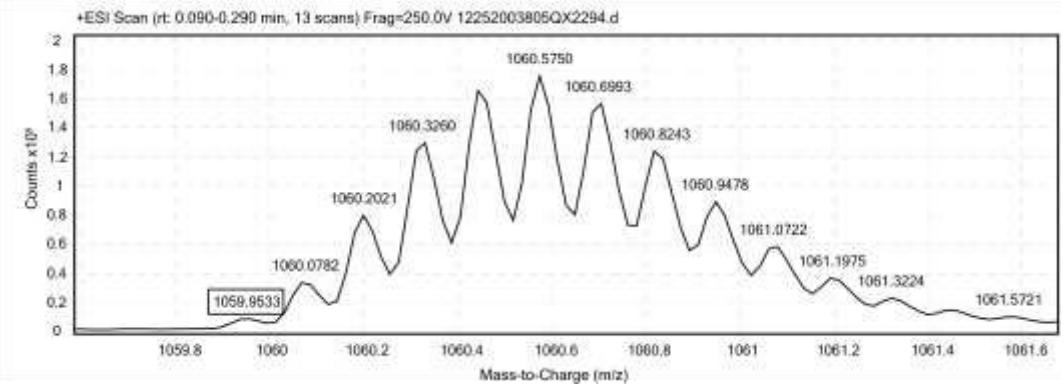

Figure S33. ESI-TOF spectrum for disulfide-bound coiled-coil variant **d27*e*/22*g*'-*z*4x** (QX2294, $C_{372}H_{617}N_{107}O_{114}S_2$). Expected $[M+8H^+]/8$ = 1059.948 Da. Observed $[M+8H^+]/8$ = 1059.953 Da.

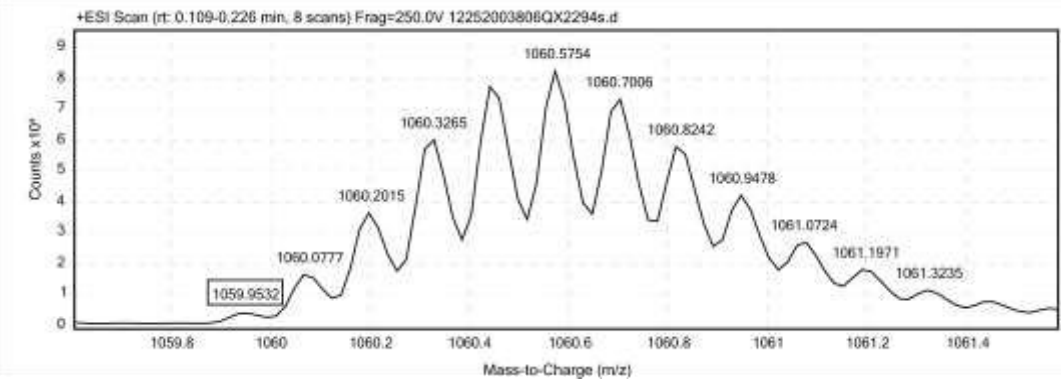

Figure S34. ESI-TOF spectrum for stapled disulfide-bound coiled-coil variant **sd27e/22g'-40** (QX2294s, $C_{372}H_{617}N_{107}O_{114}S_2$). Expected $[M+8H^+]/8$ = 1059.948 Da. Observed $[M+8H^+]/8$ = 1059.953 Da

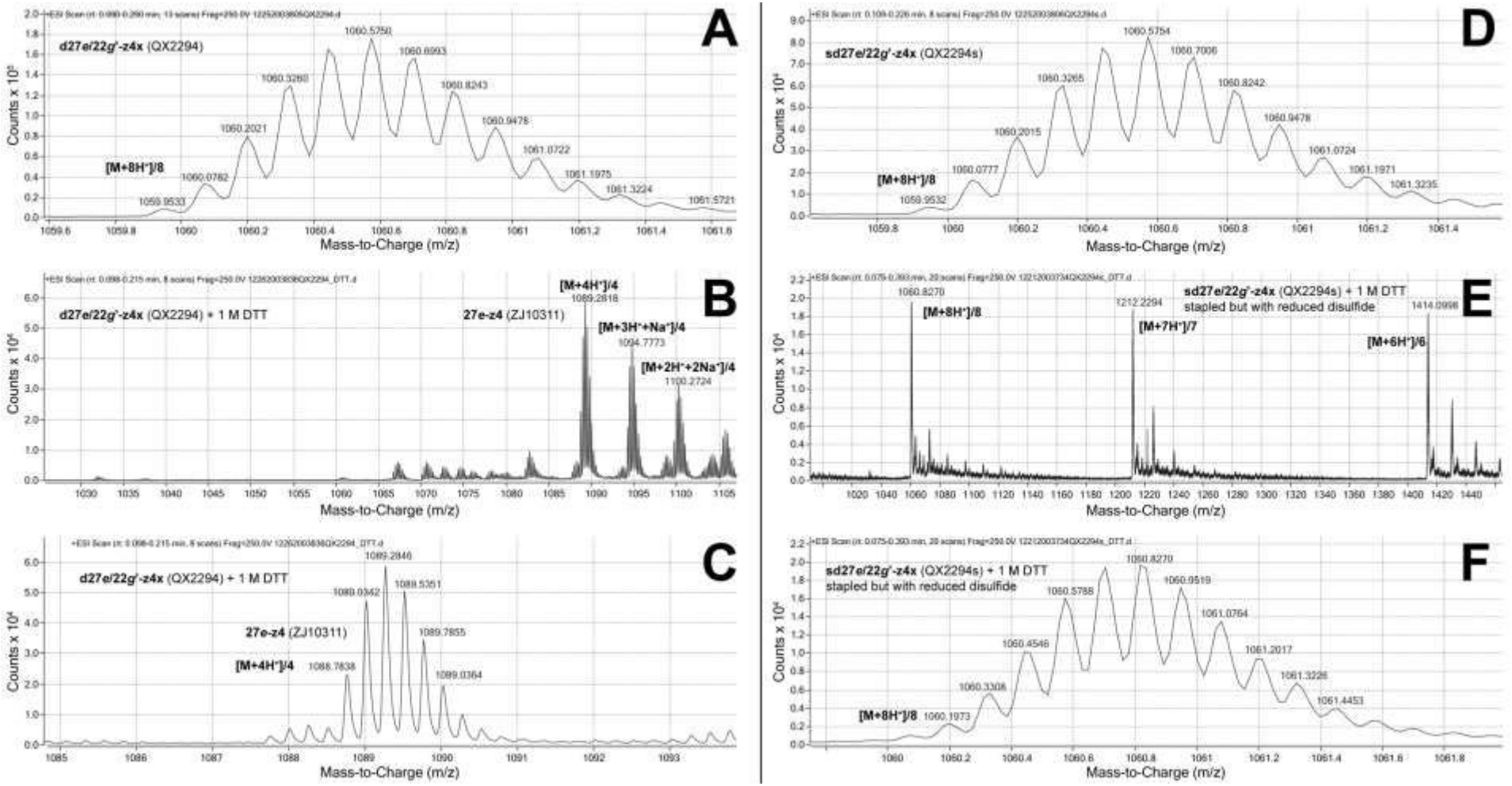

Figure S35. ESI-TOF MS data for azide-containing (A) disulfide-bound coiled-coil variant **d27*e*/22*g*'-z4x** before (QX2294; $C_{372}H_{617}N_{107}O_{114}S_2$; expected $[M+8H^+]/8$ = 1059.948 Da) and (B,C) after exposure to reducing conditions (1M DTT) for at least 8h. Following reduction, **d27*e*/22*g*'-z4x** splits into its component peptides: **27*e*-z4** (ZJ10311; $C_{185}H_{295}N_{51}O_{68}S$; expected mass $[M+4H^+]/4$ = 1088.781 Da) and **22*g*'-x** (ZJ10312; $C_{187}H_{324}N_{56}O_{46}S$; expected mass $[M+4H^+]/4$ = 1031.620 Da; does not appear in spectrum for reasons that are not clear). Also shown are ESI-TOF MS data for (D) triazole-stapled disulfide-bound coiled-coil variant **sd27*e*/22*g*'-z4x** before (QX2294s; $C_{372}H_{617}N_{107}O_{114}S_2$; expected $[M+8H^+]/8$ = 1059.948 Da) and (E,F) after exposure to reduction conditions for at least 8h ($C_{372}H_{619}N_{107}O_{114}S_2$; expected $[M+8H^+]/8$ = 1060.073 Da after reduction of disulfide bond to cysteine residues). Note that **sd27*e*/22*g*'-z4x** remains intact even after disulfide reduction due to the triazole staple.

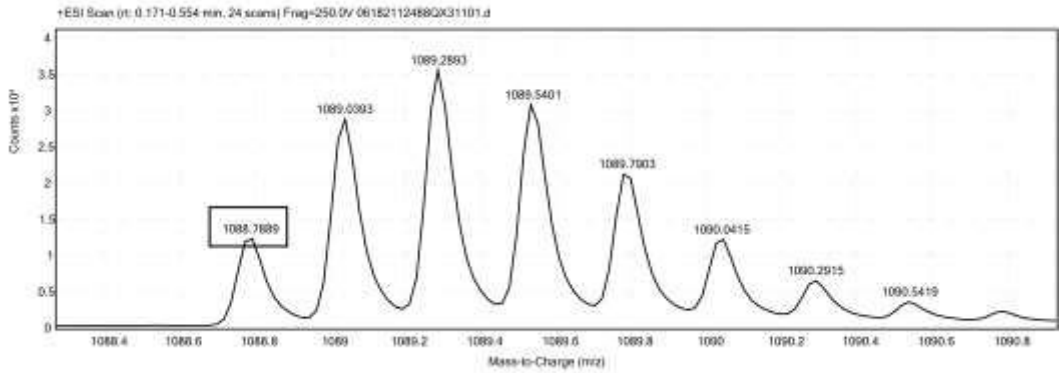

Figure S36. ESI-TOF spectrum for acidic monomer **6*e*-z4** (QX31101, $C_{185}H_{295}N_{51}O_{68}S$). Expected $[M+4H^+]/4$ = 1088.781 Da. Observed $[M+4H^+]/4$ = 1088.789 Da.

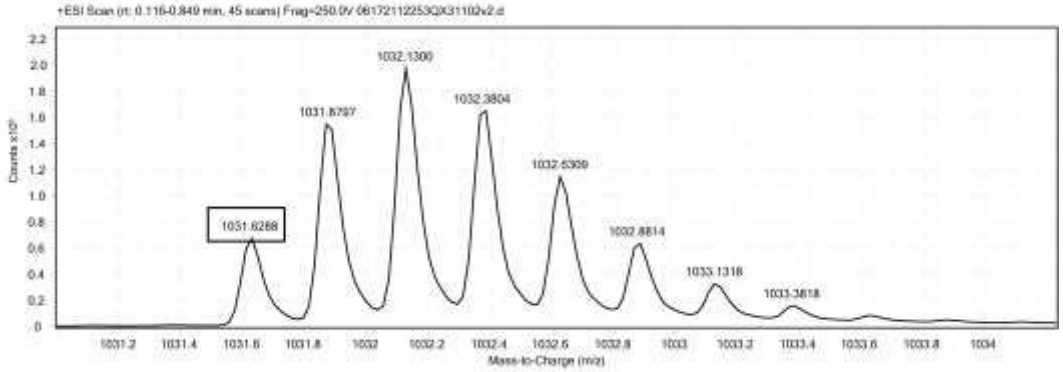

Figure S37. ESI-TOF spectrum for basic monomer **1g'-x** (QX31102, $C_{187}H_{324}N_{56}O_{46}S$). Expected $[M+4H^+]/4$ = 1031.620 Da. Observed $[M+4H^+]/4$ = 1031.629 Da.

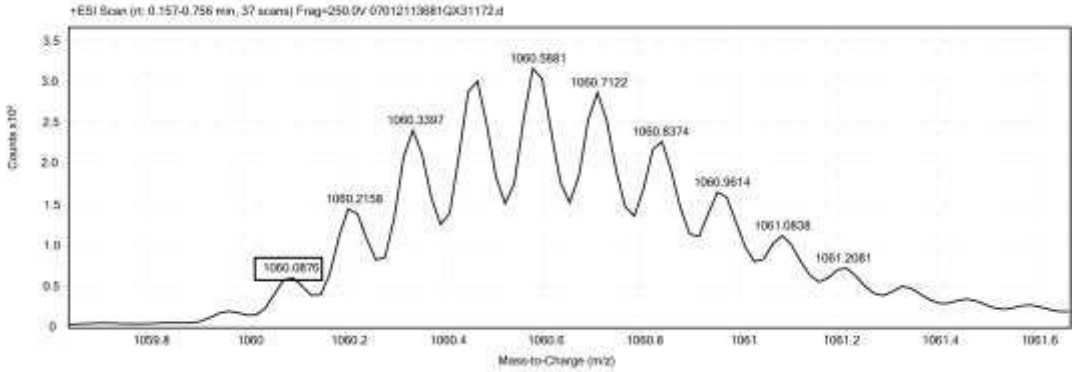

Figure S38. ESI-TOF spectrum for disulfide-bound coiled-coil variant **d6*e*/1g'-z4x** (QX31172, $C_{372}H_{617}N_{107}O_{114}S_2$). Expected $[M+8H^+]/8$ = 1059.948 Da. Observed $[M+4H^+]/4$ = 1060.088 Da.

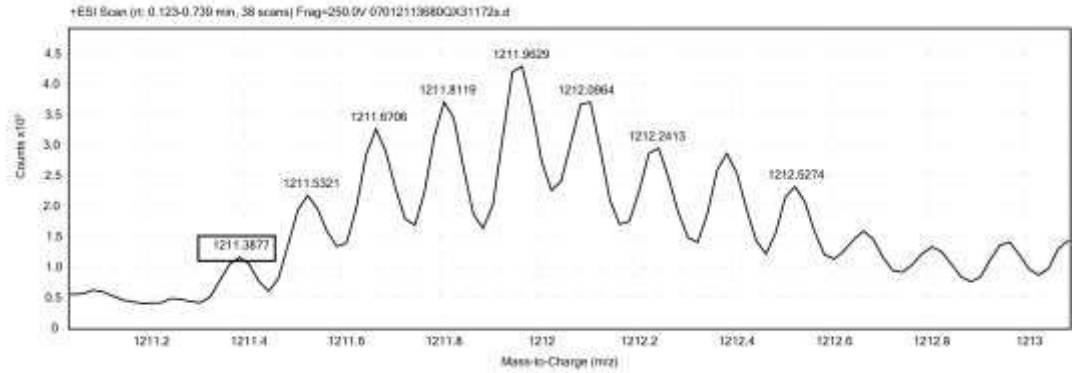

Figure S39. ESI-TOF spectrum for stapled disulfide-bound coiled-coil variant **sd6*e*/1g'-z4x** (QX31172s, $C_{372}H_{617}N_{107}O_{114}S_2$). Expected $[M+7H^+]/7$ = 1211.225 Da. Observed $[M+7H^+]/7$ = 1211.388 Da.

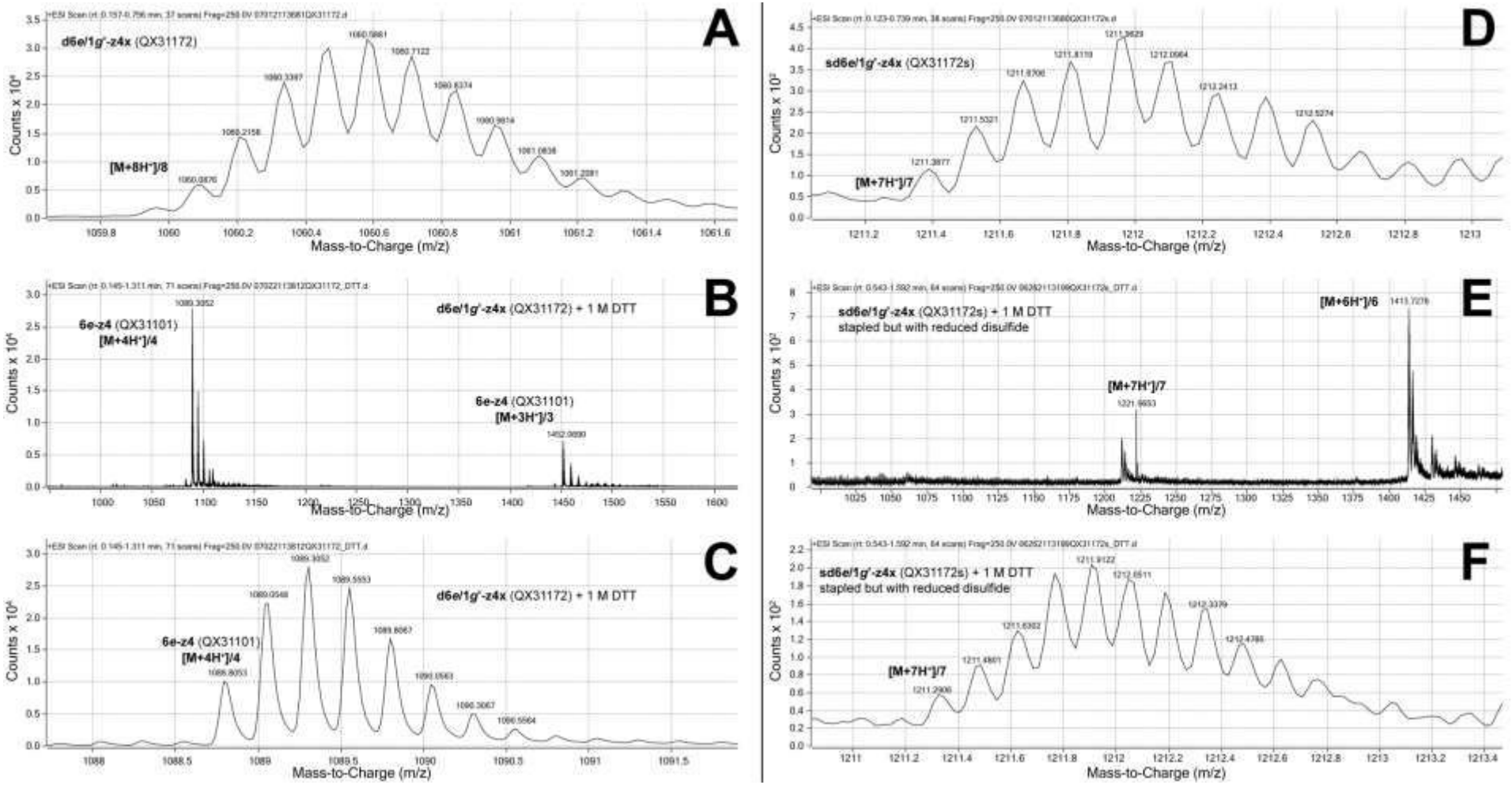

Figure S40. ESI-TOF MS data for azide-containing (A) disulfide-bound coiled-coil variant **d6*e*/1*g*'-z4x** before (QX31172; $C_{372}H_{617}N_{107}O_{114}S_2$; expected $[M+8H^+]/8$ = 1059.948 Da) and (B,C) after exposure to reducing conditions (1M DTT) for at least 8h. Following reduction, **d6*e*/1*g*'-z4x** splits into its component peptides: **6*e*-z4** (QX31101; $C_{185}H_{295}N_{51}O_{68}S$; expected mass $[M+4H^+]/4$ = 1088.781 Da) and **1*g*'-x** (QX31102; $C_{187}H_{324}N_{56}O_{46}S$; expected mass $[M+4H^+]/4$ = 1031.620 Da; does not appear in spectrum for reasons that are not clear). Also shown are ESI-TOF MS data for (D) triazole-stapled disulfide-bound coiled-coil variant **sd6*e*/1*g*'-z4x** before (QX31172s; $C_{372}H_{617}N_{107}O_{114}S_2$; expected $[M+7H^+]/7$ = 1211.225 Da) and (E,F) after exposure to reduction conditions for at least 8h ($C_{372}H_{619}N_{107}O_{114}S_2$; expected $[M+7H^+]/7$ = 1211.513 Da after reduction of disulfide bond to cysteine residues). Note that **sd6*e*/1*g*'-z4x** remains intact even after disulfide reduction due to the triazole staple.

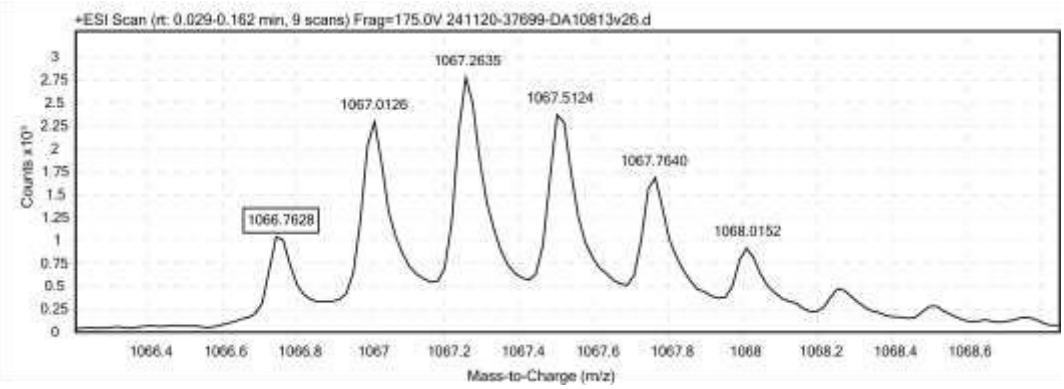

Figure S41. ESI-TOF spectrum for acidic monomer **27*e*-*z*2** (DA10813; $C_{183}H_{290}N_{48}O_{67}S$; expected $[M+4H^+]/4$ = 1066.768 Da). Observed $[M+4H^+]/4$= 1066.763 Da.

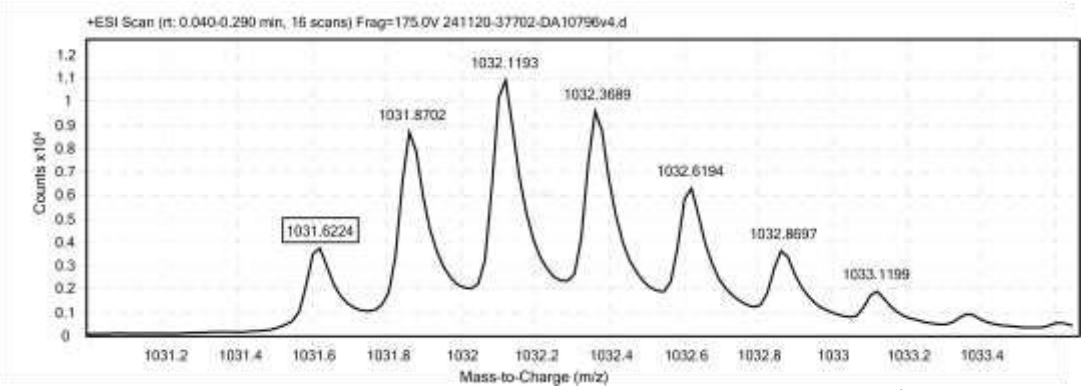

Figure S42. ESI-TOF spectrum for basic monomer **29*g*'-x** (DA10796; $C_{187}H_{324}N_{56}O_{46}S$; expected $[M+4H^+]/4$ = 1031.620 Da). Observed $[M+4H^+]/4$ = 1031.622 Da.

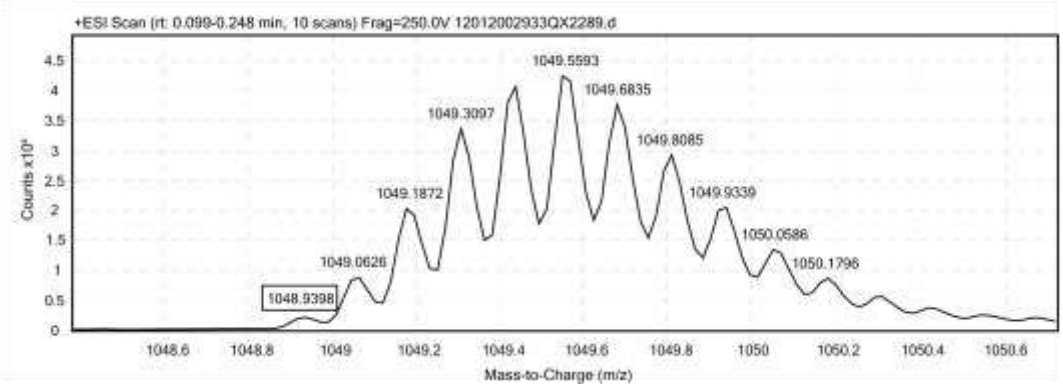

Figure S43. ESI-TOF spectrum for disulfide-bound coiled-coil variant **d27*e*/29*g*'-*z*2x** (QX2289; $C_{368}H_{609}N_{107}O_{112}S_2$; expected $[M+8H^+]/8$ = 1048.942 Da. Observed $[M+8H^+]/8$ = 1048.940 Da.

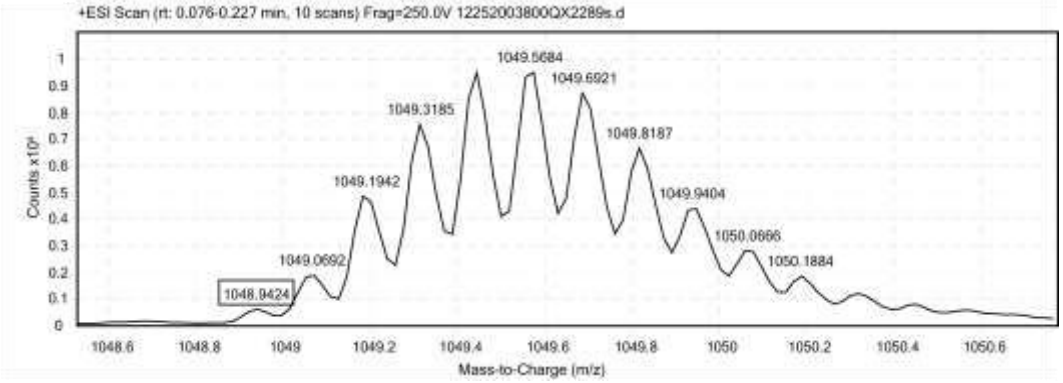

Figure S44. ESI-TOF spectrum for coiled-coil variant **sd27*e*/29*g*'-*z*2x** (QX2289s; $C_{368}H_{609}N_{107}O_{112}S_2$; expected $[M+8H^+]/8$ = 1048.942 Da). Observed $[M+8H^+]/8$ = 1048.942 Da.

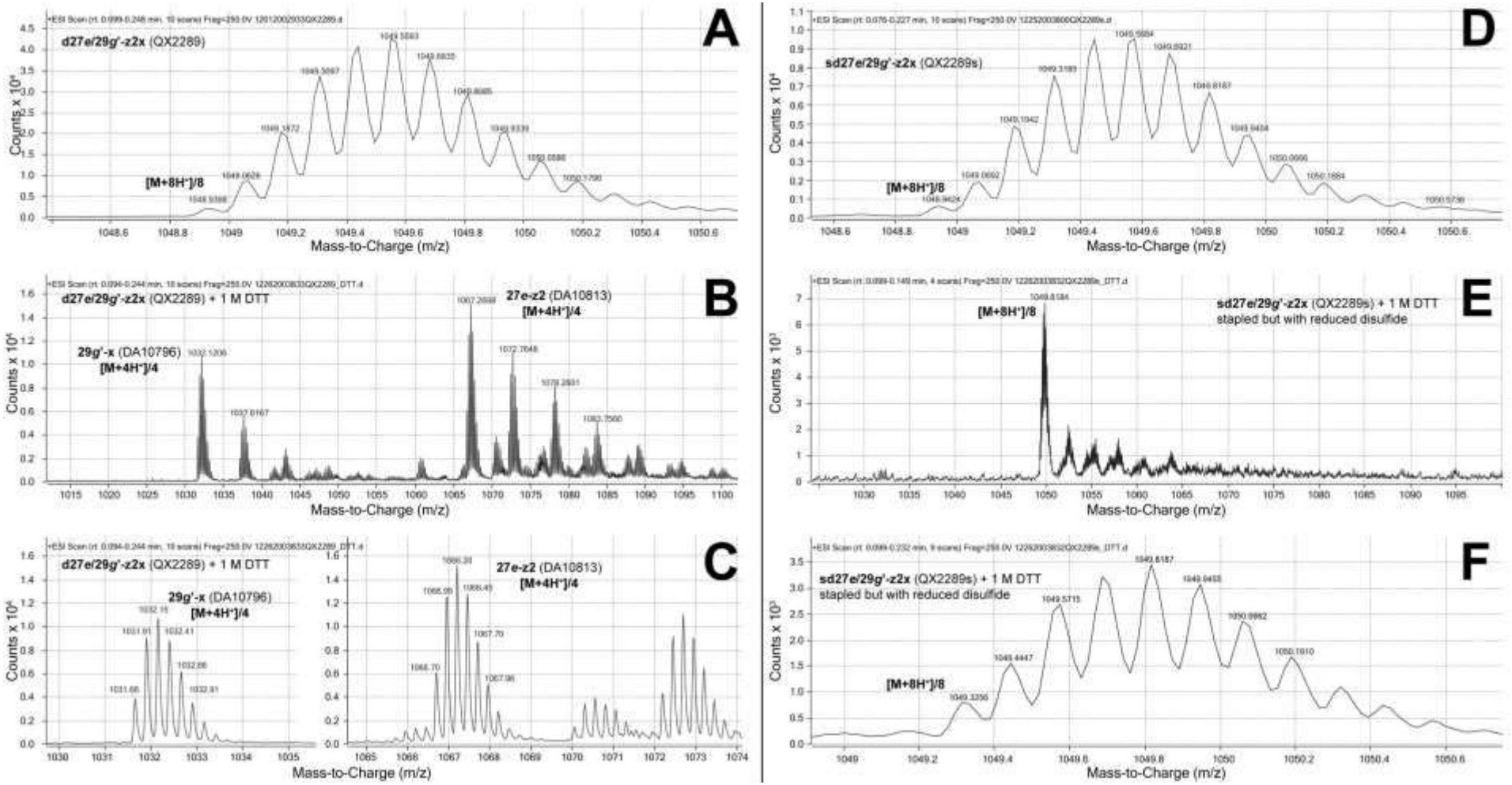

Figure S45. ESI-TOF MS data for (A) coiled-coil variant **d27*e*/29*g*'-z2x** before (QX2289; $C_{368}H_{609}N_{107}O_{112}S_2$; expected $[M+8H^+]/8$ = 1048.942 Da) and (B,C) after exposure to reducing conditions (1M DTT) for at least 8h. Following reduction, **d27*e*/29*g*'-z2x** splits into its component peptides: **27*e*-z2** (DA10813; $C_{183}H_{290}N_{48}O_{67}S$; expected mass $[M+4H^+]/4$ = 1066.7682) and **29*g*'-x** (DA10796; $C_{187}H_{324}N_{56}O_{46}S$; expected mass $[M+4H^+]/4$ = 1031.620 Da). Also shown are ESI-TOF MS data for (D) triazole-stapled **sd27*e*/29*g*'-z2x** before (QX2289s; $C_{368}H_{609}N_{107}O_{112}S_2$; expected $[M+8H^+]/8$ = 1048.942 Da and (E,F) after exposure to reducing conditions (1M DTT) for at least 8h ($C_{373}H_{619}N_{109}O_{113}S_2$; expected $[M+8H^+]/8$ = 1049.194 Da after reduction of disulfide bond to free cysteine residues). Note that **sd27*e*/29*g*'-z2x** remains intact even after disulfide reduction due to the triazole staple.

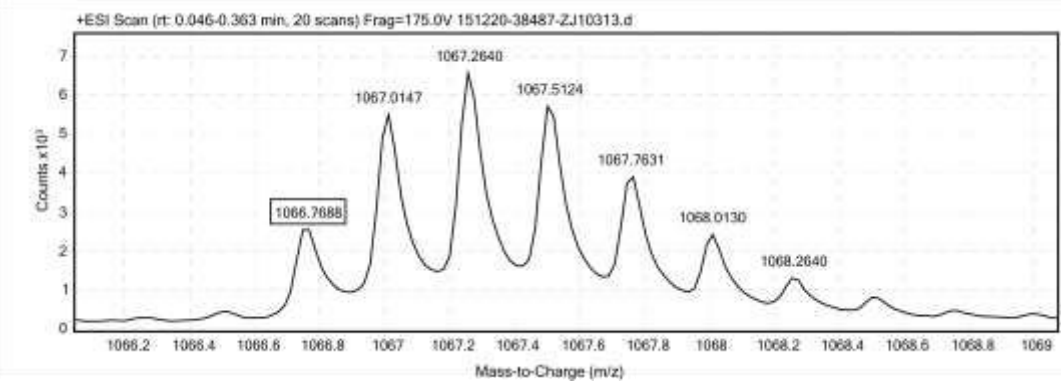

Figure S46. ESI-TOF spectrum for acidic monomer **27*e*-*z*2** (ZJ10313; $C_{181}H_{286}N_{51}O_{66}S$; expected $[M+4H^+]/4$ = 1066.768 Da). Observed $[M+4H^+]/4$ = 1066.769 Da.

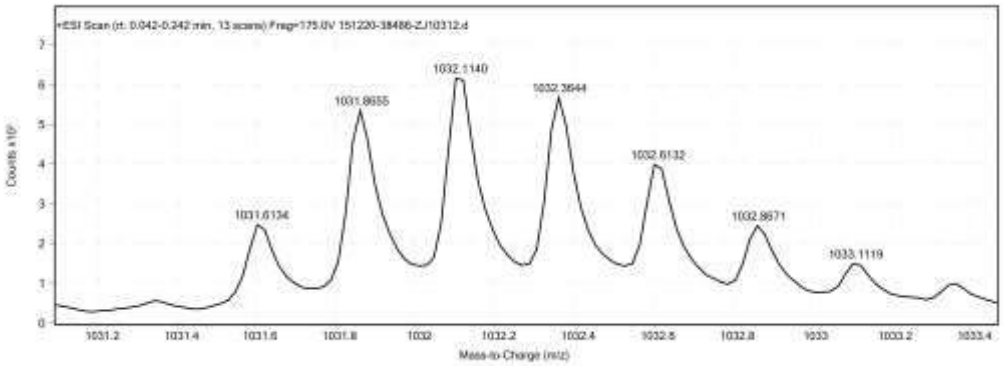

Figure S47. ESI-TOF spectrum for basic monomer **22*g*'-x** (ZJ10312; $C_{187}H_{324}N_{56}O_{46}S$; expected $[M+4H^+]/4$ = 1031.620 Da). Observed $[M+4H^+]/4$ = 1031.613 Da.

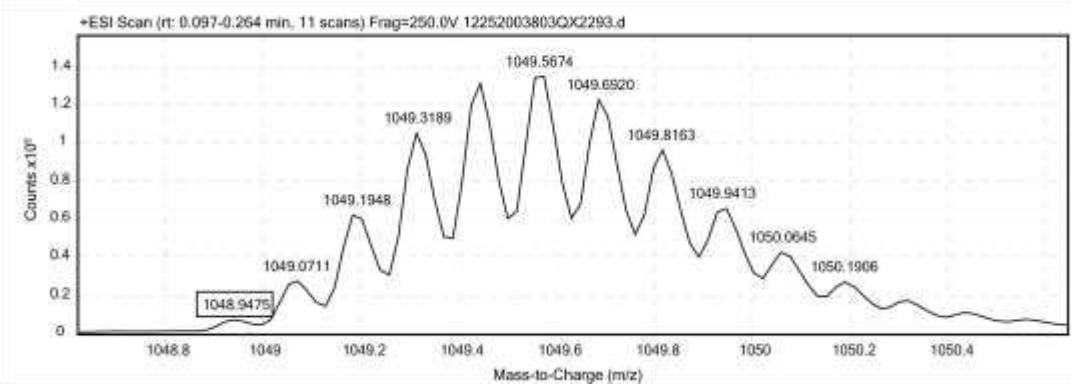

Figure S48. ESI-TOF spectrum for disulfide-bound coiled-coil variant **d27*e*/22*g*'-*z*2x** (QX2293; $C_{368}H_{609}N_{107}O_{112}S_2$; expected $[M+8H^+]/8$ = 1048.942 Da). Observed $[M+8H^+]/8$ = 1048.948 Da.

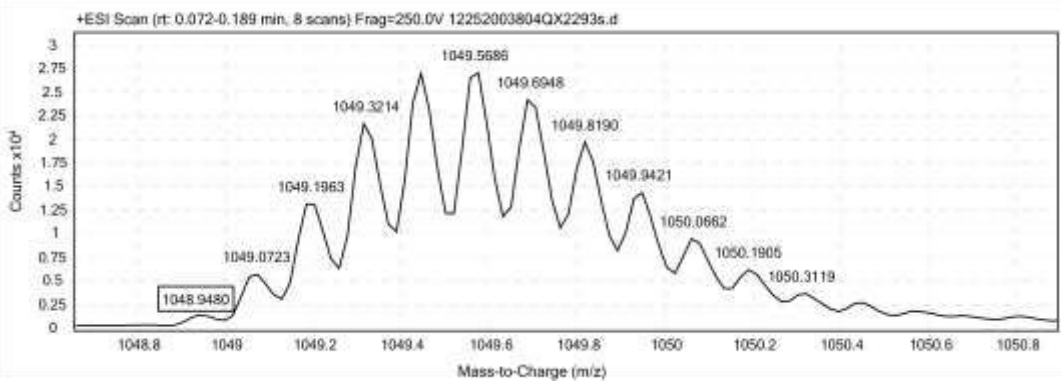

Figure S49. ESI-TOF spectrum for stapled disulfide-bound coiled-coil variant **sd27*e*/22*g*'-*z*2x** (QX2293s; $C_{368}H_{609}N_{107}O_{112}S_2$; expected $[M+8H^+]/8$ = 1048.942 Da). Observed $[M+8H^+]/8$ = 1048.948 Da.

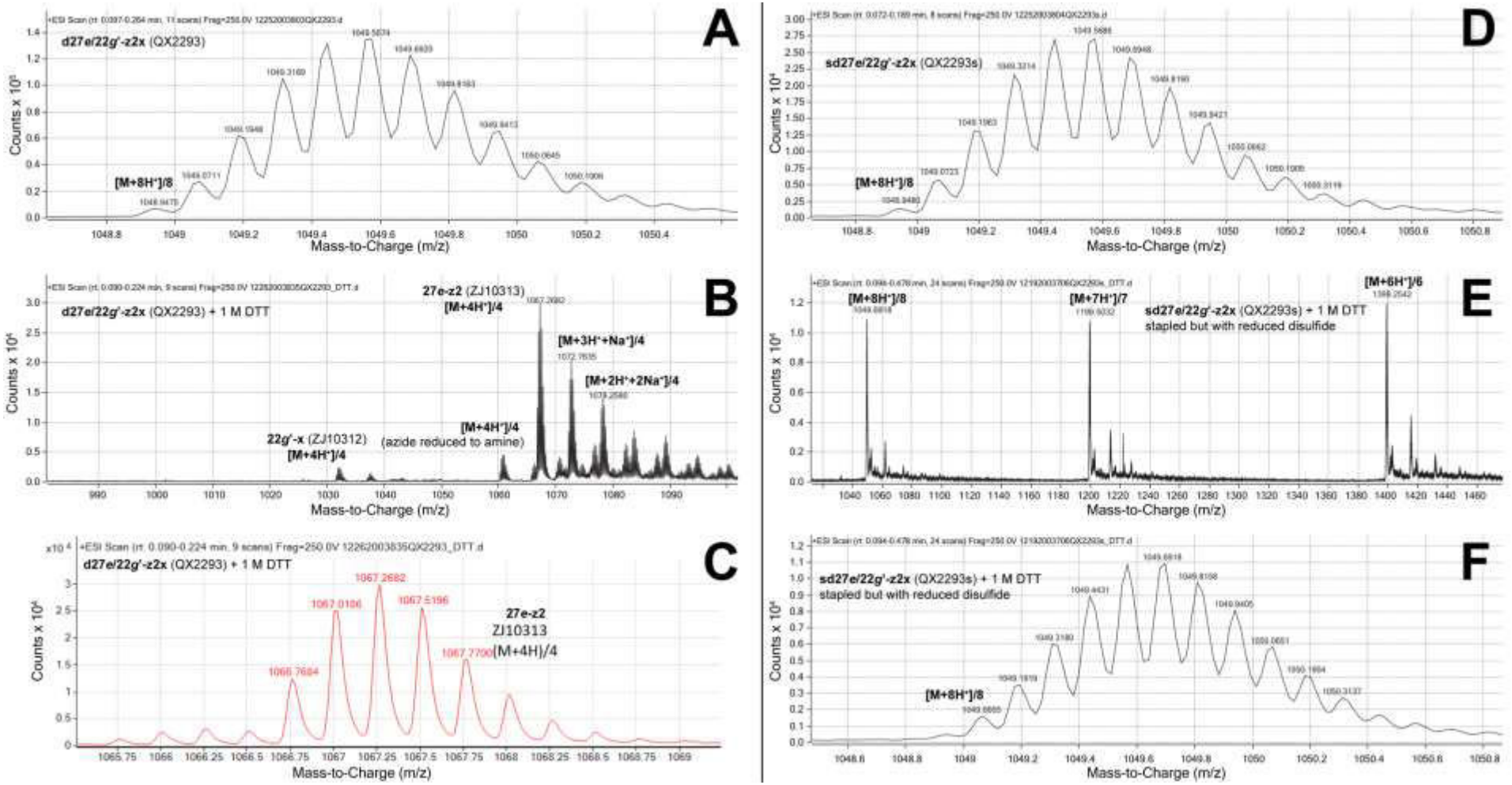

Figure S50. ESI-TOF MS data for (A) coiled-coil variant **d27*e*/22*g*'-z2x** before (QX2293; $C_{368}H_{609}N_{107}O_{112}S_2$; expected $[M+8H^+]/8$ = 1048.942 Da) and (B,C) after exposure to reducing conditions (1M DTT) for at least 8h. Following reduction, **d27*e*/22*g*'-z2x** splits into its component peptides: **27*e*-z2** (ZJ10313; $C_{181}H_{286}N_{51}O_{66}S$; expected mass $[M+4H^+]/4$ = 1066.768) and **22*g*'-x** (ZJ10312; $C_{187}H_{324}N_{56}O_{46}S$; expected mass $[M+4H^+]/4$ = 1031.620 Da). Also shown are ESI-TOF MS data for (D) triazole-stapled **sd27*e*/22*g*'-z2x** before (QX2293s; $C_{368}H_{609}N_{107}O_{112}S_2$; expected $[M+8H^+]/8$ = 1048.942 Da and (E,F) after exposure to reducing conditions (1M DTT) for at least 8h ($C_{368}H_{611}N_{107}O_{112}S_2$; expected $[M+8H^+]/8$ = 1049.194 Da after reduction of disulfide bond to free cysteine residues). Note that **sd27*e*/22*g*'-z2x** remains intact even after disulfide reduction due to the triazole staple.

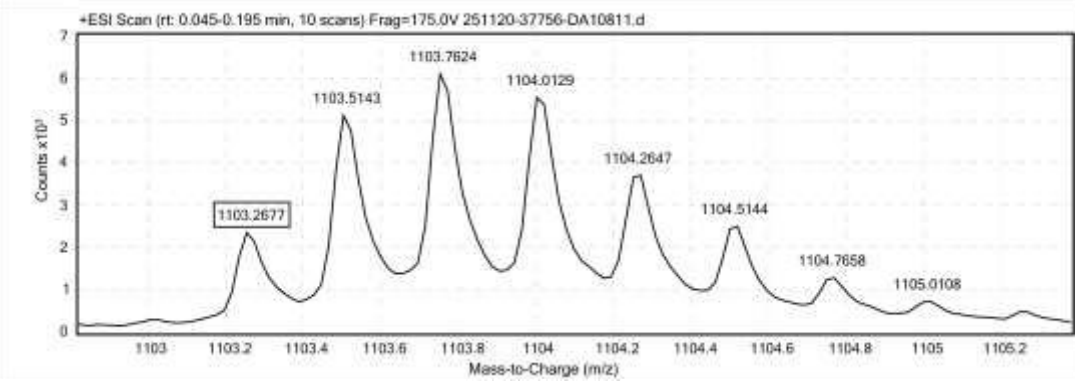

Figure S51. ESI-TOF spectrum for acidic monomer **24*b*-z4** (DA10811, $C_{187}H_{297}N_{51}O_{70}S$). Expected $[M+4H^+]/4$ = 1103.282 Da. Observed $[M+4H^+]/4$ = 1103.268 Da.

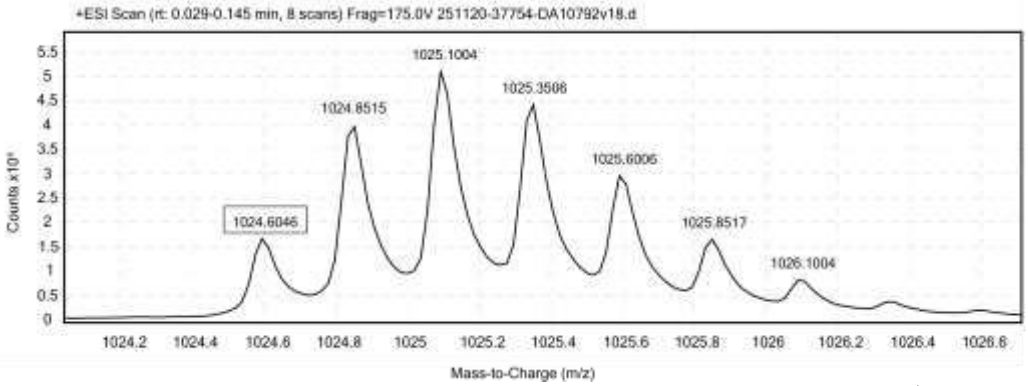

Figure S52. ESI-TOF spectrum for basic monomer **25*c*'-x** (DA10792; $C_{187}H_{324}N_{54}O_{46}S$). Expected $[M+4H^+]/4$ = 1024.618 Da. Observed $[M+4H^+]/4$ = 1024.605 Da.

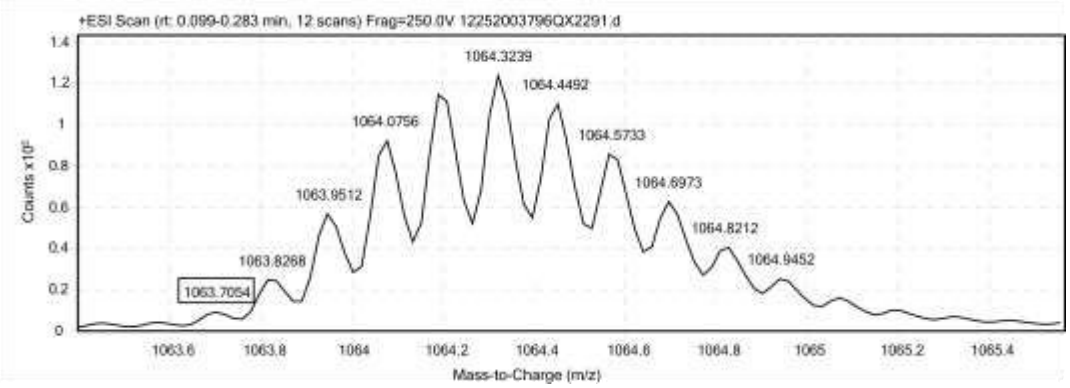

Figure S53. ESI-TOF spectrum for disulfide-bound coiled-coil variant **d24*b*/25*c*'-z4x** (QX2291, $C_{374}H_{619}N_{105}O_{116}S_2$). Expected $[M+8H^+]/8$ = 1063.698 Da. Observed $[M+8H^+]/8$ = 1063.705 Da.

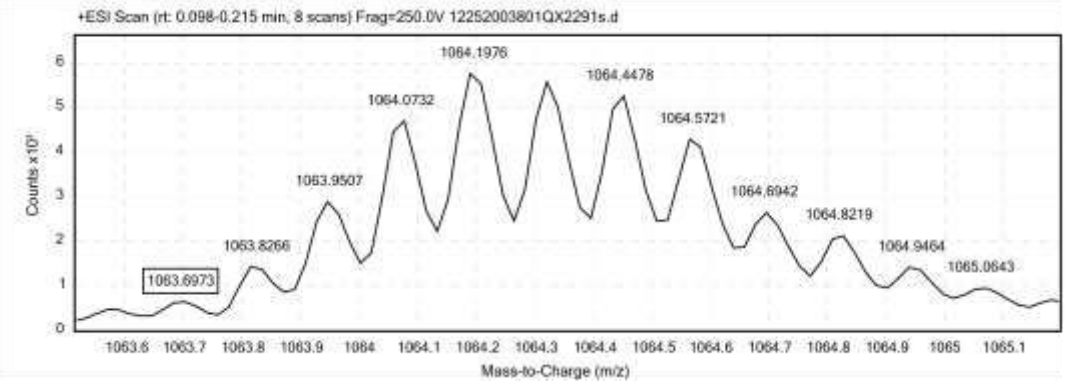

Figure S54. ESI-TOF spectrum for stapled disulfide-bound coiled-coil variant **sd24*b*/25*c*'-z4x** (QX2291s, $C_{374}H_{619}N_{105}O_{116}S_2$). Expected $[M+8H^+]/8$ = 1063.698 Da. Observed $[M+8H^+]/8$ = 1063.697 Da.

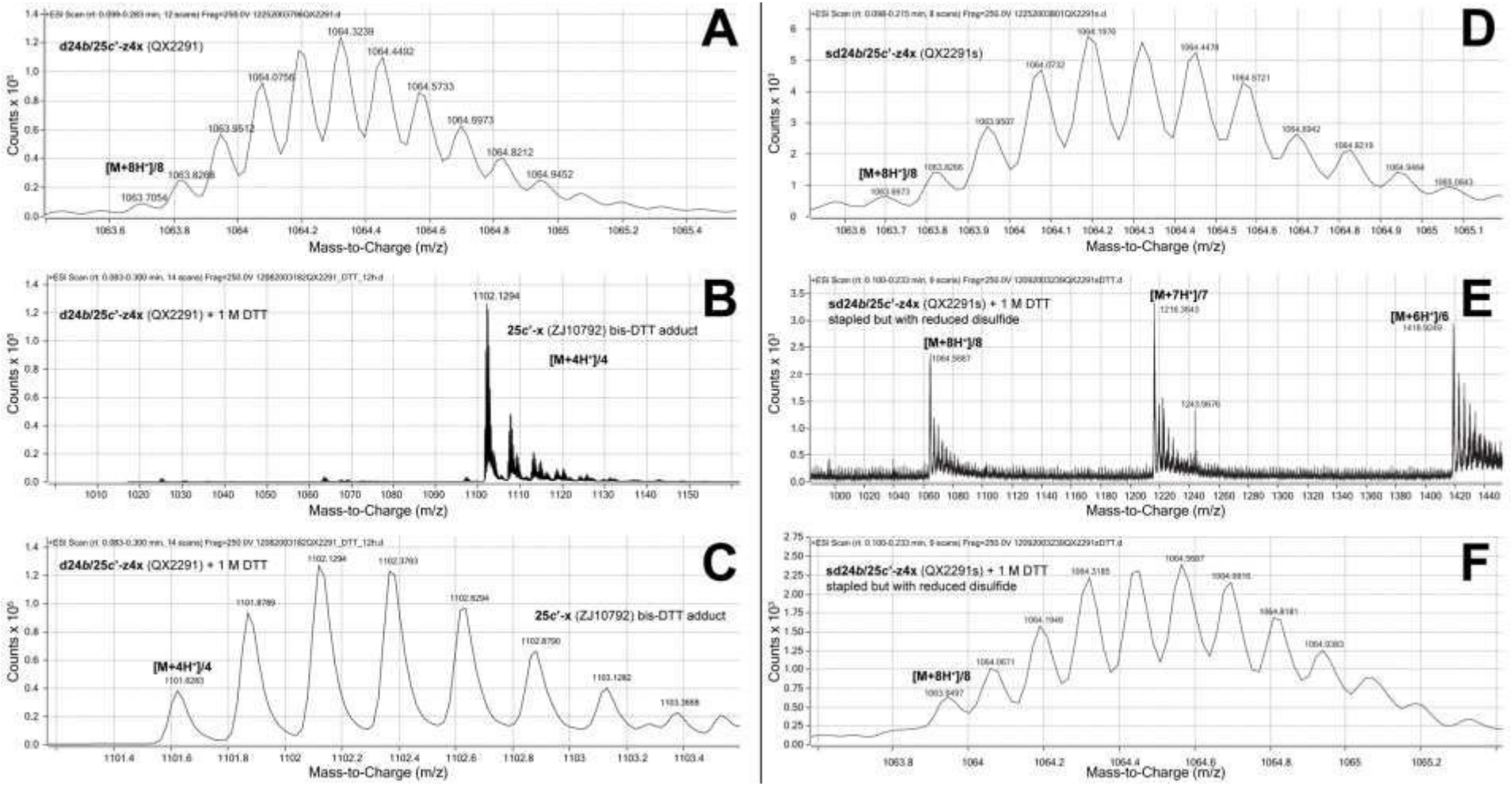

Figure S55. ESI-TOF MS data for (A) disulfide-bound coiled-coil variant **d24*b*/25*c*'-z4x** before (QX2291; $C_{374}H_{619}N_{105}O_{116}S_2$; expected $[M+8H^+]/8$ = 1063.698 Da) and (B,C) after exposure to reducing conditions (1M DTT) for at least 8h. Following reduction, **d24*b*/25*c*'-z4x** should split into its component peptides: **24*b*-z4** (DA10811; $C_{187}H_{297}N_{51}O_{70}S$; expected mass $[M+4H^+]/4$ = 1103.282) and **25*c*'-x** (DA10792; $C_{187}H_{324}N_{54}O_{46}S$; expected mass $[M+4H^+]/4$ = 1024.618 Da). However, neither of these appear in (B,C). Instead, we observe a peak with m/z = 1101.628 Da and isotopic spacing consistent with z = 4. This peak is consistent with bis-DTT adduct of **25*c*'-x** ($C_{195}H_{344}N_{54}O_{50}S_5$; expected $[M+4H^+]/4$ = 1101.624), which could be formed via tandem thiol-yne and thiol-ene reactions between the propargylglycine of **25*c*'-x** and two equivalents of DTT. Peptide **24*b*-4** does not appear in (B,C) for reasons that are unclear. Also shown are ESI-TOF MS data for (D) triazole-stapled disulfide-bound coiled-coil variant **sd24*b*/25*c*'-z4x** before (QX2291s; $C_{374}H_{619}N_{105}O_{116}S_2$; expected $[M+8H^+]/8$ = 1063.698 Da and (E,F) after exposure to reducing conditions (1M DTT) for at least 8h ($C_{374}H_{621}N_{105}O_{116}S_2$; expected $[M+8H^+]/8$ = 1063.950 Da after reduction of disulfide bond to free cysteine residues). Note that **sd24*b*/25*c*'-z4x** remains intact even after disulfide reduction due to the triazole staple.

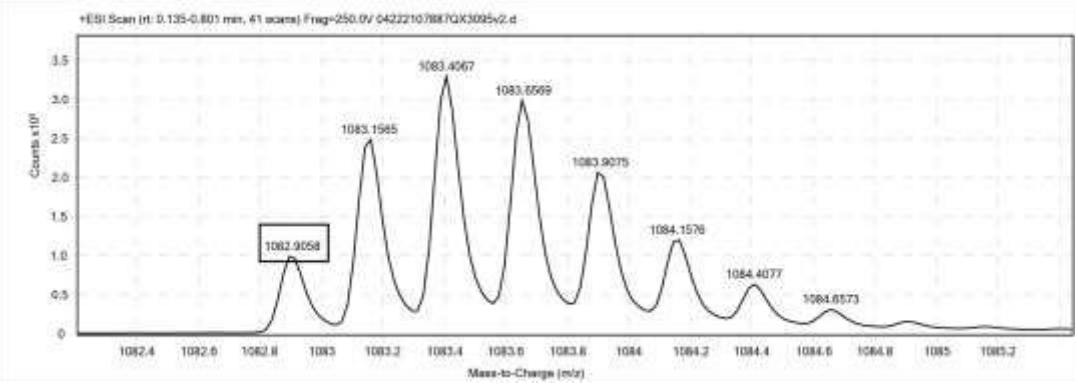

Figure S56. ESI-TOF spectrum for basic monomer variant **25*c*'-y4** (QX3095; $C_{197}H_{343}N_{55}O_{51}S$; expected $[M+4H^+]/4$ = 1082.900 Da. Observed $[M+4H^+]/4$ = 1082.906 Da.

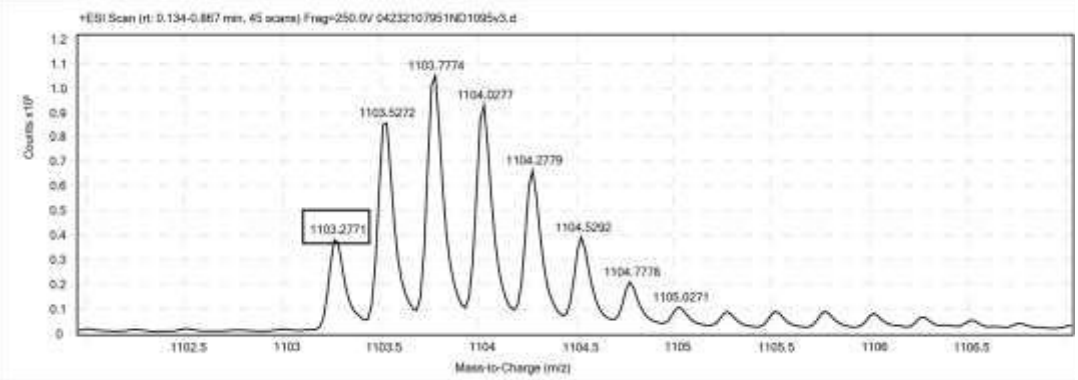

Figure S57. ESI-TOF spectrum for acidic monomer **24*b*-*z*4** (ND1095; $C_{187}H_{297}N_{51}O_{70}S$; expected $[M+4H^+]/4$ = 1103.282 Da). Observed $[M+4H^+]/4$ = 1103.277 Da.

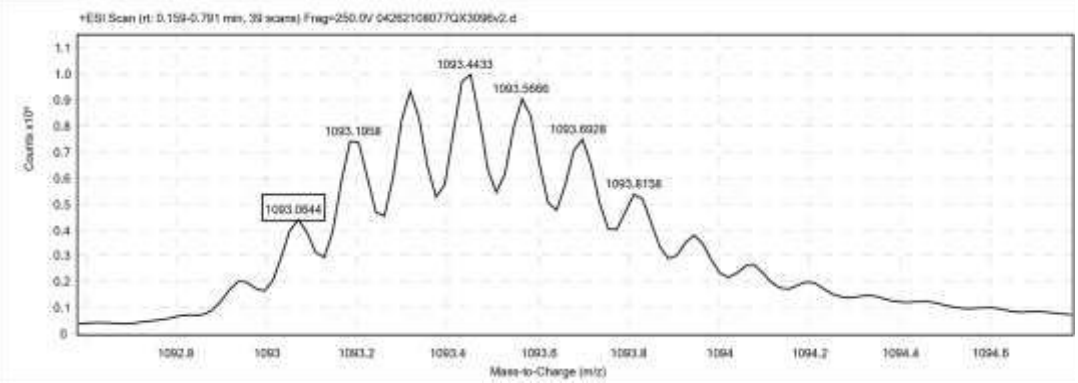

Figure S58. ESI-TOF spectrum for disulfide-bound coiled-coil variant **d24*b*/25*c*'-*z*4y4** (QX3096; $C_{384}H_{638}N_{106}O_{121}S_2$; expected $[M+8H^+]/8$ = 1092.839 Da). Observed $[M+8H^+]/8$ = 1093.064 Da.

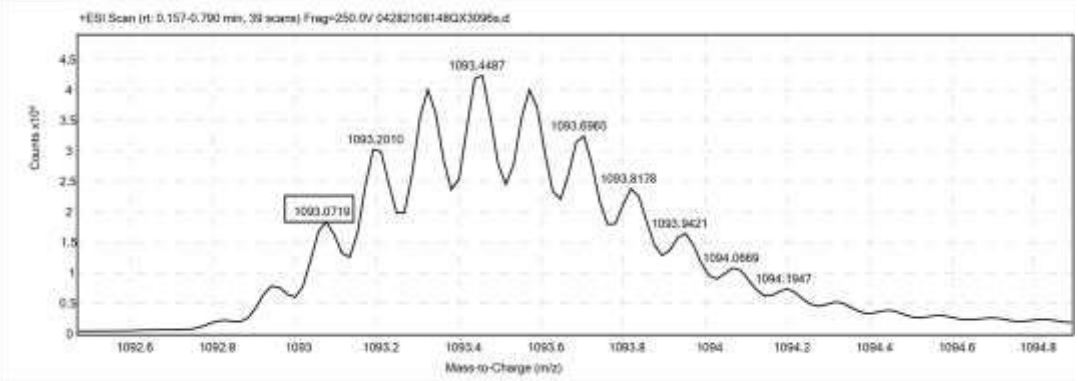

Figure S59. ESI-TOF spectrum for stapled disulfide-bound coiled-coil variant **sd24*b*/25*c*'-*z*4y4** (QX3096s; $C_{384}H_{638}N_{106}O_{121}S_2$; expected $[M+8H^+]/8$ = 1092.839 Da). Observed $[M+8H^+]/8$ = 1093.072 Da.

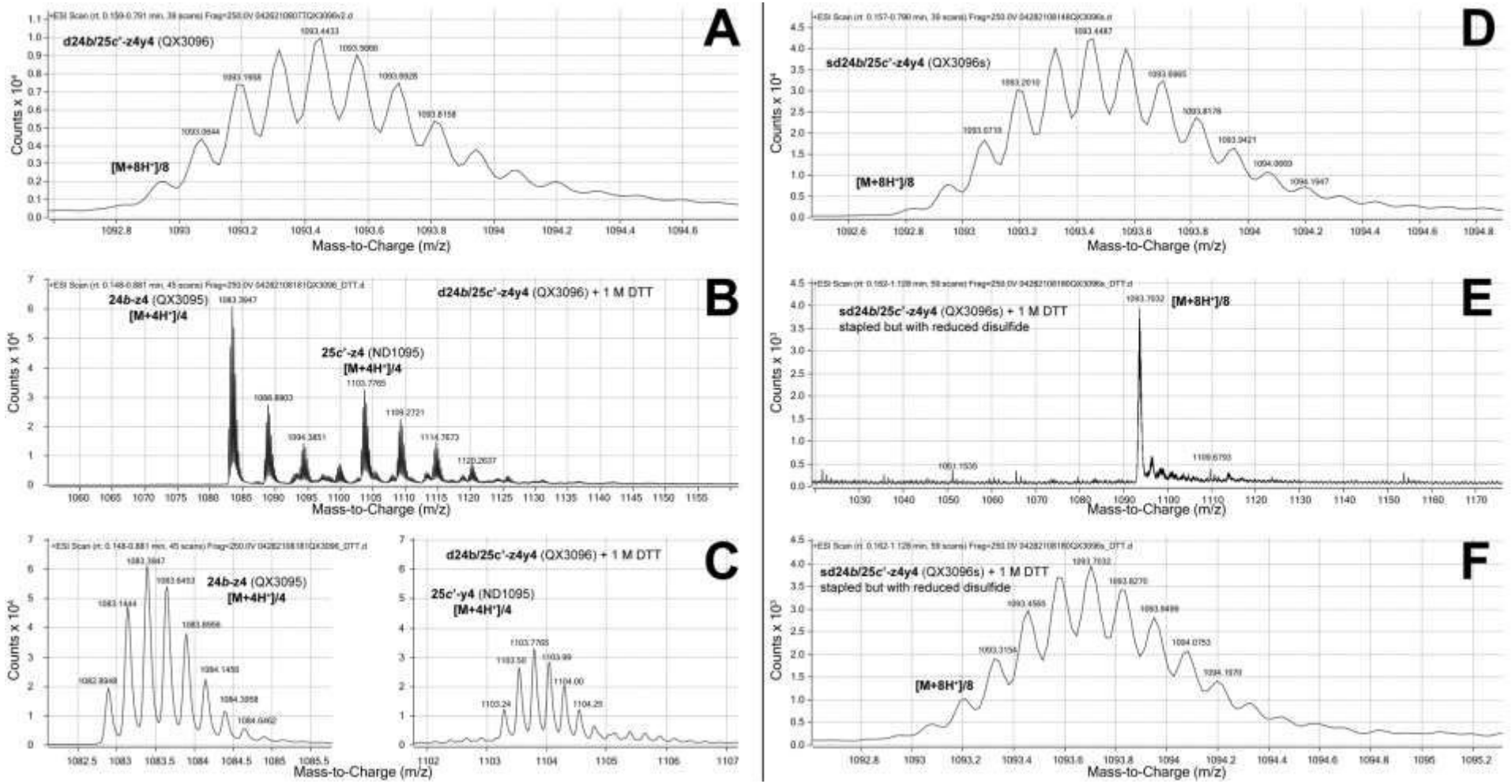

Figure S60. ESI-TOF MS data for (A) disulfide-bound coiled-coil variant **d24*b*/25*c*'-*z*4y4** before (QX3096; $C_{384}H_{638}N_{106}O_{121}S_2$; expected $[M+8H^+]/8$ = 1092.839 Da) and (B,C) after exposure to reducing conditions (1M DTT) for at least 8h. Following reduction, **d24*b*/25*c*'-*z*4y4** splits into its component peptides: **24*b*-z4** (QX3095; $C_{197}H_{343}N_{55}O_{51}S$; expected mass $[M+4H^+]/4$ = 1082.900 Da) and **25*c*'-y4** (ND1095; $C_{187}H_{297}N_{51}O_{70}S$; expected mass $[M+4H^+]/4$ = 1103.282 Da). Also shown are ESI-TOF MS data for (D) triazole-stapled disulfide-bound coiled-coil variant **sd24*b*/25*c*'-*z*4y4** before (QX3096s; $C_{384}H_{638}N_{106}O_{121}S_2$; expected $[M+8H^+]/8$ = 1092.839 Da and (E,F) after exposure to reducing conditions (1M DTT) for at least 8h ($C_{384}H_{640}N_{106}O_{121}S_2$; expected $[M+8H^+]/8$ = 1093.091 Da after reduction of disulfide bond to free cysteine residues). Note that **sd24*b*/25*c*'-*z*4y4** remains intact even after disulfide reduction due to the triazole staple.

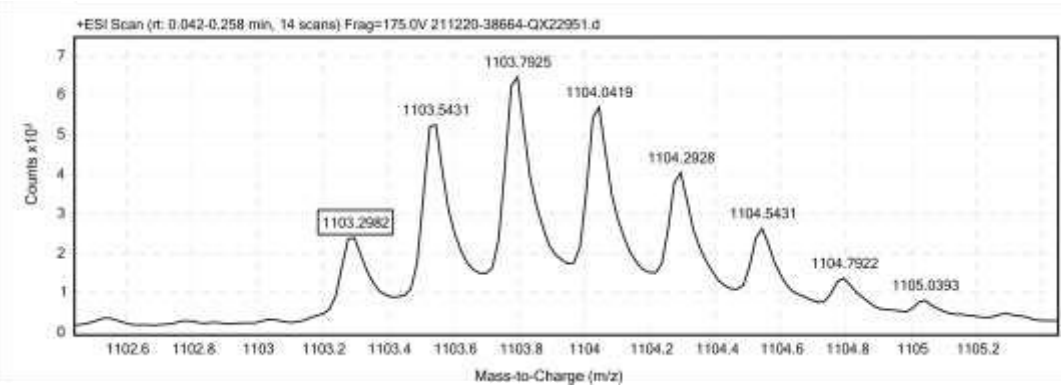

Figure S61. ESI-TOF spectrum for acidic monomer **7*f*-z4** (QX22951; $C_{187}H_{297}N_{51}O_{70}S$; expected $[M+4H^+]/4$ = 1103.282 Da). Observed $[M+4H^+]/4$ = 1103.298 Da.

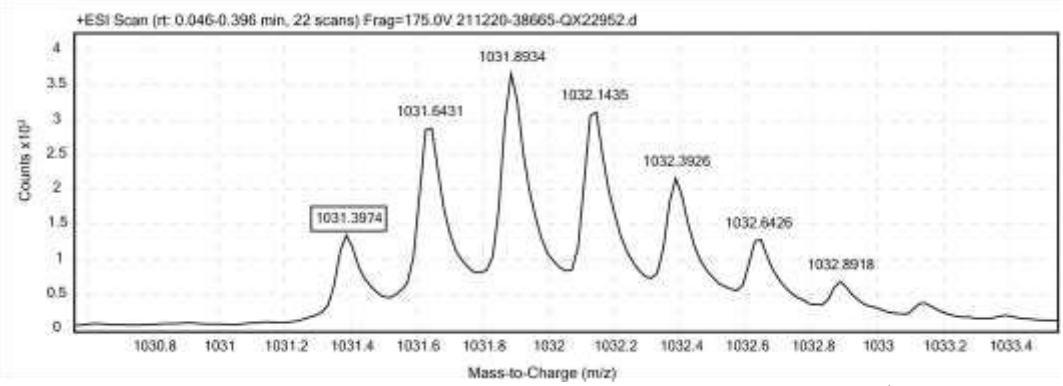

Figure S62. ESI-TOF spectrum for basic monomer **10*b*'-x** (QX22952; $C_{188}H_{329}N_{57}O_{44}S$; expected $[M+4H^+]/4$ = 1031.383 Da). Observed $[M+4H^+]/4$ = 1031.397 Da.

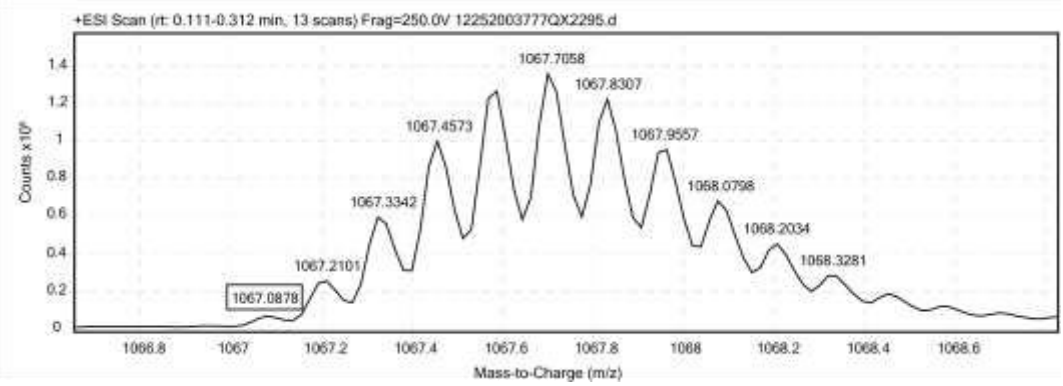

Figure S63. ESI-TOF spectrum for disulfide-bound coiled-coil **d7*f*/10*b*'-z4x** (QX2295; $C_{375}H_{624}N_{108}O_{114}S_2$; expected $[M+8H^+]/8$ = 1067.081 Da). Observed $[M+8H^+]/8$ = 1067.088 Da.

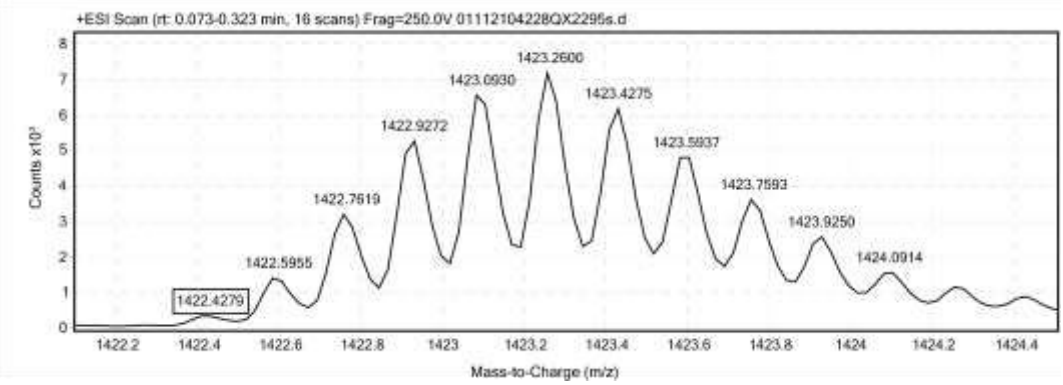

Figure S64. ESI-TOF spectrum for stapled disulfide-bound coiled-coil variant **sd7*f*/10*b*'-z4x** (QX2295s; $C_{375}H_{624}N_{108}O_{114}S_2$; expected $[M+6H^+]/6$ = 1422.438 Da). Observed $[M+6H^+]/6$ = 1422.428 Da.

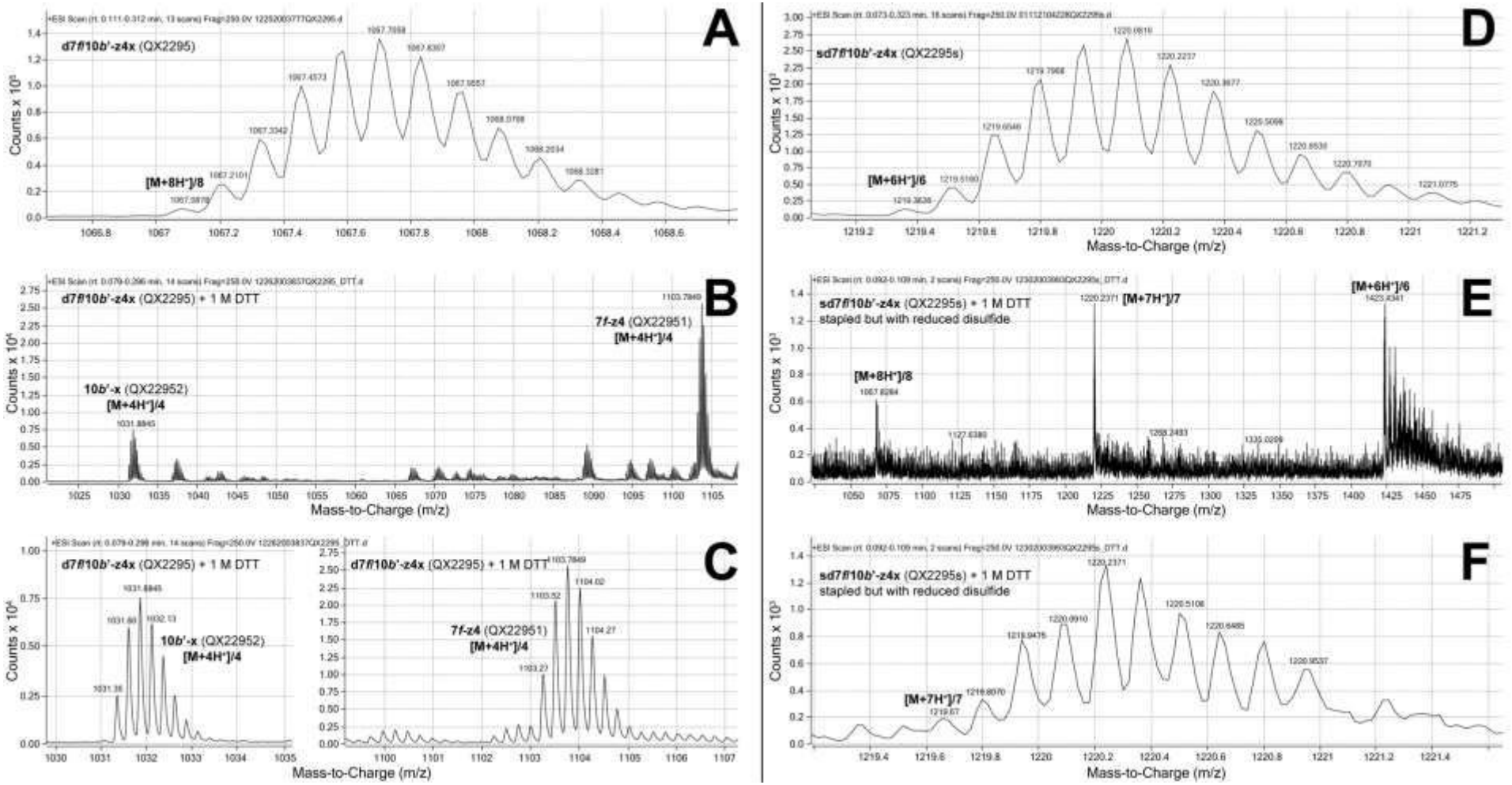

Figure S65. ESI-TOF MS data for (A) disulfide-bound coiled-coil variant **d7*f*/10*b*'-z4x** before (QX2295; $C_{375}H_{624}N_{108}O_{114}S_2$; expected $[M+8H^+]/8$ = 1067.081 Da) and (B,C) after exposure to reducing conditions (1M DTT) for at least 8h. Following reduction, **d7*f*/10*b*'-z4x** splits into its component peptides: **7*f*-z4** (QX22951; $C_{187}H_{297}N_{51}O_{70}S$; expected mass $[M+4H^+]/4$ = 1103.282) and **10*b*'-x** (QX22952; $C_{188}H_{329}N_{57}O_{44}S$; expected mass $[M+4H^+]/4$ = 1031.383 Da). Also shown are ESI-TOF MS data for (D) triazole-stapled disulfide-bound coiled-coil variant **sd7*f*/10*b*'-z4x** before (QX2295s; $C_{375}H_{624}N_{108}O_{114}S_2$; expected $[M+7H^+]/7$ = 1219.377 Da and (E,F) after exposure to reducing conditions (1M DTT) for at least 8h ($C_{375}H_{626}N_{108}O_{114}S_2$; expected $[M+7H^+]/7$ = 1219.665 Da after reduction of disulfide bond to free cysteine residues). Note that **sd7*f*/10*b*'-z4x** remains intact even after disulfide reduction due to the triazole staple.

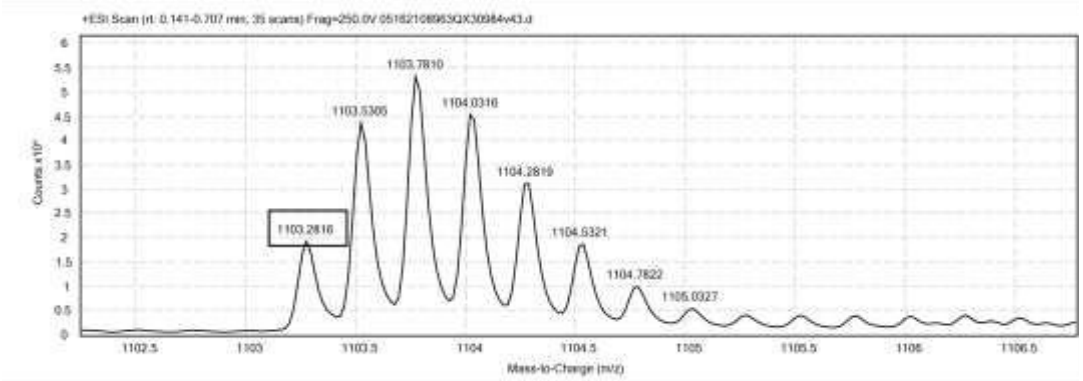

Figure S66. ESI-TOF spectrum for coiled-coil variant **7*f*-z4** (QX30984; $C_{187}H_{297}N_{51}O_{70}S$; expected $[M+4H^+]/4$ = 1103.282 Da). Observed $[M+4H^+]/4$ = 1103.282 Da.

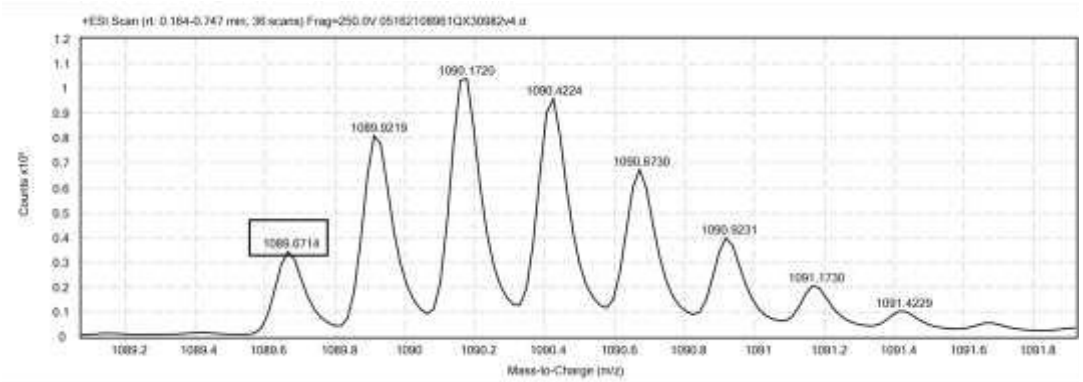

Figure S67. ESI-TOF spectrum for coiled-coil variant **10*b*'-y4** (QX30982; $C_{198}H_{348}N_{58}O_{49}S$; expected $[M+4H^+]/4$ = 1089.664 Da). Observed $[M+4H^+]/4$ = 1089.671 Da.

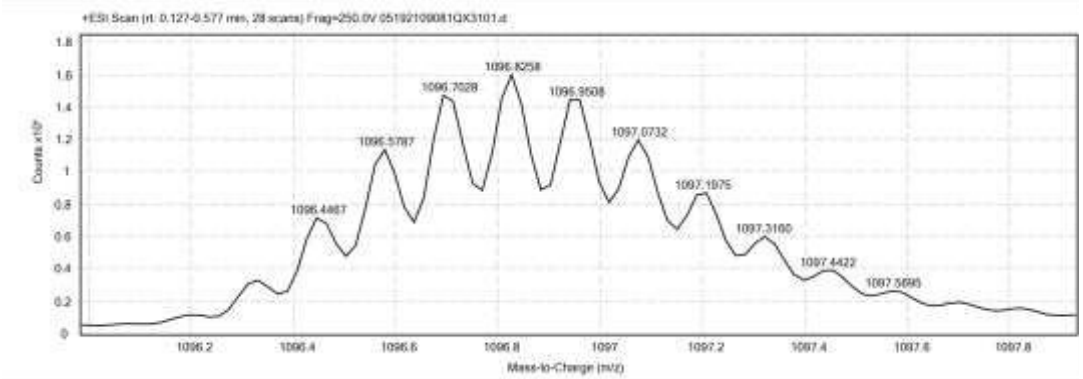

Figure S68. ESI-TOF spectrum for coiled-coil variant **d7*f*/10*b*'-*z*4y4** (QX3101; $C_{385}H_{643}N_{109}O_{119}S_2$; expected $[M+8H^+]/8$ = 1096.221 Da). Observed $[M+8H^+]/8$ = 1096.447 Da.

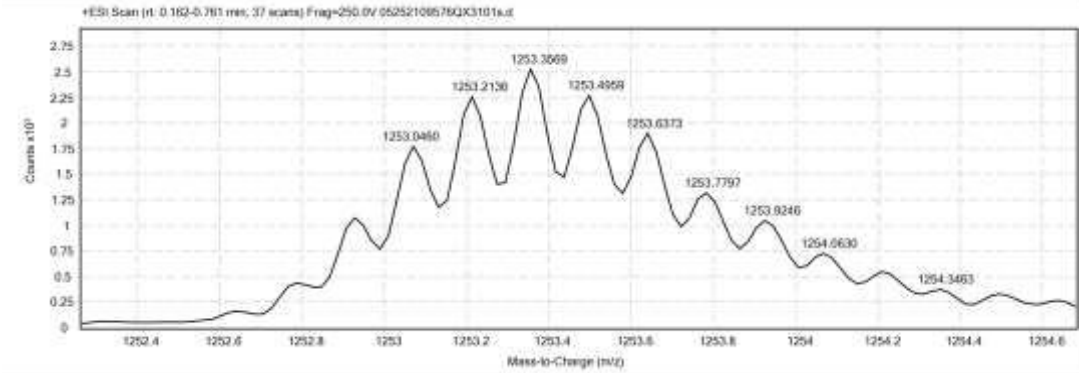

Figure S69. ESI-TOF spectrum for coiled-coil variant **sd7*f*/10*b*'-z4y4** (QX3101s; $C_{385}H_{643}N_{109}O_{119}S_2$; expected $[M+7H^+]/7$ = 1252.680 Da). Observed $[M+8H^+]/8$ = 1253.046 Da.

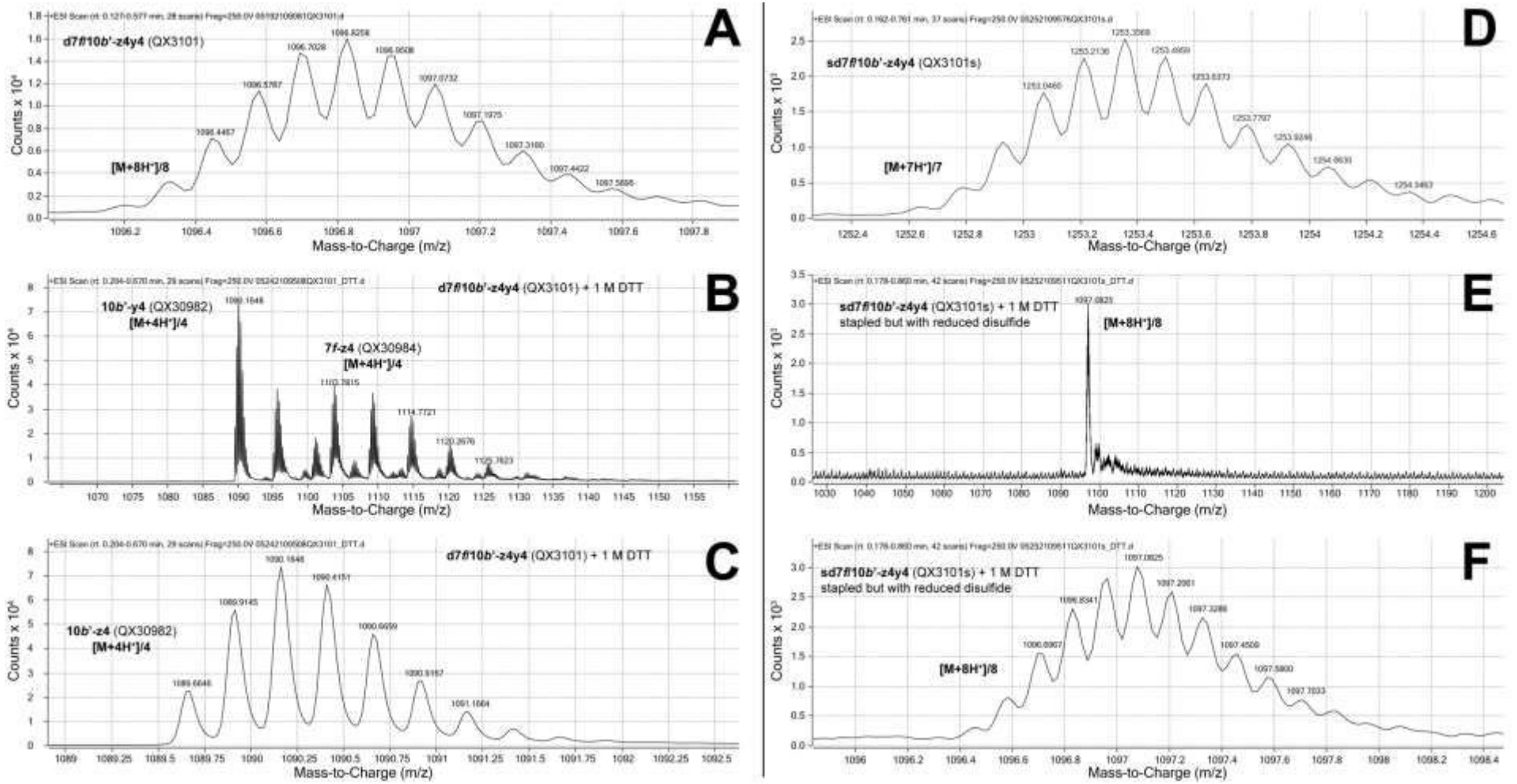

Figure S70. ESI-TOF MS data for (A) disulfide-bound coiled-coil variant **d7*f*/10*b*'-z4y4** before (QX3101; $C_{385}H_{643}N_{109}O_{119}S_2$; expected $[M+8H^+]/8$ = 1096.221 Da) and (B,C) after exposure to reducing conditions (1M DTT) for at least 8h. Following reduction, **d7*f*/10*b*'-z4y4** splits into its component peptides: **7*f*-z4** (QX30984; $C_{187}H_{297}N_{51}O_{70}S$; expected mass $[M+4H^+]/4$ = 1103.282 Da) and **10*b*'-y4** (QX30982; $C_{198}H_{348}N_{58}O_{49}S$; expected mass $[M+4H^+]/4$ = 1089.664 Da). Also shown are ESI-TOF MS data for (D) triazole-stapled disulfide-bound coiled-coil variant **sd7*f*/10*b*'-z4y4** before (QX3101s; $C_{385}H_{643}N_{109}O_{119}S_2$; expected $[M+8H^+]/8$ = 1096.221 Da and (E,F) after exposure to reducing conditions (1M DTT) for at least 8h ($C_{385}H_{645}N_{109}O_{119}S_2$; expected $[M+8H^+]/8$ = 1096.473 Da after reduction of disulfide bond to free cysteine residues). Note that **sd7*f*/10*b*'-z4y4** remains intact even after disulfide reduction due to the triazole staple.

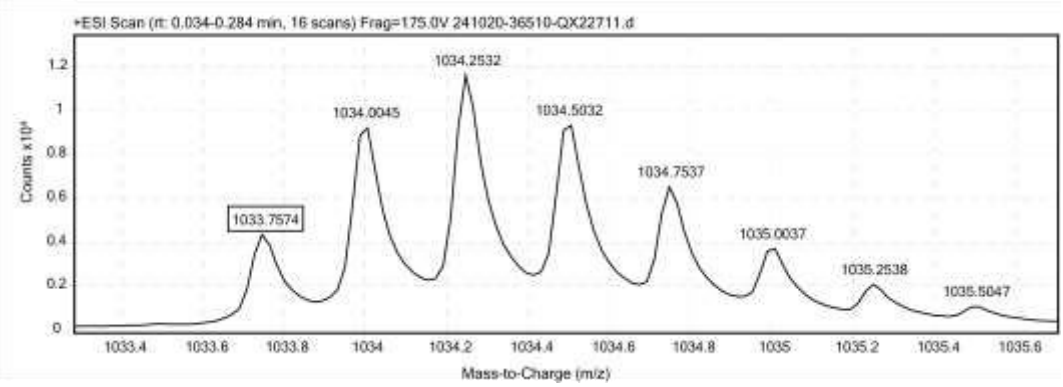

Figure S71. ESI-TOF spectrum for acidic monomer **27*e*-x** (QX22711; $C_{178}H_{279}N_{47}O_{64}S$; expected $[M+4H^+]/4$ = 1033.752 Da). Observed $[M+4H^+]/4$ = 1033.757 Da.

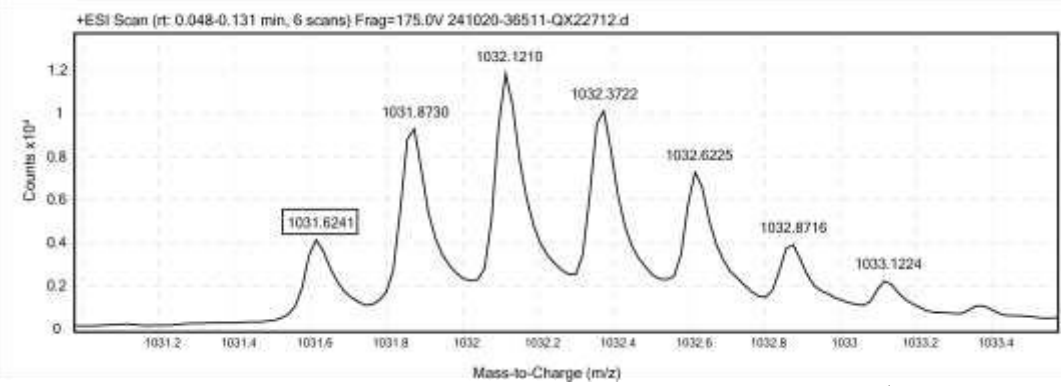

Figure S72. ESI-TOF spectrum for basic monomer **29*g*'-x** (QX22712; $C_{187}H_{324}N_{56}O_{46}S$; expected $[M+4H^+]/4$ = 1031.620 Da. Observed $[M+4H^+]/4$ = 1031.624 Da.

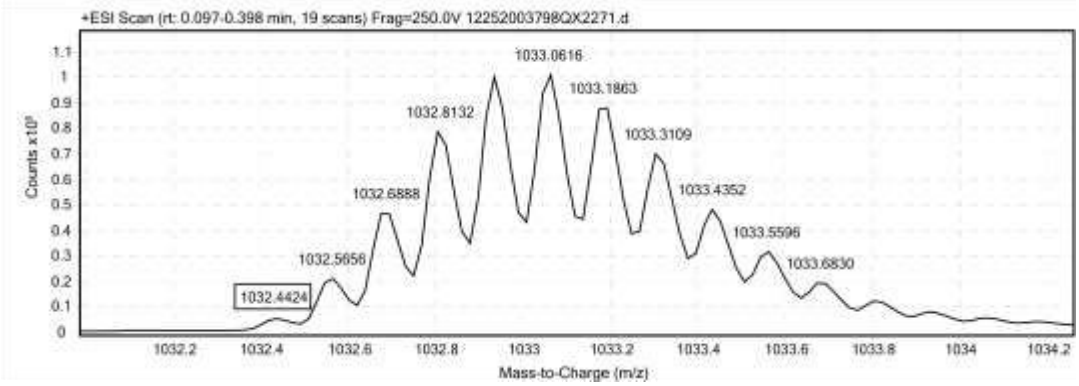

Figure S73. ESI-TOF spectrum for disulfide-bound coiled-coil variant **d27*e*/29*g*'-xx** (QX2271; $C_{365}H_{601}N_{103}O_{110}S_2$; expected $[M+8H^+]/8$ = 1032.434 Da). Observed $[M+8H^+]/8$ = 1032.442 Da.

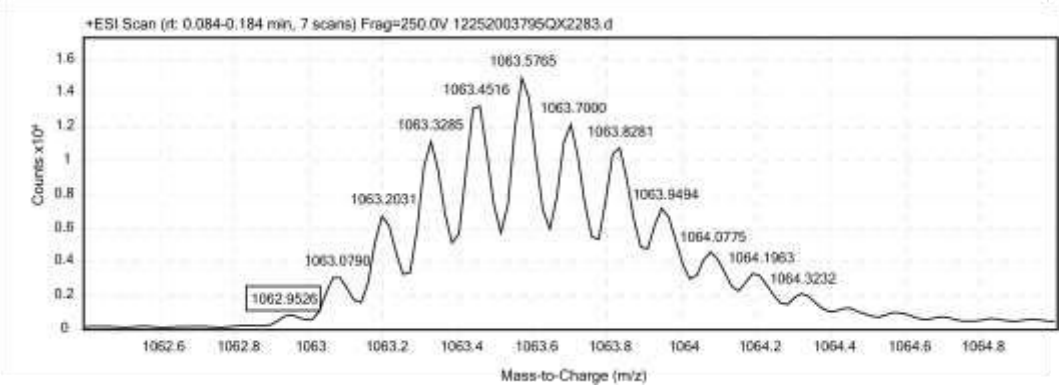

Figure S74. ESI-TOF spectrum for stapled disulfide-bound coiled-coil variant **sd27*e*/29*g*'-x4x** (QX2283; $C_{373}H_{617}N_{109}O_{113}S_2$; expected $[M+8H^+]/8$ = 1062.950 Da). Observed $[M+8H^+]/8$ = 1062.952 Da.

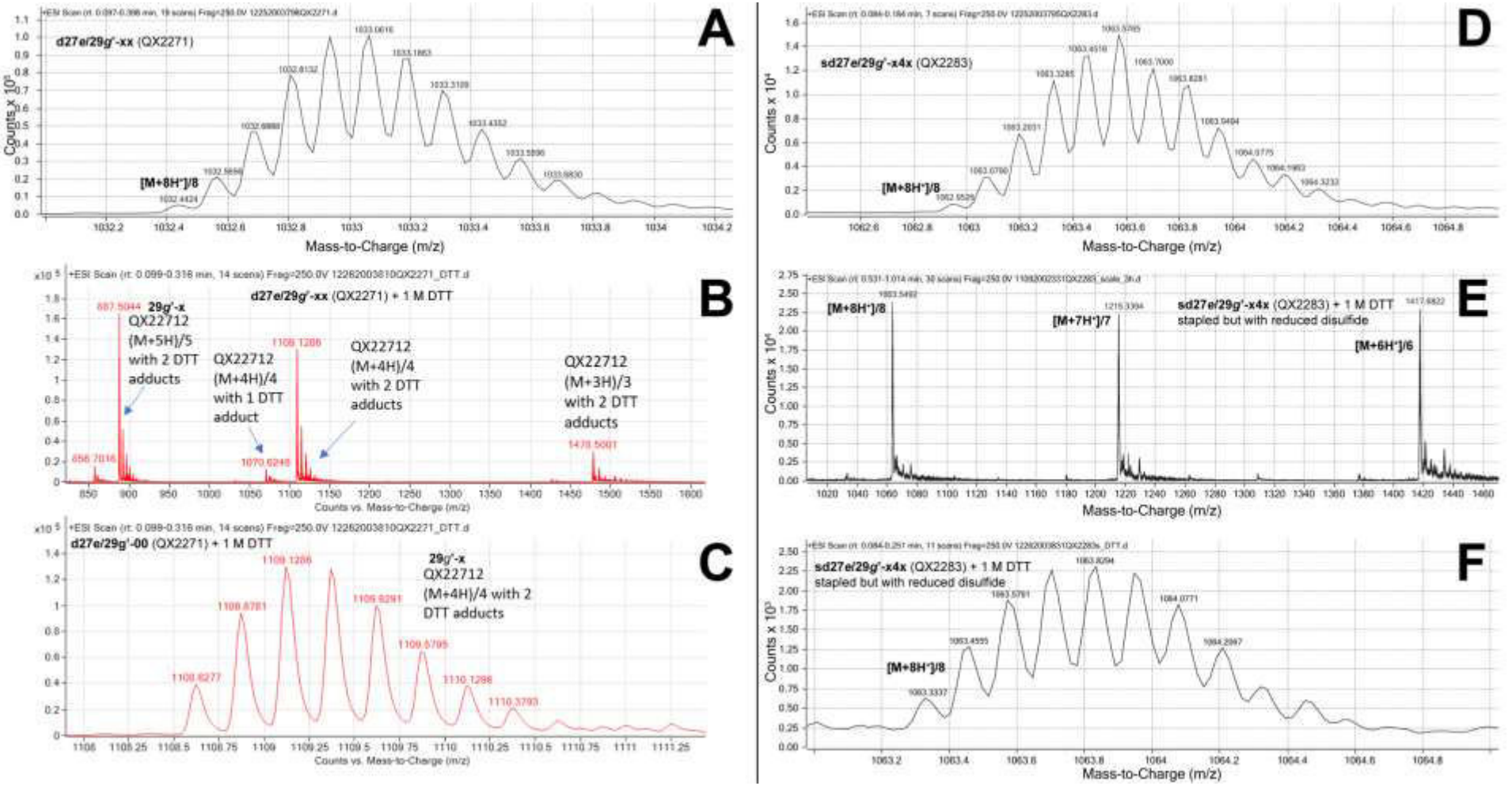

Figure S75. ESI-TOF MS data for (A) disulfide-bound coiled-coil variant **d27*e*/29*g*'-xx** before (QX2271; $C_{365}H_{601}N_{103}O_{110}S_2$; expected $[M+8H^+]/8$ = 1032.434 Da) and (B,C) after exposure to reducing conditions (1M DTT) for at least 8h. Following reduction, **d27*e*/29*g*'-xx** splits into its component peptides: **27*e*-x** (QX22711; $C_{178}H_{279}N_{47}O_{64}S$; expected mass $[M+4H^+]/4$ = 1033.752) and **29*g*'-x** (QX22712; $C_{187}H_{324}N_{56}O_{46}S$; expected mass $[M+4H^+]/4$ = 1031.620 Da). However, neither of these appear in (B,C). Instead, we observe a peak with m/z = 1108.6277 Da and isotopic spacing consistent with z = 4. This peak is consistent with bis-DTT adduct of **29*g*'-x** ($C_{195}H_{344}N_{56}O_{50}S_5$; expected $[M+4H^+]/4$ = 1108.626), which could be formed via tandem thiol-yne and thiol-ene reactions between the propargylglycine of **29*g*'-x** and two equivalents of DTT. Peptide **27*e*-x** does not appear in (B,C) for reasons that are unclear. Also shown are ESI-TOF MS data for (D) triazole-stapled disulfide-bound coiled-coil variant **sd27*e*/29*g*'-x4x** before (QX2283; $C_{373}H_{617}N_{109}O_{113}S_2$; expected $[M+8H^+]/8$ = 1062.950 Da and (E,F) after exposure to reducing conditions (1M DTT) for at least 8h ($C_{373}H_{619}N_{109}O_{113}S_2$; expected $[M+8H^+]/8$ = 1063.202 Da after reduction of disulfide bond to free cysteine residues). Note that **sd27*e*/29*g*'-x4x** remains intact even after disulfide reduction due to the triazole staple.

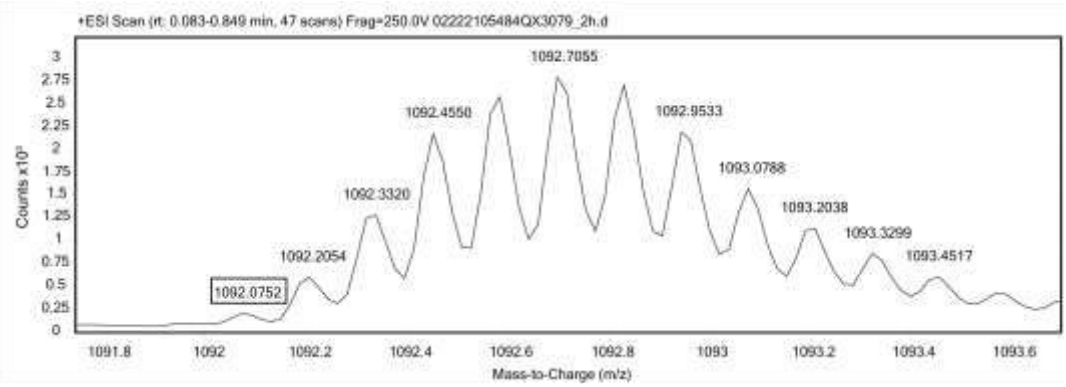

Figure S76. ESI-TOF spectrum for stapled disulfide-bound coiled-coil variant **sd27*e*/29*g*'-x4px** (QX3079; $C_{383}H_{636}N_{110}O_{118}S_2$; expected $[M+8H^+]/8$ = 1092.090 Da). Observed $[M+8H^+]/8$ = 1092.075 Da.

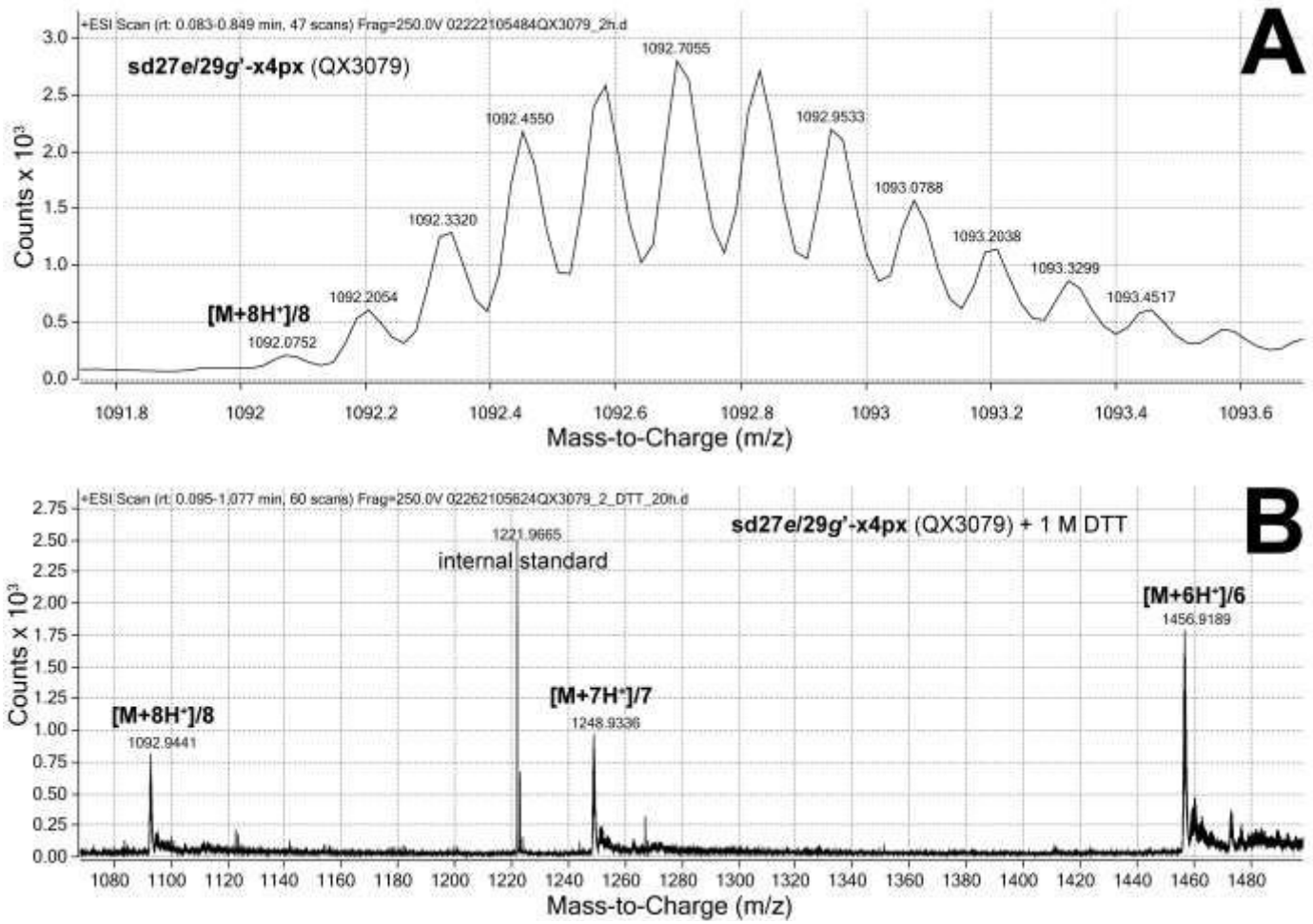

Figure S77. ESI-TOF MS data for (A) bis-triazole-stapled disulfide-bound coiled-coil variant **sd27*e*/29*g*'-x4px** (QX3079; $C_{383}H_{636}N_{110}O_{118}S_2$; expected $[M+8H^+]/8$ = 1092.090 Da) and (B) after exposure to reducing conditions (1M DTT) for at least 8h ($C_{383}H_{638}N_{110}O_{118}S_2$; expected $[M+8H^+]/8$ = 1092.342 Da after reduction of disulfide bond to free cysteine residues). Note that **sd27*e*/29*g*'-x4px** remains intact even after disulfide reduction due to the bis-triazole staple.

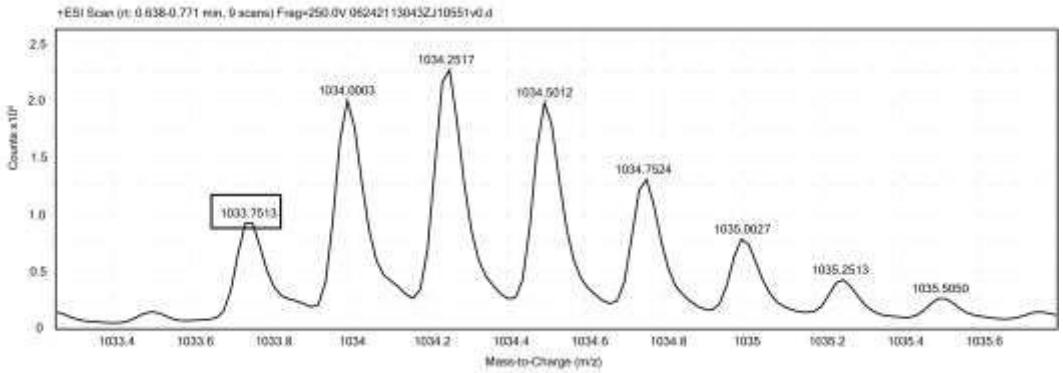

Figure S78. ESI-TOF spectrum for acidic monomer **(*R*)-27*e*-x** (ZJ10551; $C_{178}H_{279}N_{47}O_{64}S$; expected $[M+8H^+]/8$ = 1033.752 Da). Observed $[M+8H^+]/8$ = 1033.751 Da.

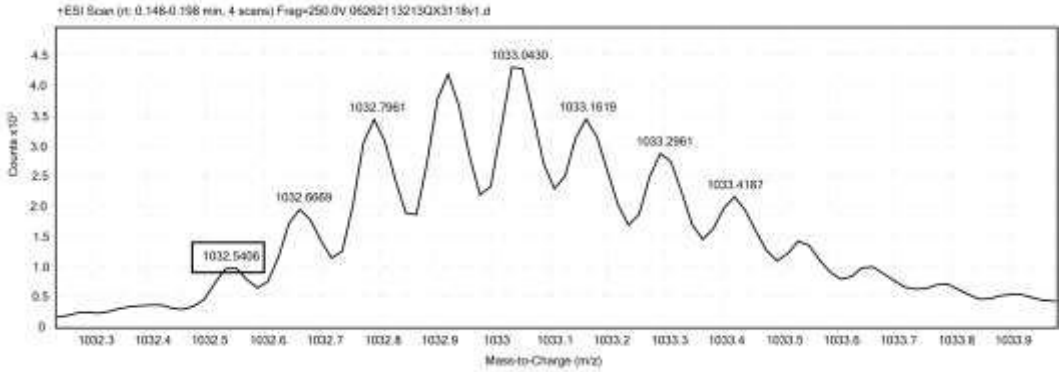

Figure S79. ESI-TOF spectrum for disulfide-bound coiled-coil variant **(*R*,*S*)-d27*e*/29*g*'-xx** (QX3118; $C_{365}H_{601}N_{103}O_{110}S_2$; expected $[M+8H^+]/8$ = 1032.434 Da). Observed $[M+8H^+]/8$ = 1033.541 Da.

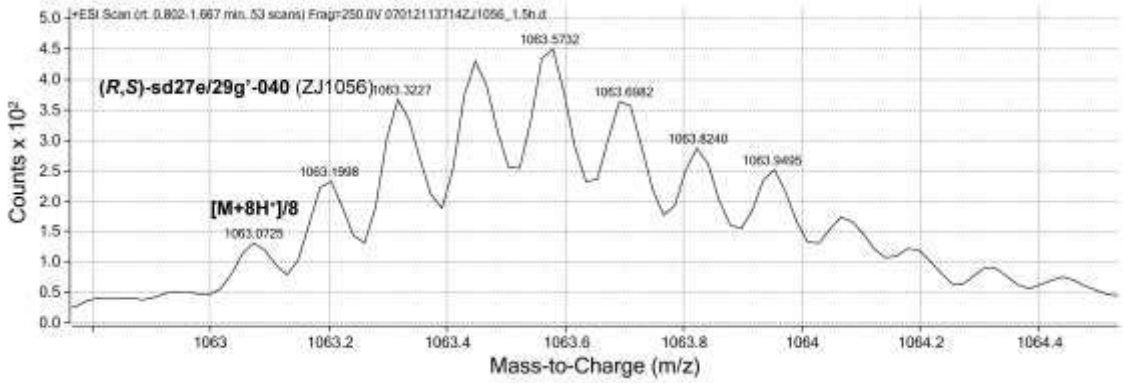

Figure S80. ESI-TOF spectrum for stapled disulfide-bound coiled-coil variant **(*R*,*S*)-sd27*e*/29*g*'-x4x** (ZJ1056; $C_{373}H_{617}N_{109}O_{113}S_2$; expected $[M+8H^+]/8$ = 1062.950 Da). Observed $[M+8H^+]/8$ = 1063.073 Da.

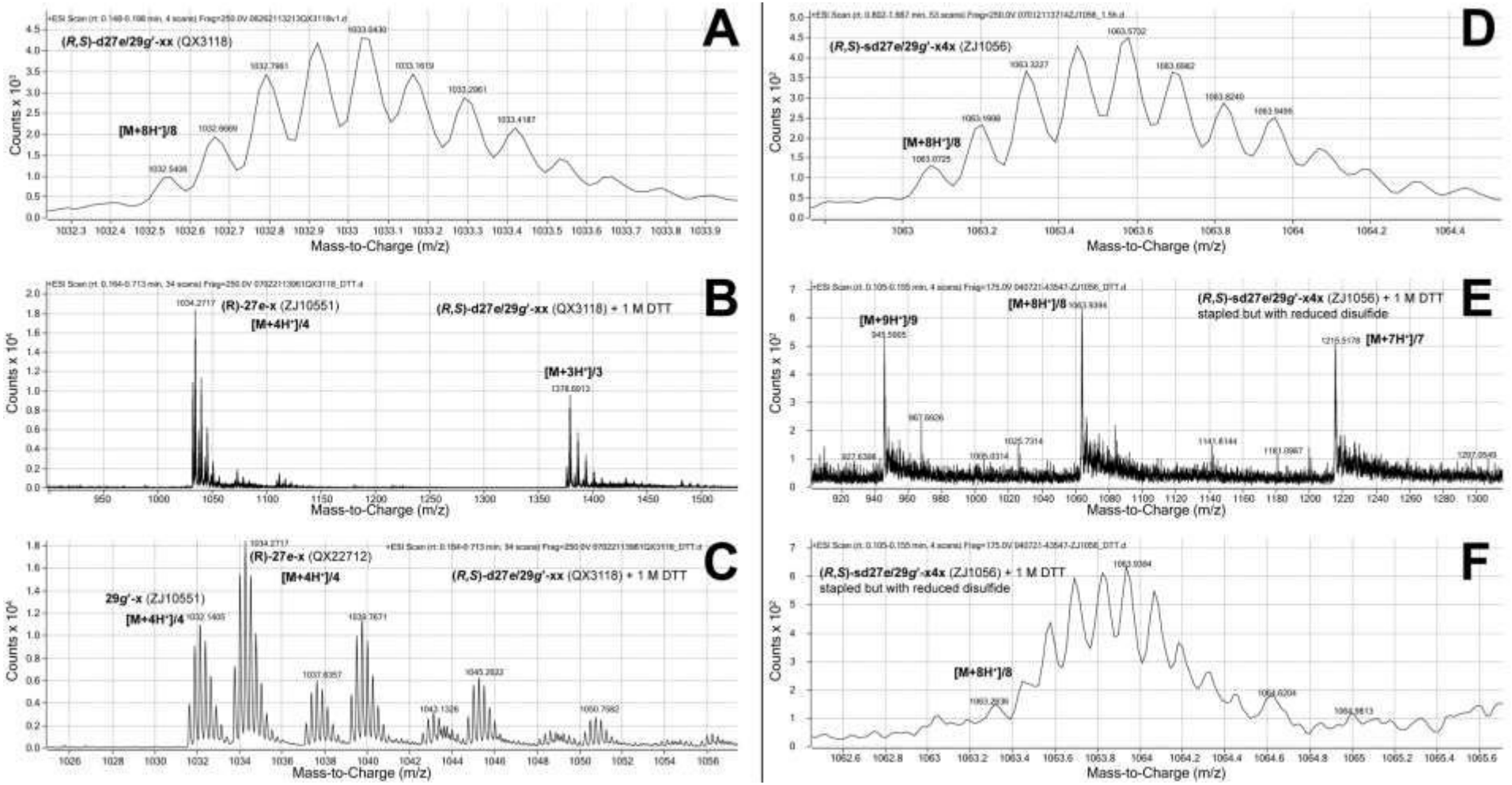

Figure S81. ESI-TOF MS data for (A) disulfide-bound coiled-coil variant **(*R*,*S*)-d27*e*/29*g*'-xx** before (QX3118; $C_{365}H_{601}N_{103}O_{110}S_2$; expected $[M+8H^+]/8$ = 1032.434 Da) and (B,C) after exposure to reducing conditions (1M DTT) for at least 8h. Following reduction, **(*R*,*S*)-d27*e*/29*g*'-xx** splits into its component peptides: **(*R*)-27*e*-x** (ZJ10551; $C_{178}H_{279}N_{47}O_{64}S$; expected mass $[M+4H^+]/4$ = 1033.752) and **29*g*'-x** (QX22712; $C_{187}H_{324}N_{56}O_{46}S$; expected mass $[M+4H^+]/4$ = 1031.620 Da). Also shown are ESI-TOF MS data for (D) triazole-stapled disulfide-bound coiled-coil variant **(*R*,*S*)-sd27*e*/29*g*'-x4x** before (ZJ1056; $C_{373}H_{617}N_{109}O_{113}S_2$; expected $[M+8H^+]/8$ = 1062.950 Da and (E,F) after exposure to reducing conditions (1M DTT) for at least 8h ($C_{373}H_{619}N_{109}O_{113}S_2$; expected $[M+8H^+]/8$ = 1063.202 Da after reduction of disulfide bond to free cysteine residues). Note that **(*R*,*S*)-sd27*e*/29*g*'-x4x** remains intact even after disulfide reduction due to the triazole staple.

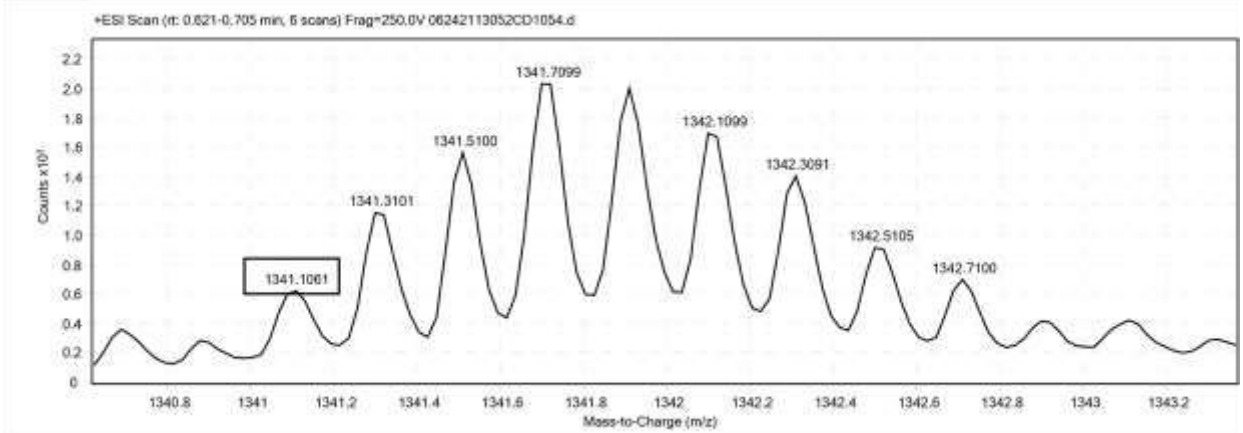

Figure S82. ESI-TOF MS spectrum for affibody **a** (CD1054). Expected [M+5H$^+$]/5 = 1341.102 Da. Observed [M+5H$^+$]/5 = 1341.106 Da.

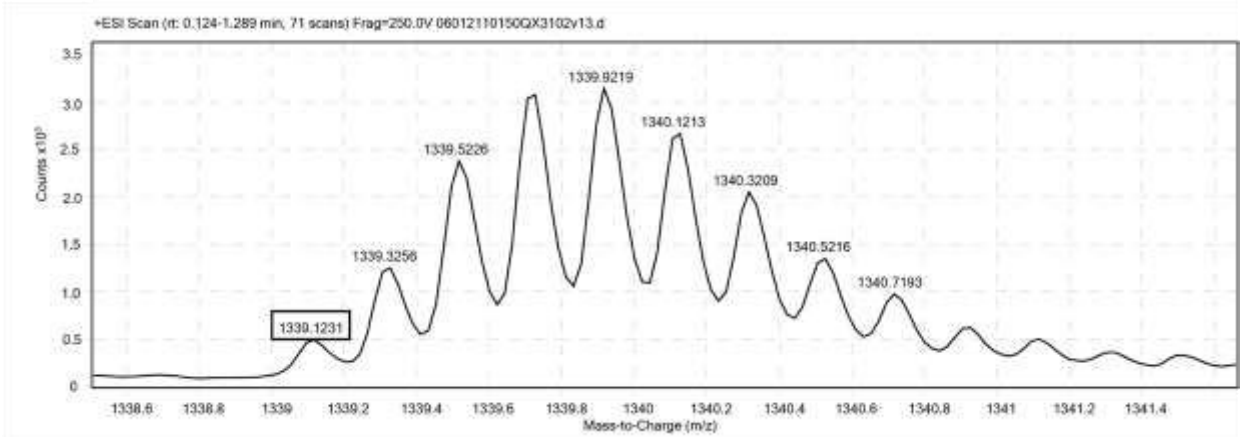

Figure S83. ESI-TOF MS spectrum for affibody variant **a8/42-xx** (QX3102). Expected [M+5H$^+$]/5 = 1339.102 Da. Observed [M+5H$^+$]/5 = 1339.123 Da.

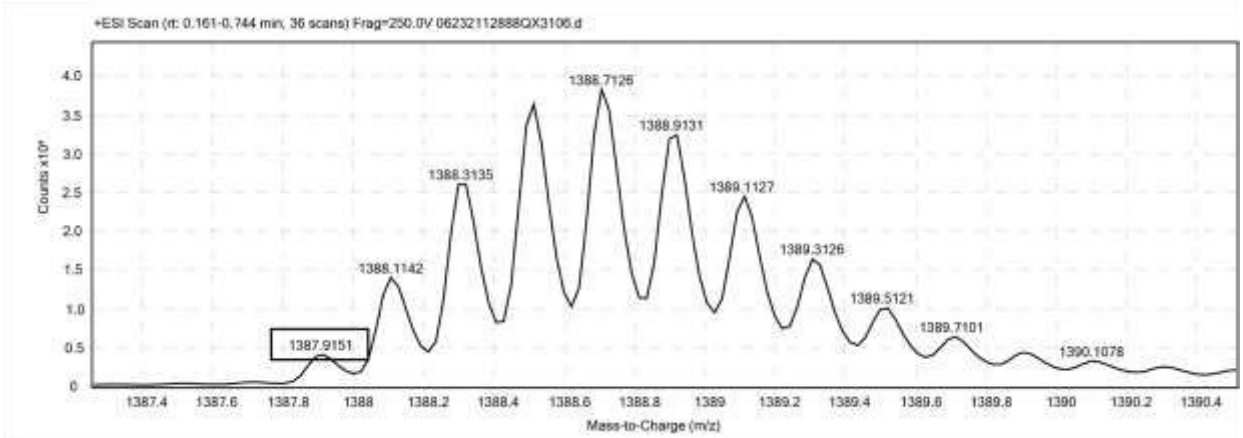

Figure S84. ESI-TOF MS spectrum for affibody variant **sa8/42-x4x** (QX3106). Expected [M+5H$^+$]/5 = 1387.927 Da. Observed [M+5H$^+$]/5 = 1387.915 Da.

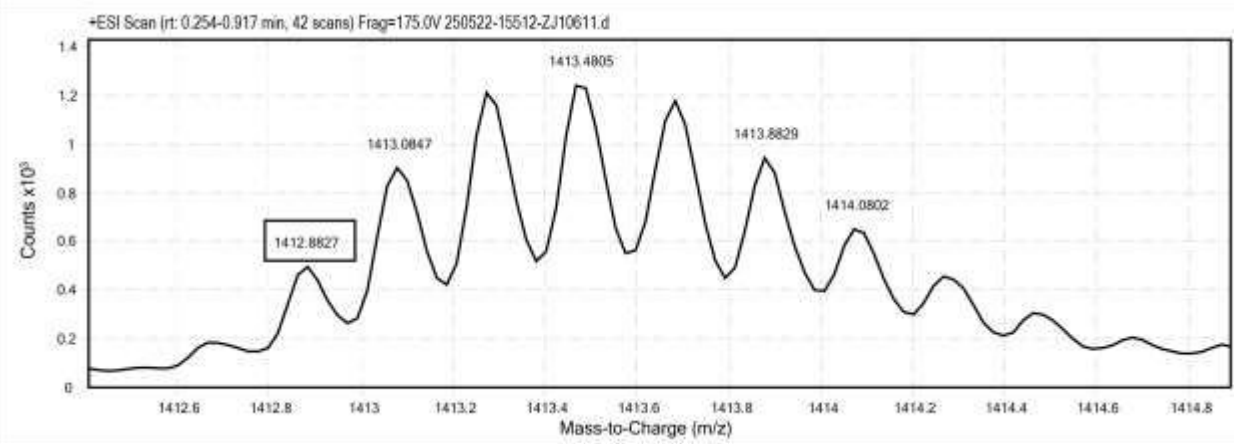

Figure S85. ESI-TOF MS spectrum for fluorescent affibody variant **fa** (ZJ10611). Expected [M+5H$^+$]/5 = 1412.914 Da. Observed [M+5H$^+$]/5 = 1412.883 Da.

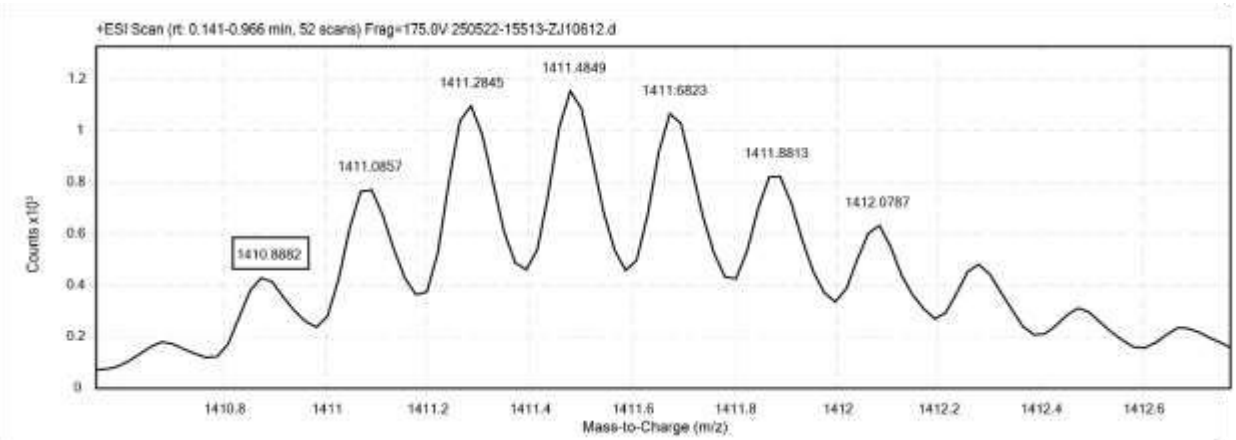

Figure S86. ESI-TOF MS spectrum for fluorescent affibody variant **fa8/42-xx** (ZJ10612). Expected [M+5H$^+$]/5 = 1410.913 Da. Observed [M+5H$^+$]/5 = 1410.888 Da.

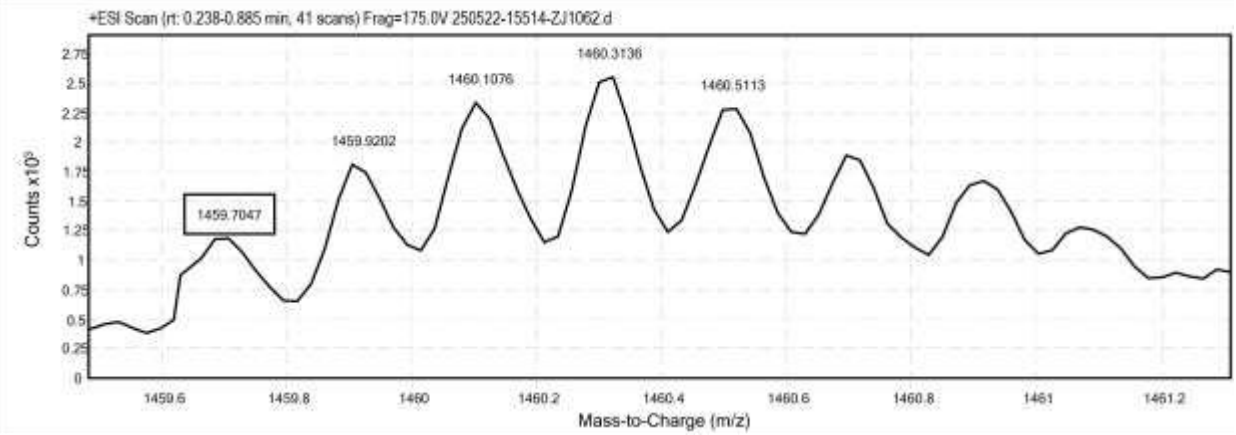

Figure S87. ESI-TOF MS spectrum for fluorescent affibody variant **fsa8/42-x4x** (ZJ1062). Expected [M+5H$^+$]/5 = 1459.738 Da. Observed [M+5H$^+$]/5 = 1459.705 Da.

4. Analytical HPLC data

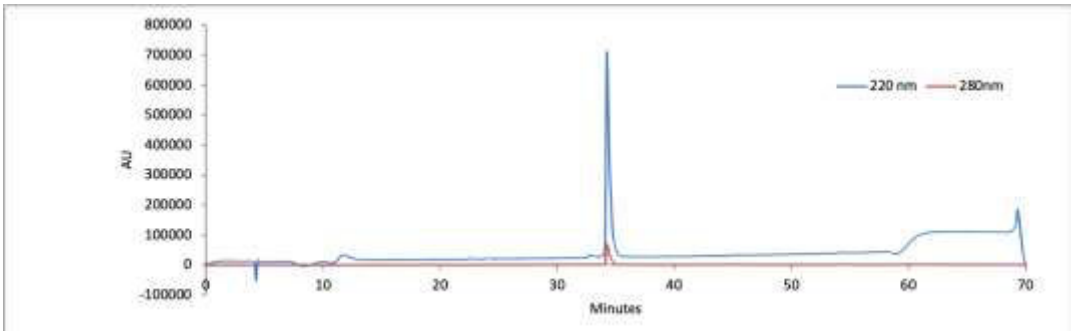

Figure S88. Analytical HPLC Data for variant **d20*e*/22*g*'-z4x** (ZJ10511). Protein solution was injected onto a C18 analytical column and eluted using a linear gradient of 10-60% B (A = H_2O, 0.1% TFA; B = MeCN, 0.1% TFA) over 50 minutes, followed by a 10-minute rinse (95% B), and a 10-minute column re-equilibration.

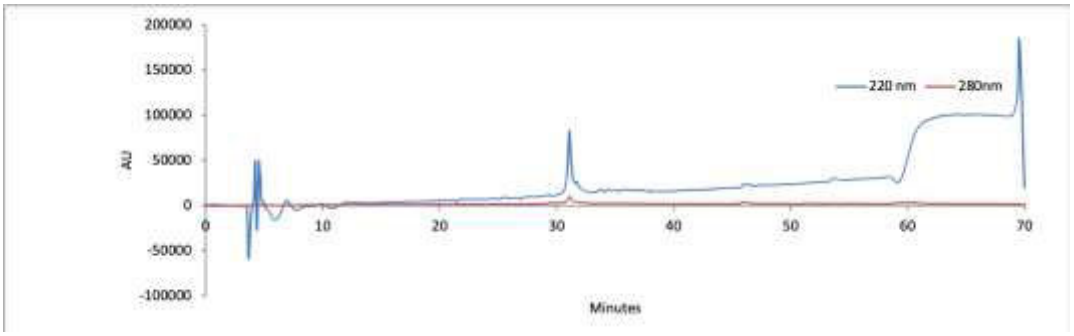

Figure S89. Analytical HPLC Data for variant **sd20*e*/22*g*'-z4x** (ZJ10511s). Protein solution was injected onto a C18 analytical column and eluted using a linear gradient of 10-60% B (A = H_2O, 0.1% TFA; B = MeCN, 0.1% TFA) over 50 minutes, followed by a 10-minute rinse (95% B), and a 10-minute column re-equilibration.

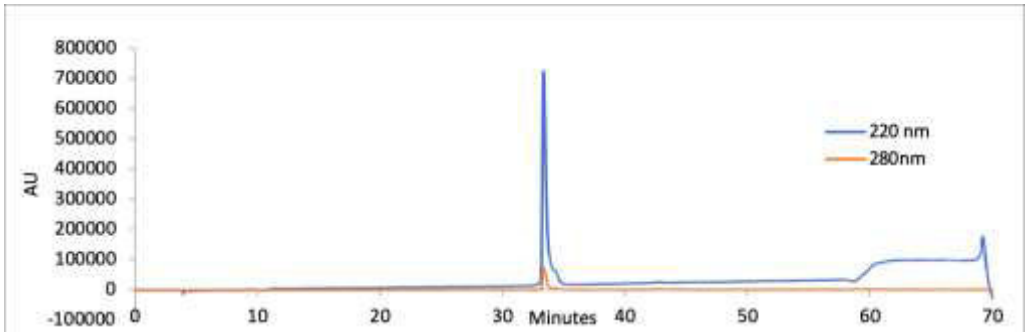

Figure S90. Analytical HPLC Data for variant **d27*e*/29*g*'-xx** (QX2271). Protein solution was injected onto a C18 analytical column and eluted using a linear gradient of 10-60% B (A = H_2O, 0.1% TFA; B = MeCN, 0.1% TFA) over 50 minutes, followed by a 10-minute rinse (95% B), and a 10-minute column re-equilibration.

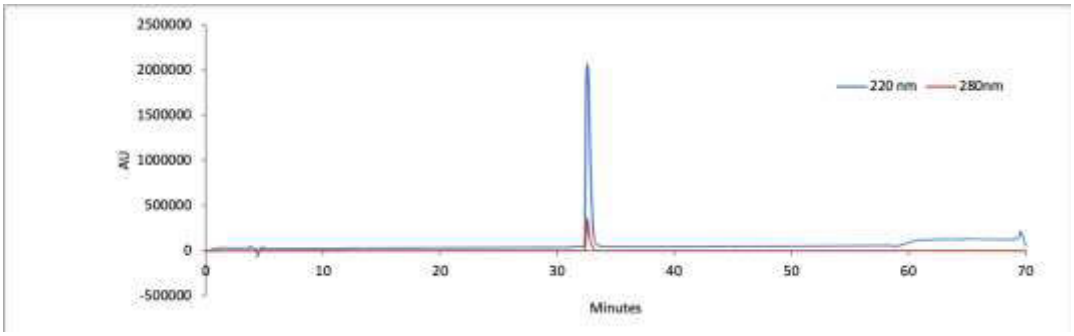

Figure S91. Analytical HPLC Data for variant **d13*e*/15*g*'-z4x** (QX31171). Protein solution was injected onto a C18 analytical column and eluted using a linear gradient of 10-60% B (A = H_2O, 0.1% TFA; B = MeCN, 0.1% TFA) over 50 minutes, followed by a 10-minute rinse (95% B), and a 10-minute column re-equilibration.

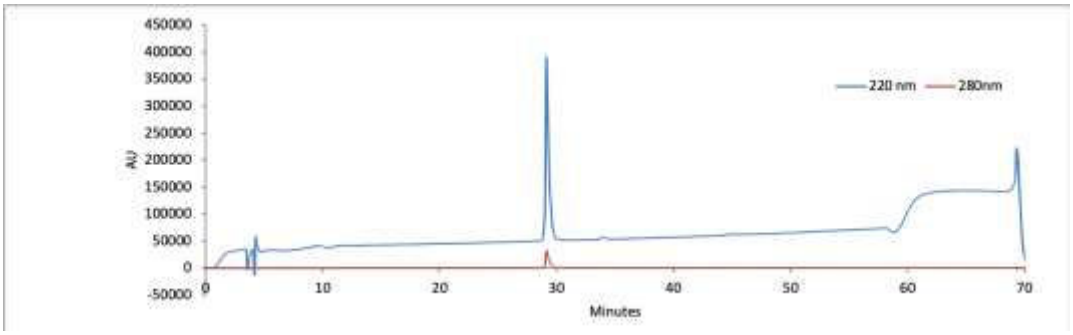

Figure S852. Analytical HPLC Data for variant **sd13*e*/15*g*'-z4x** (QX31171s). Protein solution was injected onto a C18 analytical column and eluted using a linear gradient of 10-60% B (A = H_2O, 0.1% TFA; B = MeCN, 0.1% TFA) over 50 minutes, followed by a 10-minute rinse (95% B), and a 10-minute column re-equilibration.

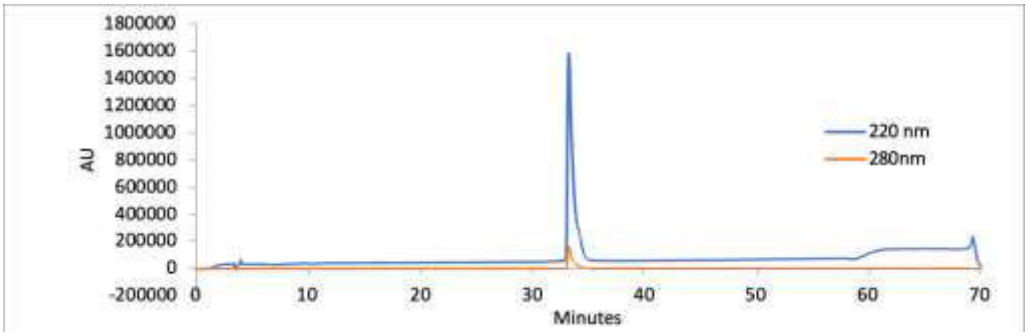

Figure S93. Analytical HPLC Data for variant **d6*e*/8*g*'-z4x** (QX2292). Protein solution was injected onto a C18 analytical column and eluted using a linear gradient of 10-60% B (A = H_2O, 0.1% TFA; B = MeCN, 0.1% TFA) over 50 minutes, followed by a 10-minute rinse (95% B), and a 10-minute column re-equilibration.

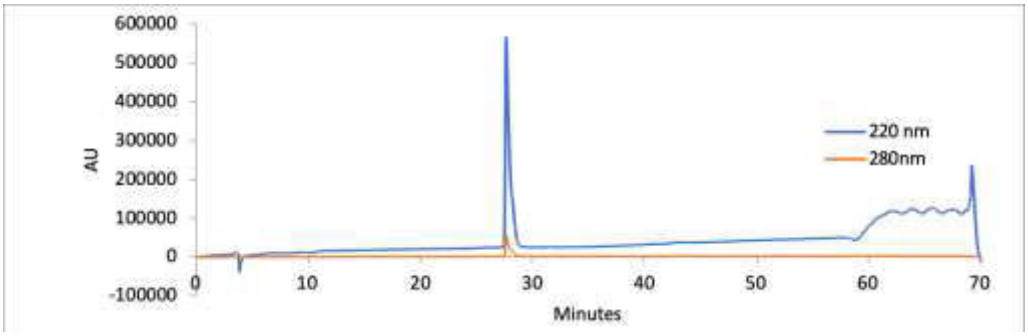

Figure S94. Analytical HPLC Data for variant **sd6*e*/8*g*'-z4x** (QX2292s). Protein solution was injected onto a C18 analytical column and eluted using a linear gradient of 10-60% B (A = H_2O, 0.1% TFA; B = MeCN, 0.1% TFA) over 50 minutes, followed by a 10-minute rinse (95% B), and a 10-minute column re-equilibration.

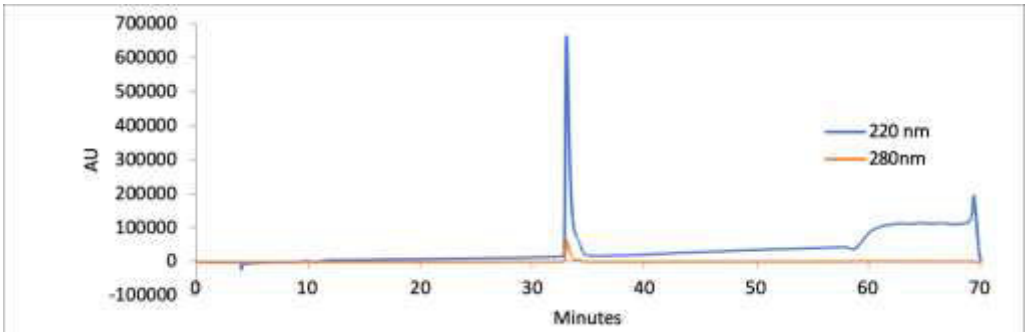

Figure S95. Analytical HPLC Data for variant **d27*e*/22*g*'-z4x** (QX2294). Protein solution was injected onto a C18 analytical column and eluted using a linear gradient of 10-60% B (A = H_2O, 0.1% TFA; B = MeCN, 0.1% TFA) over 50 minutes, followed by a 10-minute rinse (95% B), and a 10-minute column re-equilibration.

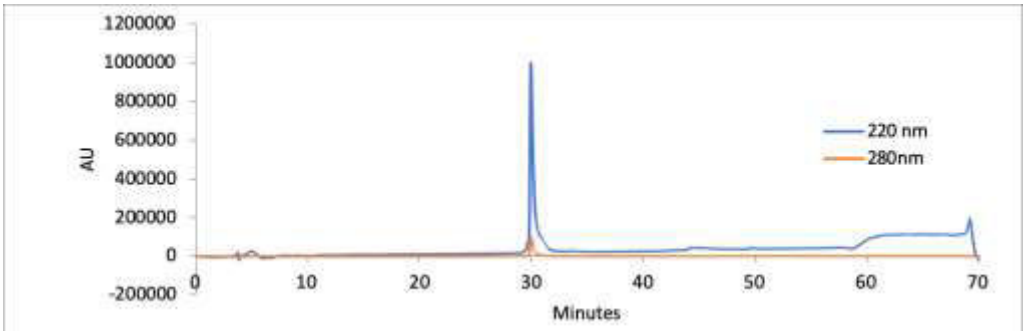

Figure S96. Analytical HPLC Data for variant **sd27*e*/22*g*'-z4x** (QX2294s). Protein solution was injected onto a C18 analytical column and eluted using a linear gradient of 10-60% B (A = H_2O, 0.1% TFA; B = MeCN, 0.1% TFA) over 50 minutes, followed by a 10-minute rinse (95% B), and a 10-minute column re-equilibration.

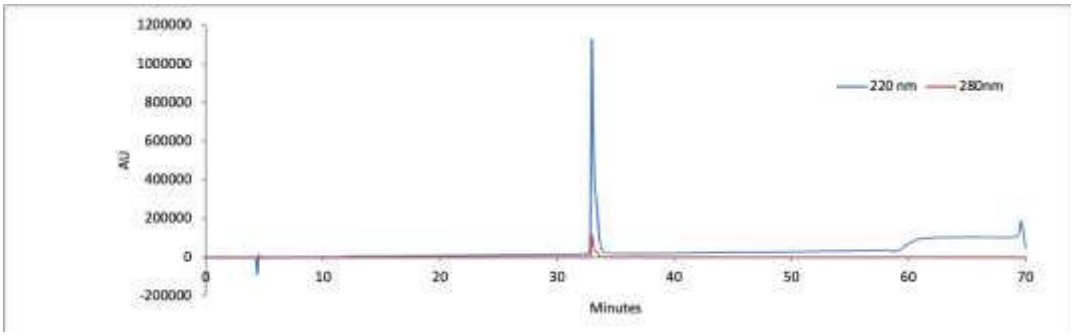

Figure S97. Analytical HPLC Data for variant **d6*e*/1*g*'-z4x** (QX31172). Protein solution was injected onto a C18 analytical column and eluted using a linear gradient of 10-60% B (A = H_2O, 0.1% TFA; B = MeCN, 0.1% TFA) over 50 minutes, followed by a 10-minute rinse (95% B), and a 10-minute column re-equilibration.

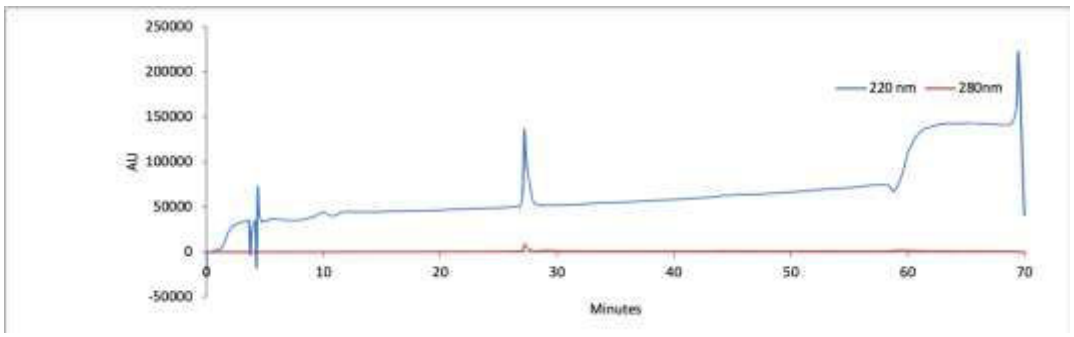

Figure S98. Analytical HPLC Data for variant **sd6*e*/1*g*'-z4x** (QX31172s). Protein solution was injected onto a C18 analytical column and eluted using a linear gradient of 10-60% B (A = H_2O, 0.1% TFA; B = MeCN, 0.1% TFA) over 50 minutes, followed by a 10-minute rinse (95% B), and a 10-minute column re-equilibration.

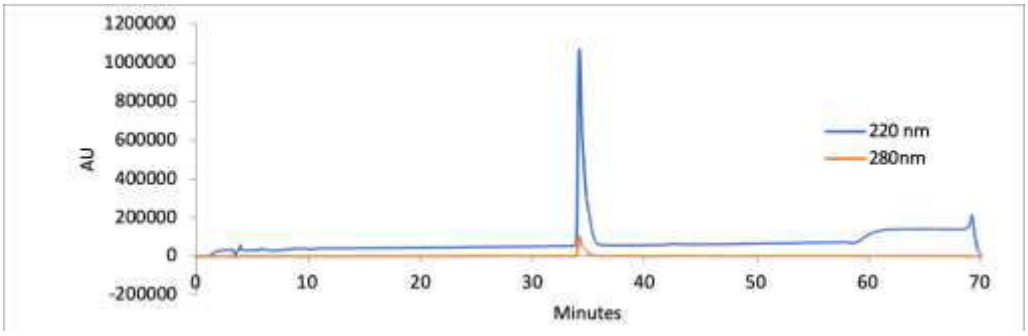

Figure S99. Analytical HPLC Data for variant **d27*e*/29*g*'-z2x** (QX2289). Protein solution was injected onto a C18 analytical column and eluted using a linear gradient of 10-60% B (A = H_2O, 0.1% TFA; B = MeCN, 0.1% TFA) over 50 minutes, followed by a 10-minute rinse (95% B), and a 10-minute column re-equilibration.

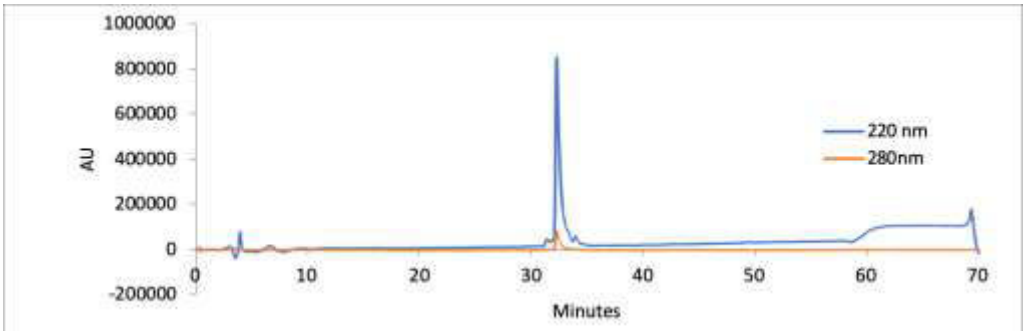

Figure S100. Analytical HPLC Data for variant **sd27*e*/29*g*'-z2x** (QX2289s). Protein solution was injected onto a C18 analytical column and eluted using a linear gradient of 10-60% B (A = H_2O, 0.1% TFA; B = MeCN, 0.1% TFA) over 50 minutes, followed by a 10-minute rinse (95% B), and a 10-minute column re-equilibration.

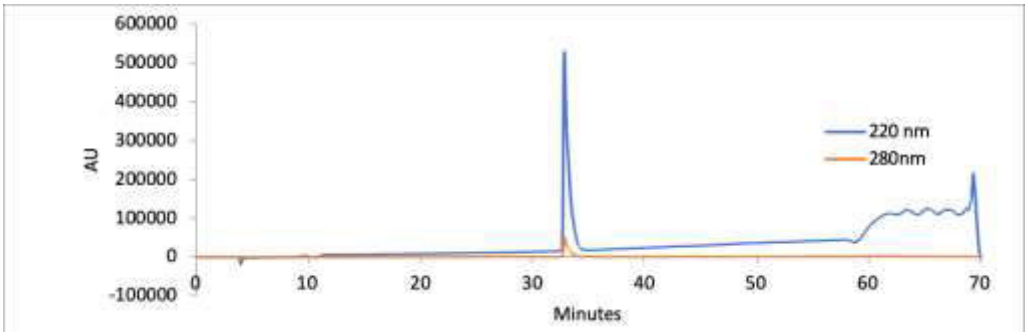

Figure S101. Analytical HPLC Data for variant **d27*e*/22*g*'-z2x** (QX2293). Protein solution was injected onto a C18 analytical column and eluted using a linear gradient of 10-60% B (A = H_2O, 0.1% TFA; B = MeCN, 0.1% TFA) over 50 minutes, followed by a 10-minute rinse (95% B), and a 10-minute column re-equilibration.

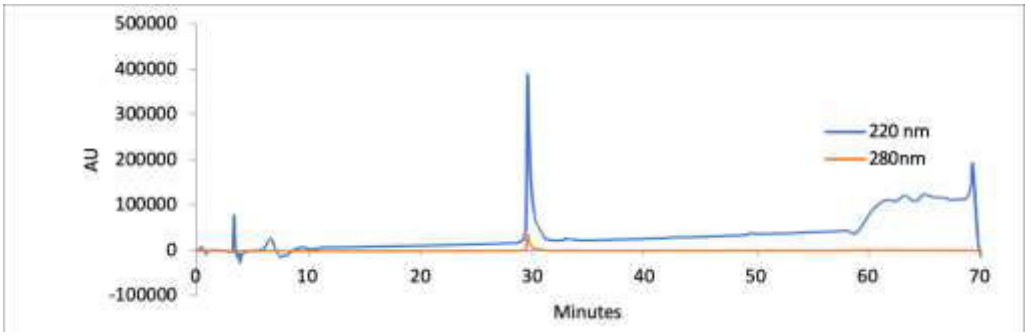

Figure S102. Analytical HPLC Data for variant **sd27*e*/22*g*'-z2x** (QX2293s). Protein solution was injected onto a C18 analytical column and eluted using a linear gradient of 10-60% B (A = H_2O, 0.1% TFA; B = MeCN, 0.1% TFA) over 50 minutes, followed by a 10-minute rinse (95% B), and a 10-minute column re-equilibration.

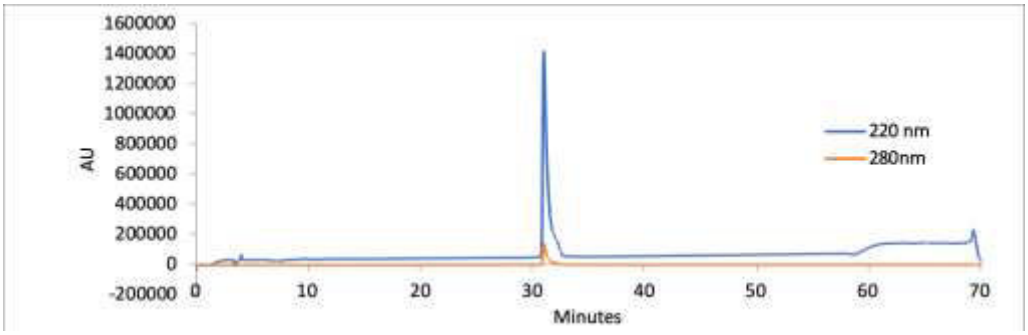

Figure S103. Analytical HPLC Data for variant **d24*b*/25*c*'-z4x** (QX2291). Protein solution was injected onto a C18 analytical column and eluted using a linear gradient of 10-60% B (A = $_{H2O}$, 0.1% TFA; B = MeCN, 0.1% TFA) over 50 minutes, followed by a 10-minute rinse (95% B), and a 10-minute column re-equilibration.

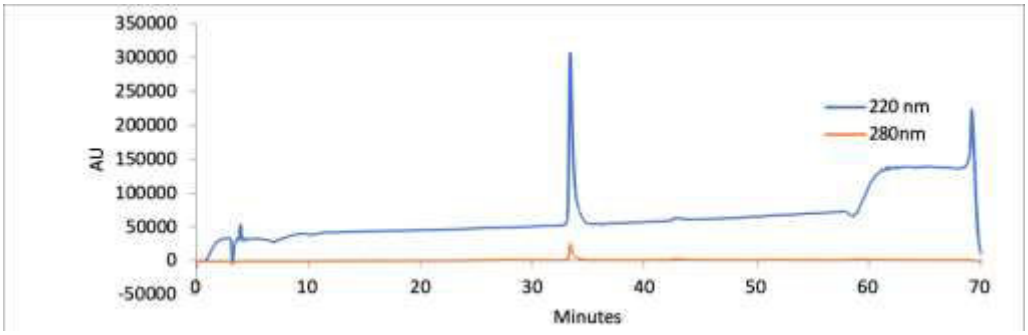

Figure S104. Analytical HPLC Data for variant **sd24*b*/25*c*'-z4x** (QX2291s). Protein solution was injected onto a C18 analytical column and eluted using a linear gradient of 10-60% B (A = H_2O, 0.1% TFA; B = MeCN, 0.1% TFA) over 50 minutes, followed by a 10-minute rinse (95% B), and a 10-minute column re-equilibration.

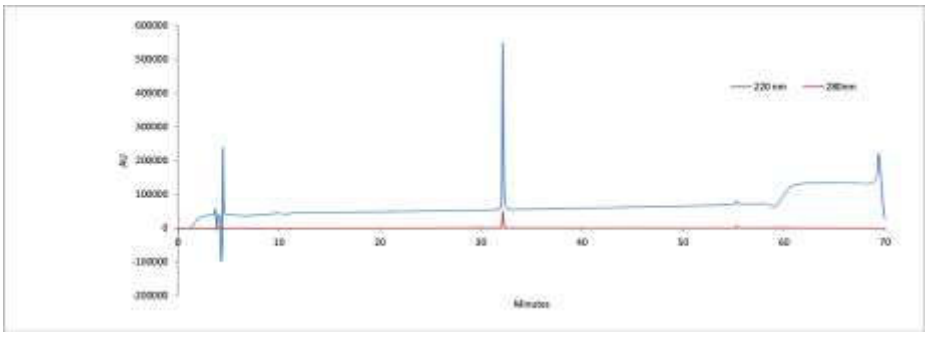

Figure S105. Analytical HPLC Data for variant **d24*b*/25*c*'-z4y4** (QX3096). Protein solution was injected onto a C18 analytical column and eluted using a linear gradient of 10-60% B (A = H_2O, 0.1% TFA; B = MeCN, 0.1% TFA) over 50 minutes, followed by a 10-minute rinse (95% B), and a 10-minute column re-equilibration.

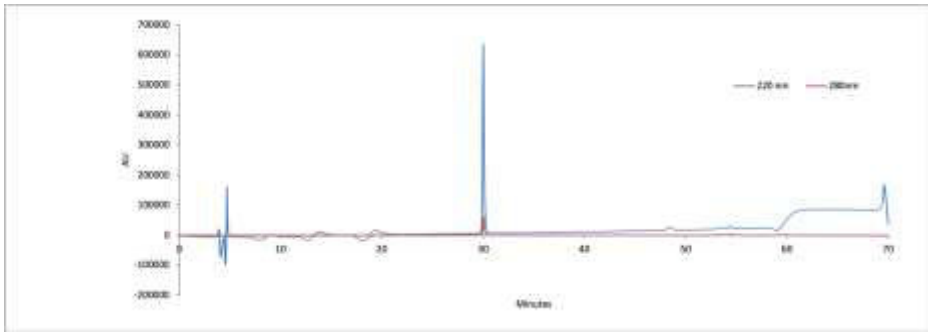

Figure S106. Analytical HPLC Data for variant **sd24*b*/25*c*'-z4y4** (QX3096s). Protein solution was injected onto a C18 analytical column and eluted using a linear gradient of 10-60% B (A = H_2O, 0.1% TFA; B = MeCN, 0.1% TFA) over 50 minutes, followed by a 10-minute rinse (95% B), and a 10-minute column re-equilibration.

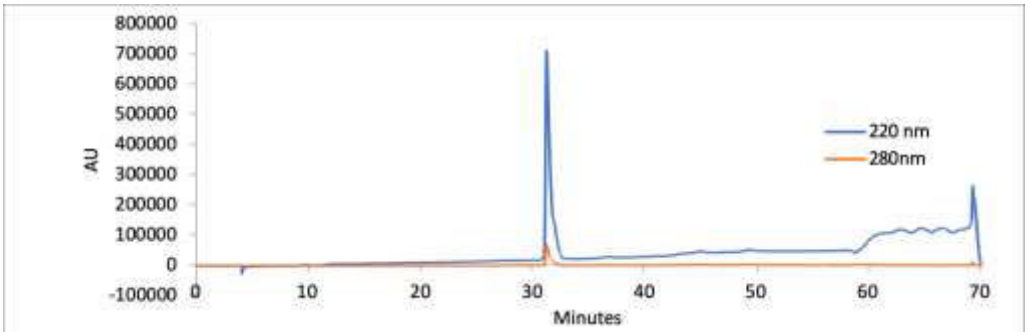

Figure S107. Analytical HPLC Data for variant **d7*f*/10*b*'-z4x** (QX2295). Protein solution was injected onto a C18 analytical column and eluted using a linear gradient of 10-60% B (A = H_2O, 0.1% TFA; B = MeCN, 0.1% TFA) over 50 minutes, followed by a 10-minute rinse (95% B), and a 10-minute column re-equilibration.

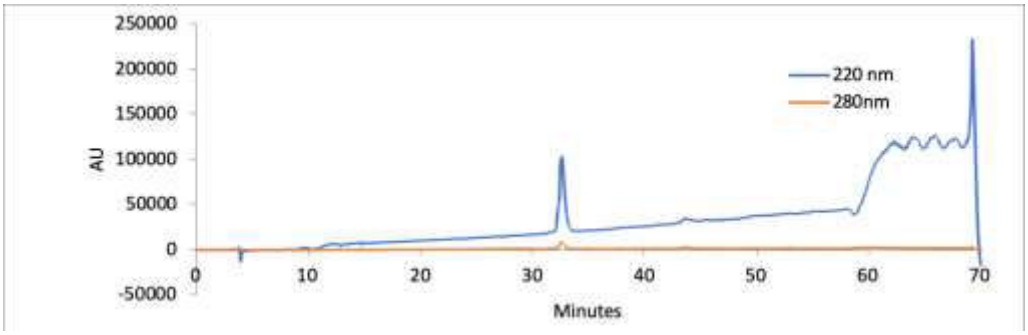

Figure S108. Analytical HPLC Data for variant **sd7*f*/10*b*'-z4x** (QX2295). Protein solution was injected onto a C18 analytical column and eluted using a linear gradient of 10-60% B (A = H_2O, 0.1% TFA; B = MeCN, 0.1% TFA) over 50 minutes, followed by a 10-minute rinse (95% B), and a 10-minute column re-equilibration.

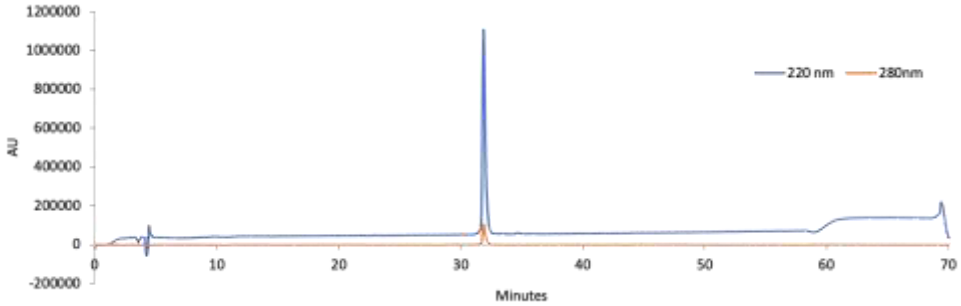

Figure S109. Analytical HPLC Data for variant **d7*f*/10*b*'-z4y4** (QX3101). Protein solution was injected onto a C18 analytical column and eluted using a linear gradient of 10-60% B (A = H_2O, 0.1% TFA; B = MeCN, 0.1% TFA) over 50 minutes, followed by a 10-minute rinse (95% B), and a 10-minute column re-equilibration.

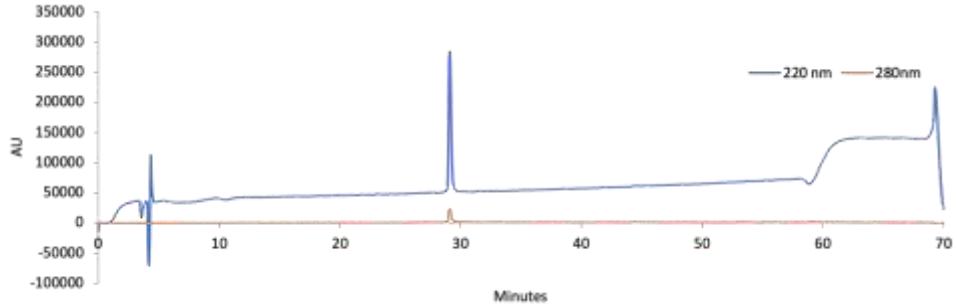

Figure S110. Analytical HPLC Data for variant **sd7*f*/10*b*'-z4y4** (QX3101s). Protein solution was injected onto a C18 analytical column and eluted using a linear gradient of 10-60% B (A = H_2O, 0.1% TFA; B = MeCN, 0.1% TFA) over 50 minutes, followed by a 10-minute rinse (95% B), and a 10-minute column re-equilibration.

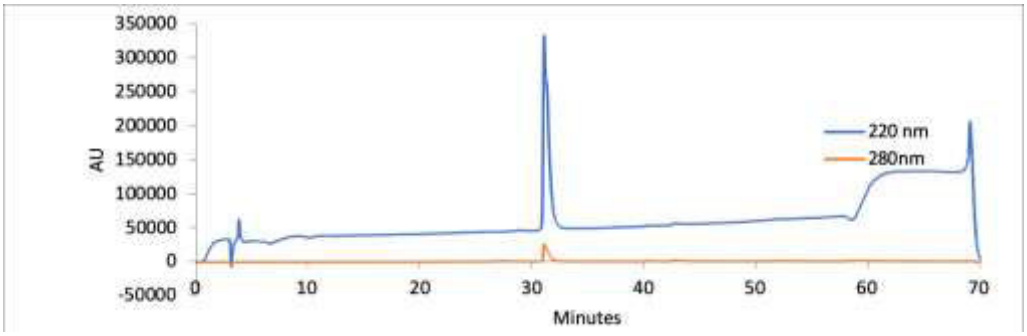

Figure S111. Analytical HPLC Data for coiled-coil variant **sd27*e*/29*g*'-x4x** (QX2283). Protein solution was injected onto a C18 analytical column and eluted using a linear gradient of 10-60% B (A = H_2O, 0.1% TFA; B = MeCN, 0.1% TFA) over 50 minutes, followed by a 10-minute rinse (95% B), and a 10-minute column re-equilibration.

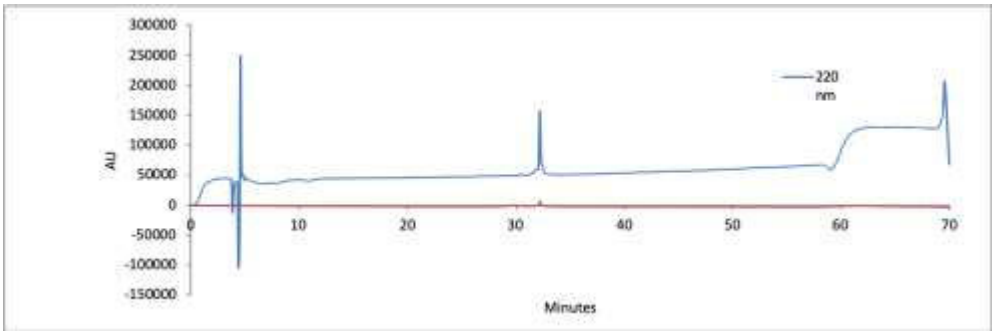

Figure S112. Analytical HPLC Data for variant **sd27e/29e'-x4px** (QX3079). Protein solution was injected onto a C18 analytical column and eluted using a linear gradient of 10-60% B (A = H_2O, 0.1% TFA; B = MeCN, 0.1% TFA) over 50 minutes, followed by a 10-minute rinse (95% B), and a 10-minute column re-equilibration.

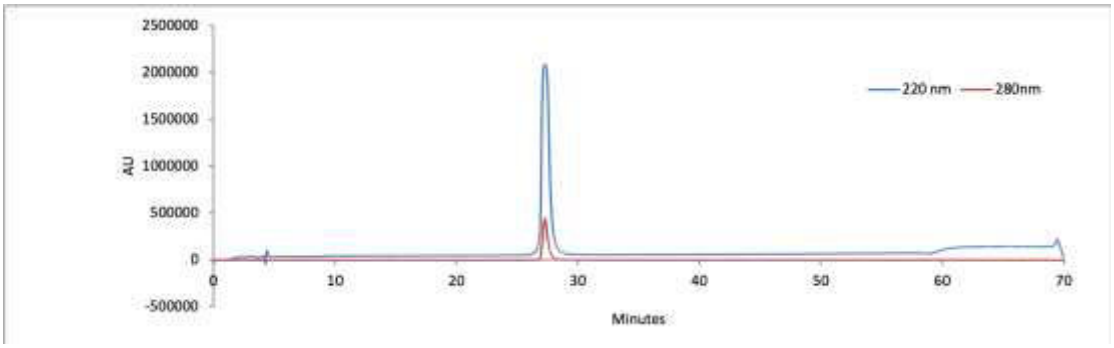

Figure S113. Analytical HPLC Data for native affibody **a** (CD1054). Protein solution was injected onto a C18 analytical column and eluted using a linear gradient of 10-60% B (A = H2O, 0.1% TFA; B = MeCN, 0.1% TFA) over 50 minutes, followed by a 10-minute rinse (95% B), and a 10-minute column re-equilibration.

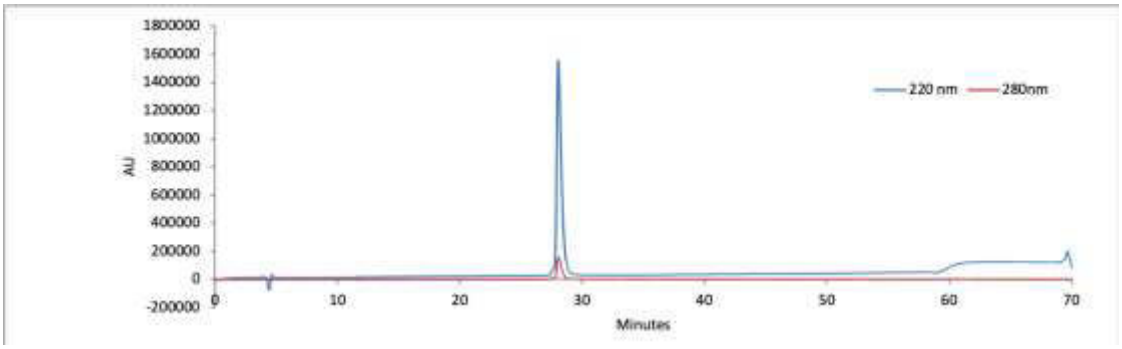

Figure S114. Analytical HPLC Data for affibody variant **a8/42-xx** (QX3102). Protein solution was injected onto a C18 analytical column and eluted using a linear gradient of 10-60% B (A = H2O, 0.1% TFA; B = MeCN, 0.1% TFA) over 50 minutes, followed by a 10-minute rinse (95% B), and a 10-minute column re-equilibration.

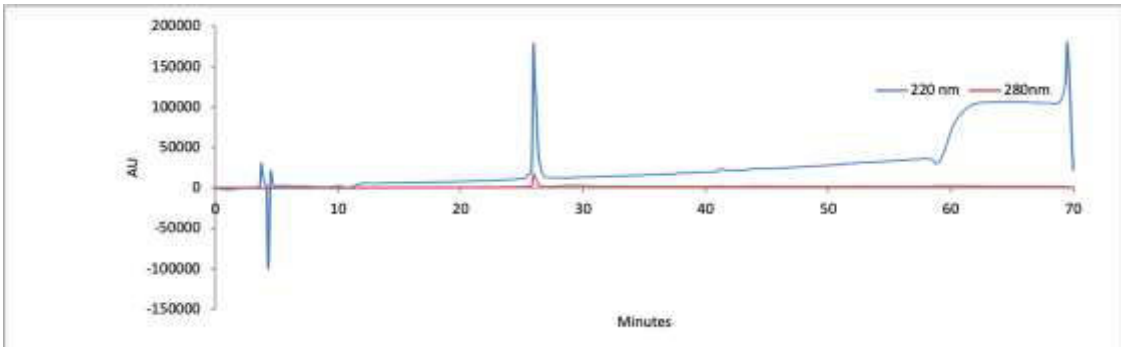

Figure S115. Analytical HPLC Data for stapled affibody variant **sa8/42-x4x** (QX3106). Protein solution was injected onto a C18 analytical column and eluted using a linear gradient of 10-60% B (A = H2O, 0.1% TFA; B = MeCN, 0.1% TFA) over 50 minutes, followed by a 10-minute rinse (95% B), and a 10-minute column re-equilibration.

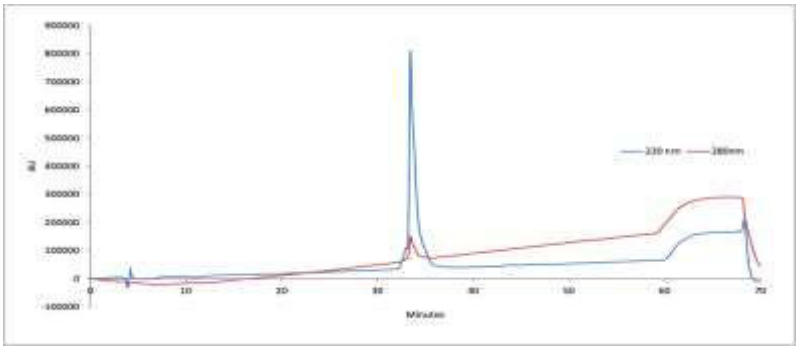

Figure S116. Analytical HPLC Data for fluorescent affibody variant **fa** (ZJ10611). Protein solution was injected onto a C18 analytical column and eluted using a linear gradient of 10-60% B (A = H2O, 0.1% TFA; B = MeCN, 0.1% TFA) over 50 minutes, followed by a 10-minute rinse (95% B), and a 10-minute column re-equilibration.

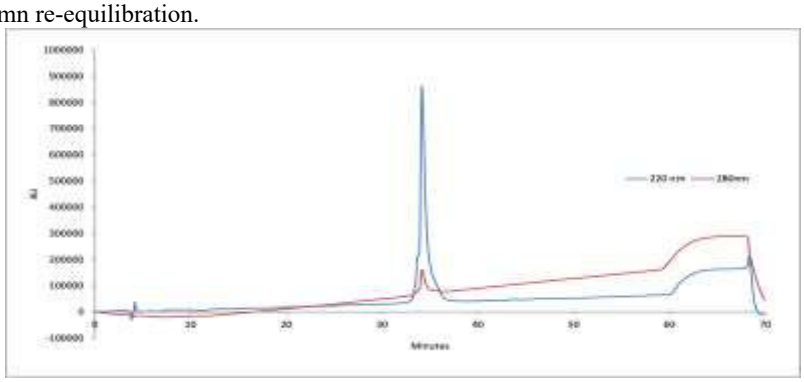

Figure S117. Analytical HPLC Data for fluorescent affibody f variant **fa8/42-xx** (ZJ10612). Protein solution was injected onto a C18 analytical column and eluted using a linear gradient of 10-60% B (A = H2O, 0.1% TFA; B = MeCN, 0.1% TFA) over 50 minutes, followed by a 10-minute rinse (95% B), and a 10-minute column re-equilibration.

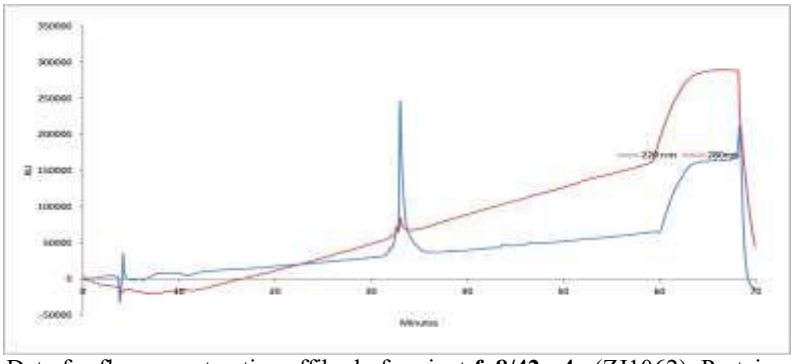

Figure S118. Analytical HPLC Data for fluorescent native affibody f variant **fa8/42-x4x** (ZJ1062). Protein solution was injected onto a C18 analytical column and eluted using a linear gradient of 10-60% B (A = H2O, 0.1% TFA; B = MeCN, 0.1% TFA) over 50 minutes, followed by a 10-minute rinse (95% B), and a 10-minute column re-equilibration.

5. Global Fitting of Variable Temperature CD Data

The conformational stability of stapled variants and their non-stapled counterparts was assessed by variable-temperature circular dichroism spectropolarimetry. Data from three replicate variable temperature CD experiments were each fit globally to a model for a two-state thermally induced unfolding transition using the program Mathematica (Wolfram Research). We used a model based on two-state monomer folding/unfolding equilibrium for stapled coiled-coil variants **sd20*e*/22*g*'-z4x**, **sd13*e*/15*g*'-z4x**, **sd6*e*/8*g*'-z4x**, **sd27*e*/22*g*'-z4x**, **sd6*e*/1*g*'-z4x**, **sd27*e*/29*g*'-z2x**, **sd27*e*/22*g*'-z2x**, **sd24*b*/25*c*'-z4x**, **sd24*b*/25*c*'-z4y4**, **sd7*f*/10*b*'-z4x**, **sd7*f*/10*b*'-z4y4**, **sd27*e*/29*g*'-x4x**, **sd27*e*/29*g*'-x4px**, and (***R***,***S***)-**sd27*e*/29*g*'-x4x**; for their non-stapled counterparts variants **d20*e*/22*g*'-z4x**, **d13*e*/15*g*'-z4x**, **d6*e*/8*g*'-z4x**, **d27*e*/22*g*'-z4x**, **d6*e*/1*g*'-z4x**, **d27*e*/29*g*'-z2x**, **d27*e*/22*g*'-z2x**, **d24*b*/25*c*'-z4x**, **d24*b*/25*c*'-z4y4**, **d7*f*/10*b*'-z4x**, **d7*f*/10*b*'-z4y4**, **d27*e*/29*g*'-xx**, and (***R***,***S***)-**d27*e*/29*g*'-xx**; for stapled HER2 affibody **sa8/42-xx**; for its non-stapled counterpart **a8/42-x4x**; and for native HER2 affibody **a**. This model is described in equation S1:

$$[\theta] = \frac{[K\cdot(a_n+b_n\cdot T)+(c_n+d_n\cdot T)]}{1+K}, \quad \text{(S1)}$$

where T is temperature in Kelvin, a_n is the *y*-intercept and b_n is the slope of the pre-transition baseline for melt *n* (a_1 and b_1 for replicate 1, a_2 and b_2 for replicate 2, a_3 and b_3 for replicate 3, etc.); c_n is the *y*-intercept and d_n is the slope of the post-transition baseline for replicate *n* (c_1 and d_1 for replicate 1, c_2 and d_2 for replicate 2, c_3 and d_3 for replicate 3, etc.); and K is the temperature-dependent folding equilibrium constant. K is related to the temperature-dependent free energy of folding ΔG according to the following equation:

$$K = \exp\left[-\frac{\Delta G}{RT}\right], \quad \text{(S2)}$$

where R is the universal gas constant (0.0019872 kcal/mol/K). ΔG is a function of temperature, as shown in the following equation:

$$\Delta G = \frac{\Delta H_0\cdot(T_m-T)}{T_m} + \Delta C_p\cdot(T - T_m - T\cdot\ln\left[\frac{T}{T_m}\right]), \quad \text{(S3)}$$

where T_m is the midpoint of the unfolding transition and the temperature at which $\Delta G_f = 0$; ΔH_0 is the change in enthalpy upon folding at $T = T_m$; and ΔC_p is the change in heat capacity upon folding. In some cases, we found that some fit parameters had sufficiently high standard errors as to render them indistinguishable from zero and therefore not essential to the fit (as judged by their p-values). When this occurred, we repeated the fitting process without the non-essential parameters. We used the fit parameters for each variant to calculate the ΔG values given in the main text; we calculated the uncertainty for each ΔG value by propagation of error using the standard errors of the fit parameters.

Molar ellipticity data at 222 nm ($[\theta]_{222}$), melting temperatures (T_m), and folding free energies ΔG for variants **d27*e*/29*g*'-z4x** and **sd27*e*/29*g*'-z4x**; **d27*e*/22*g*'-z4x** and **sd27*e*/22*g*'-z4x**; **d24*b*/25*c*'-z4x** and **sd24*b*/25*c*'-z4x**; **d20*e*/22*g*'-z4x** and **sd20*e*/22*g*'-z4x**; **d13*e*/15*g*'-z4x** and **sd13*e*/15*g*'-z4x**; **d6*e*/8*g*'-z4x** and **sd6*e*/8*g*'-z4x**; **d6*e*/1*g*'-z4x** and **sd6*e*/1*g*'-z4x**; **d27*e*/29*g*'-z2x** and **sd27*e*/29*g*'-z2x**; **d27*e*/22*g*'-z2x** and **sd27*e*/22*g*'-z2x**; **d24*b*/25*c*'-z4y4** and **sd24*b*/25*c*'-z4y4**; **d7*f*/10*b*'-z4x** and **sd7*f*/10*b*'-z4x**; **d7*f*/10*b*'-z4y4** and **sd7*f*/10*b*'-z4y4**; **d27*e*/29*g*'-xx**, **sd27*e*/29*g*'-x4x**, and **sd27*e*/29*g*'-x4px**; and HER2 affibody variants **a**, **a8/42-xx** and **sa8/42-x4x** are given in Table S2. $[\theta]_{222}$ is a well-known indicator of α-helical secondary structure, whereas T_m values are indicators of tertiary/quaternary structural stability. Values of the ratio $[\theta]_{222}/[\theta]_{208}$ near 1.1 are also considered diagnostic of coiled-coil tertiary/quaternary structures. However, we were not able to measure $[\theta]_{208}$ due to the excessively high dynode values we observed at wavelengths less than 210 nm in solutions of these variants in 20 mM phosphate buffer (pH 7) + 4 M guanidinium chloride (which was necessary to observe complete or nearly complete thermal unfolding transitions). Therefore, our assessment of coiled-coil tertiary structural stability must rely on T_m values alone.

$[\theta]_{222}$ values for these variants are consistent with α-helical secondary structure and T_m values are consistent with coiled-coil tertiary structure. However, the magnitude of $[\theta]_{222}$ varies widely from variant to variant and is not well correlated with T_m (Figure S113). Increases in T_m associated with PEG stapling are sometimes associated with increases in $[\theta]_{222}$ (compare variants **d27*e*/29*g*'-z4x** vs. **sd27*e*/29*g*'-z4x**; **d20*e*/22*g*'-z4x** vs. **sd20*e*/22*g*'-z4x**; **d13*e*/15*g*'-z4x** vs. **sd13*e*/15*g*'-z4x**; **d27*e*/22*g*'-z4x** vs. **sd27*e*/22*g*'-z4x**; **d6*e*/1*g*'-z4x** vs. **sd6*e*/1*g*'-z4x**; **d7*f*/10*b*'-z4y4** vs. **sd7*f*/10*b*'-z4y4**; **d27*e*/22*g*'-z4x** vs. **sd27*e*/22*g*'-z4x**; and **d27*e*/29*g*'-xx** vs. **sd27*e*/29*g*'-x4x**), but not always (compare variants **d6*e*/8*g*'-z4x** vs. **sd6*e*/8*g*'-z4x**; **d7*f*/10*b*'-z4x** vs. **sd7*f*/10*b*'-z4x**; **sd27*e*/29*g*'-x4px** vs. **sd27*e*/29*g*'-x4x**; and **a8/42-xx** vs. **sa8/42-x4x**). This observation is interesting because it is generally accepted that α-helical secondary structure forms concomitantly with coiled-coil association: that is, individual subunits are only α-helical within the coiled-coil assembly, not on their own. It is possible that the covalent linkages between helices in the disulfide-bound coiled-coil variants and their stapled counterparts attenuate the connection between secondary and tertiary structural stability. However, we previously[3] observed a similar lack of correlation between $[\theta]_{222}$ and T_m values in a study of non-stapled non-disulfide-bound trimeric α-helical coiled coils. Despite this anomaly, crystallography confirmed that these previously characterized variants adopted their intended trimeric coiled-coil quaternary structures. Therefore, we believe that the lack of correlation we observed here between $[\theta]_{222}$ and T_m, while interesting, does not substantially change the conclusions

described in the main text.

CD spectra and variable temperature CD data for each variant are shown in Figures S114–S143, along with the fit parameters ± standard error. Standard parameter errors were used to estimate the uncertainty in the thermodynamic values given in the main text by propagation of error.

Table S2. Molar ellipticity, melting temperatures and folding free energies for non-stapled variants and their PEG-stapled counterparts.[a]

Protein	Distance between staple positions (Å)	Calculated Staple Length (Å)	$[\theta]_{222}$ (deg cm^2 dmol^{-1} x 10^3)	T_m (°C)	Impact of Stapling		
					ΔΔG (kcal/mol)	ΔΔH (kcal/mol)	-TΔΔS (kcal/mol)
d27*e*/29*g*'-z4x			-24.6	41.1 ± 0.2			
sd27*e*/29*g*'-z4x	9.2	18.5	-34.5	48.2 ± 0.1	-0.65 ± 0.02	1.3 ± 0.6	-1.9 ± 0.6
d20*e*/22*g*'-z4x			-24.0	41.8 ± 0.2			
sd20*e*/22*g*'-z4x	9.2	18.5	-31.3	54.3 ± 0.1	-1.09 ± 0.02	1.6 ± 0.6	-2.7 ± 0.6
d13*e*/15*g*'-z4x			-28.2	42.4 ± 0.1			
sd13*e*/15*g*'-z4x	9.7	18.5	-29.7	57.7 ± 0.1	-1.33 ± 0.02	2.1 ± 0.5	-3.4 ± 0.5
d6*e*/8*g*'-z4x			-31.6	39.5 ± 0.2			
sd6*e*/8*g*'-z4x	10.6	18.5	-18.2	69.1 ± 0.1	-2.53 ± 0.04	-1.9 ± 0.6	-0.7 ± 0.6
d27*e*/22*g*'-z4x			-22.5	43.2 ± 0.1			
sd27*e*/22*g*'-z4x	6.3	18.5	-40.4	63.6 ± 0.1	-2.01 ± 0.02	-2.7 ± 0.5	0.6 ± 0.5
d6*e*/1*g*'-z4x			-24.7	45.0 ± 0.1			
sd6*e*/1*g*'-z4x	6.0	18.5	-27.6	73.7 ± 0.2	-2.30 ± 0.04	1.7 ± 0.6	-4.0 ± 0.6
d24*b*/25*c*'-z4x			-38.0	43.4 ± 0.1			
sd24*b*/25*c*'-z4x	14.3	18.5	-11.4	33.0 ± 0.2	0.65 ± 0.02	8.1 ± 0.5	-7.4 ± 0.5
d7*f*/10*b*'-z4x			-24.9	42.6 ± 0.2			
sd7*f*/10*b*'-z4x	15.6	18.5	-11.1	51.4 ± 0.3	-0.61 ± 0.03	8.8 ± 0.9	-9.4 ± 0.9
d24*b*/25*c*'-z4y4			-21.3	46.5 ± 0.1			
sd24*b*/25*c*'-z4y4	14.3	28.5	-16.5	44.5 ± 0.2	0.17 ± 0.02	0.8 ± 0.6	-0.6 ± 0.6
d7*f*/10*b*'-z4y4			-16.4	43.7 ± 0.2			
sd7*f*/10*b*'-z4y4	15.6	28.5	-30.2	54.2 ± 0.2	-0.68 ± 0.01	6.6 ± 0.6	-7.2 ± 0.6
d27*e*/29*g*'-z2x			-24.2	38.8 ± 0.2			
sd27*e*/29*g*'-z2x	9.2	8.1	-16.3	33.7 ± 0.1	0.31 ± 0.01	6.1 ± 0.4	-5.8 ± 0.4
d27*e*/22*g*'-z2x			-20.4	43.4 ± 0.1			
sd27*e*/22*g*'-z2x	6.3	8.1	-23.1	64.9 ± 0.3	-2.04 ± 0.03	-0.5 ± 0.6	-1.5 ± 0.6
d27*e*/29*g*'-xx			-22.4	39.8 ± 0.2			
sd27*e*/29*g*'-x4x	9.2	19.3	-52.2	52.9 ± 0.2	-1.08 ± 0.03	-2.0 ± 0.5	0.9 ± 0.5
sd27*e*/29*g*'-x4px			-28.1	53.4 ± 0.1	-1.21 ± 0.02	-4.1 ± 0.5	2.9 ± 0.5
affibody a			-7.0	66.4 ± 0.2			
a8/42-xx	7.4	19.3	-38.5	60.9 ± 0.1	0.64 ± 0.02	-2.1 ± 1.1	2.8 ± 1.1
sa8/42-x4x			-16.1	76.1 ± 0.1	-1.09 ± 0.03	3.5 ± 1.3	-4.6 ± 1.3

[a]Distance between staple positions for each variant were calculated by measuring the distance between the centers of mass of the corresponding side chains in the crystal structure of the parent disulfide-bound coiled-coil heterodimer **dA/B** (PDB ID: 1KD9). Calculated staple length measured from β-carbon to β-carbon within model staple structures (see supporting information) optimized in Gaussian 16 using density functional theory APFD and the 6-31G+d,p basis set. ΔΔG, ΔΔH, and -TΔΔS values for each variant are given ± std. error in kcal/mol at the melting temperature of its corresponding non-stapled counterpart at 15 μM protein concentration in 20 mM sodium phosphate buffer (pH 7) + 4.0 M GdnHCl, except for affibody **a**, non-stapled **a8/42-xx**, and stapled **sa8/42-x4x**, which were characterized without denaturant.

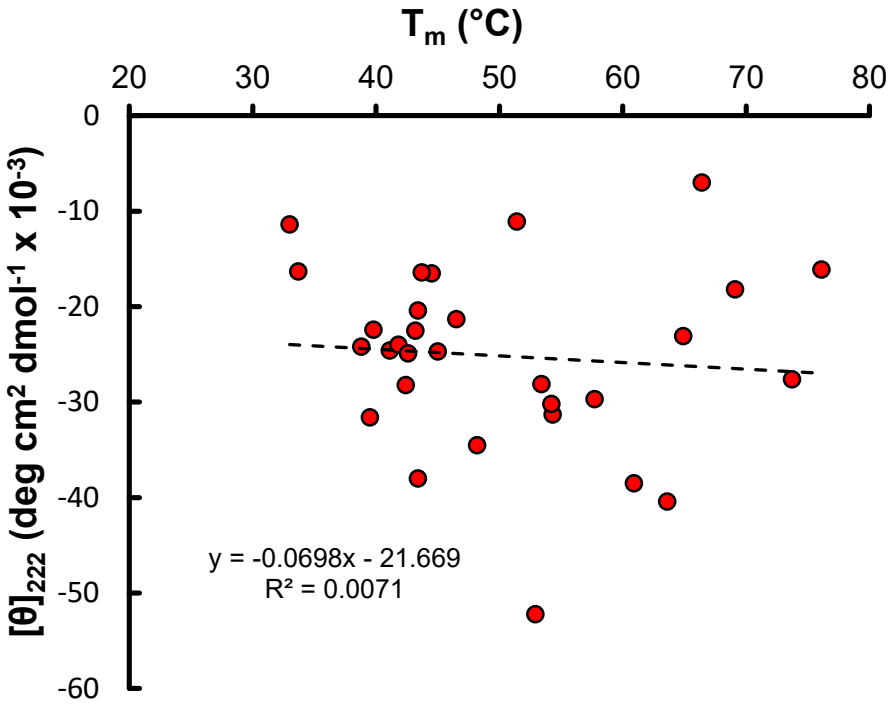

Figure S119. Plot of $[\theta]_{222}$ vs. melting temperature for variants **d27*e*/29*g*'-z4x** and **sd27*e*/29*g*'-z4x; d27*e*/22*g*'-z4x** and **sd27*e*/22*g*'-z4x; d24*b*/25*c*'-z4x** and **sd24*b*/25*c*'-z4x; d20*e*/22*g*'-z4x** and **sd20*e*/22*g*'-z4x; d13*e*/15*g*'-z4x** and **sd13*e*/15*g*'-z4x; d6*e*/8*g*'-z4x** and **sd6*e*/8*g*'-z4x; d6*e*/1*g*'-z4x** and **sd6*e*/1*g*'-z4x; d27*e*/29*g*'-z2x** and **sd27*e*/29*g*'-z2x; d27*e*/22*g*'-z2x** and **sd27*e*/22*g*'-z2x; d24*b*/25*c*'-z4y4** and **sd24*b*/25*c*'-z4y4; d7*f*/10*b*'-z4x** and **sd7*f*/10*b*'-z4x; d7*f*/10*b*'-z4y4** and **sd7*f*/10*b*'-z4y4; d27*e*/29*g*'-xx, sd27*e*/29*g*'-x4x,** and **sd27*e*/29*g*'-x4px;** and HER2 affibody variants **a**, **a8/42-xx** and **sa8/42-x4x**.

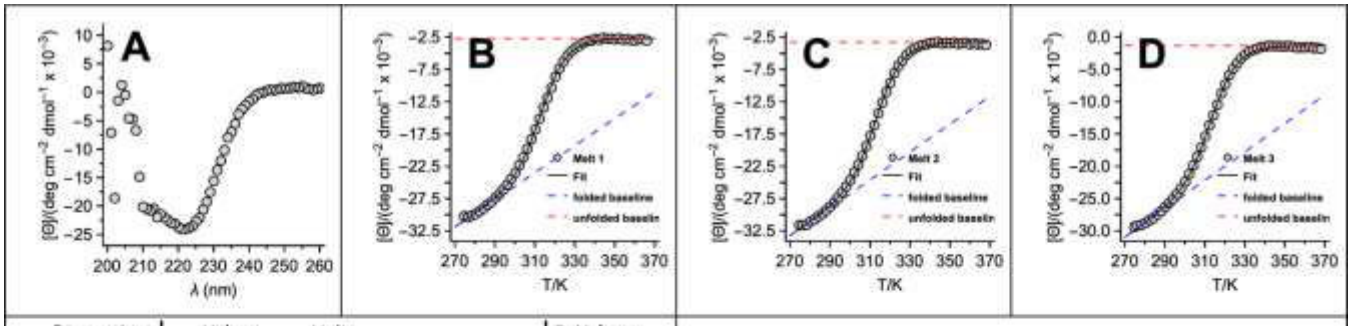

Parameters	Values	Units	P–Values
ΔH_0	−30.27 ± 0.43	kcal/mol	<0.001
T_m	41.8 ± 0.2	°C	<0.001
ΔC_p	---	---	---
a1	−88.5 ± 2.2	deg cm^{-2} dmol^{-1} x 10^{-3}	<0.001
b1	0.210 ± 0.008	deg cm^{-2} dmol^{-1} K^{-1} x 10^{-3}	<0.001
c1	−2.66 ± 0.06	deg cm^{-2} dmol^{-1} x 10^{-3}	<0.001
d1	---	---	---
a2	−91.5 ± 2.2	deg cm^{-2} dmol^{-1} x 10^{-3}	<0.001
b2	0.216 ± 0.008	deg cm^{-2} dmol^{-1} K^{-1} x 10^{-3}	<0.001
c2	−3.27 ± 0.05	deg cm^{-2} dmol^{-1} x 10^{-3}	<0.001
d2	---	---	---
a3	−90.4 ± 2.2	deg cm^{-2} dmol^{-1} x 10^{-3}	<0.001
b3	0.220 ± 0.008	deg cm^{-2} dmol^{-1} K^{-1} x 10^{-3}	<0.001
c3	−1.30 ± 0.05	deg cm^{-2} dmol^{-1} x 10^{-3}	<0.001
d3	---	---	---

$R^2 = 0.99984$
sum residuals^2 = 6.72397

For **d20*e*/22*g*'–z4x**, at 315.0 K,
$\Delta G = 0.00 \pm 0.02$ kcal/mol
$\Delta H = -30.3 \pm 0.4$ kcal/mol
$-T\Delta S = 30.3 \pm 0.4$ kcal/mol

Figure S120. (A) CD spectra and (B–D) variable temperature CD data (triplicate) for 15 μM disulfide-bound coiled-coil variant **d20*e*/22*g*'-z4x** (ZJ10511) in 20 mM sodium phosphate (pH 7) with 4 M GdnHCl. Fit parameters from eq. S1–S3 appear in the table, as do calculated values of ΔG_f, ΔH_f, and $-T\Delta S_f \pm$ standard error at the indicated temperature.

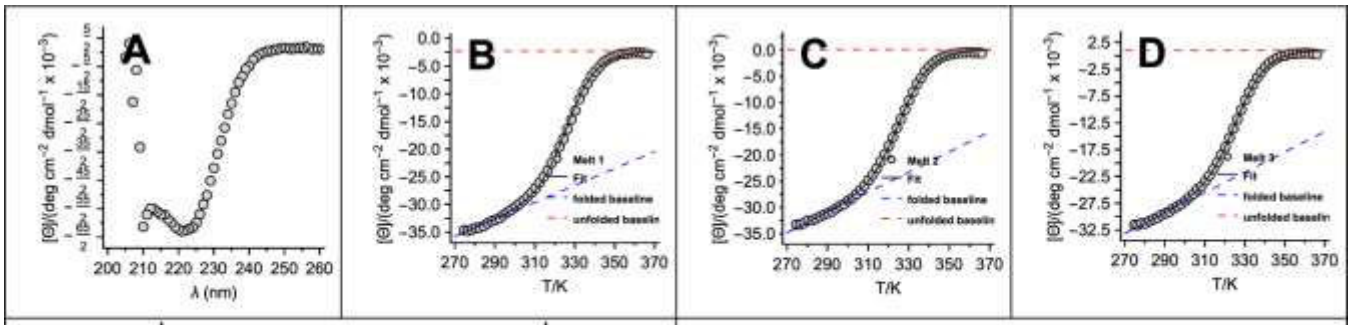

Parameters	Values	Units	P–Values
ΔH_0	−28.63 ± 0.40	kcal/mol	<0.001
T_m	54.3 ± 0.1	°C	<0.001
ΔC_p	---	---	---
a1	−77.0 ± 1.7	deg cm^{-2} dmol^{-1} x 10^{-3}	<0.001
b1	0.153 ± 0.006	deg cm^{-2} dmol^{-1} K^{-1} x 10^{-3}	<0.001
c1	−2.24 ± 0.09	deg cm^{-2} dmol^{-1} x 10^{-3}	<0.001
d1	---	---	---
a2	−86.7 ± 1.7	deg cm^{-2} dmol^{-1} x 10^{-3}	<0.001
b2	0.192 ± 0.006	deg cm^{-2} dmol^{-1} K^{-1} x 10^{-3}	<0.001
c2	0.12 ± 0.09	deg cm^{-2} dmol^{-1} x 10^{-3}	0.161
d2	---	---	---
a3	−84.3 ± 1.6	deg cm^{-2} dmol^{-1} x 10^{-3}	<0.001
b3	0.190 ± 0.006	deg cm^{-2} dmol^{-1} K^{-1} x 10^{-3}	<0.001
c3	1.08 ± 0.09	deg cm^{-2} dmol^{-1} x 10^{-3}	<0.001
d3	---	---	---

$R^2 = 0.99986$
sum residuals^2 = 9.04439

For **sd20e/22g'–z4x**, at 315.0 K,
$\Delta G = -1.09 \pm 0.02$ kcal/mol
$\Delta H = -28.6 \pm 0.4$ kcal/mol
$-T\Delta S = 27.5 \pm 0.4$ kcal/mol

Figure S121. (A) CD spectra and (B–D) variable temperature CD data (triplicate) for 15 μM stapled disulfide-bound coiled-coil variant **sd20*e*/22*g*'-z4x** (ZJ10511s) in 20 mM sodium phosphate (pH 7) with 4 M GdnHCl. Fit parameters from eq. S1–S3 appear in the table, as do calculated values of ΔG_f, ΔH_f, and $-T\Delta S_f \pm$ standard error at the indicated temperature.

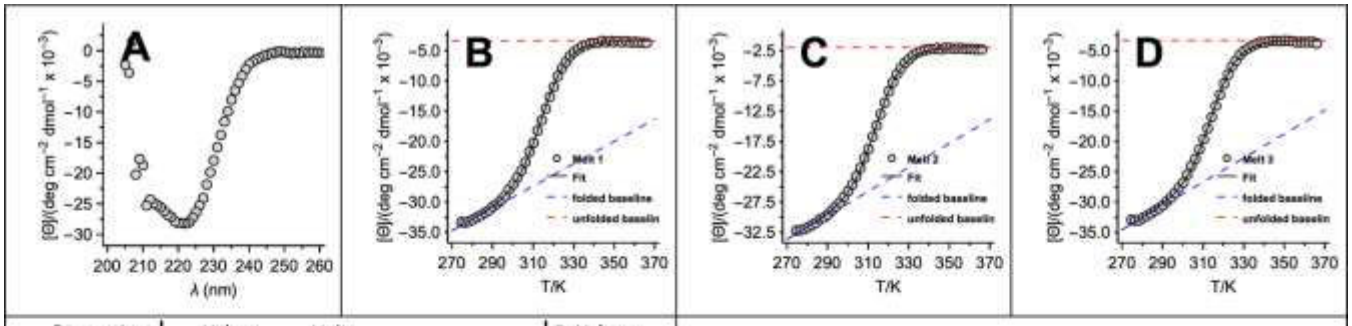

Parameters	Values	Units	P–Values
ΔH_0	−30.82 ± 0.38	kcal/mol	<0.001
T_m	42.4 ± 0.1	°C	<0.001
ΔC_p	---	---	---
a1	−84.5 ± 2.1	deg cm^{-2} dmol^{-1} x 10^{-3}	<0.001
b1	0.184 ± 0.007	deg cm^{-2} dmol^{-1} K^{-1} x 10^{-3}	<0.001
c1	−3.32 ± 0.06	deg cm^{-2} dmol^{-1} x 10^{-3}	<0.001
d1	---	---	---
a2	−87.1 ± 2.1	deg cm^{-2} dmol^{-1} x 10^{-3}	<0.001
b2	0.198 ± 0.007	deg cm^{-2} dmol^{-1} K^{-1} x 10^{-3}	<0.001
c2	−1.92 ± 0.06	deg cm^{-2} dmol^{-1} x 10^{-3}	<0.001
d2	---	---	---
a3	−88.0 ± 2.1	deg cm^{-2} dmol^{-1} x 10^{-3}	<0.001
b3	0.198 ± 0.007	deg cm^{-2} dmol^{-1} K^{-1} x 10^{-3}	<0.001
c3	−3.25 ± 0.06	deg cm^{-2} dmol^{-1} x 10^{-3}	<0.001
d3	---	---	---

$R^2 = 0.99987$
sum residuals^2 = 6.49581

For **d13*e*/15*g*'–z4x**, at 315.5 K,
$\Delta G = 0.00 \pm 0.01$ kcal/mol
$\Delta H = -30.8 \pm 0.4$ kcal/mol
$-T\Delta S = 30.8 \pm 0.4$ kcal/mol

Figure S122. (A) CD spectra and (B–D) variable temperature CD data (triplicate) for 15 μM disulfide-bound coiled-coil variant **d13*e*/15*g*'-z4x** (QX31171) in 20 mM sodium phosphate (pH 7) with 4 M GdnHCl. Fit parameters from eq. S1–S3 appear in the table, as do calculated values of ΔG_f, ΔH_f, and $-T\Delta S_f \pm$ standard error at the indicated temperature.

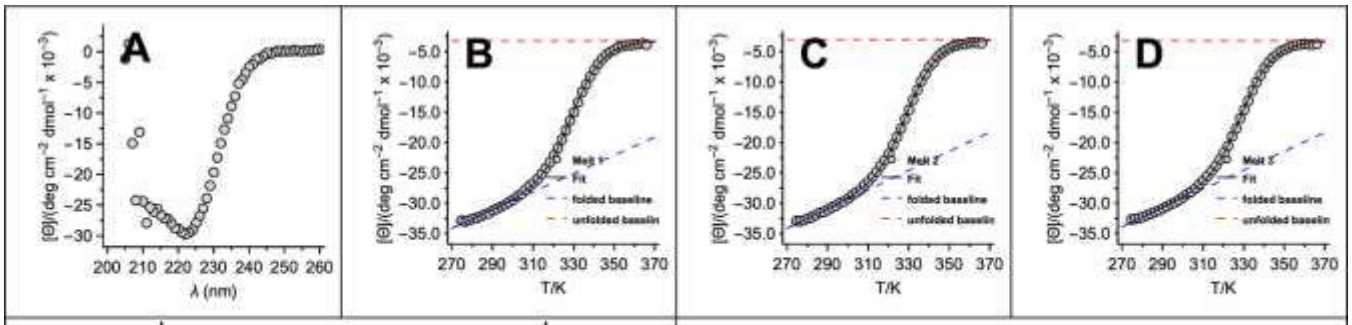

Parameters	Values	Units	P–Values
ΔH_0	−28.71 ± 0.31	kcal/mol	<0.001
T_m	57.7 ± 0.1	°C	<0.001
ΔC_p	---	---	---
a1	−74.9 ± 1.0	deg cm^{-2} dmol^{-1} x 10^{-3}	<0.001
b1	0.151 ± 0.003	deg cm^{-2} dmol^{-1} K^{-1} x 10^{-3}	<0.001
c1	−3.18 ± 0.07	deg cm^{-2} dmol^{-1} x 10^{-3}	<0.001
d1	---	---	---
a2	−77.0 ± 1.0	deg cm^{-2} dmol^{-1} x 10^{-3}	<0.001
b2	0.159 ± 0.003	deg cm^{-2} dmol^{-1} K^{-1} x 10^{-3}	<0.001
c2	−2.95 ± 0.07	deg cm^{-2} dmol^{-1} x 10^{-3}	<0.001
d2	---	---	---
a3	−75.8 ± 1.0	deg cm^{-2} dmol^{-1} x 10^{-3}	<0.001
b3	0.155 ± 0.003	deg cm^{-2} dmol^{-1} K^{-1} x 10^{-3}	<0.001
c3	−3.16 ± 0.07	deg cm^{-2} dmol^{-1} x 10^{-3}	<0.001
d3	---	---	---

$R^2 = 0.99994$
sum residuals^2 = 4.08798

For **sd13e/15g'–z4x**, at 315.5 K,
$\Delta G = -1.33 \pm 0.02$ kcal/mol
$\Delta H = -28.7 \pm 0.3$ kcal/mol
$-T\Delta S = 27.4 \pm 0.3$ kcal/mol

Figure S123. (A) CD spectra and (B–D) variable temperature CD data (triplicate) for 15 μM stapled disulfide-bound coiled-coil variant **sd13*e*/15*g*'-z4x** (QX31171s) in 20 mM sodium phosphate (pH 7) with 4 M GdnHCl. Fit parameters from eq. S1–S3 appear in the table, as do calculated values of ΔG_f, ΔH_f, and $-T\Delta S_f \pm$ standard error at the indicated temperature.

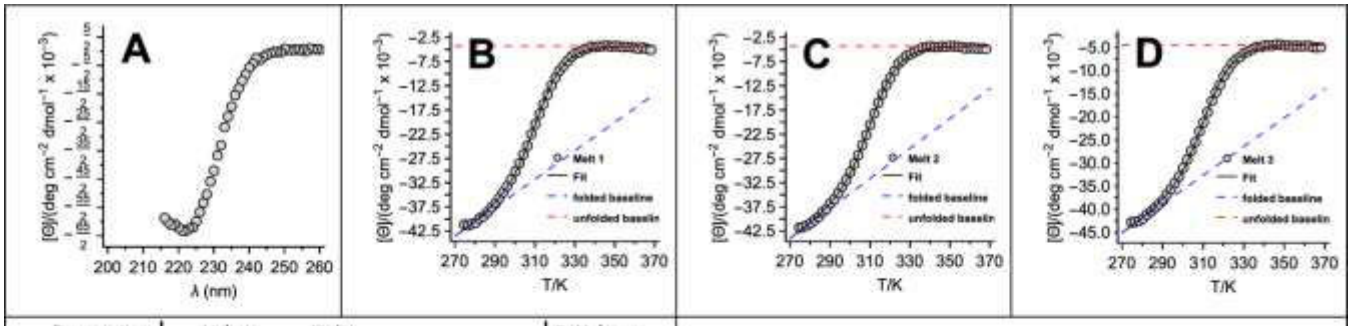

Parameters	Values	Units	P–Values
ΔH_0	−27.33 ± 0.40	kcal/mol	<0.001
T_m	39.5 ± 0.2	°C	<0.001
ΔC_p	---	---	---
a1	−123.0 ± 3.7	deg cm^{-2} dmol^{-1} x 10^{-3}	<0.001
b1	0.294 ± 0.013	deg cm^{-2} dmol^{-1} K^{-1} x 10^{-3}	<0.001
c1	−4.24 ± 0.07	deg cm^{-2} dmol^{-1} x 10^{-3}	<0.001
d1	---	---	---
a2	−127.8 ± 3.7	deg cm^{-2} dmol^{-1} x 10^{-3}	<0.001
b2	0.310 ± 0.013	deg cm^{-2} dmol^{-1} K^{-1} x 10^{-3}	<0.001
c2	−4.25 ± 0.07	deg cm^{-2} dmol^{-1} x 10^{-3}	<0.001
d2	---	---	---
a3	−129.0 ± 3.8	deg cm^{-2} dmol^{-1} x 10^{-3}	<0.001
b3	0.311 ± 0.013	deg cm^{-2} dmol^{-1} K^{-1} x 10^{-3}	<0.001
c3	−4.43 ± 0.07	deg cm^{-2} dmol^{-1} x 10^{-3}	<0.001
d3	---	---	---

$R^2 = 0.99983$
sum residuals^2 = 12.65339

For **d6e/8g'–z4x**, at 312.6 K,
$\Delta G = 0.00 \pm 0.02$ kcal/mol
$\Delta H = -27.3 \pm 0.4$ kcal/mol
$-T\Delta S = 27.3 \pm 0.4$ kcal/mol

Figure S124. (A) CD spectra and (B–D) variable temperature CD data (triplicate) for 15 μM disulfide-bound coiled-coil variant **d6*e*/8*g*'-z4x** (QX2292) in 20 mM sodium phosphate (pH 7) with 4 M GdnHCl. Fit parameters from eq. S1–S3 appear in the table, as do calculated values of ΔG_f, ΔH_f, and $-T\Delta S_f$ ± standard error at the indicated temperature.

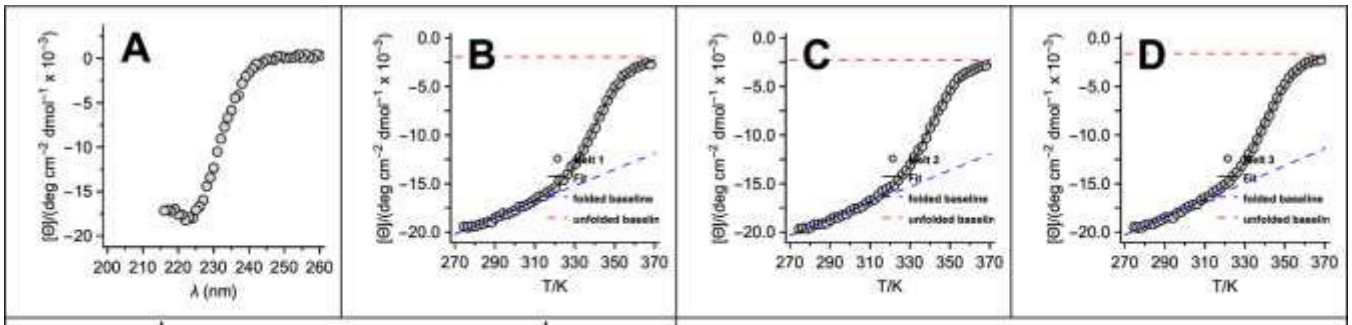

Parameters	Values	Units	P–Values
ΔH_0	−29.20 ± 0.49	kcal/mol	<0.001
T_m	69.1 ± 0.1	°C	<0.001
ΔC_p	---	---	---
a1	−42.7 ± 0.6	deg cm^{-2} dmol^{-1} x 10^{-3}	<0.001
b1	0.083 ± 0.002	deg cm^{-2} dmol^{-1} K^{-1} x 10^{-3}	<0.001
c1	−1.93 ± 0.08	deg cm^{-2} dmol^{-1} x 10^{-3}	<0.001
d1	---	---	---
a2	−43.0 ± 0.6	deg cm^{-2} dmol^{-1} x 10^{-3}	<0.001
b2	0.084 ± 0.002	deg cm^{-2} dmol^{-1} K^{-1} x 10^{-3}	<0.001
c2	−2.23 ± 0.08	deg cm^{-2} dmol^{-1} x 10^{-3}	<0.001
d2	---	---	---
a3	−44.3 ± 0.6	deg cm^{-2} dmol^{-1} x 10^{-3}	<0.001
b3	0.089 ± 0.002	deg cm^{-2} dmol^{-1} K^{-1} x 10^{-3}	<0.001
c3	−1.55 ± 0.08	deg cm^{-2} dmol^{-1} x 10^{-3}	<0.001
d3	---	---	---

$R^2 = 0.99991$
sum residuals^2 = 2.62711

For **sd6e/8g'–z4x**, at 312.6 K,
$\Delta G = -2.53 \pm 0.04$ kcal/mol
$\Delta H = -29.2 \pm 0.5$ kcal/mol
$-T\Delta S = 26.7 \pm 0.5$ kcal/mol

Figure S125. (A) CD spectra and (B–D) variable temperature CD data (triplicate) for 15 μM stapled disulfide-bound coiled-coil variant **sd6*e*/8*g*'-z4x** (QX2292s) in 20 mM sodium phosphate (pH 7) with 4 M GdnHCl. Fit parameters from eq. S1–S3 appear in the table, as do calculated values of ΔG_f, ΔH_f, and $-T\Delta S_f$ ± standard error at the indicated temperature.

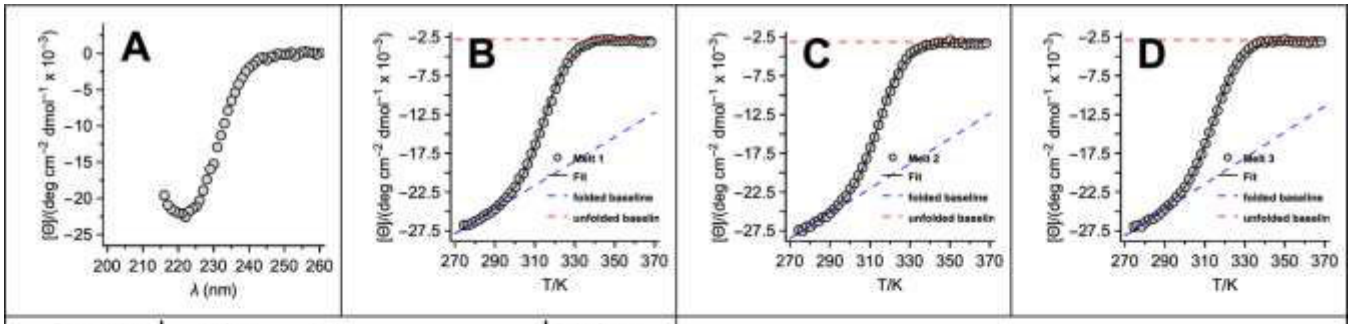

Parameters	Values	Units	P–Values
ΔH_0	−30.68 ± 0.40	kcal/mol	<0.001
T_m	43.2 ± 0.2	°C	<0.001
ΔC_p	---	---	---
a1	−70.0 ± 1.7	deg cm^{-2} dmol^{-1} x 10^{-3}	<0.001
b1	0.156 ± 0.006	deg cm^{-2} dmol^{-1} K^{-1} x 10^{-3}	<0.001
c1	−2.78 ± 0.05	deg cm^{-2} dmol^{-1} x 10^{-3}	<0.001
d1	---	---	---
a2	−71.9 ± 1.7	deg cm^{-2} dmol^{-1} x 10^{-3}	<0.001
b2	0.161 ± 0.006	deg cm^{-2} dmol^{-1} K^{-1} x 10^{-3}	<0.001
c2	−3.11 ± 0.05	deg cm^{-2} dmol^{-1} x 10^{-3}	<0.001
d2	---	---	---
a3	−73.3 ± 1.7	deg cm^{-2} dmol^{-1} x 10^{-3}	<0.001
b3	0.167 ± 0.006	deg cm^{-2} dmol^{-1} K^{-1} x 10^{-3}	<0.001
c3	−2.87 ± 0.05	deg cm^{-2} dmol^{-1} x 10^{-3}	<0.001
d3	---	---	---

$R^2 = 0.99987$
sum residuals^2 = 4.68638

For **d27e/22g'–z4x**, at 316.4 K,
$\Delta G = 0.00 \pm 0.01$ kcal/mol
$\Delta H = -30.7 \pm 0.4$ kcal/mol
$-T\Delta S = 30.7 \pm 0.4$ kcal/mol

Figure S126. (A) CD spectra and (B–D) variable temperature CD data (triplicate) for 15 μM disulfide-bound coiled-coil variant **d27*e*/22*g*'-z4x** (QX2294) in 20 mM sodium phosphate (pH 7) with 4 M GdnHCl. Fit parameters from eq. S1–S3 appear in the table, as do calculated values of ΔG_f, ΔH_f, and $-T\Delta S_f \pm$ standard error at the indicated temperature.

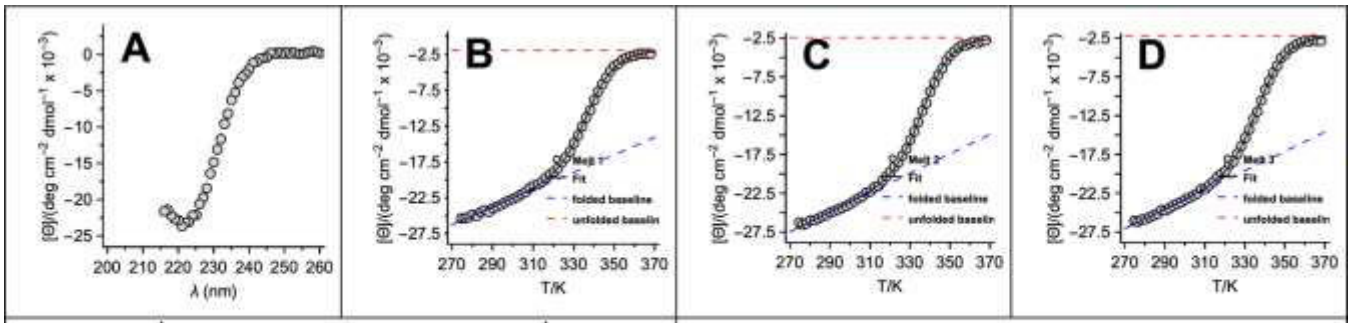

Parameters	Values	Units	P–Values
ΔH_0	−32.06 ± 0.42	kcal/mol	<0.001
T_m	64.9 ± 0.1	°C	---
ΔC_p	---	---	---
a1	−59.3 ± 0.7	deg cm^{-2} dmol^{-1} x 10^{-3}	<0.001
b1	0.122 ± 0.002	deg cm^{-2} dmol^{-1} K^{-1} x 10^{-3}	<0.001
c1	−1.90 ± 0.07	deg cm^{-2} dmol^{-1} x 10^{-3}	<0.001
d1	---	---	---
a2	−61.3 ± 0.7	deg cm^{-2} dmol^{-1} x 10^{-3}	<0.001
b2	0.126 ± 0.002	deg cm^{-2} dmol^{-1} K^{-1} x 10^{-3}	<0.001
c2	−2.40 ± 0.07	deg cm^{-2} dmol^{-1} x 10^{-3}	<0.001
d2	---	---	---
a3	−60.6 ± 0.7	deg cm^{-2} dmol^{-1} x 10^{-3}	<0.001
b3	0.124 ± 0.002	deg cm^{-2} dmol^{-1} K^{-1} x 10^{-3}	<0.001
c3	−2.22 ± 0.07	deg cm^{-2} dmol^{-1} x 10^{-3}	<0.001
d3	---	---	---

$R^2 = 0.99992$
sum residuals^2 = 3.59157

For **sd27e/22g'–z2x**, at 316.6 K,
$\Delta G = -2.04 \pm 0.03$ kcal/mol
$\Delta H = -32.1 \pm 0.4$ kcal/mol
$-T\Delta S = 30.0 \pm 0.4$ kcal/mol

Figure S127. (A) CD spectra and (B–D) variable temperature CD data (triplicate) for 15 μM disulfide-bound coiled-coil variant **sd27*e*/22*g*'-z4x** (QX2294s) in 20 mM sodium phosphate (pH 7) with 4 M GdnHCl. Fit parameters from eq. S1–S3 appear in the table, as do calculated values for ΔG_f, ΔH_f, and $-T\Delta S_f \pm$ standard error at the indicated temperature.

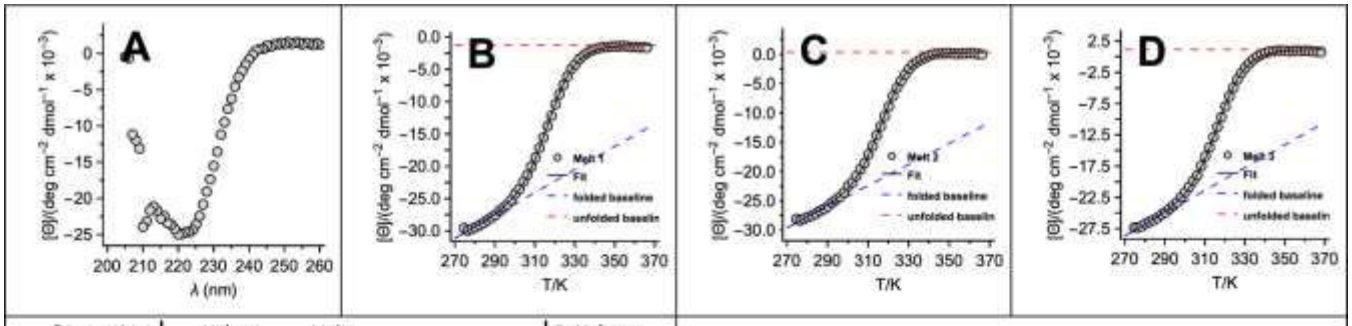

Parameters	Values	Units	P–Values
ΔH_0	−29.59 ± 0.35	kcal/mol	<0.001
T_m	45.0 ± 0.1	°C	<0.001
ΔC_p	---	---	---
a1	−79.2 ± 1.7	deg cm^{-2} dmol^{-1} x 10^{-3}	<0.001
b1	0.178 ± 0.006	deg cm^{-2} dmol^{-1} K^{-1} x 10^{-3}	<0.001
c1	−1.23 ± 0.05	deg cm^{-2} dmol^{-1} x 10^{-3}	<0.001
d1	---	---	---
a2	−78.2 ± 1.7	deg cm^{-2} dmol^{-1} x 10^{-3}	<0.001
b2	0.180 ± 0.006	deg cm^{-2} dmol^{-1} K^{-1} x 10^{-3}	<0.001
c2	0.42 ± 0.05	deg cm^{-2} dmol^{-1} x 10^{-3}	<0.001
d2	---	---	---
a3	−77.6 ± 1.7	deg cm^{-2} dmol^{-1} x 10^{-3}	<0.001
b3	0.182 ± 0.006	deg cm^{-2} dmol^{-1} K^{-1} x 10^{-3}	<0.001
c3	1.17 ± 0.05	deg cm^{-2} dmol^{-1} x 10^{-3}	<0.001
d3	---	---	---

$R^2 = 0.99986$
sum residuals^2 = 5.37545

For **d6e/1g'–z4x**, at 318.2 K,
$\Delta G = 0.00 \pm 0.01$ kcal/mol
$\Delta H = -29.6 \pm 0.4$ kcal/mol
$-T\Delta S = 29.6 \pm 0.4$ kcal/mol

Figure S128. (A) CD spectra and (B–D) variable temperature CD data (triplicate) for 15 μM disulfide-bound coiled-coil variant **d6*e*/1*g*'-z4x** (QX31172) in 20 mM sodium phosphate (pH 7) with 4 M GdnHCl. Fit parameters from eq. S1–S3 appear in the table, as do calculated values of ΔG_f, ΔH_f, and $-T\Delta S_f \pm$ standard error at the indicated temperature.

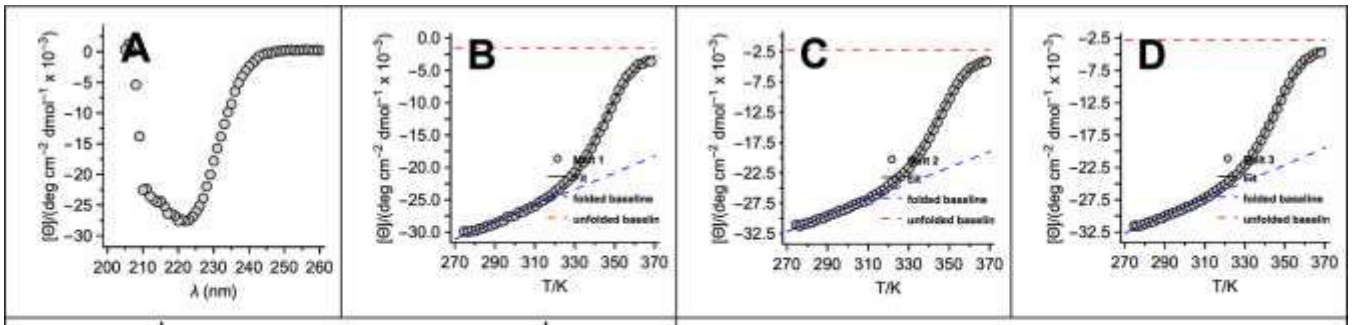

Parameters	Values	Units	P–Values
ΔH_0	−27.92 ± 0.49	kcal/mol	<0.001
T_m	73.7 ± 0.2	°C	<0.001
ΔC_p	---	---	---
a1	−65.7 ± 0.8	deg cm^{-2} dmol^{-1} x 10^{-3}	<0.001
b1	0.128 ± 0.003	deg cm^{-2} dmol^{-1} K^{-1} x 10^{-3}	<0.001
c1	−1.49 ± 0.16	deg cm^{-2} dmol^{-1} x 10^{-3}	<0.001
d1	---	---	---
a2	−67.8 ± 0.8	deg cm^{-2} dmol^{-1} x 10^{-3}	<0.001
b2	0.132 ± 0.003	deg cm^{-2} dmol^{-1} K^{-1} x 10^{-3}	<0.001
c2	−2.17 ± 0.16	deg cm^{-2} dmol^{-1} x 10^{-3}	<0.001
d2	---	---	---
a3	−68.0 ± 0.8	deg cm^{-2} dmol^{-1} x 10^{-3}	<0.001
b3	0.131 ± 0.003	deg cm^{-2} dmol^{-1} K^{-1} x 10^{-3}	<0.001
c3	−2.78 ± 0.16	deg cm^{-2} dmol^{-1} x 10^{-3}	<0.001
d3	---	---	---

$R^2 = 0.99993$
sum residuals^2 = 5.51575

For **sd6e/1g'–z4x**, at 318.2 K,
$\Delta G = -2.30 \pm 0.04$ kcal/mol
$\Delta H = -27.9 \pm 0.5$ kcal/mol
$-T\Delta S = 25.6 \pm 0.5$ kcal/mol

Figure S129. (A) CD spectra and (B–D) variable temperature CD data (triplicate) for 15 μM stapled disulfide-bound coiled-coil variant **sd6*e*/1*g*'-z4x** (QX31172s) in 20 mM sodium phosphate (pH 7) with 4 M GdnHCl. Fit parameters from eq. S1–S3 appear in the table, as do calculated values of ΔG_f, ΔH_f, and $-T\Delta S_f \pm$ standard error at the indicated temperature.

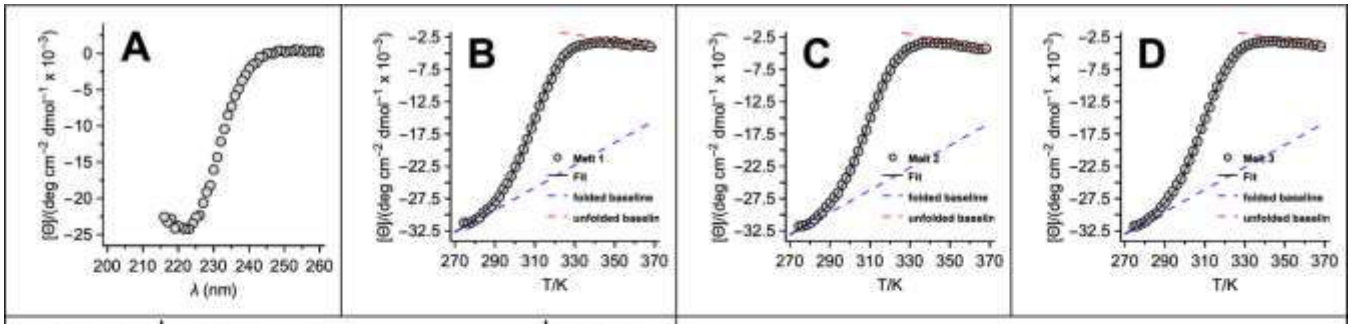

Parameters	Values	Units	P–Values
ΔH_0	−24.50 ± 0.31	kcal/mol	<0.001
T_m	38.8 ± 0.2	°C	<0.001
ΔC_p	---	---	---
a1	−79.6 ± 2.4	deg cm^{-2} dmol^{-1} x 10^{-3}	<0.001
b1	0.174 ± 0.008	deg cm^{-2} dmol^{-1} K^{-1} x 10^{-3}	<0.001
c1	14.10 ± 1.24	deg cm^{-2} dmol^{-1} x 10^{-3}	<0.001
d1	−0.05 ± 0.00	deg cm^{-2} dmol^{-1} x 10^{-3}	<0.001
a2	−79.9 ± 2.4	deg cm^{-2} dmol^{-1} x 10^{-3}	<0.001
b2	0.173 ± 0.009	deg cm^{-2} dmol^{-1} K^{-1} x 10^{-3}	<0.001
c2	19.14 ± 1.26	deg cm^{-2} dmol^{-1} x 10^{-3}	<0.001
d2	−0.064 ± 0.004	deg cm^{-2} dmol^{-1} K^{-1} x 10^{-3}	<0.001
a3	−79.6 ± 2.4	deg cm^{-2} dmol^{-1} x 10^{-3}	<0.001
b3	0.173 ± 0.009	deg cm^{-2} dmol^{-1} K^{-1} x 10^{-3}	<0.001
c3	15.08 ± 1.25	deg cm^{-2} dmol^{-1} x 10^{-3}	<0.001
d3	−0.052 ± 0.004	deg cm^{-2} dmol^{-1} K^{-1} x 10^{-3}	<0.001

$R^2 = 0.99994$
sum residuals^2 = 2.63360

For **d27e/29g'–z2x**, at 312.0 K,
$\Delta G = 0.00 \pm 0.01$ kcal/mol
$\Delta H = -24.5 \pm 0.3$ kcal/mol
$-T\Delta S = 24.5 \pm 0.3$ kcal/mol

Figure S130. (A) CD spectra and (B–D) variable temperature CD data (triplicate) for 15 μM disulfide-bound coiled-coil variant **d27*e*/29*g*'-z2x** (QX2289) in 20 mM sodium phosphate (pH 7) with 4 M GdnHCl. Fit parameters from equations S1–S3 appear in the table, as do calculated values for ΔG_f, ΔH_f, and $-T\Delta S_f$ at ± standard error at the indicated temperature.

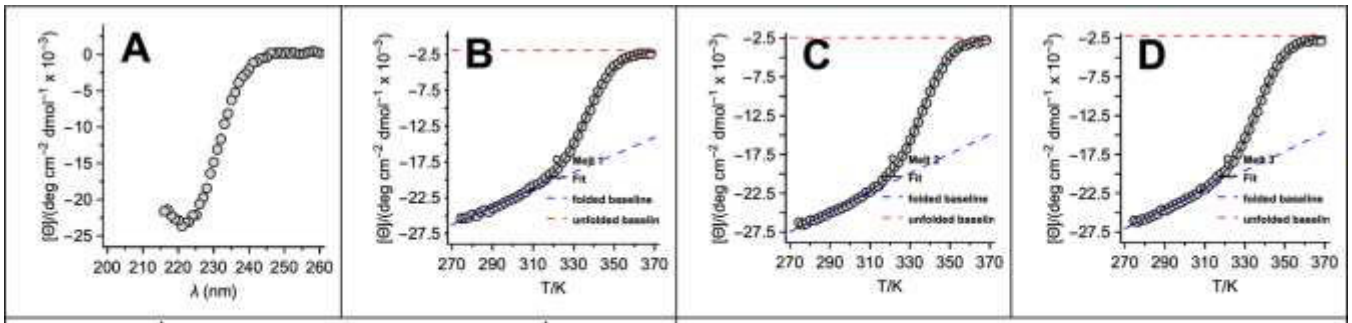

Parameters	Values	Units	P–Values
ΔH_0	−32.06 ± 0.42	kcal/mol	<0.001
T_m	64.9 ± 0.1	°C	---
ΔC_p	---	---	---
a1	−59.3 ± 0.7	deg cm^{-2} dmol^{-1} x 10^{-3}	<0.001
b1	0.122 ± 0.002	deg cm^{-2} dmol^{-1} K^{-1} x 10^{-3}	<0.001
c1	−1.90 ± 0.07	deg cm^{-2} dmol^{-1} x 10^{-3}	<0.001
d1	---	---	---
a2	−61.3 ± 0.7	deg cm^{-2} dmol^{-1} x 10^{-3}	<0.001
b2	0.126 ± 0.002	deg cm^{-2} dmol^{-1} K^{-1} x 10^{-3}	<0.001
c2	−2.40 ± 0.07	deg cm^{-2} dmol^{-1} x 10^{-3}	<0.001
d2	---	---	---
a3	−60.6 ± 0.7	deg cm^{-2} dmol^{-1} x 10^{-3}	<0.001
b3	0.124 ± 0.002	deg cm^{-2} dmol^{-1} K^{-1} x 10^{-3}	<0.001
c3	−2.22 ± 0.07	deg cm^{-2} dmol^{-1} x 10^{-3}	<0.001
d3	---	---	---

$R^2 = 0.99992$
sum residuals^2 = 3.59157

For **sd27e/22g'–z2x**, at 316.6 K,
$\Delta G = -2.04 \pm 0.03$ kcal/mol
$\Delta H = -32.1 \pm 0.4$ kcal/mol
$-T\Delta S = 30.0 \pm 0.4$ kcal/mol

Figure S131. (A) CD spectra and (B–D) variable temperature CD data (triplicate) for 15 μM stapled disulfide-bound coiled-coil variant **sd27*e*/29*g*'-z2x** (QX2289s) in 20 mM sodium phosphate (pH 7) with 4 M GdnHCl. Fit parameters from equations S1–S3 appear in the table, as do calculated values for ΔG_f, ΔH_f, and $-T\Delta S_f$ ± standard errors at the indicated temperature.

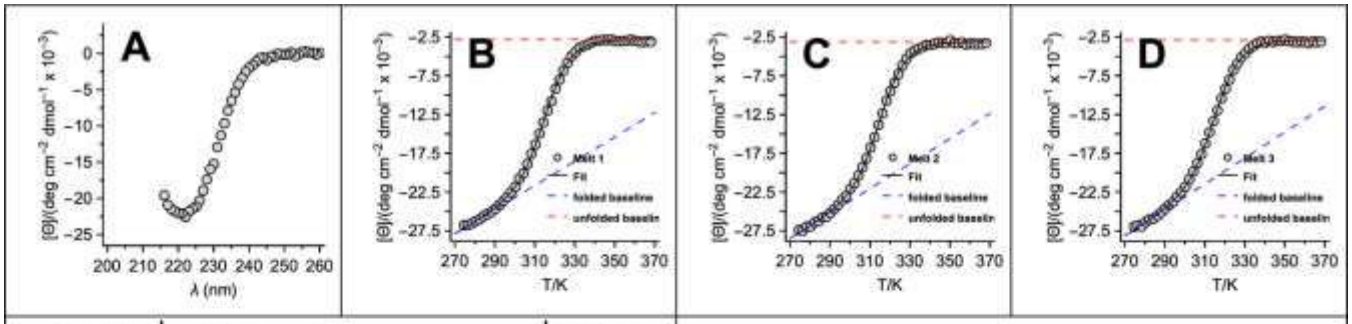

Parameters	Values	Units	P–Values
ΔH_0	−30.68 ± 0.40	kcal/mol	<0.001
T_m	43.2 ± 0.2	°C	<0.001
ΔC_p	---	---	---
a1	−70.0 ± 1.7	deg cm^{-2} dmol^{-1} x 10^{-3}	<0.001
b1	0.156 ± 0.006	deg cm^{-2} dmol^{-1} K^{-1} x 10^{-3}	<0.001
c1	−2.78 ± 0.05	deg cm^{-2} dmol^{-1} x 10^{-3}	<0.001
d1	---	---	---
a2	−71.9 ± 1.7	deg cm^{-2} dmol^{-1} x 10^{-3}	<0.001
b2	0.161 ± 0.006	deg cm^{-2} dmol^{-1} K^{-1} x 10^{-3}	<0.001
c2	−3.11 ± 0.05	deg cm^{-2} dmol^{-1} x 10^{-3}	<0.001
d2	---	---	---
a3	−73.3 ± 1.7	deg cm^{-2} dmol^{-1} x 10^{-3}	<0.001
b3	0.167 ± 0.006	deg cm^{-2} dmol^{-1} K^{-1} x 10^{-3}	<0.001
c3	−2.87 ± 0.05	deg cm^{-2} dmol^{-1} x 10^{-3}	<0.001
d3	---	---	---

$R^2 = 0.99987$
sum residuals^2 = 4.68638

For **d27e/22g'–z4x**, at 316.4 K,
ΔG = 0.00 ± 0.01 kcal/mol
ΔH = −30.7 ± 0.4 kcal/mol
−TΔS = 30.7 ± 0.4 kcal/mol

Figure S132. (A) CD spectra and (B–D) variable temperature CD data (triplicate) for 15 μM disulfide-bound coiled-coil variant **d27*e*/22*g*'-*z*2x** (QX2293) in 20 mM sodium phosphate (pH 7) with 4 M GdnHCl. Fit parameters from equations S1–S3 appear in the table, as do calculated values for ΔG_f, ΔH_f, and $-T\Delta S_f$ ± standard error at the indicated temperature.

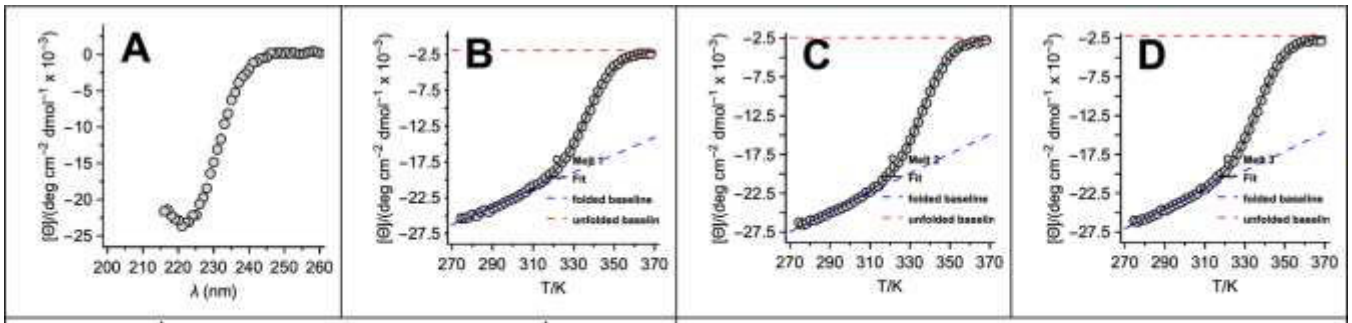

Parameters	Values	Units	P–Values
ΔH_0	−32.06 ± 0.42	kcal/mol	<0.001
T_m	64.9 ± 0.1	°C	---
ΔC_p	---	---	---
a1	−59.3 ± 0.7	deg cm^{-2} dmol^{-1} x 10^{-3}	<0.001
b1	0.122 ± 0.002	deg cm^{-2} dmol^{-1} K^{-1} x 10^{-3}	<0.001
c1	−1.90 ± 0.07	deg cm^{-2} dmol^{-1} x 10^{-3}	<0.001
d1	---	---	---
a2	−61.3 ± 0.7	deg cm^{-2} dmol^{-1} x 10^{-3}	<0.001
b2	0.126 ± 0.002	deg cm^{-2} dmol^{-1} K^{-1} x 10^{-3}	<0.001
c2	−2.40 ± 0.07	deg cm^{-2} dmol^{-1} x 10^{-3}	<0.001
d2	---	---	---
a3	−60.6 ± 0.7	deg cm^{-2} dmol^{-1} x 10^{-3}	<0.001
b3	0.124 ± 0.002	deg cm^{-2} dmol^{-1} K^{-1} x 10^{-3}	<0.001
c3	−2.22 ± 0.07	deg cm^{-2} dmol^{-1} x 10^{-3}	<0.001
d3	---	---	---

$R^2 = 0.99992$
sum residuals^2 = 3.59157

For **sd27e/22g'–z2x**, at 316.6 K,
ΔG = −2.04 ± 0.03 kcal/mol
ΔH = −32.1 ± 0.4 kcal/mol
−TΔS = 30.0 ± 0.4 kcal/mol

Figure S133. (A) CD spectra and (B–D) variable temperature CD data (triplicate) for 15 μM stapled disulfide-bound coiled-coil variant **sd27*e*/22*g*'-*z*4x** (QX2293s) in 20 mM sodium phosphate (pH 7) with 4 M GdnHCl. Fit parameters from equations S1–S3 appear in the table, as do calculated values for ΔG_f, ΔH_f, and $-T\Delta S_f$ ± standard error at the indicated temperature.

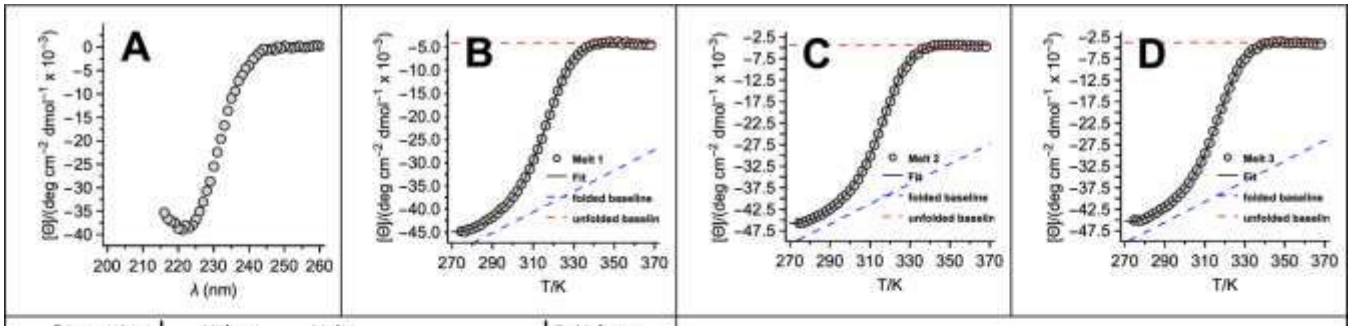

Parameters	Values	Units	P–Values
ΔH_0	−27.22 ± 0.27	kcal/mol	<0.001
T_m	43.4 ± 0.1	°C	<0.001
ΔC_p	−0.794 ± 0.020	kcal/mol/K	<0.001
a1	−110.2 ± 3.7	deg cm^{-2} dmol^{-1} x 10^{-3}	<0.001
b1	0.225 ± 0.013	deg cm^{-2} dmol^{-1} K^{-1} x 10^{-3}	<0.001
c1	−4.06 ± 0.04	deg cm^{-2} dmol^{-1} x 10^{-3}	<0.001
d1	---	---	---
a2	−113.4 ± 3.7	deg cm^{-2} dmol^{-1} x 10^{-3}	<0.001
b2	0.233 ± 0.013	deg cm^{-2} dmol^{-1} K^{-1} x 10^{-3}	<0.001
c2	−4.32 ± 0.04	deg cm^{-2} dmol^{-1} x 10^{-3}	<0.001
d2	---	---	---
a3	−114.2 ± 3.8	deg cm^{-2} dmol^{-1} x 10^{-3}	<0.001
b3	0.237 ± 0.013	deg cm^{-2} dmol^{-1} K^{-1} x 10^{-3}	<0.001
c3	−3.72 ± 0.04	deg cm^{-2} dmol^{-1} x 10^{-3}	<0.001
d3	---	---	---

$R^2 = 0.99996$
sum residuals^2 = 3.87501

For **d24*b*/25*c*'–z4x**, at 316.5 K,
$\Delta G = 0.00 \pm 0.01$ kcal/mol
$\Delta H = -27.2 \pm 0.3$ kcal/mol
$-T\Delta S = 27.2 \pm 0.3$ kcal/mol

Figure S134. (A) CD spectra and (B–D) variable temperature CD data (triplicate) for 15 μM disulfide-bound coiled-coil variant **d24*b*/25*c*'-z4x** (QX2291) in 20 mM sodium phosphate (pH 7) with 4 M GdnHCl. Fit parameters from eq. S1–S3 appear in the table, as do calculated values for ΔG_f, ΔH_f, and $-T\Delta S_f \pm$ standard error at the indicated temperature.

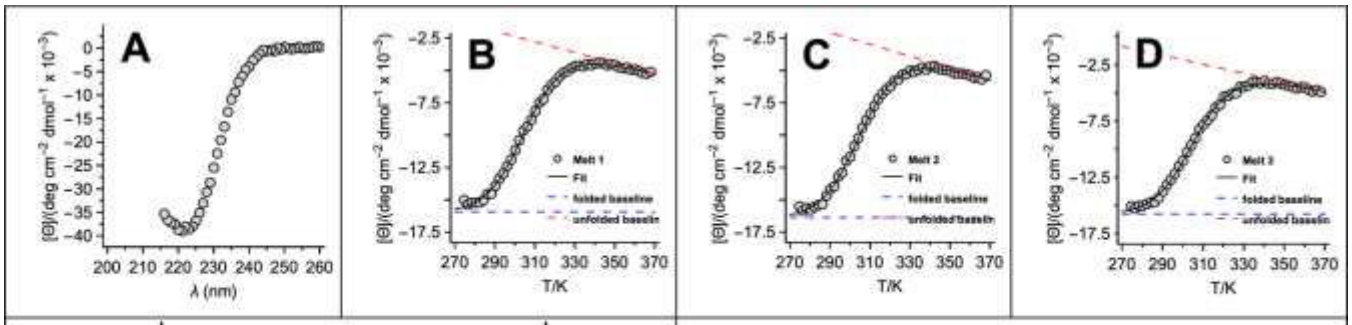

Parameters	Values	Units	P–Values
ΔH_0	−19.15 ± 0.36	kcal/mol	<0.001
T_m	33.0 ± 0.2	°C	<0.001
ΔC_p	---	---	---
a1	−15.9 ± 0.1	deg cm^{-2} dmol^{-1} x 10^{-3}	<0.001
b1	---	---	---
c1	9.97 ± 1.11	deg cm^{-2} dmol^{-1} x 10^{-3}	<0.001
d1	−0.04 ± 0.00	deg cm^{-2} dmol^{-1} x 10^{-3}	<0.001
a2	−16.4 ± 0.1	deg cm^{-2} dmol^{-1} x 10^{-3}	<0.001
b2	---	---	---
c2	11.10 ± 1.13	deg cm^{-2} dmol^{-1} x 10^{-3}	<0.001
d2	−0.045 ± 0.003	deg cm^{-2} dmol^{-1} K^{-1} x 10^{-3}	<0.001
a3	−15.7 ± 0.1	deg cm^{-2} dmol^{-1} x 10^{-3}	<0.001
b3	---	---	---
c3	9.99 ± 1.12	deg cm^{-2} dmol^{-1} x 10^{-3}	<0.001
d3	−0.040 ± 0.003	deg cm^{-2} dmol^{-1} K^{-1} x 10^{-3}	<0.001

$R^2 = 0.99976$
sum residuals^2 = 2.87262

For **sd24b/25c'–z4x**, at 316.5 K,
$\Delta G = 0.65 \pm 0.02$ kcal/mol
$\Delta H = -19.1 \pm 0.4$ kcal/mol
$-T\Delta S = 19.8 \pm 0.4$ kcal/mol

Figure S135. (A) CD spectra and (B–D) variable temperature CD data (triplicate) for 15 μM stapled disulfide-bound coiled-coil variant **sd24*b*/25*c*'-z4x** (QX2291s) in 20 mM sodium phosphate (pH 7) with 4 M GdnHCl. Fit parameters from eq. S1–S3 appear in the table, as do calculated values for ΔG_f, ΔH_f, and $-T\Delta S_f \pm$ standard error at the indicated temperature.

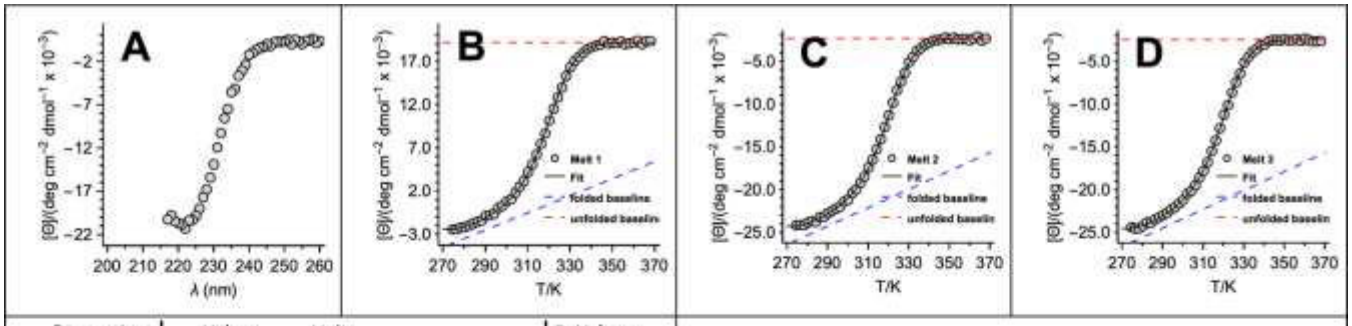

Parameters	Values	Units	P–Values
ΔH_0	−28.54 ± 0.33	kcal/mol	<0.001
T_m	46.5 ± 0.1	°C	<0.001
ΔC_p	−0.783 ± 0.023	kcal/mol/K	<0.001
a1	−31.2 ± 2.0	deg cm^{-2} dmol^{-1} x 10^{-3}	<0.001
b1	0.099 ± 0.007	deg cm^{-2} dmol^{-1} K^{-1} x 10^{-3}	<0.001
c1	19.20 ± 0.03	deg cm^{-2} dmol^{-1} x 10^{-3}	<0.001
d1	---	---	---
a2	−55.4 ± 2.0	deg cm^{-2} dmol^{-1} x 10^{-3}	<0.001
b2	0.107 ± 0.007	deg cm^{-2} dmol^{-1} K^{-1} x 10^{-3}	<0.001
c2	−2.30 ± 0.03	deg cm^{-2} dmol^{-1} x 10^{-3}	<0.001
d2	---	---	---
a3	−56.4 ± 2.0	deg cm^{-2} dmol^{-1} x 10^{-3}	<0.001
b3	0.110 ± 0.007	deg cm^{-2} dmol^{-1} K^{-1} x 10^{-3}	<0.001
c3	−2.45 ± 0.03	deg cm^{-2} dmol^{-1} x 10^{-3}	<0.001
d3	---	---	---

$R^2 = 0.99994$
sum residuals^2 = 1.70878

For **d24*b*/25*c*'–z4y4**, at 319.6 K,
$\Delta G = 0.00 \pm 0.01$ kcal/mol
$\Delta H = -28.5 \pm 0.3$ kcal/mol
$-T\Delta S = 28.5 \pm 0.4$ kcal/mol

Figure S136. (A) CD spectra and (B–D) variable temperature CD data (triplicate) for 15 μM disulfide-bound coiled-coil variant **d24*b*/25*c*'-z4y4** (QX3096) in 20 mM sodium phosphate (pH 7) with 4 M GdnHCl. Fit parameters from equations S1–S3 appear in the table, as do calculated values for ΔG_f, ΔH_f, and $-T\Delta S_f \pm$ standard error at the indicated temperature.

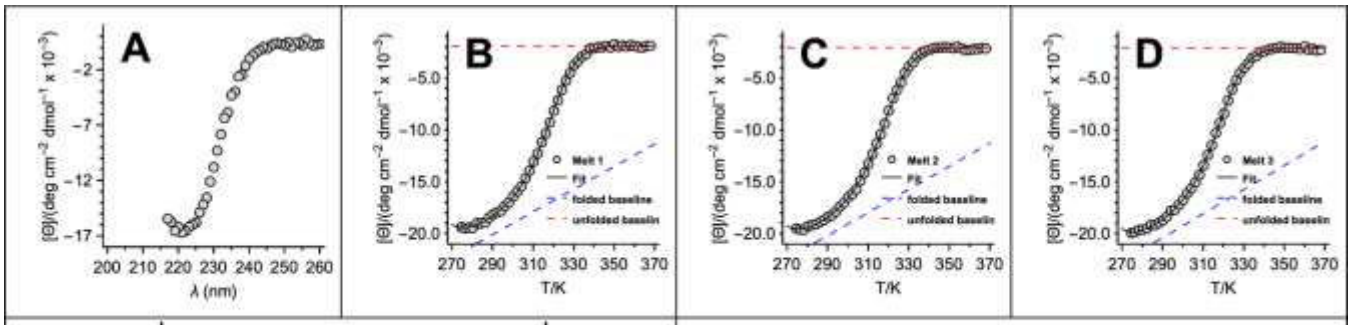

Parameters	Values	Units	P–Values
ΔH_0	−26.11 ± 0.43	kcal/mol	<0.001
T_m	44.5 ± 0.2	°C	<0.001
ΔC_p	−0.798 ± 0.022	kcal/mol/K	<0.001
a1	−51.8 ± 2.3	deg cm^{-2} dmol^{-1} x 10^{-3}	<0.001
b1	0.109 ± 0.008	deg cm^{-2} dmol^{-1} K^{-1} x 10^{-3}	<0.001
c1	−1.89 ± 0.03	deg cm^{-2} dmol^{-1} x 10^{-3}	<0.001
d1	---	---	---
a2	−52.6 ± 2.3	deg cm^{-2} dmol^{-1} x 10^{-3}	<0.001
b2	0.112 ± 0.008	deg cm^{-2} dmol^{-1} K^{-1} x 10^{-3}	<0.001
c2	−2.04 ± 0.03	deg cm^{-2} dmol^{-1} x 10^{-3}	<0.001
d2	---	---	---
a3	−54.2 ± 2.3	deg cm^{-2} dmol^{-1} x 10^{-3}	<0.001
b3	0.116 ± 0.008	deg cm^{-2} dmol^{-1} K^{-1} x 10^{-3}	<0.001
c3	−2.09 ± 0.03	deg cm^{-2} dmol^{-1} x 10^{-3}	<0.001
d3	---	---	---

$R^2 = 0.99993$
sum residuals^2 = 1.48000

For **sd24b/24c'–z4y4**, at 319.6 K,
$\Delta G = 0.17 \pm 0.02$ kcal/mol
$\Delta H = -27.7 \pm 0.5$ kcal/mol
$-T\Delta S = 27.9 \pm 0.5$ kcal/mol

Figure S137. (A) CD spectra and (B–D) variable temperature CD data (triplicate) for 15 μM stapled disulfide-bound coiled-coil variant **sd24*b*/25*c*'-z4y4** (QX3096s) in 20 mM sodium phosphate (pH 7) with 4 M GdnHCl. Fit parameters from equations S1–S3 appear in the table, as do calculated values for ΔG_f, ΔH_f, and $-T\Delta S_f \pm$ standard error at the indicated temperature.

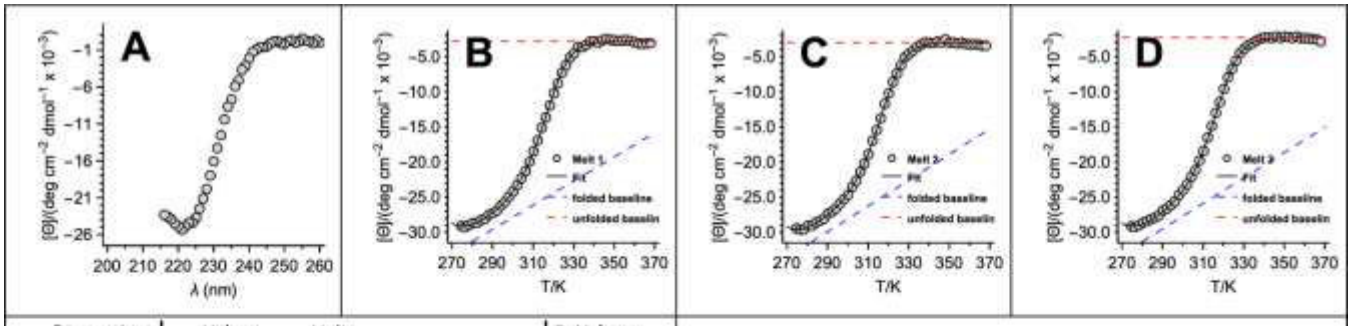

Parameters	Values	Units	P–Values
ΔH_0	−28.59 ± 0.49	kcal/mol	<0.001
T_m	42.6 ± 0.2	°C	<0.001
ΔC_p	−0.913 ± 0.028	kcal/mol/K	<0.001
a1	−79.4 ± 3.6	deg cm^{-2} dmol^{-1} x 10^{-3}	<0.001
b1	0.172 ± 0.012	deg cm^{-2} dmol^{-1} K^{-1} x 10^{-3}	<0.001
c1	−2.79 ± 0.04	deg cm^{-2} dmol^{-1} x 10^{-3}	<0.001
d1	---	---	---
a2	−83.1 ± 3.6	deg cm^{-2} dmol^{-1} x 10^{-3}	<0.001
b2	0.183 ± 0.013	deg cm^{-2} dmol^{-1} K^{-1} x 10^{-3}	<0.001
c2	−2.98 ± 0.04	deg cm^{-2} dmol^{-1} x 10^{-3}	<0.001
d2	---	---	---
a3	−81.9 ± 3.7	deg cm^{-2} dmol^{-1} x 10^{-3}	<0.001
b3	0.181 ± 0.013	deg cm^{-2} dmol^{-1} K^{-1} x 10^{-3}	<0.001
c3	−2.27 ± 0.04	deg cm^{-2} dmol^{-1} x 10^{-3}	<0.001
d3	---	---	---

$R^2 = 0.99991$
sum residuals^2 = 3.87271

For **d7f/10b'–z4x**, at 315.7 K,
$\Delta G = 0.00 \pm 0.02$ kcal/mol
$\Delta H = -28.6 \pm 0.5$ kcal/mol
$-T\Delta S = 28.6 \pm 0.5$ kcal/mol

Figure S138. (A) CD spectra and (B–D) variable temperature CD data (triplicate) for 15 μM stapled disulfide-bound coiled-coil variant **d7*f*/10*b*'-z4x** (QX2295) in 20 mM sodium phosphate (pH 7) with 4 M GdnHCl. Fit parameters from equations S1–S3 appear in the table, as do calculated values for ΔG_f, ΔH_f, and $-T\Delta S_f \pm$ standard error at the indicated temperature.

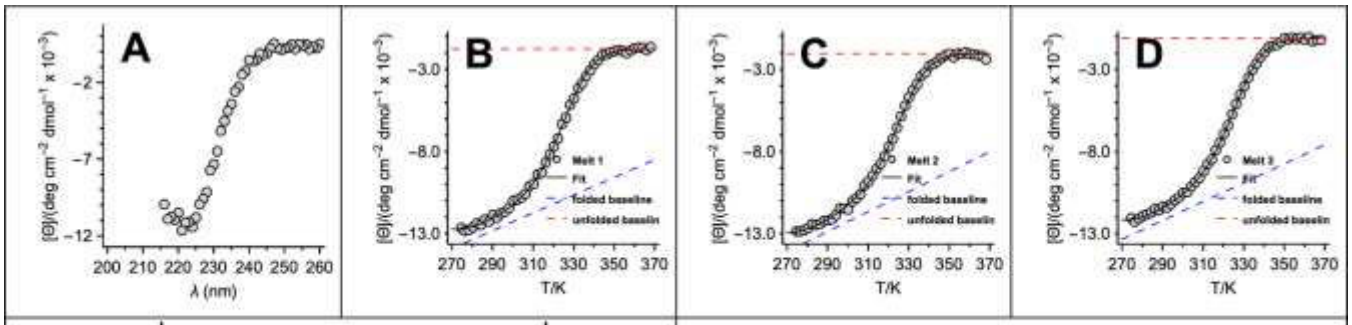

Parameters	Values	Units	P–Values
ΔH_0	−25.32 ± 0.57	kcal/mol	<0.001
T_m	51.4 ± 0.3	°C	<0.001
ΔC_p	−0.629 ± 0.033	kcal/mol/K	<0.001
a1	−28.5 ± 1.7	deg cm^{-2} dmol^{-1} x 10^{-3}	<0.001
b1	0.054 ± 0.006	deg cm^{-2} dmol^{-1} K^{-1} x 10^{-3}	<0.001
c1	−1.74 ± 0.03	deg cm^{-2} dmol^{-1} x 10^{-3}	<0.001
d1	---	---	---
a2	−30.5 ± 1.6	deg cm^{-2} dmol^{-1} x 10^{-3}	<0.001
b2	0.061 ± 0.005	deg cm^{-2} dmol^{-1} K^{-1} x 10^{-3}	<0.001
c2	−2.02 ± 0.03	deg cm^{-2} dmol^{-1} x 10^{-3}	<0.001
d2	---	---	---
a3	−28.9 ± 1.7	deg cm^{-2} dmol^{-1} x 10^{-3}	<0.001
b3	0.057 ± 0.006	deg cm^{-2} dmol^{-1} K^{-1} x 10^{-3}	<0.001
c3	−1.08 ± 0.03	deg cm^{-2} dmol^{-1} x 10^{-3}	<0.001
d3	---	---	---

$R^2 = 0.99986$
sum residuals^2 = 1.34394

For **sd7f/10b'–z4x**, at 315.7 K,
$\Delta G = -0.61 \pm 0.03$ kcal/mol
$\Delta H = -19.8 \pm 0.7$ kcal/mol
$-T\Delta S = 19.2 \pm 0.7$ kcal/mol

Figure S139. (A) CD spectra and (B–D) variable temperature CD data (triplicate) for 15 μM stapled disulfide-bound coiled-coil variant **sd7*f*/10*b*'-z4x** (QX2295s) in 20 mM sodium phosphate (pH 7) with 4 M GdnHCl. Fit parameters from equations S1–S3 appear in the table, as do calculated values for ΔG_f, ΔH_f, and $-T\Delta S_f \pm$ standard error at the indicated temperature.

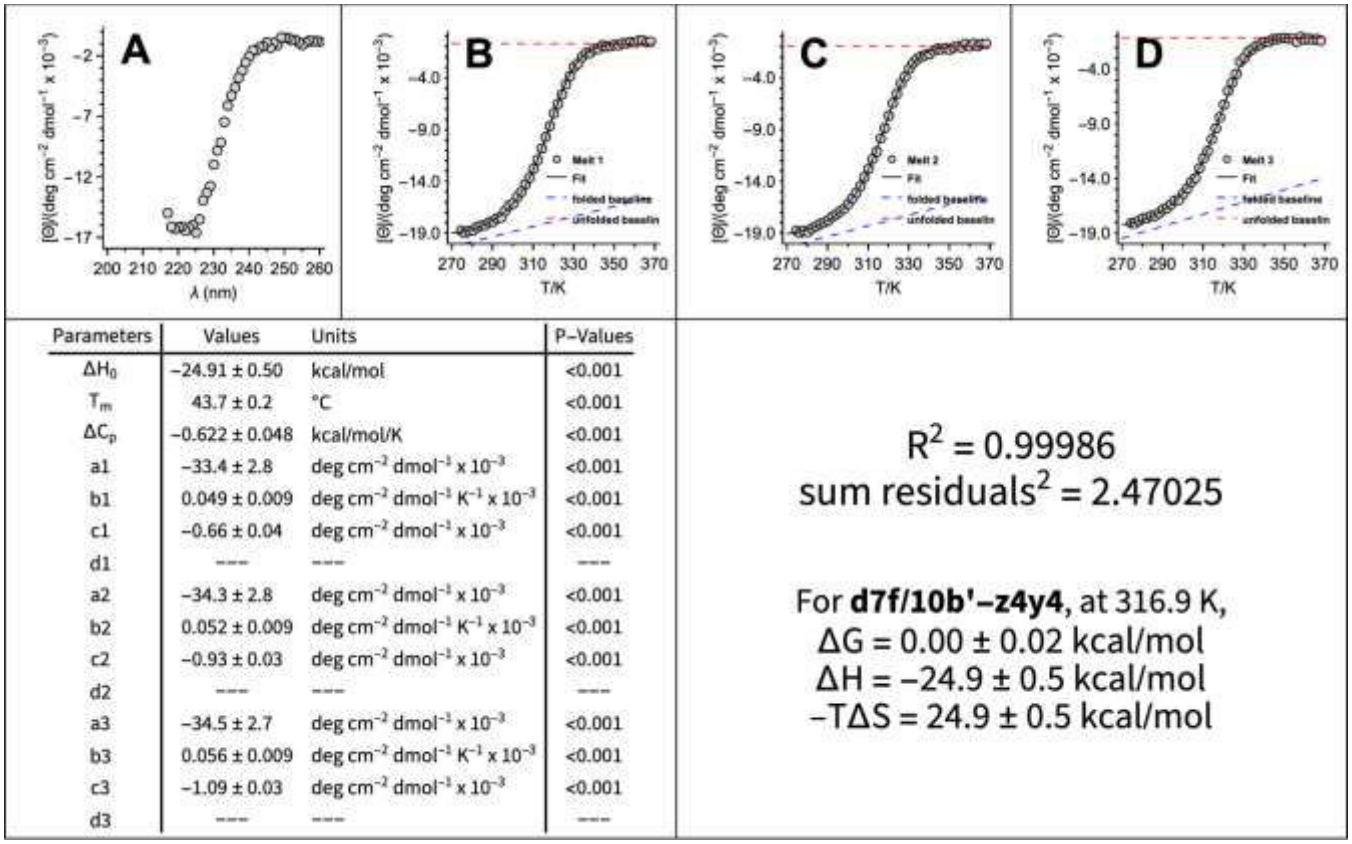

Parameters	Values	Units	P–Values
ΔH_0	−24.91 ± 0.50	kcal/mol	<0.001
T_m	43.7 ± 0.2	°C	<0.001
ΔC_p	−0.622 ± 0.048	kcal/mol/K	<0.001
a1	−33.4 ± 2.8	deg cm^{-2} dmol^{-1} x 10^{-3}	<0.001
b1	0.049 ± 0.009	deg cm^{-2} dmol^{-1} K^{-1} x 10^{-3}	<0.001
c1	−0.66 ± 0.04	deg cm^{-2} dmol^{-1} x 10^{-3}	<0.001
d1	---	---	---
a2	−34.3 ± 2.8	deg cm^{-2} dmol^{-1} x 10^{-3}	<0.001
b2	0.052 ± 0.009	deg cm^{-2} dmol^{-1} K^{-1} x 10^{-3}	<0.001
c2	−0.93 ± 0.03	deg cm^{-2} dmol^{-1} x 10^{-3}	<0.001
d2	---	---	---
a3	−34.5 ± 2.7	deg cm^{-2} dmol^{-1} x 10^{-3}	<0.001
b3	0.056 ± 0.009	deg cm^{-2} dmol^{-1} K^{-1} x 10^{-3}	<0.001
c3	−1.09 ± 0.03	deg cm^{-2} dmol^{-1} x 10^{-3}	<0.001
d3	---	---	---

$R^2 = 0.99986$
sum residuals^2 = 2.47025

For **d7f/10b'–z4y4**, at 316.9 K,
$\Delta G = 0.00 \pm 0.02$ kcal/mol
$\Delta H = -24.9 \pm 0.5$ kcal/mol
$-T\Delta S = 24.9 \pm 0.5$ kcal/mol

Figure S860. (A) CD spectra and (B–D) variable temperature CD data (triplicate) for 15 μM disulfide-bound coiled-coil variant **d7*f*/10*b*'-z4y4** (QX3101) in 20 mM sodium phosphate (pH 7) with 4 M GdnHCl. Fit parameters from equations S1–S3 appear in the table, as do calculated values for ΔG_f, ΔH_f, and $-T\Delta S_f$ ± standard error at the indicated temperature.

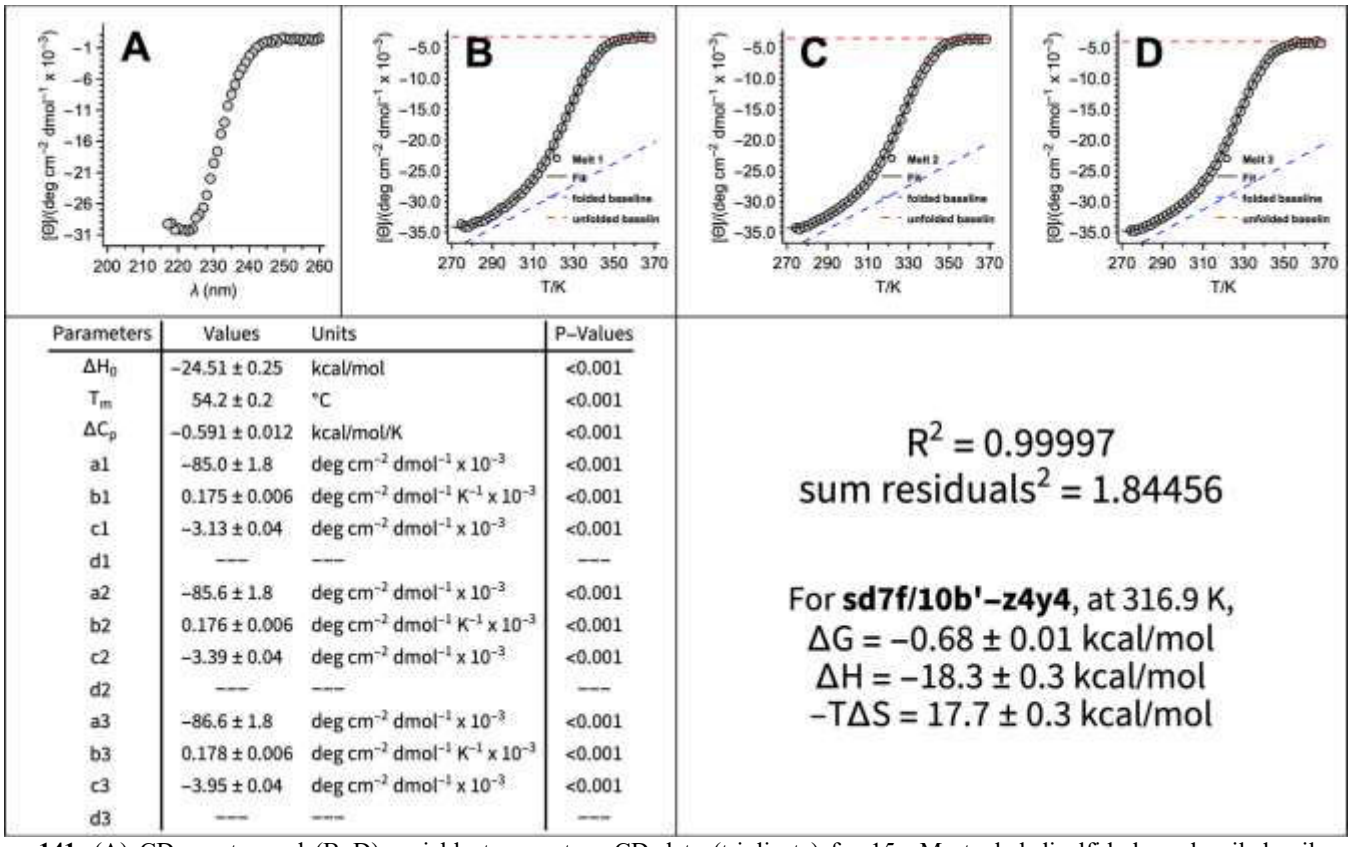

Parameters	Values	Units	P–Values
ΔH_0	−24.51 ± 0.25	kcal/mol	<0.001
T_m	54.2 ± 0.2	°C	<0.001
ΔC_p	−0.591 ± 0.012	kcal/mol/K	<0.001
a1	−85.0 ± 1.8	deg cm^{-2} dmol^{-1} x 10^{-3}	<0.001
b1	0.175 ± 0.006	deg cm^{-2} dmol^{-1} K^{-1} x 10^{-3}	<0.001
c1	−3.13 ± 0.04	deg cm^{-2} dmol^{-1} x 10^{-3}	<0.001
d1	---	---	---
a2	−85.6 ± 1.8	deg cm^{-2} dmol^{-1} x 10^{-3}	<0.001
b2	0.176 ± 0.006	deg cm^{-2} dmol^{-1} K^{-1} x 10^{-3}	<0.001
c2	−3.39 ± 0.04	deg cm^{-2} dmol^{-1} x 10^{-3}	<0.001
d2	---	---	---
a3	−86.6 ± 1.8	deg cm^{-2} dmol^{-1} x 10^{-3}	<0.001
b3	0.178 ± 0.006	deg cm^{-2} dmol^{-1} K^{-1} x 10^{-3}	<0.001
c3	−3.95 ± 0.04	deg cm^{-2} dmol^{-1} x 10^{-3}	<0.001
d3	---	---	---

$R^2 = 0.99997$
sum residuals^2 = 1.84456

For **sd7f/10b'–z4y4**, at 316.9 K,
$\Delta G = -0.68 \pm 0.01$ kcal/mol
$\Delta H = -18.3 \pm 0.3$ kcal/mol
$-T\Delta S = 17.7 \pm 0.3$ kcal/mol

Figure 141. (A) CD spectra and (B–D) variable temperature CD data (triplicate) for 15 μM stapled disulfide-bound coiled-coil variant **sd7*f*/10*b*'-z4y4** (QX3101s) in 20 mM sodium phosphate (pH 7) with 4 M GdnHCl. Fit parameters from equations S1–S3 appear in the table, as do calculated values for ΔG_f, ΔH_f, and $-T\Delta S_f$ ± standard error at the indicated temperature.

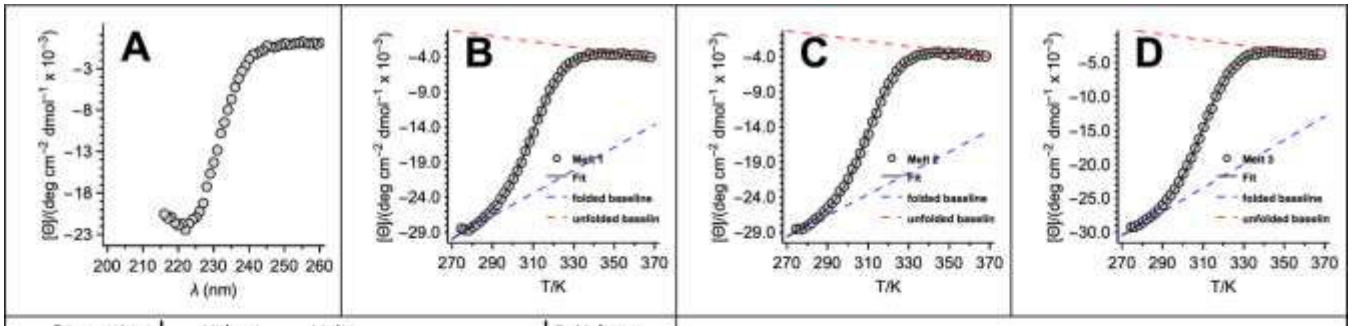

Parameters	Values	Units	P–Values
ΔH_0	−24.89 ± 0.38	kcal/mol	<0.001
T_m	39.8 ± 0.2	°C	<0.001
ΔC_p	---	---	---
a1	−74.0 ± 2.3	deg cm^{-2} dmol^{-1} x 10^{-3}	<0.001
b1	0.163 ± 0.008	deg cm^{-2} dmol^{-1} K^{-1} x 10^{-3}	<0.001
c1	10.06 ± 1.34	deg cm^{-2} dmol^{-1} x 10^{-3}	<0.001
d1	−0.04 ± 0.00	deg cm^{-2} dmol^{-1} x 10^{-3}	<0.001
a2	−70.5 ± 2.4	deg cm^{-2} dmol^{-1} x 10^{-3}	<0.001
b2	0.151 ± 0.008	deg cm^{-2} dmol^{-1} K^{-1} x 10^{-3}	<0.001
c2	9.44 ± 1.35	deg cm^{-2} dmol^{-1} x 10^{-3}	<0.001
d2	−0.036 ± 0.004	deg cm^{-2} dmol^{-1} K^{-1} x 10^{-3}	<0.001
a3	−78.0 ± 2.4	deg cm^{-2} dmol^{-1} x 10^{-3}	<0.001
b3	0.176 ± 0.008	deg cm^{-2} dmol^{-1} K^{-1} x 10^{-3}	<0.001
c3	10.75 ± 1.35	deg cm^{-2} dmol^{-1} x 10^{-3}	<0.001
d3	−0.040 ± 0.004	deg cm^{-2} dmol^{-1} K^{-1} x 10^{-3}	<0.001

$R^2 = 0.99992$
sum residuals^2 = 2.96509

For **d27e/29g'–xx**, at 313.0 K,
$\Delta G = 0.00 \pm 0.01$ kcal/mol
$\Delta H = -24.9 \pm 0.4$ kcal/mol
$-T\Delta S = 24.9 \pm 0.4$ kcal/mol

Figure S142. (A) CD spectra and (B–D) variable temperature CD data (triplicate) for 15 μM disulfide-bound coiled-coil variant **d27e/29g'-xx** (QX2271) in 20 mM sodium phosphate (pH 7) with 4 M GdnHCl. Fit parameters from equations S1–S3 appear in the table, as do calculated values for ΔG_f, ΔH_f, and $-T\Delta S_f \pm$ standard error at the indicated temperature.

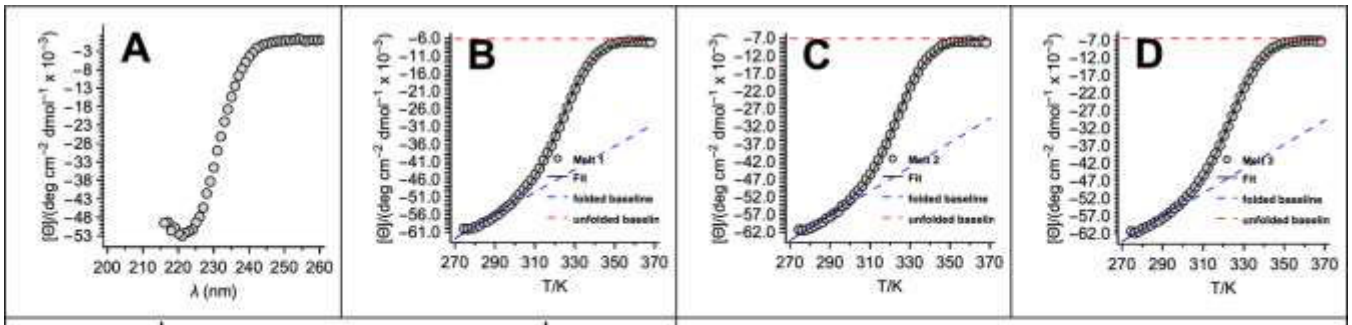

Parameters	Values	Units	P–Values
ΔH_0	−26.88 ± 0.39	kcal/mol	<0.001
T_m	52.9 ± 0.2	°C	<0.001
ΔC_p	---	---	---
a1	−150.8 ± 3.0	deg cm^{-2} dmol^{-1} x 10^{-3}	<0.001
b1	0.326 ± 0.010	deg cm^{-2} dmol^{-1} K^{-1} x 10^{-3}	<0.001
c1	−6.17 ± 0.14	deg cm^{-2} dmol^{-1} x 10^{-3}	<0.001
d1	---	---	---
a2	−157.6 ± 3.0	deg cm^{-2} dmol^{-1} x 10^{-3}	<0.001
b2	0.346 ± 0.010	deg cm^{-2} dmol^{-1} K^{-1} x 10^{-3}	<0.001
c2	−7.08 ± 0.14	deg cm^{-2} dmol^{-1} x 10^{-3}	<0.001
d2	---	---	---
a3	−157.3 ± 3.0	deg cm^{-2} dmol^{-1} x 10^{-3}	<0.001
b3	0.345 ± 0.011	deg cm^{-2} dmol^{-1} K^{-1} x 10^{-3}	<0.001
c3	−6.49 ± 0.14	deg cm^{-2} dmol^{-1} x 10^{-3}	<0.001
d3	---	---	---

$R^2 = 0.99988$
sum residuals^2 = 25.36095

For **sd27e/29g'–x4x**, at 313.0 K,
$\Delta G = -1.08 \pm 0.02$ kcal/mol
$\Delta H = -26.9 \pm 0.4$ kcal/mol
$-T\Delta S = 25.8 \pm 0.4$ kcal/mol

Figure S143. (A) CD spectra and (B–D) variable temperature CD data (triplicate) for 15 μM stapled disulfide-bound coiled-coil variant **sd27*e*/29*g*'-x4x** (QX2283) in 20 mM sodium phosphate (pH 7) with 4 M GdnHCl. Fit parameters from equations S1–S3 appear in the table, as do calculated values for ΔG_f, ΔH_f, and $-T\Delta S_f \pm$ standard error at the indicated temperature.

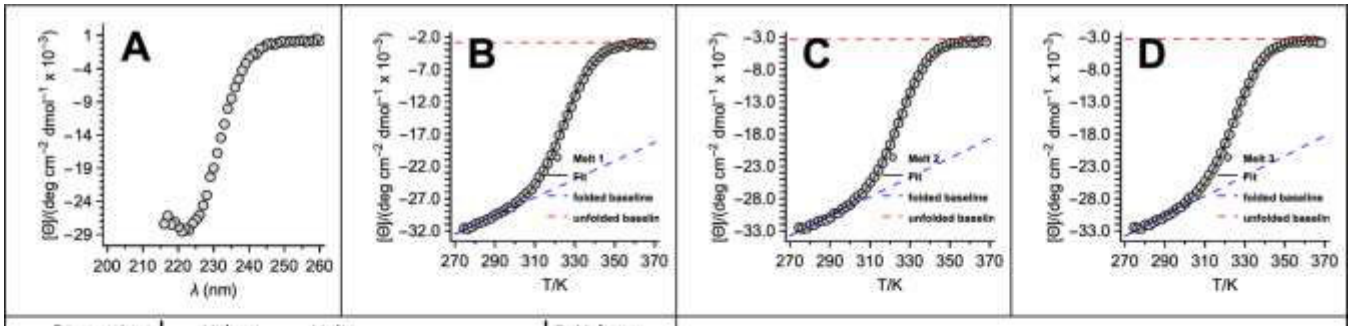

Parameters	Values	Units	P–Values
ΔH_0	−29.03 ± 0.29	kcal/mol	<0.001
T_m	53.4 ± 0.1	°C	---
ΔC_p	---	---	---
a1	−70.7 ± 1.1	deg cm^{-2} dmol^{-1} x 10^{-3}	<0.001
b1	0.142 ± 0.004	deg cm^{-2} dmol^{-1} K^{-1} x 10^{-3}	<0.001
c1	−2.81 ± 0.05	deg cm^{-2} dmol^{-1} x 10^{-3}	<0.001
d1	---	---	---
a2	−74.3 ± 1.1	deg cm^{-2} dmol^{-1} x 10^{-3}	<0.001
b2	0.150 ± 0.004	deg cm^{-2} dmol^{-1} K^{-1} x 10^{-3}	<0.001
c2	−3.33 ± 0.05	deg cm^{-2} dmol^{-1} x 10^{-3}	<0.001
d2	---	---	---
a3	−75.6 ± 1.1	deg cm^{-2} dmol^{-1} x 10^{-3}	<0.001
b3	0.155 ± 0.004	deg cm^{-2} dmol^{-1} K^{-1} x 10^{-3}	<0.001
c3	−3.27 ± 0.05	deg cm^{-2} dmol^{-1} x 10^{-3}	<0.001
d3	---	---	---

$R^2 = 0.99993$
sum residuals^2 = 4.04561

For **sd27e/29g'–x4px**, at 313.0 K,
$\Delta G = -1.21 \pm 0.02$ kcal/mol
$\Delta H = -29.0 \pm 0.3$ kcal/mol
$-T\Delta S = 27.8 \pm 0.3$ kcal/mol

Figure S144. (A) CD spectra and (B–D) variable temperature CD data (triplicate) for 15 μM branched PEG-stapled disulfide-bound coiled-coil variant **sd27*e*/29*g*'-x4px** (QX3079) in 20 mM sodium phosphate (pH 7) with 4 M GdnHCl. Fit parameters from equations S1–S3 appear in the table, as do calculated values for ΔG_f, ΔH_f, and $-T\Delta S_f \pm$ standard error at the indicated temperature.

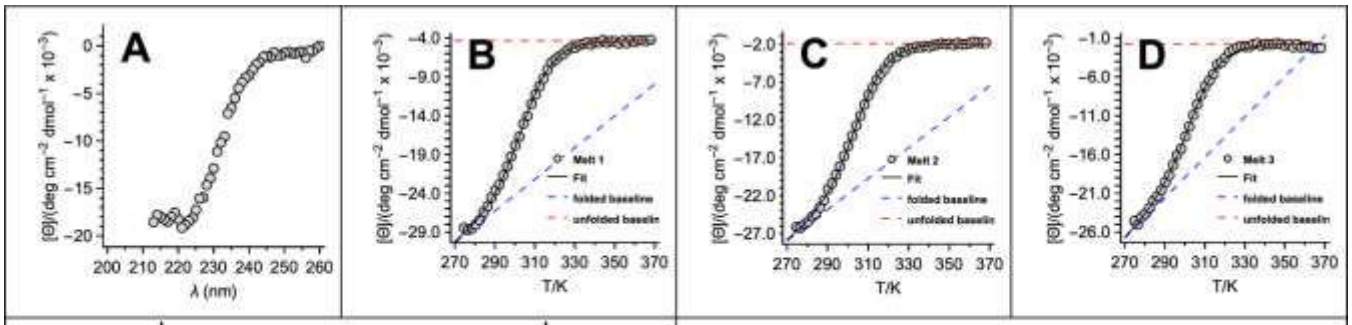

Parameters	Values	Units	P–Values
ΔH_0	−23.56 ± 0.40	kcal/mol	<0.001
T_m	33.1 ± 0.5	°C	<0.001
ΔC_p	---	---	---
a1	−85.5 ± 4.9	deg cm^{-2} dmol^{-1} x 10^{-3}	<0.001
b1	0.204 ± 0.018	deg cm^{-2} dmol^{-1} K^{-1} x 10^{-3}	<0.001
c1	−4.32 ± 0.06	deg cm^{-2} dmol^{-1} x 10^{-3}	<0.001
d1	---	---	---
a2	−83.1 ± 4.9	deg cm^{-2} dmol^{-1} x 10^{-3}	<0.001
b2	0.204 ± 0.018	deg cm^{-2} dmol^{-1} K^{-1} x 10^{-3}	<0.001
c2	−1.89 ± 0.06	deg cm^{-2} dmol^{-1} x 10^{-3}	<0.001
d2	---	---	---
a3	−97.1 ± 4.2	deg cm^{-2} dmol^{-1} x 10^{-3}	<0.001
b3	0.260 ± 0.015	deg cm^{-2} dmol^{-1} K^{-1} x 10^{-3}	<0.001
c3	−1.75 ± 0.05	deg cm^{-2} dmol^{-1} x 10^{-3}	<0.001
d3	---	---	---

$R^2 = 0.99972$
sum residuals^2 = 7.08461

For **(R,S)–d27e/29g'–xx**, at 306.2 K,
$\Delta G = 0.00 \pm 0.04$ kcal/mol
$\Delta H = -23.6 \pm 0.4$ kcal/mol
$-T\Delta S = 23.6 \pm 0.4$ kcal/mol

Figure S145. (A) CD spectra and (B–D) variable temperature CD data (triplicate) for 15 μM stapled disulfide-bound coiled-coil variant **(*R*,*S*)-d27e/29g'-xx** (QX3118) in 20 mM sodium phosphate (pH 7) with 4 M GdnHCl. Fit parameters from equations S1–S3 appear in the table, as do calculated values for ΔG_f, ΔH_f, and $-T\Delta S_f \pm$ standard error at the indicated temperature.

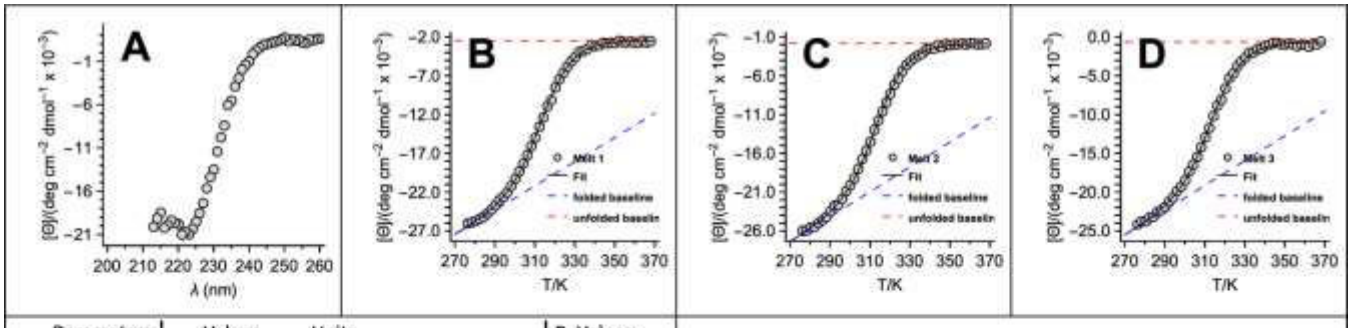

Parameters	Values	Units	P–Values
ΔH_0	−25.25 ± 0.33	kcal/mol	<0.001
T_m	42.2 ± 0.2	°C	<0.001
ΔC_p	---	---	---
a1	−69.6 ± 2.3	deg cm^{-2} dmol^{-1} x 10^{-3}	<0.001
b1	0.156 ± 0.008	deg cm^{-2} dmol^{-1} K^{-1} x 10^{-3}	<0.001
c1	−2.43 ± 0.05	deg cm^{-2} dmol^{-1} x 10^{-3}	<0.001
d1	---	---	---
a2	−70.7 ± 2.3	deg cm^{-2} dmol^{-1} x 10^{-3}	<0.001
b2	0.160 ± 0.008	deg cm^{-2} dmol^{-1} K^{-1} x 10^{-3}	<0.001
c2	−1.81 ± 0.05	deg cm^{-2} dmol^{-1} x 10^{-3}	<0.001
d2	---	---	---
a3	−68.6 ± 2.2	deg cm^{-2} dmol^{-1} x 10^{-3}	<0.001
b3	0.160 ± 0.008	deg cm^{-2} dmol^{-1} K^{-1} x 10^{-3}	<0.001
c3	−0.62 ± 0.05	deg cm^{-2} dmol^{-1} x 10^{-3}	<0.001
d3	---	---	---

$R^2 = 0.99985$
sum residuals^2 = 4.18787

For **(R,S)–sd27e/29g'–x4x**, at 306.2 K,
$\Delta G = -0.73 \pm 0.02$ kcal/mol
$\Delta H = -25.2 \pm 0.3$ kcal/mol
$-T\Delta S = 24.5 \pm 0.3$ kcal/mol

Figure S146. (A) CD spectra and (B–D) variable temperature CD data (triplicate) for 15 μM stapled disulfide-bound coiled-coil variant ***(R,S)*-sd27e/29g'-xx** (QX3118) in 20 mM sodium phosphate (pH 7) with 4 M GdnHCl. Fit parameters from equations S1–S3 appear in the table, as do calculated values for ΔG_f, ΔH_f, and $-T\Delta S_f \pm$ standard error at the indicated temperature.

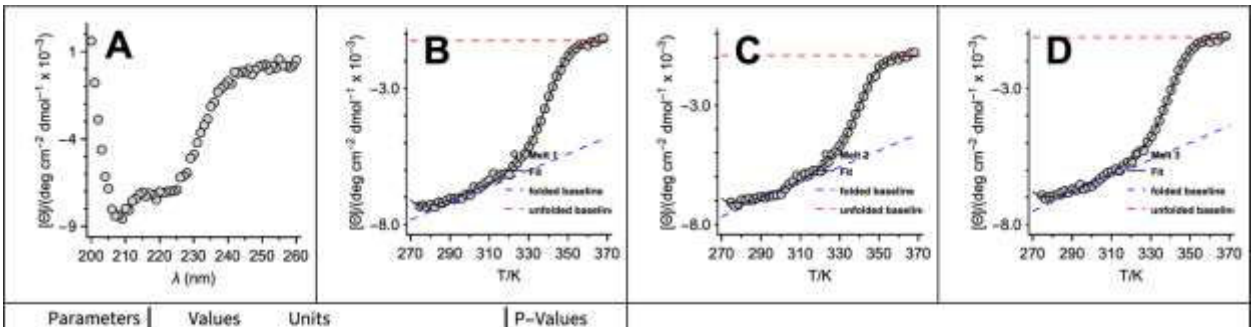

Parameters	Values	Units	P–Values
ΔH_0	−38.42 ± 1.02	kcal/mol	<0.001
T_m	66.4 ± 0.2	°C	<0.001
ΔC_p	−0.880 ± 0.034	kcal/mol/K	<0.001
a1	−16.0 ± 0.4	deg cm^{-2} dmol^{-1} x 10^{-3}	<0.001
b1	0.030 ± 0.001	deg cm^{-2} dmol^{-1} K^{-1} x 10^{-3}	<0.001
c1	−1.24 ± 0.03	deg cm^{-2} dmol^{-1} x 10^{-3}	<0.001
d1	---	---	---
a2	−17.0 ± 0.4	deg cm^{-2} dmol^{-1} x 10^{-3}	<0.001
b2	0.035 ± 0.001	deg cm^{-2} dmol^{-1} K^{-1} x 10^{-3}	<0.001
c2	−0.89 ± 0.03	deg cm^{-2} dmol^{-1} x 10^{-3}	<0.001
d2	---	---	---
a3	−15.9 ± 0.4	deg cm^{-2} dmol^{-1} x 10^{-3}	<0.001
b3	0.031 ± 0.001	deg cm^{-2} dmol^{-1} K^{-1} x 10^{-3}	<0.001
c3	−1.11 ± 0.03	deg cm^{-2} dmol^{-1} x 10^{-3}	<0.001
d3	---	---	---

$R^2 = 0.99981$
sum residuals^2 = 0.75005

For **a**, at 339.6 K,
$\Delta G = 0.00 \pm 0.02$ kcal/mol
$\Delta H = -38.4 \pm 1.0$ kcal/mol
$-T\Delta S = 38.4 \pm 1.0$ kcal/mol

Figure S147. (A) CD spectra and (B–D) variable temperature CD data (triplicate) for 15 μM HER2 native affibody variant **a** (CD1054) in 20 mM sodium phosphate (pH 7). Fit parameters from equations S1–S3 appear in the table, as do calculated values for ΔG_f, ΔH_f, and $-T\Delta S_f \pm$ standard error at the indicated temperature.

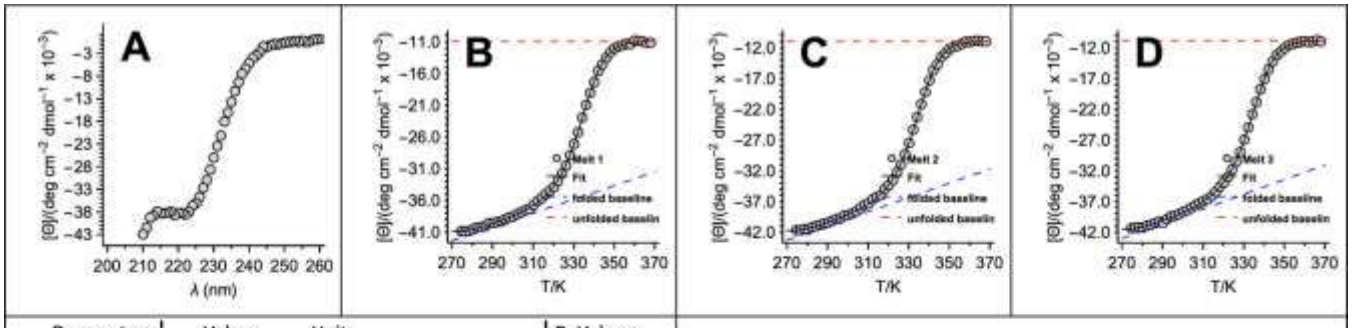

Parameters	Values	Units	P–Values
ΔH_0	−36.08 ± 0.27	kcal/mol	<0.001
T_m	60.9 ± 0.1	°C	<0.001
ΔC_p	−0.810 ± 0.015	kcal/mol/K	<0.001
a1	−71.6 ± 0.9	deg cm^{-2} dmol^{-1} x 10^{-3}	<0.001
b1	0.109 ± 0.003	deg cm^{-2} dmol^{-1} K^{-1} x 10^{-3}	<0.001
c1	−10.91 ± 0.04	deg cm^{-2} dmol^{-1} x 10^{-3}	<0.001
d1	---	---	---
a2	−74.4 ± 0.9	deg cm^{-2} dmol^{-1} x 10^{-3}	<0.001
b2	0.116 ± 0.003	deg cm^{-2} dmol^{-1} K^{-1} x 10^{-3}	<0.001
c2	−10.92 ± 0.04	deg cm^{-2} dmol^{-1} x 10^{-3}	<0.001
d2	---	---	---
a3	−75.3 ± 0.9	deg cm^{-2} dmol^{-1} x 10^{-3}	<0.001
b3	0.120 ± 0.003	deg cm^{-2} dmol^{-1} K^{-1} x 10^{-3}	<0.001
c3	−10.80 ± 0.04	deg cm^{-2} dmol^{-1} x 10^{-3}	<0.001
d3	---	---	---

$R^2 = 0.99999$
sum residuals^2 = 1.91732

For **a8/42–xx**, at 339.6 K,
$\Delta G = 0.64 \pm 0.01$ kcal/mol
$\Delta H = -40.6 \pm 0.3$ kcal/mol
$-T\Delta S = 41.2 \pm 0.3$ kcal/mol

Figure S148. (A) CD spectra and (B–D) variable temperature CD data (triplicate) for 15 μM stapled affibody variant **a8/42-xx** (QX3102) in 20 mM sodium phosphate (pH 7). Fit parameters from equations S1–S3 appear in the table, as do calculated values for ΔG_f, ΔH_f, and $-T\Delta S_f \pm$ standard error at the indicated temperature.

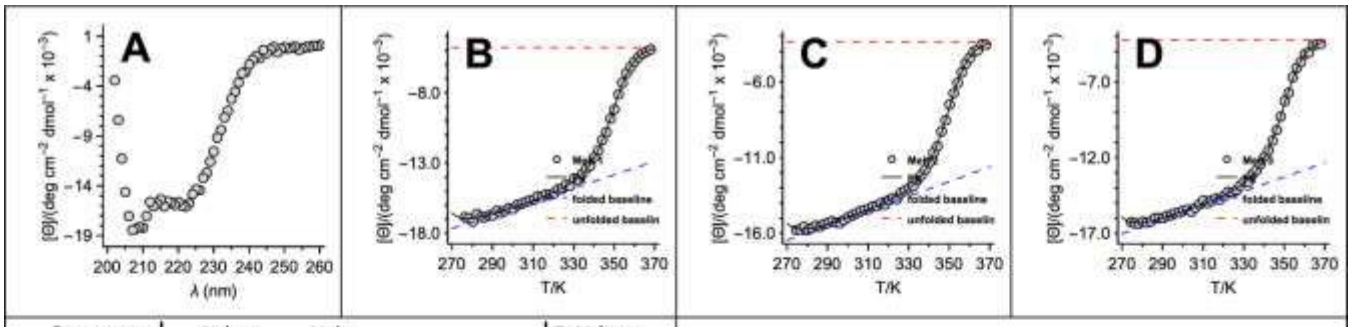

Parameters	Values	Units	P–Values
ΔH_0	−43.47 ± 0.71	kcal/mol	<0.001
T_m	76.1 ± 0.1	°C	<0.001
ΔC_p	−0.880 ± 0.022	kcal/mol/K	<0.001
a1	−30.6 ± 0.4	deg cm^{-2} dmol^{-1} x 10^{-3}	<0.001
b1	0.048 ± 0.001	deg cm^{-2} dmol^{-1} K^{-1} x 10^{-3}	<0.001
c1	−4.76 ± 0.05	deg cm^{-2} dmol^{-1} x 10^{-3}	<0.001
d1	---	---	---
a2	−29.6 ± 0.4	deg cm^{-2} dmol^{-1} x 10^{-3}	<0.001
b2	0.049 ± 0.001	deg cm^{-2} dmol^{-1} K^{-1} x 10^{-3}	<0.001
c2	−3.34 ± 0.05	deg cm^{-2} dmol^{-1} x 10^{-3}	<0.001
d2	---	---	---
a3	−29.7 ± 0.4	deg cm^{-2} dmol^{-1} x 10^{-3}	<0.001
b3	0.047 ± 0.001	deg cm^{-2} dmol^{-1} K^{-1} x 10^{-3}	<0.001
c3	−4.23 ± 0.05	deg cm^{-2} dmol^{-1} x 10^{-3}	<0.001
d3	---	---	---

$R^2 = 0.99995$
sum residuals^2 = 1.17004

For **sa8/42–x4x**, at 339.6 K,
$\Delta G = -1.09 \pm 0.02$ kcal/mol
$\Delta H = -34.9 \pm 0.7$ kcal/mol
$-T\Delta S = 33.9 \pm 0.7$ kcal/mol

Figure S149. (A) CD spectra and (B–D) variable temperature CD data (triplicate) for 15 μM stapled affibody variant **sa8/42-x4x** (QX3106s) in 20 mM sodium phosphate (pH 7). Fit parameters from equations S1–S3 appear in the table, as do calculated values for ΔG_f, ΔH_f, and $-T\Delta S_f$ ± standard error at the indicated temperature.

6. Proteolysis of coiled-coil variants

15 μM protein solutions in 20 mM sodium phosphate buffer (pH 7) were incubated at ambient temperature with 17 μg/mL proteinase K respectively for up to 5 hours. At each of the several time points, the proteolysis reaction was quenched by adding 40 μL of aqueous trifluoroacetic acid (1% v/v) to 40 uL of the reaction mixture. The quenched mixture was then analyzed in triplicate by reverse phase HPLC analytical column, monitored by a UV-Vis detector at 220 nm. The degradation of the proteins was assessed using the integrated HPLC peak area to account for how much of the full-length protein remained at each time point. The protein half-lives were calculated by fitting the integrated peak areas as a function of time to a mono exponential decay equation:

$$\text{Area}(t) = A \bullet \exp[-kt],$$

where t is time in minutes, A is a constant corresponding to relative integrated peak area at t = 0, and τ is the decay time, which is related to the protein half-life $t_{1/2}$ ($t_{1/2} = \tau \ln 2$). Decay traces for proteins coiled-coil variants, **d27*e*/29*g*'-xx** (QX2271); **sd27*e*/29*g*'-x4x** (QX2283); **d27*e*/29*g*'-z2x** (QX2289); **sd27*e*/29*g*'-z2x** (QX2289s); **d24*b*/25*c*'-z4x** (QX2291); **sd24*b*/25*c*'-z4x** (QX2291s); **d6*e*/8*g*'-z4x** (QX2292); **sd6*e*/8*g*'-z4x** (QX2292s); **d27*e*/22*g*'-z2x** (QX2293); **sd27*e*/22*g*'-z2x** (QX2292s); **d27*e*/22*g*'-z4x** (QX2294); **sd27*e*/22*g*'-z4x** (QX2294s) are shown in Figures S142–S156.

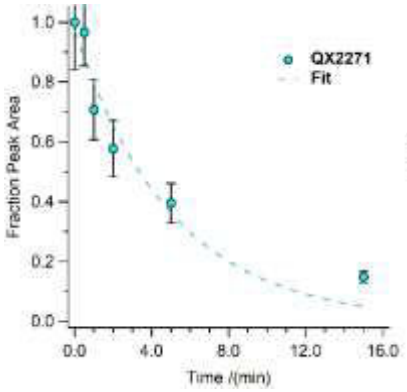

QX2271 Parameters	Values	P-Values
A	0.97 ± 0.1	<0.001
k	0.20 ± 0.04	0.012
R^2	0.9888	

Figure S150. Proteolysis of **d27*e*/29*g*'-xx** (QX2271) at 50 μM protein concentration in 20 mM sodium phosphate buffer pH 7 by proteinase K (17 μg/mL) as monitored by HPLC. Data points are shown as blue circles; each represents the average of three replicate experiments, with error bars representing standard error. The dashed line represents fit of the data to a mono exponential decay function, which was used to calculate the indicated apparent proteolysis rate constant.

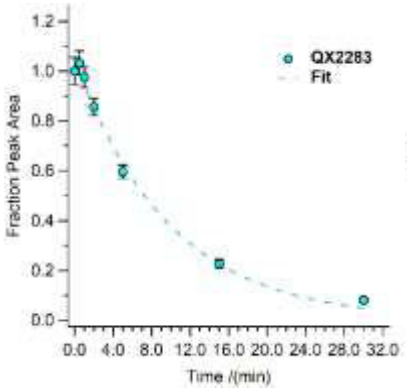

QX2283 Parameters	Values	P-Values
A	1.05 ± 0.0	<0.001
k	0.10 ± 0.01	<0.001
R^2	0.9984	

Figure S151. Proteolysis of **sd27*e*/29*g*'-x4x** (QX2283) at 50 μM protein concentration in 20 mM sodium phosphate buffer pH 7 by proteinase K (17 μg/mL) as monitored by HPLC. Data points for are shown as blue circles; each represents the average of three replicate experiments, with error bars representing standard error. The dashed line represents fit of the data to a mono exponential decay function, which was used to calculate the indicated apparent proteolysis rate constant.

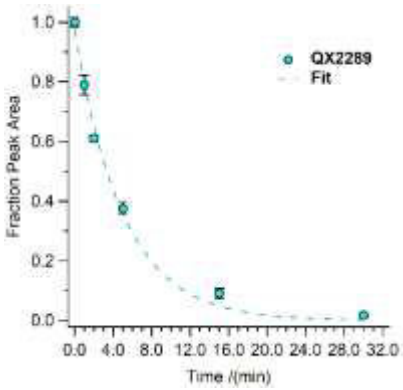

QX2289 Parameters	Values	P-Values
A	0.97 ± 0.0	<0.001
k	0.20 ± 0.02	<0.001
R^2	0.9977	

Figure S152. Proteolysis of **d27*e*/29*g*'-z2x** (QX2289) at 50 μM protein concentration in 20 mM sodium phosphate buffer pH 7 by proteinase K (17 μg/mL) as monitored by HPLC. Data points are shown as blue circles; each represents the average of three replicate experiments, with error bars representing standard error. The dashed line represents fit of the data to a mono exponential decay function, which was used to calculate the indicated apparent proteolysis rate constant.

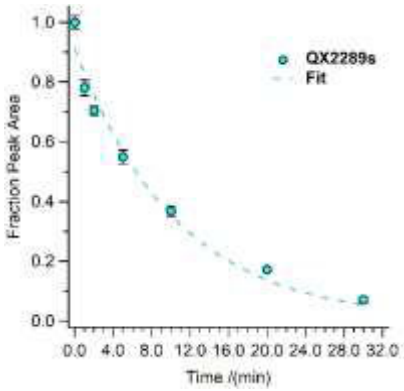

QX2289s Parameters	Values	P-Values
A	0.91 ± 0.0	<0.001
k	0.09 ± 0.01	<0.001
R^2	0.9942	

Figure S153. Proteolysis of **sd27*e*/29*g*'-z2x** (QX2289s) at 50 μM protein concentration in 20 mM sodium phosphate buffer pH 7 by proteinase K (17 μg/mL) as monitored by HPLC. Data points are shown as blue circles; each represents the average of three replicate experiments, with error bars representing standard error. The dashed line represents fit of the data to a mono exponential decay function, which was used to calculate the indicated apparent proteolysis rate constant.

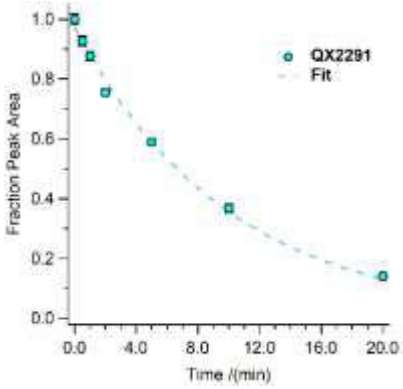

QX2291 Parameters	Values	P-Values
A	0.97 ± 0.0	<0.001
k	0.10 ± 0.00	<0.001
R^2	0.9993	

Figure S154. Proteolysis of **d24*b*/25*c*'-z4x** (QX2291) at 50 μM protein concentration in 20 mM sodium phosphate buffer pH 7 by proteinase K (17 μg/mL) as monitored by HPLC. Data points for are shown as blue circles; each represents the average of three replicate experiments, with error bars representing standard error. The dashed line represents fit of the data to a mono exponential decay function, which was used to calculate the indicated apparent proteolysis rate constant.

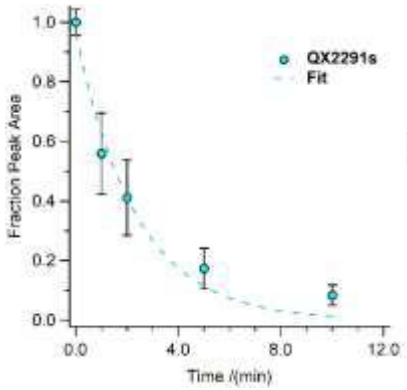

QX2291s Parameters	Values	P–Values
A	0.96 ± 0.1	<0.001
k	0.43 ± 0.07	0.009
R^2	0.9903	

Figure S155. Proteolysis of **sd24*b*/25*c*'-z4x** (QX2291s) at 50 μM protein concentration in 20 mM sodium phosphate buffer pH 7 by proteinase K (17 μg/mL) as monitored by HPLC. Data points are shown as blue circles; each represents the average of three replicate experiments, with error bars representing standard error. The dashed line represents fit of the data to a mono exponential decay function, which was used to calculate the indicated apparent proteolysis rate constant.

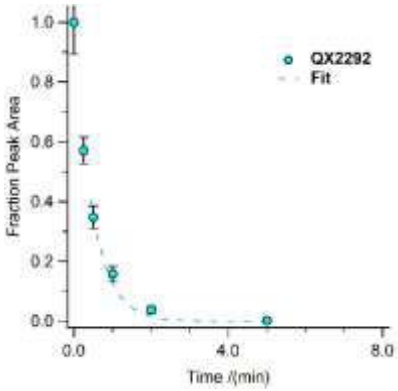

QX2292 Parameters	Values	P–Values
A	0.99 ± 0.0	<0.001
k	2.04 ± 0.10	<0.001
R^2	0.9986	

Figure S156. Proteolysis of **d6*e*/8*g*'-z4x** (QX2292) at 50 μM protein concentration in 20 mM sodium phosphate buffer pH 7 by proteinase K (17 μg/mL) as monitored by HPLC. Data points are shown as blue circles; each represents the average of three replicate experiments, with error bars representing standard error. The dashed line represents fit of the data to a mono exponential decay function, which was used to calculate the indicated apparent proteolysis rate constant.

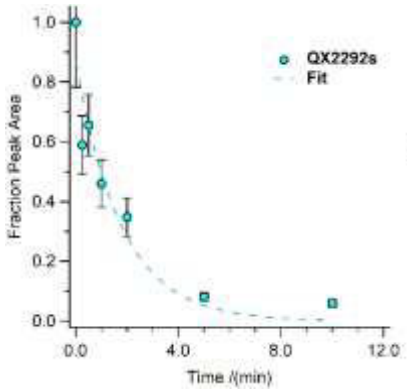

QX2292s Parameters	Values	P–Values
A	0.86 ± 0.1	<0.001
k	0.56 ± 0.15	0.013
R^2	0.9744	

Figure S157. Proteolysis of **sd6*e*/8*g*'-z4x** (QX2292s) at 50 μM protein concentration in 20 mM sodium phosphate buffer pH 7 by proteinase K (17 μg/mL) as monitored by HPLC. Data points are shown as blue circles; each represents the average of three replicate experiments, with error bars representing standard error. The dashed line represents fit of the data to a mono exponential decay function, which was used to calculate the indicated apparent proteolysis rate constant.

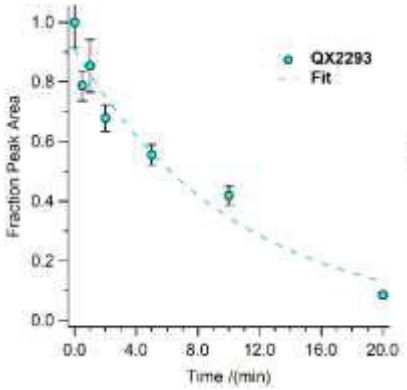

QX2293 Parameters	Values	P–Values
A	0.91 ± 0.0	<0.001
k	0.10 ± 0.02	0.002
R^2	0.9916	

Figure S158. Proteolysis of **d27*e*/22*g*'-*z*2x** (QX2293) at 50 µM protein concentration in 20 mM sodium phosphate buffer pH 7 by proteinase K (17 µg/mL) as monitored by HPLC. Data points are shown as blue circles; each represents the average of three replicate experiments, with error bars representing standard error. The dashed line represents fit of the data to a mono exponential decay function, which was used to calculate the indicated apparent proteolysis rate constant.

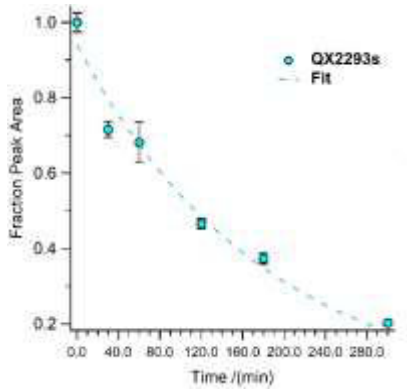

QX2293s Parameters	Values	P–Values
A	0.94 ± 0.0	<0.001
k	0.01 ± 0.00	<0.001
R^2	0.9951	

Figure S159. Proteolysis of **sd27*e*/22*g*'-*z*2x** (QX2293s) at 50 µM protein concentration in 20 mM sodium phosphate buffer pH 7 by proteinase K (17 µg/mL) as monitored by HPLC. Data points are shown as blue circles; each represents the average of three replicate experiments, with error bars representing standard error. The dashed line represents fit of the data to a mono exponential decay function, which was used to calculate the indicated apparent proteolysis rate constant.

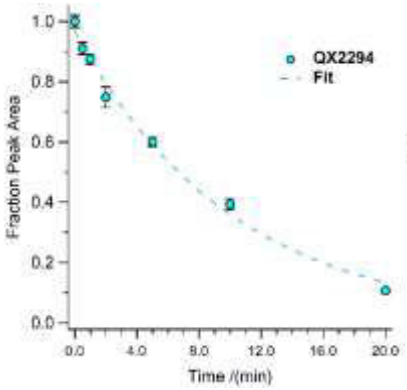

QX2294 Parameters	Values	P–Values
A	0.97 ± 0.0	<0.001
k	0.10 ± 0.01	<0.001
R^2	0.9986	

Figure S160. Proteolysis of **d27*e*/22*g*'-*z*4x** (QX2294) at 50 µM protein concentration in 20 mM sodium phosphate buffer pH 7 by proteinase K (17 µg/mL) as monitored by HPLC. Data points are shown as blue circles; each represents the average of three replicate experiments, with error bars representing standard error. The dashed line represents fit of the data to a mono exponential decay function, which was used to calculate the indicated apparent proteolysis rate constant.

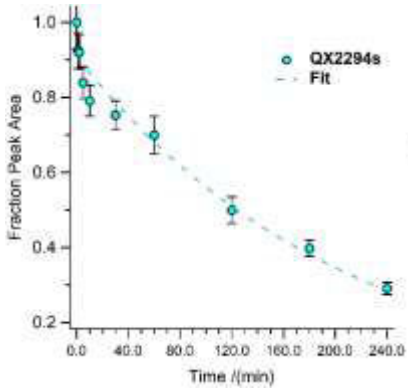

QX2294s Parameters	Values	P–Values
A	0.91 ± 0.0	<0.001
k	0.00 ± 0.00	<0.001
R^2	0.9966	

Figure S161. Proteolysis of **sd27*e*/22*g*'-z4x** (QX2294s) at 50 μM protein concentration in 20 mM sodium phosphate buffer pH 7 by proteinase K (17 μg/mL) as monitored by HPLC. Data points are shown as blue circles; each represents the average of three replicate experiments, with error bars representing standard error. The dashed line represents fit of the data to a mono exponential decay function, which was used to calculate the indicated apparent proteolysis rate constant.

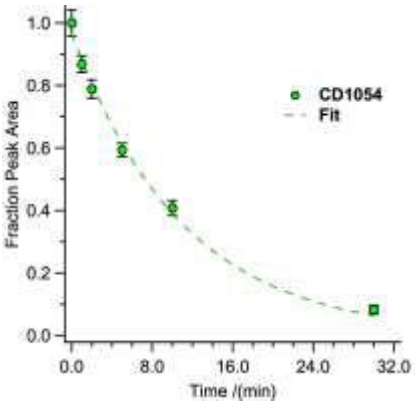

CD1054 Parameters	Values	P–Values
A	0.97 ± 0.0	<0.001
k	0.09 ± 0.01	<0.001
R^2	0.9991	

Figure S162. Proteolysis of native HER2 affibody **a** (CD1054) at 15 μM protein concentration in 20 mM sodium phosphate buffer pH 7 by proteinase K (17 μg/mL) as monitored by HPLC. Data points are shown as green circles; each represents the average of three replicate experiments, with error bars representing standard error. The dashed line represents fit of the data to a mono exponential decay function, which was used to calculate the indicated apparent proteolysis rate constant.

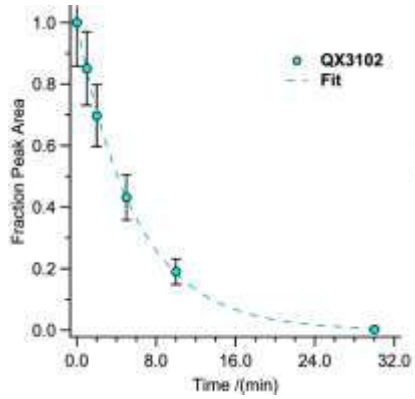

QX3102 Parameters	Values	P–Values
A	1.00 ± 0.0	<0.001
k	0.17 ± 0.00	<0.001
R^2	0.9999	

Figure S163. Proteolysis of **a8/42-xx** (QX3102) at 15 μM protein concentration in 20 mM sodium phosphate buffer pH 7 by proteinase K (17 μg/mL) as monitored by HPLC. Data points are shown as blue circles; each represents the average of three replicate experiments, with error bars representing standard error. The dashed line represents fit of the data to a mono exponential decay function, which was used to calculate the indicated apparent proteolysis rate constant.

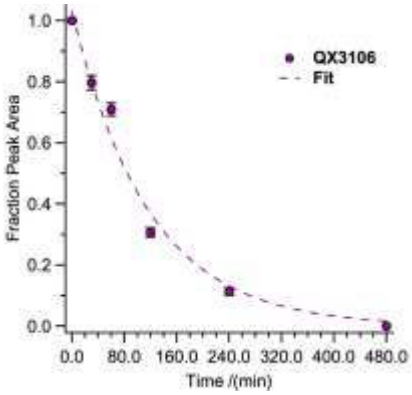

QX3106 Parameters	Values	P–Values
A	1.03 ± 0.1	<0.001
k	0.01 ± 0.00	0.001
R^2	0.9938	

Figure S164. Proteolysis of **sa8/42-x4x** (QX3106) at 15 μM protein concentration in 20 mM sodium phosphate buffer pH 7 by proteinase K (17 μg/mL) as monitored by HPLC. Data points are shown as dark magenta circles; each represents the average of three replicate experiments, with error bars representing standard error. The dashed line represents fit of the data to a mono exponential decay function, which was used to calculate the indicated apparent proteolysis rate constant.

7. Fluorescence polarization binding assay

Fluorescent affibody solutions of peptides **fa** (ZJ10611), **fa8/42-xx** (ZJ10612), and **fsa8/42-x4x** (ZJ1062)**,** with concentrations of 247 μM, 263 μM, and 57 μM, respectively, were diluted with phosphate buffer (pH 7.4) to 100 nM. The His-tagged recombinant HER2/ERBB2 extracellular domain (hereafter called the HER2 protein) was obtained from SinoBiological and prepared at a concentration of 2.7 μM. We performed direct binding fluorescence polarization assays using a constant concentration of fluorescent affibody against varying concentrations of the recombinant HER2 extra-cellular domain. We prepared the fluorescent affibody solution in a glass tube with 4970 μL of PBS solution, 25 μL β-casein blocking agent (final concentration 0.1 mg/mL) and 5 μL of fluorescent affibody stock solution (100 nM), yielding a final affibody concentration of 100 pM. The glass tube containing the fluorescent stock solution was inverted several times gently to mix. We aliquoted 200 μL of fluorescent affibody solution into each well of a 96-well plate and then added varying concentrations of the HER2 protein via serial dilution as follows: To the first well of the dilution series, we added an additional 190 μL of fluorescent affibody solution along with 10 μL of a 2.7 μM solution of the HER2 protein, bringing the total volume in the first well to 400 μL, such that the concentration of the HER2 protein in the first well was 65 nM. We then transferred 200 μL of the solution from the first well into the second well, leading to a two-fold dilution of the HER2 protein. We continued this dilution series by transferring 200 μL from well to well to generate a total of 19 different concentrations of HER2 protein, with the lowest concentration at 0.124 pM. Three 60 μL aliquots from each well were then transferred to a 384-well plate. We allowed 30 minutes for equilibration and measured the fluorescence polarization in each well using a Biotek Synergy Neo microplate reader with fluorescent polarization filters #4 (Dual FP) and #65 (FP 485/530, FP 530/590). We averaged the fluorescence polarization for these three replicate wells at each concentration of HER2 protein. We repeated this experiment for each affibody variant a total of three times on separate occasions. Data for **fa** (ZJ10611), **fa8/42-xx** (ZJ10612), and **fsa8/42-x4x** (ZJ1062) are shown in Figures S165-167. The data for the native variant **fa** were too noisy to justify further analysis. However, we fit the data for variant **fa8/42-xx** and its stapled counterpart **fsa8/42-x4x** to the following equation:

$$P = \frac{B_n \cdot [\text{affibody}]}{K_d + [\text{affibody}]}, \tag{S4}$$

where P is fluorescence polarization, [affibody] is the concentration of fluorescent affibody in M; B_n is the maximum fluorescence polarization (B_1 for replicate 1; B_2 for replicate 2; B_3 for replicate 3); K_d is the dissociation constant in M for binding of the fluorescent affibody to the HER2 protein. K_d values, fit parameters, and statistics appear in Figure S166–S167.

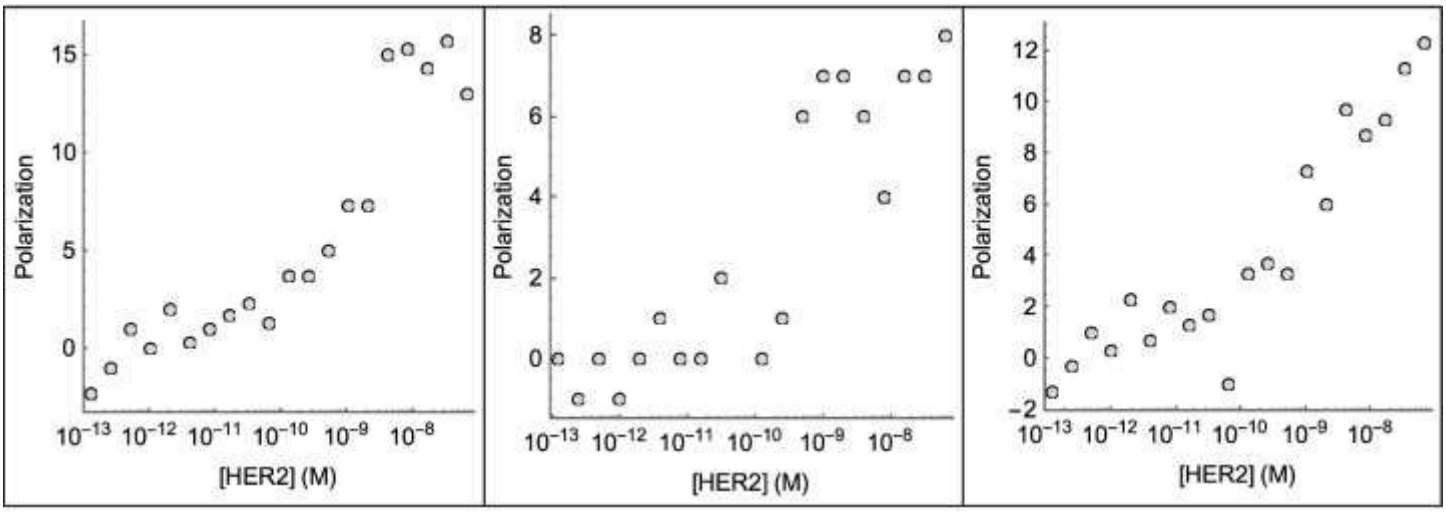

Figure S165. Fluorescence polarization data of native fluorescent affibody **fa** (ZJ10611) at 100 pM in PBS with varying concentrations of the HER2 protein. Data points are shown as grey circles; each represents the average of three wells; the three panels represent replicate data collected on three separate occasions.

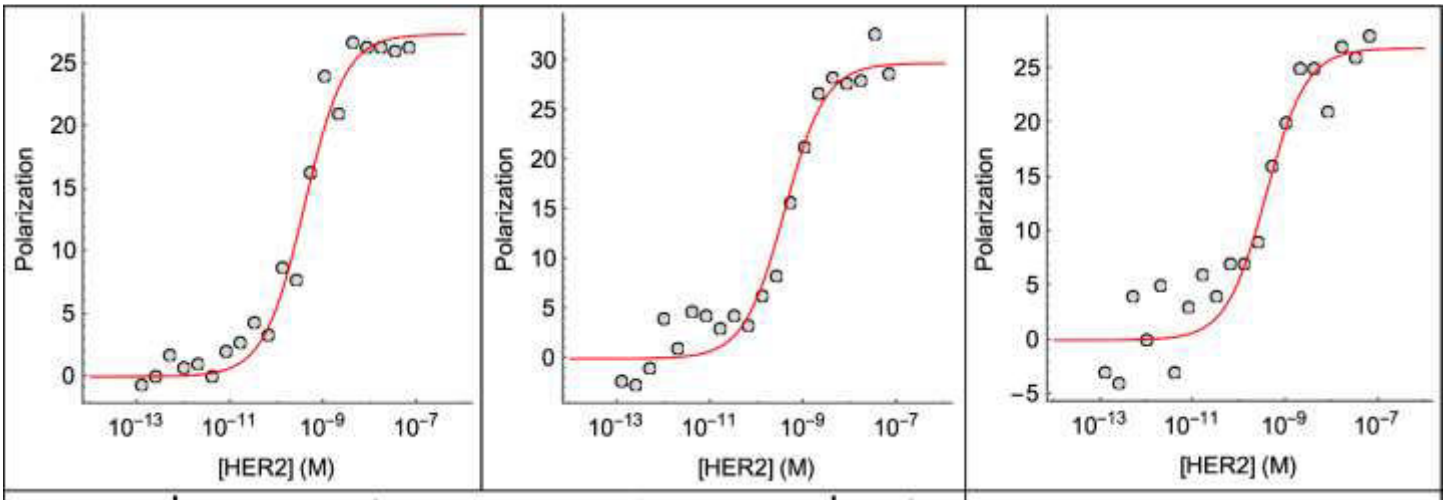

Parameters	Values	Units	P–Values
Kd	3.76E−10 ± 4.54E−11	M	<0.001
B_1	27.4 ± 1.0	polarization units	<0.001
B_2	29.791 ± 1.007	polarization units	<0.001
B_3	26.9 ± 1.0	polarization units	<0.001

$R^2 = 0.98007$

$\text{sum residuals}^2 = 312.05565$

Figure S166. Fluorescence polarization data for unstapled affibody **fa8/42-xx (ZJ10612)** at 100 pM in PBS with varying concentrations of the HER2 protein. Data points are shown as grey circles; each represents the average of three wells; the three panels represent replicate data collected on three separate occasions. The red line represents fit of the data to a binding curve given by equation S4.

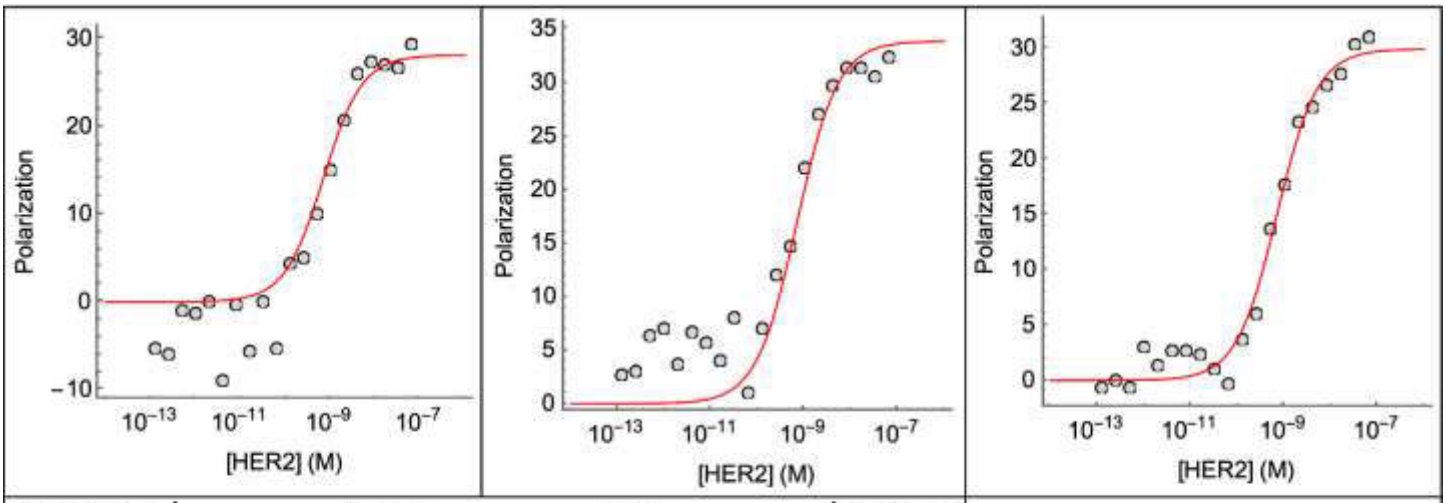

Parameters	Values	Units	P–Values
Kd	6.94E−10 ± 1.09E−10	M	<0.001
B_1	28.1 ± 1.5	polarization units	<0.001
B_2	33.835 ± 1.527	polarization units	<0.001
B_3	29.9 ± 1.5	polarization units	<0.001

$R^2 = 0.96416$

sum residuals^2 = 592.67501

Figure S167. Fluorescence polarization data of stapled affibody **fa8/42-x4x (ZJ1062)** at 100 pM protein concentration in PBS. Data points are shown as grey circles; each represents the average of three wells; the three panels represent replicate data collected on three separate occasions. The red line represents fit of the data to a binding curve given by equation S4.

8. Stapling between heterochiral residues

For monomeric helical peptide stapling crossing one helical turn or two, application of heterochiral residues can further enhance the stabilizing effect from stapling on α-helices, since the heterochiral residues are oriented toward to each other, adopting a more favorable geometry for crosslinking. The favorable geometry derived from the heterochiral residues has been applied to disulfide-bond-based stapling[4, 5] and metathesis-based stapling[6, 7] on monomeric helical peptides. We found that both the residue 27*e* and 29*g*' are oriented toward the same N-terminus direction of the coiled-coil heterodimer from the crystal structure. We wondered whether heterochiral residues at position 27*e* and 29*g*' will be more favorable for interhelical PEG stapling. Accordingly, we incorporated D-propargylglycine at *e*-position 27 on the acidic monomer, and L-propargylglycine at *g*-position 29' on the basic monomer to get heterodimer **(*R*,*S*)-d27e/29g'-xx** and its stapled counterpart **(*R*,*S*)-sd27e/29g'-x4x**. The stapled variant **(*R*,*S*)-d27e/29g'-xx** is -0.73 ± 0.04 kcal/mol more stable than its non-stapled counterpart **(*R*,*S*)-d27e/29g'-xx**, which is similar to that of the difference between **d27e/29g'-xx** vs. **sd27e/29g'-x4x**, in which L-propargylglycine was incorporated at both position 27*e* and 29*g*', indicating that stapling between residues of opposite chirality residues dose not contribute much stabilization to the impact of interhelical PEG stapling.

9. Synthesis and Characterization of PEGylated Asparagine Derivatives, bis-azido PEG, branched Y-shaped bis-azido PEG

Oxybis(ethane-2,1-diyl) dimethanesulfonate (QX2227)

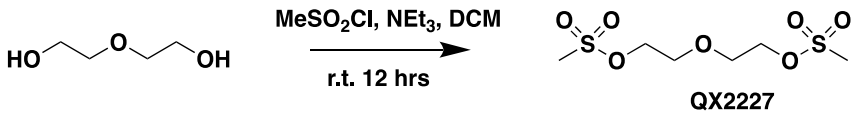

QX2227

Methanesulfonyl chloride (14.3 g, 125 mmol) was added dropwise to a stirred solution of 2,2'-oxybis(ethan-1-ol) (5.3 g, 50 mmol) and triethyl amine (15.2 g, 150 mmol) in dichloromethane (200 mL) at 0 °C. After the

addition was complete, the resulting mixture was stirred at r.t. for 12 hrs. Water was added to quench the reaction. The organic phase was separated, and the aqueous phase was extracted with dichloromethane (2 × 100 mL). The combined organic layers were washed with brine (3 × 100 mL), dried with anhydrous sodium sulfate, filtered, and the solvent was removed by rotary evaporation to afford 13.1 g of colorless oil, which was used in the next step without purification. Yield quantitative. MS(ESI-TOF) m/z calc. for $C_6H_{15}O_7S_2^+$ 263.03, found 263.02 [M+H$^+$]; calc. for $C_6H_{18}NO_7S_2^+$ 280.05, found 280.05 [M+NH$_4^+$].

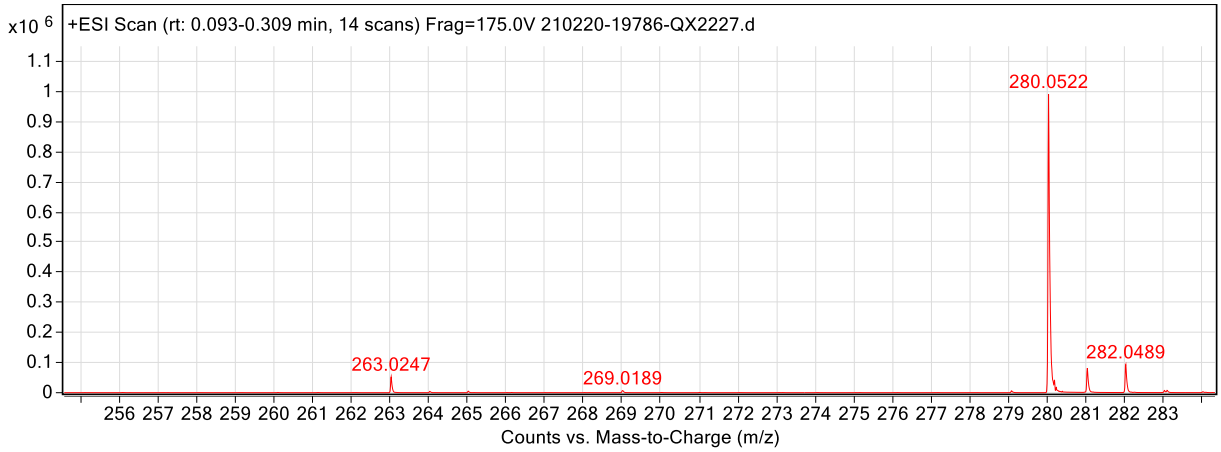

Figure S168. ESI-TOF MS data for QX2227.

1-Azido-2-(2-azidoethoxy)ethane (QX2228)

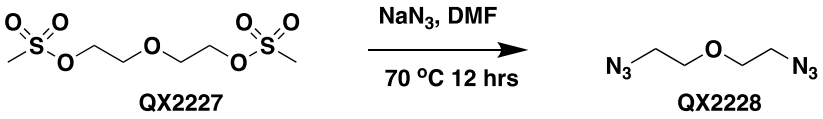

To a solution of NaN_3 (9.7 g, 150 mmol) in DMF (200 mL) was added QX2227 (13.1 g, 50 mmol) at room temperature. The reaction mixture was heated to 70 °C and stirred for 12 hours. The crude mixture was diluted with 400 mL of water and extracted with DCM (200 mL) for 3 times. The combined organic phases were washed with saturated brine and dried over anhydrous sodium sulfate, filtered, and the solvent was removed by rotary evaporation to afford 8.32 g of yellow oil. Yield quantitative. The crude product was used in the next step without further purification. The product was confirmed by Crude NMR: ^{1}H-NMR (300 MHz, Chloroform-d) δ 3.71 (t, J = 4.8 Hz, 4H), 3.44 (t, J = 4.8 Hz, 4H). ^{13}C-NMR (126 MHz, Chloroform-d) δ 70.10, 50.76.

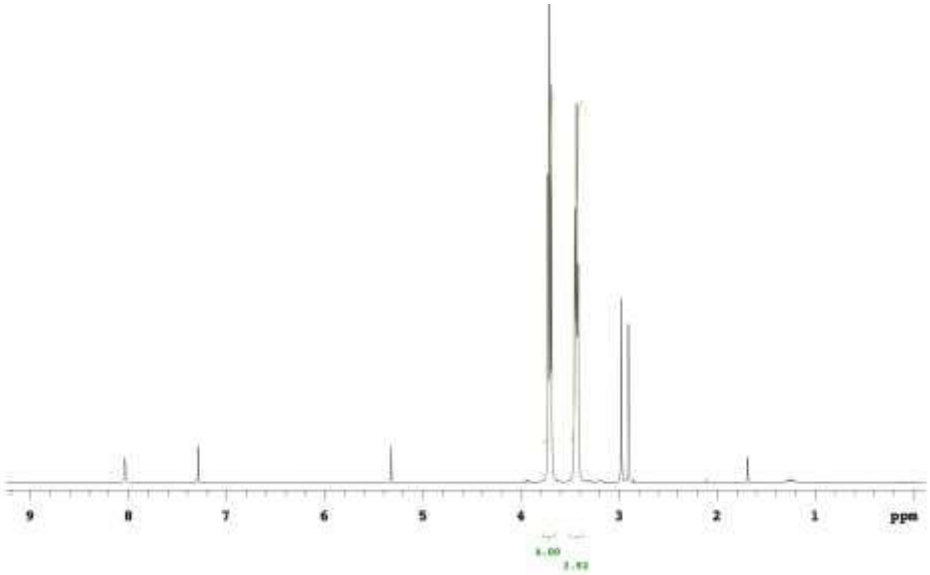

Figure S169. [1]H NMR data for QX2228.

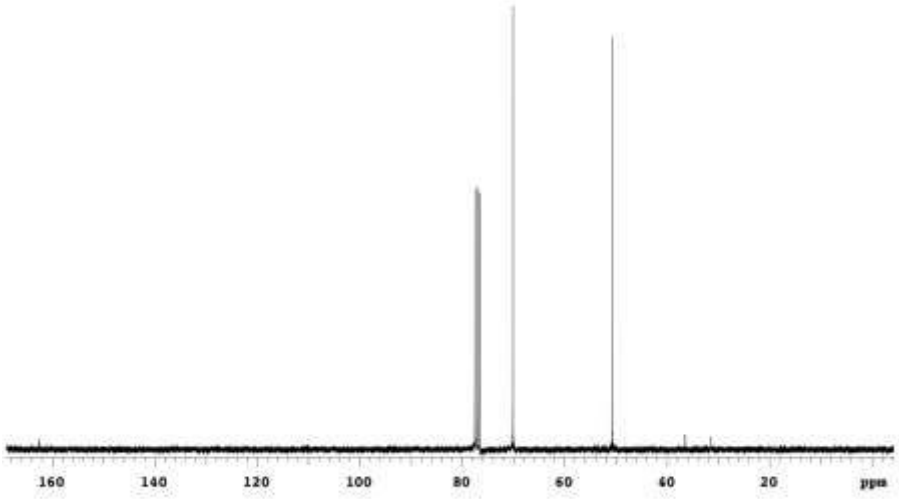

Figure S170. [13]C NMR data for QX2228.

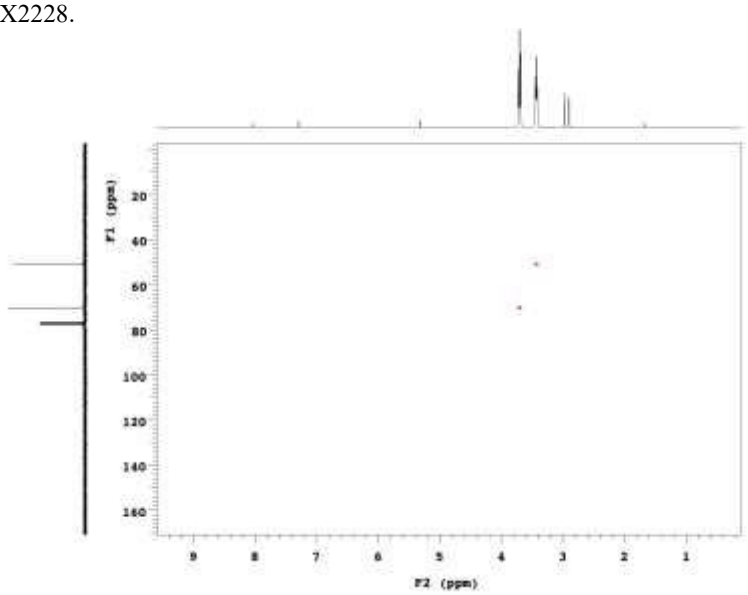

Figure S171. HSQC data for QX2228.

2-(2-Azidoethoxy)ethan-1-amine (QX2229)

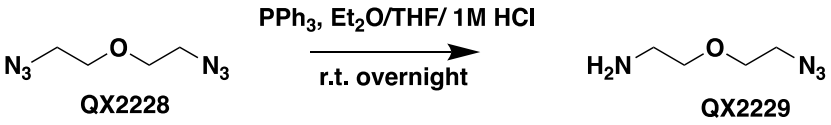

Triphenylphosphine (11 g, 45 mmol, 0.9 eq.) dissolved in ether (80 mL) was added to a solution of QX2228 (8.32 g, 50 mmol) in Ether/THF/ 1M aqueous HCl (50 mL/100 mL/50mL). Addition was performed over a period of 3 hours at room temperature and the reaction was stirred overnight. Phases were separated by a separation funnel and the organic layer was washed with 4M HCl aqueous solution. The combined aqueous layer was adjusted to pH 14 with sodium hydroxide powder. Product was then extracted with DCM (3 × 80 mL). Combined organic layer was dried over anhydrous sodium sulfate and filtered. After removal of the solvent under reduced pressure, a yellow oil was afforded (4.3 g, yield 66%), which was used in the next step without purification. MS(ESI-TOF) m/z calc. for $C_4H_{11}N_4O^+$ 131.09, found 131.09 [$M+H^+$].

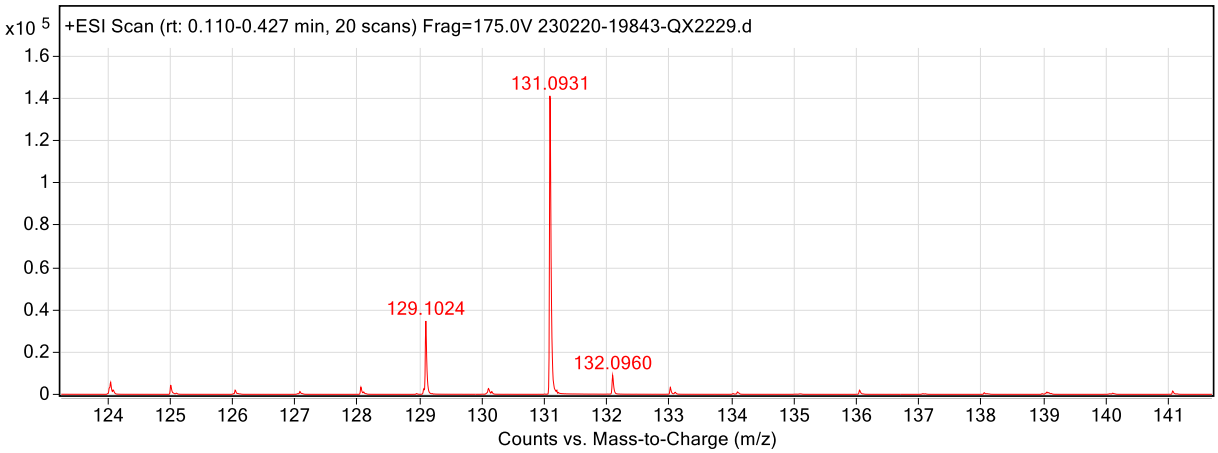

Figure S172. ESI-TOF MS data for QX2229.

tert-Butyl N^2-(((9H-fluoren-9-yl)methoxy)carbonyl)-N^4-(2-(2-azidoethoxy)ethyl)-L-asparaginate (QX2230)

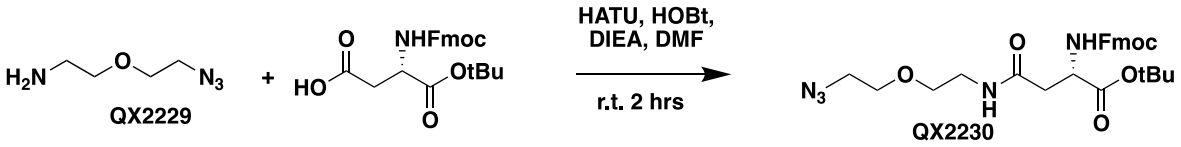

To N-Fmoc-O-tBu Asp (4.9 g, 12 mmol) dissolved in dry DMF (60 ml) was added HATU (7.4 g, 18 mmol), HOBT (2.4 g, 18 mmol), DIPEA (6.3 ml, 36 mmol). Then the mixture was stirred for 15 minutes at room temperature. Then compound QX2229 (1.9 g, 15 mmol, dissolved in 10 ml DMF) was added to the mixture and the mixture was stirred for another 2 hours at room temperature. Upon completion of the reaction monitored by TLC, 120 ml water was added to the flask and extracted 3 times with ethyl acetate (50 mL). The organic phases were combined, washed with brine, dried over anhydrous sodium sulfate and evaporated to dryness. The crude was purified by chromatography (EA/Hexane 1:1 to 1:0); MS(ESI-TOF) m/z calc. for $C_{27}H_{34}N_5O_6^+$ 524.25, found 524.25 [M+H$^+$]; ^{1}H NMR (500 MHz, Chloroform-*d*) δ 7.75 (d, *J* = 7.5 Hz, 2H), 7.60 (dd, *J* = 7, 3.5 Hz, 2H), 7.38 (t, *J* = 7.5 Hz, 2H), 7.30 (t, *J* = 7.5 Hz, 2H), 6.25 (br.s., 1H), 6.15 (d, *J* = 8 Hz, 1H), 4.52-4.48 (m., 1H), 4.39 (t, *J* = 7.5 Hz, 1H), 4.31 (t, *J* = 7.5 Hz, 1H), 4.22 (t, *J* = 7.5 Hz, 1H), 3.58 (t, *J* = 5 Hz, 2H), 3.50 (t, *J* = 5 Hz, 2H), 3.44 (d, *J* = 4.5 Hz, 2H), 3.29 (t, *J* = 4 Hz, 2H), 2.87 (dd, *J* = 15.5, 4.5 Hz, 1H), 2.72 (dd, *J* = 15.5, 4.5Hz, 1H), 1.47 (s, 9H). ^{13}C NMR (500 MHz, Chloroform-*d*) 170.15, 170.01, 156.24, 143.93, 143.81, 141.25, 127.71, 127.10, 127.08, 125.25, 125.20, 119.96, 82.29, 70.05, 69.59, 67.14, 51.42, 50.49, 47.10, 39.19, 37.91, 27.91.

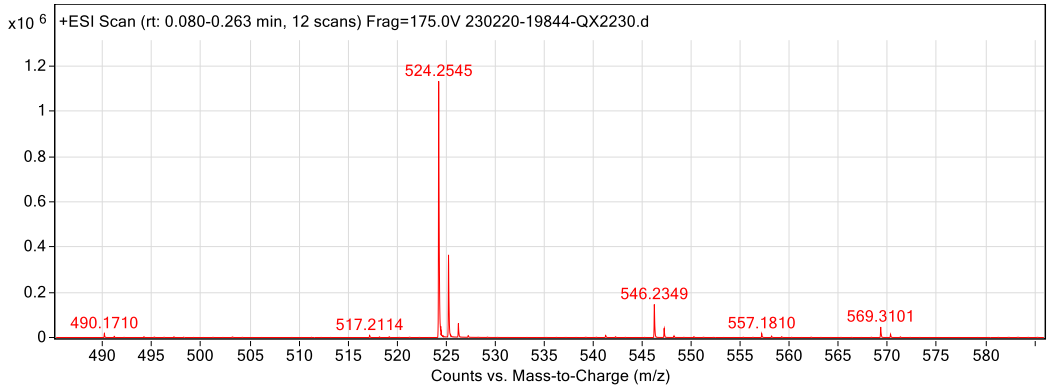

Figure S173. ESI-TOF MS data for QX2230.

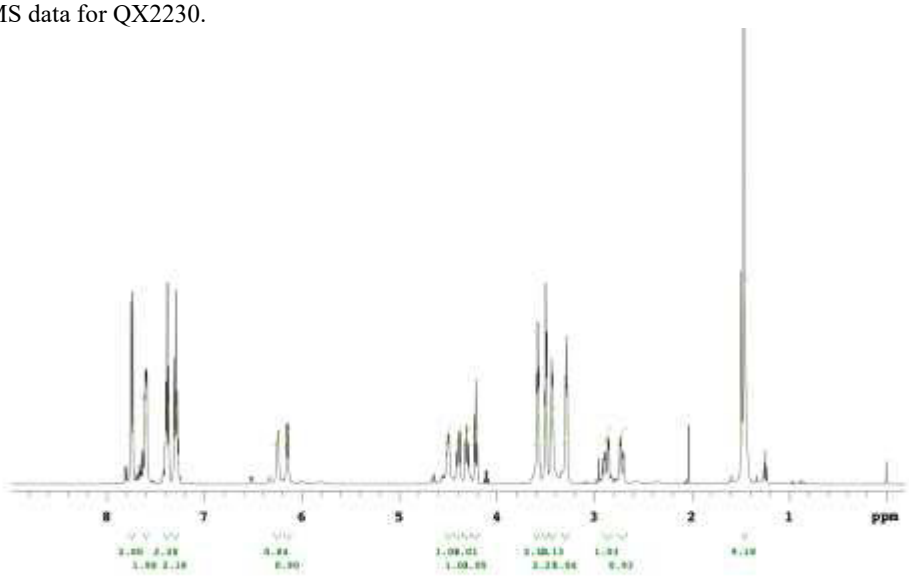

Figure S174. ^{1}H NMR data for QX2230.

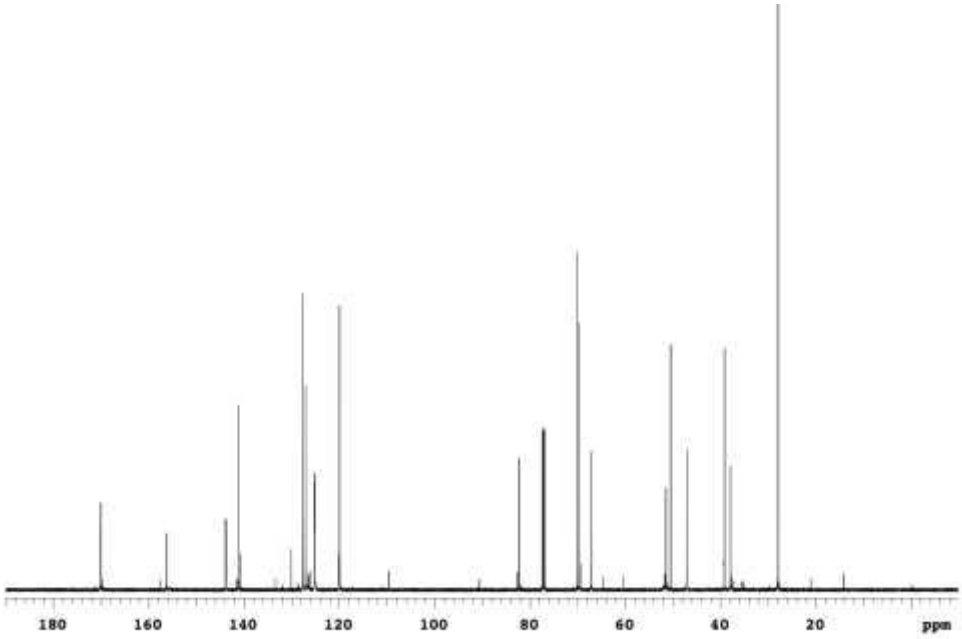

Figure S175. ^{13}C NMR data for QX2230.

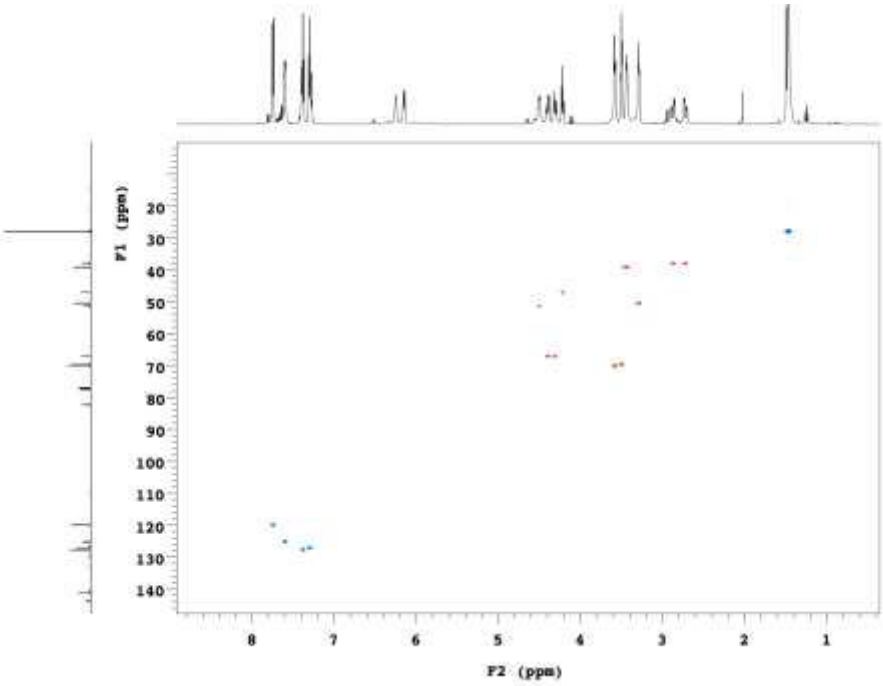

Figure S176. HSQC data for QX2230.

N^2-(((9H-fluoren-9-yl)methoxy)carbonyl)-N^4-(2-(2-azidoethoxy)ethyl)-L-asparagine (QX2232)

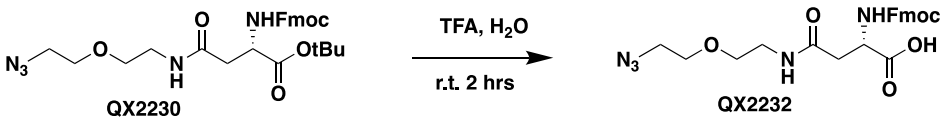

QX2230 QX2232

Compound QX2230 (1.0 g, 1.9 mmol) was dissolved in a mixture of TFA (3 ml) and water (150 uL). Then the reaction mixture was stirred at room temperature for 2 hours. After completion of the reaction, TFA and water were removed by rotary evaporation. Yield quantitative. The crude was used directly for peptide synthesis without purification. MS(ESI-TOF) m/z calc. for $C_{23}H_{27}N_5O_6^+$ 469.20, found 469.19 [$M+H^+$].

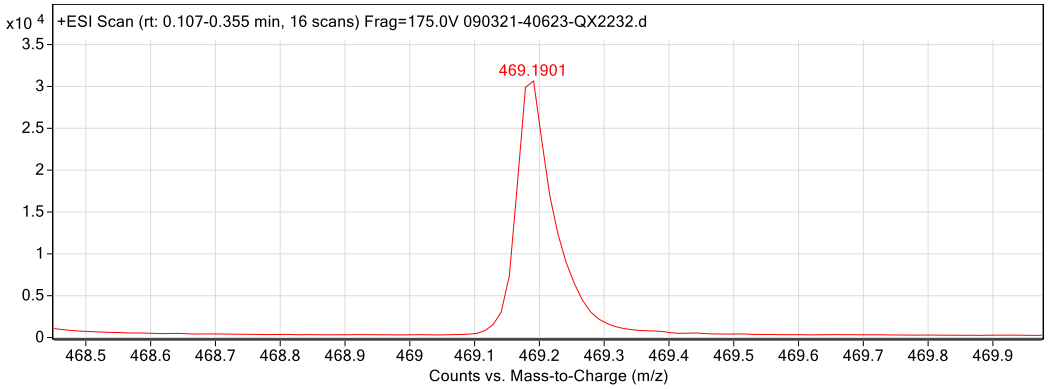

Figure S177. ESI-TOF MS data for QX2232.

2,5-Dioxopyrrolidin-1-yl (2,5,8,11-tetraoxatridecan-13-yl) carbonate (QX3065)

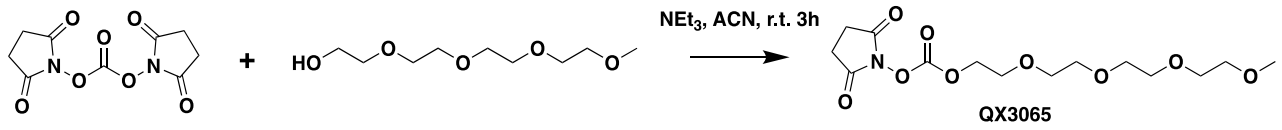

To a solution of 2,5,8,11-tetraoxatridecan-13-ol (2.08 g, 10 mmol), and bis(2,5-dioxopyrrolidin-1-yl) carbonate (3.84 g, 15 mmol), was added 4.16 mL (30 mmol) TEA. The resulting solution was stirred at r.t. for 3 hours. After the reaction was completed, monitored by TLC, the ACN solvent was removed and 100 mL DCM was added. Then the solution was washed with 5% sodium bicarbonate (50 mL× 3) then with water (50 mL × 2). The organic layer was then dried over sodium sulfate, filtered, and evaporated with reduced pressure to give us the crude product as colorless oil. Yield quantative. The crude was used in the next step without purification. MS(ESI-TOF) m/z calc. for $C_{14}H_{24}NO_9^+$ 350.14, found 350.15 [M+H$^+$]; calc. for $C_{14}H_{27}N_2O_9^+$ 367.17, found 367.17 [M+NH_4^+].

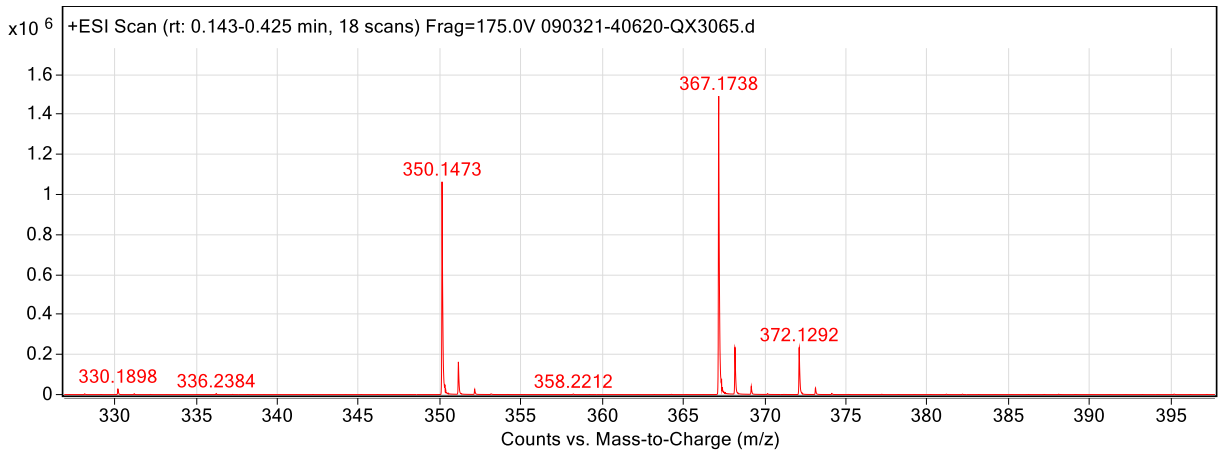

Figure S178. ESI-TOF MS data for QX3065.

2,2'-((Azanediylbis(ethane-2,1-diyl))bis(oxy))bis(ethan-1-ol) (QX3061)

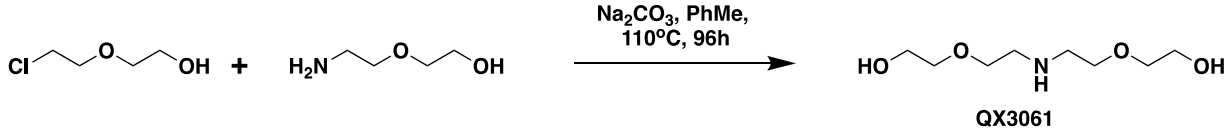

Add a solution of 2-(2-chloroethoxy)ethanol (6.4 mL, 60 mmol) in toluene(15 mL) dropwise to a stirred refluxing mixture of 2-(2-aminoethoxy)ethanol (24 mL, 240 mmol) and Na_2CO_3 (7 g, 66 mmol) in toluene (150 mL) in a flask fitted with Dean-Stark apparatus. Then the mixture was heated to 120 Celsius degree for 4 days. The solids were removed by filtration after the mixture was cooled to room temperature. The residue was washed by ether and the combined filtrates were concentrated in vacuo. The crude residue was purified by distillation. MS(ESI-TOF) m/z calc. for $C_8H_{20}NO_4^+$ 194.14, found 194.14 [M+H$^+$]. ^{1}H NMR (300 MHz, Chloroform-*d*) δ 3.72 (t, *J* = 4 Hz, 4H), 3.66-3.60 (m, 8H), 2.86 (t, *J* = 5.1 Hz, 1H). ^{13}C NMR (126 MHz, Chloroform-*d*) 72.71, 69.79, 61.63, 48.94.

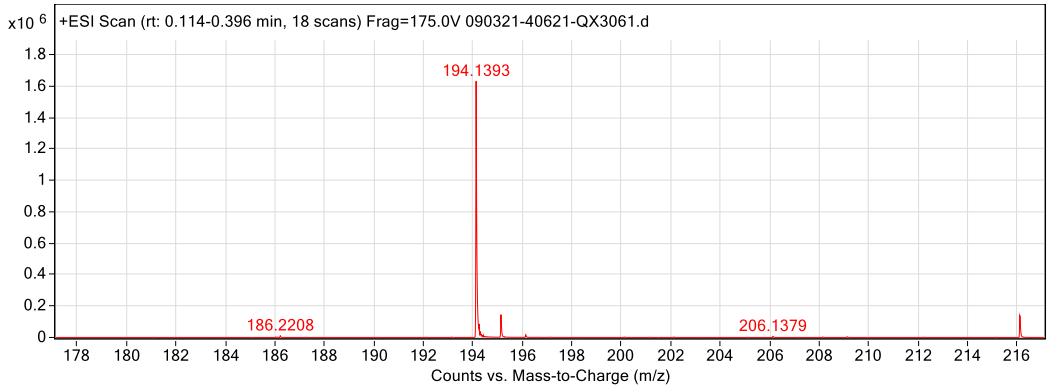

Figure S179. ESI-TOF MS data for QX3061.

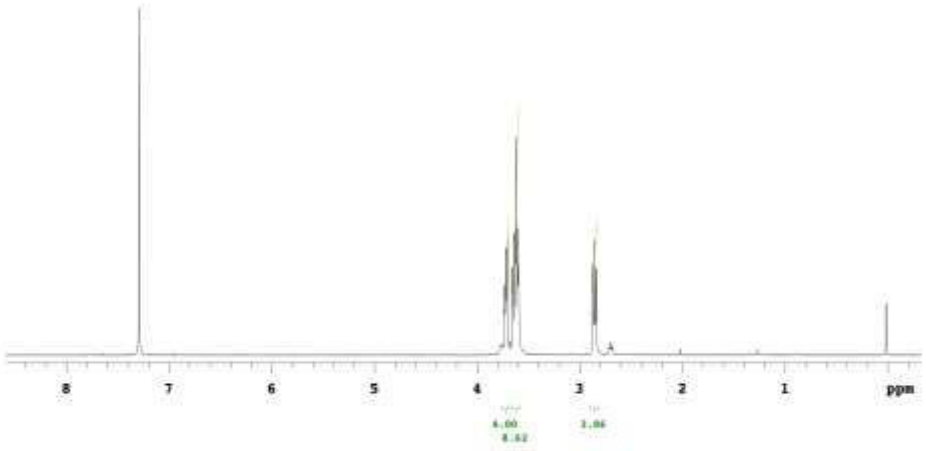

Figure S180. ^{1}H NMR data for QX3061.

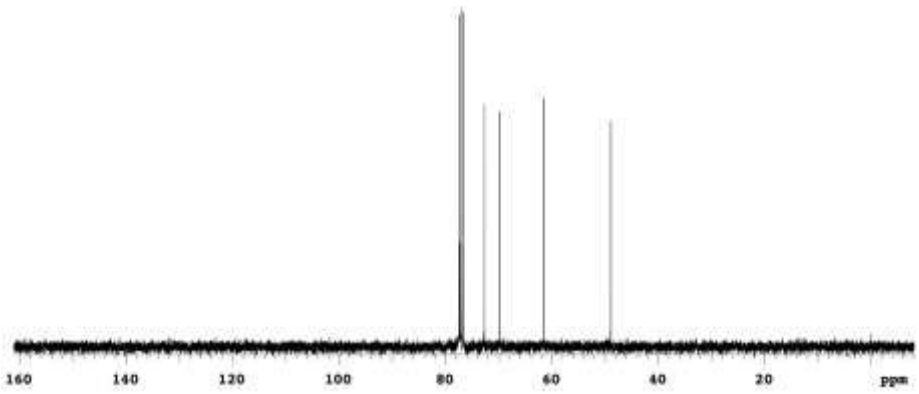

Figure S181. ^{13}C NMR for QX3061.

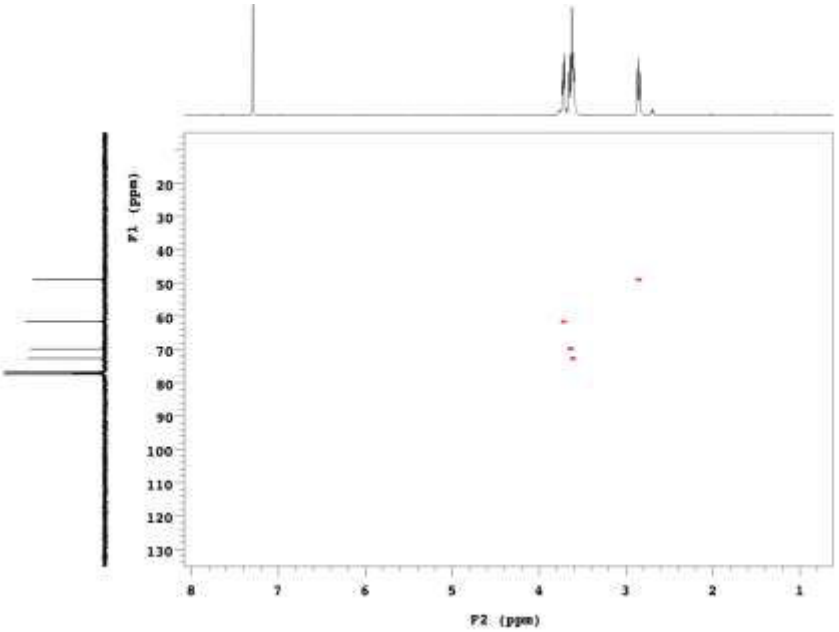

Figure S182. HSQC for QX3061.

15-Oxo-16-(2-(2-(tosyloxy)ethoxy)ethyl)-2,5,8,11,14,19-hexaoxa-16-azahenicosan-21-yl 4-methylbenzenesulfonate (QX3072)

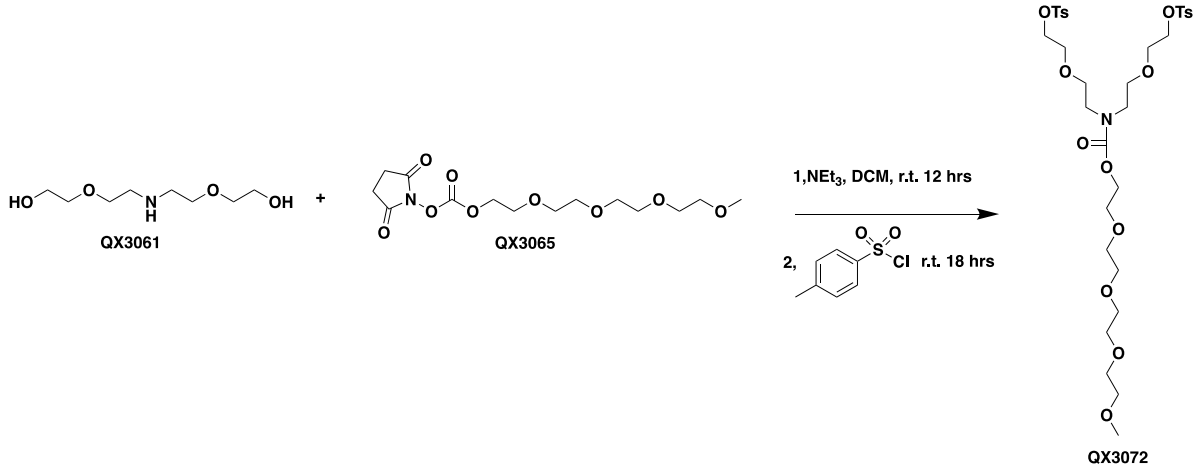

QX3065 (525 mg, 1.5 mmol) was added to a mixture of QX3061 (193 mg, 1.0 mmol) and TEA (415 uL, 3.0 mmol) in DCM (5 mL) at room temperature. Then the mixture was stirred at room temperature for 12 hours. Then additional TEA (276 uL, 2.0 mmol) was added to the mixture followed by 762 mg of TsCl (4.0 mmol). The reaction was stirred at room termperature for another 18 hours. Then the reaction was quenched with water, and the organic layer was further washed with sodium bicarbonate (5%) and brine. The crude was purified by chromatography (pure EA as mobile phase). MS(ESI-TOF) m/z calc. for $C_{32}H_{52}N_2O_{14}S_2^+$ 753.29, found 753.29 [M+NH_4^+]. ^{1}H NMR (300 MHz, Chloroform-*d*) δ 7.82 (t, *J* = 8.1 Hz, 4H), 7.37 (t, *J* = 8.1 Hz, 4H), 4.23 (t, *J* = 5.1 Hz, 2H), 4.16 (t, *J* = 4.5 Hz, 4H), 3.71-3.65 (m, 16H), 3.58-3.52 (m, 6H), 3.42 (t, *J* = 5.4 Hz, 4H), 3.40 (s, 3H) 2.47 (s, 6H). ^{13}C NMR (126 MHz, Chloroform-*d*) 156.05, 144.90, 132.93, 129.91, 127.97, 71.94, 70.61, 70.59, 70.54, 70.44, 70.01, 69.72, 69.51, 69.24, 68.44, 68.34, 67.45, 59.07, 48.20, 47.75, 21.69.

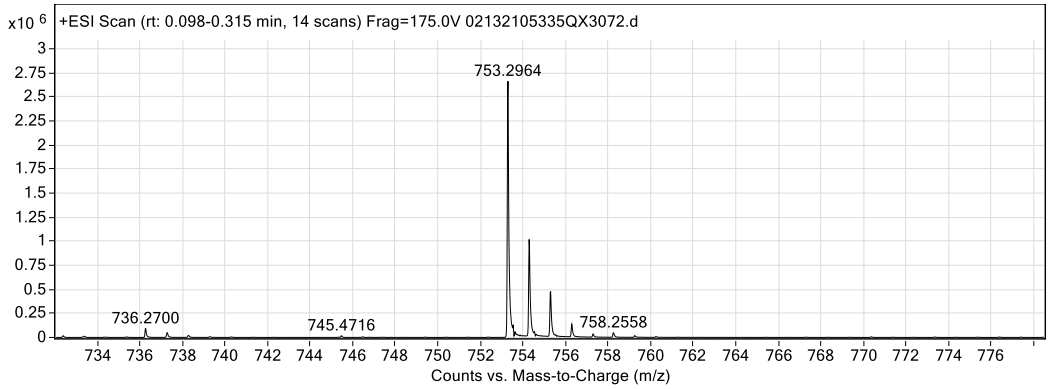

Figure S183. ESI-TOF MS data for QX3072.

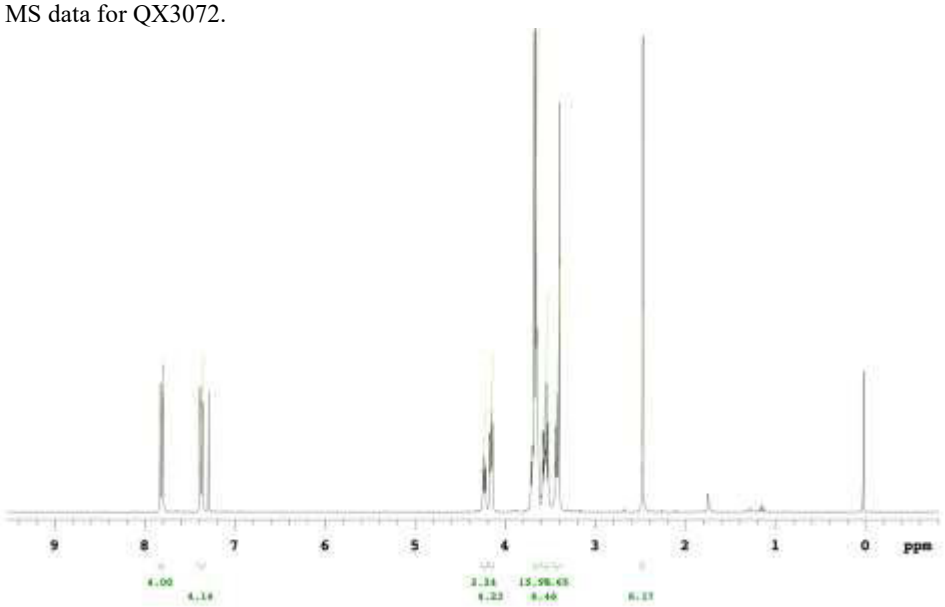

Figure S184. ^{1}H NMR data for QX3072.

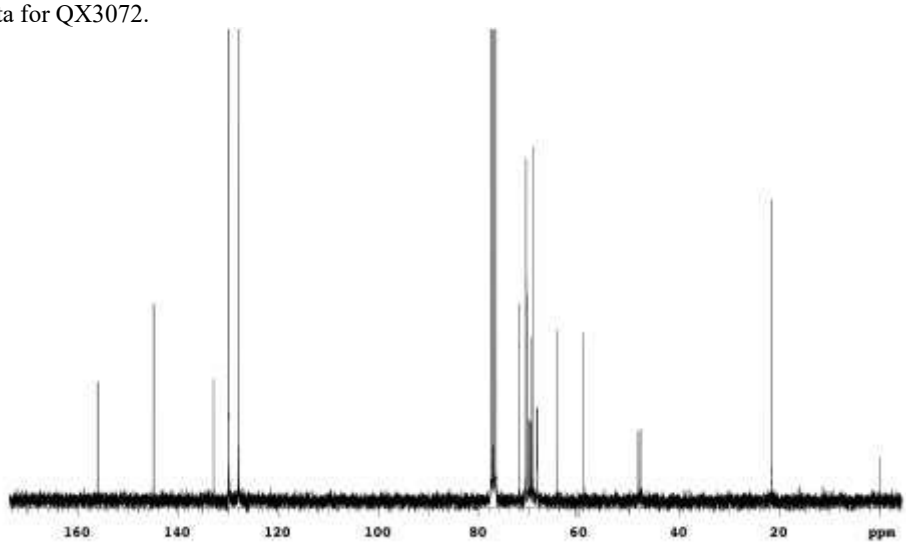

Figure S185. ^{13}C NMR data for QX3072

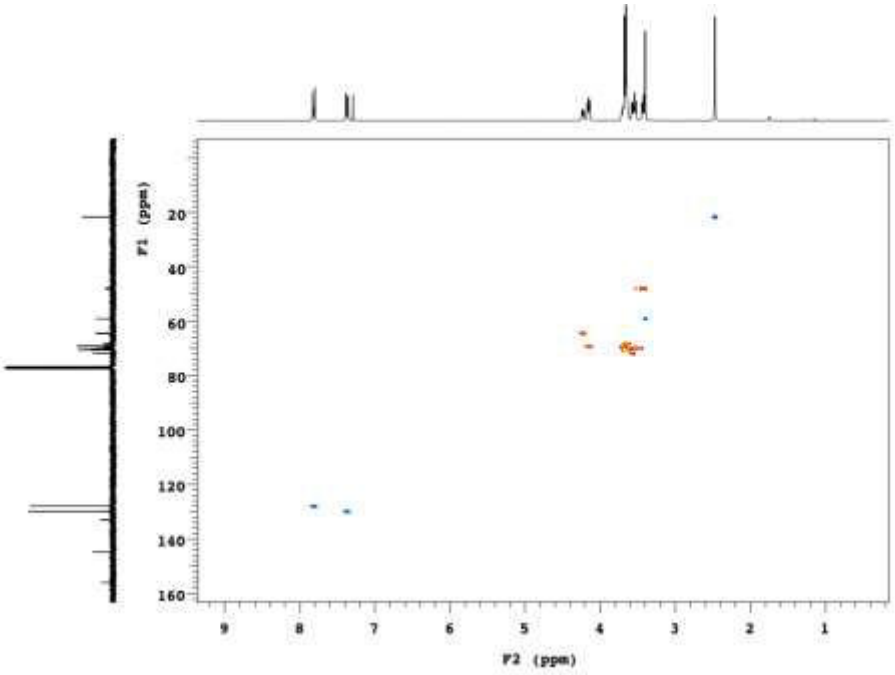

Figure S186. HSQC data for QX3072.

2,5,8,11-Tetraoxatridecan-13-yl bis(2-(2-azidoethoxy)ethyl)carbamate (QX3075)

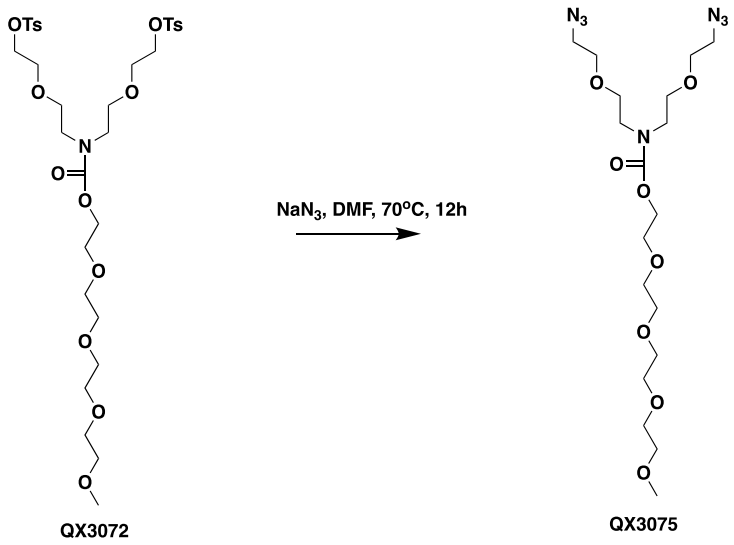

To a solution of NaN_3 (77 mg, 1.2 mmol) in DMF (2 mL) was added QX3072 (219 mg, 0.29 mmol) at room temperature. The reaction mixture was heated to 70 Celsius degree and stirred for 12 hours. The crude mixture was diluted with 4 mL of water and extracted with DCM (2 mL) for 3 times. The combined organic phases were washed with saturated brine and dried over anhydrous sodium sulfate, filtered, and the solvent was removed by rotary evaporation to afford 138 mg of product as colorless oil. Yield quantitative. MS(ESI-TOF) m/z calc. for $C_{18}H_{39}N_8O_8^+$ 495.29, found 495.29 [M+NH_4^+]. ^{1}H NMR (300 MHz, Chloroform-*d*) δ 4.23 (t, *J* = 5.1 Hz, 2H), 3.69 (t, *J* = 4.5 Hz, 2H), 3.66-3.61 (m, 18H), 3.55-3.54 (m, 6H), 3.38 (s, 3H), 3.37-3.35 (m, 4H),. ^{13}C NMR (126 MHz, Chloroform-*d*) 156.05, 71.93, 70.61, 70.53, 70.44, 69.92, 69.86, 69.78, 69.66, 69.53, 64.41, 59.03, 50.77, 48.37, 47.94.

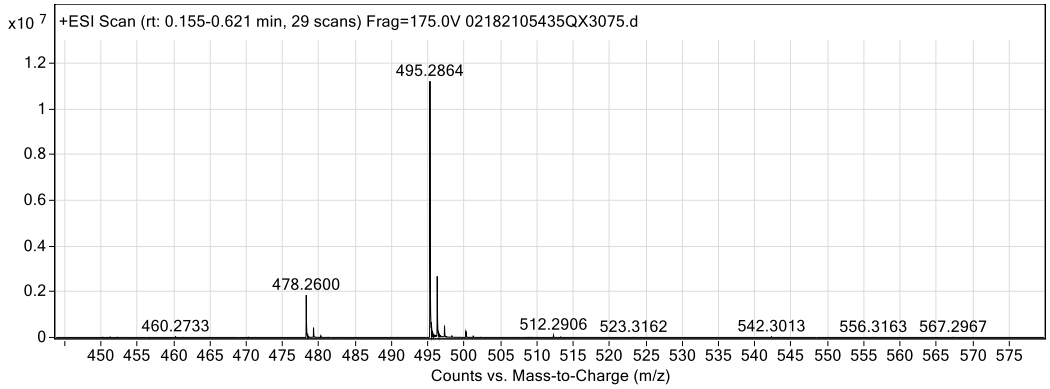

Figure S187. ESI-TOF MS data for QX3075.

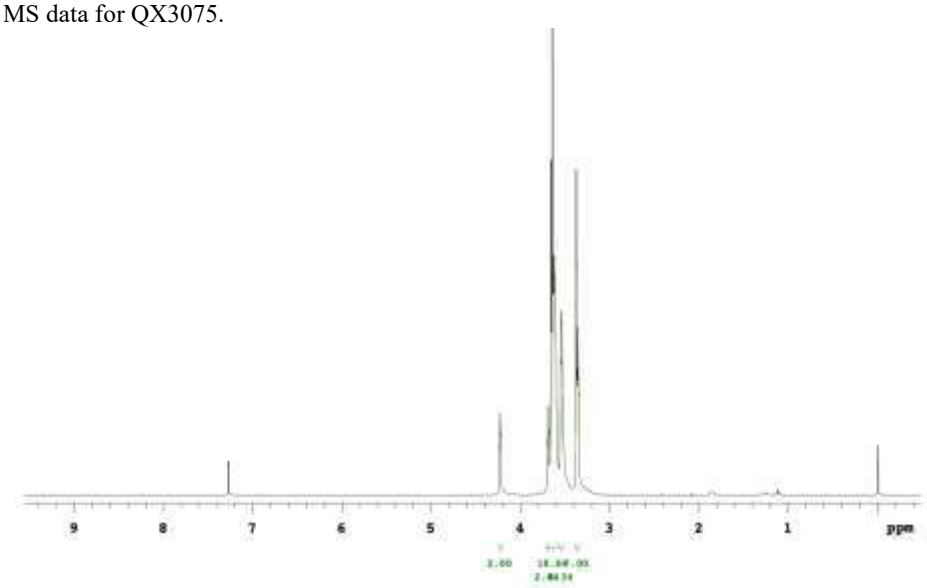

Figure S188. ^{1}H NMR data for QX3075.

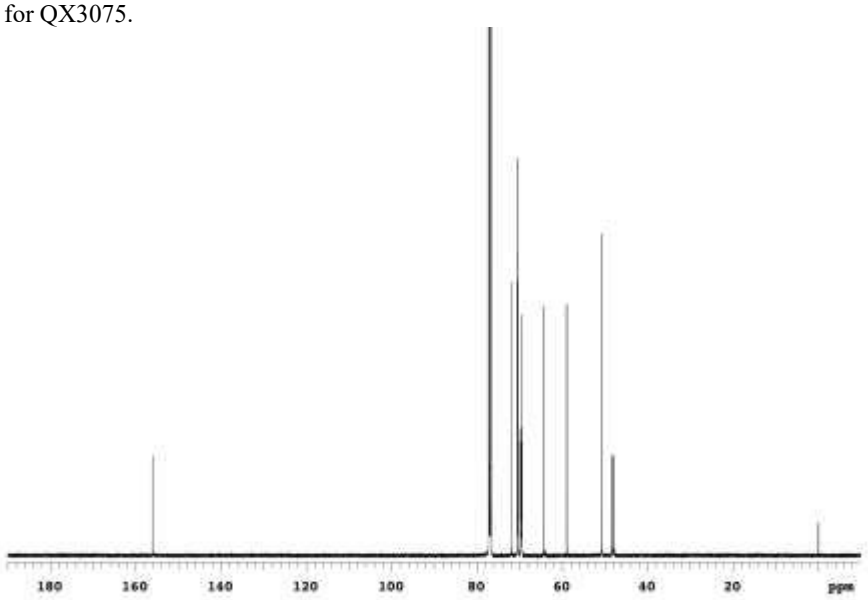

Figure S189. ^{13}C NMR data for QX3075.

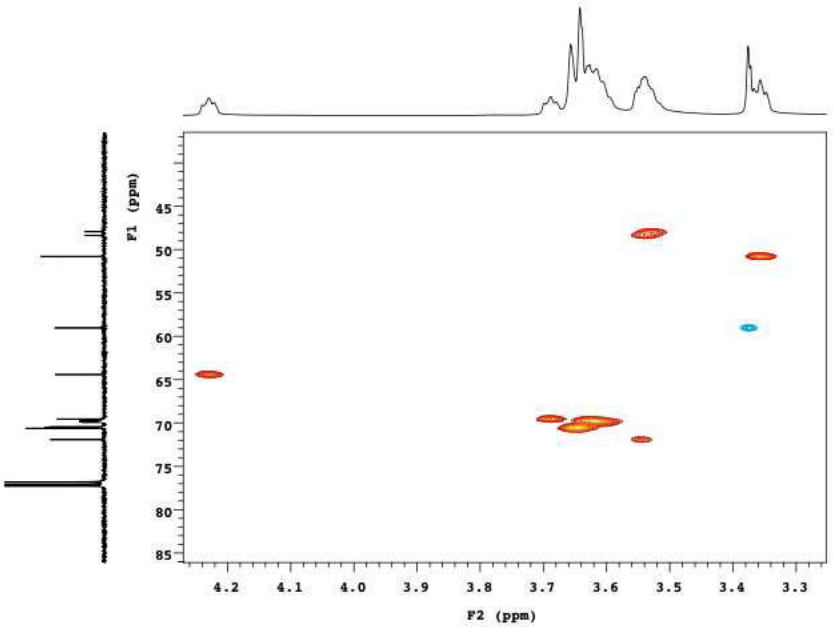

Figure S190. HSQC data for QX3075.

ESI References

1. Q. Xiao, D. S. Ashton, Z. B. Jones, K. P. Thompson and J. L. Price, *RSC Chem. Biol.*, 2020, **1**, 273–280.
2. P. B. Lawrence, Y. Gavrilov, S. S. Matthews, M. I. Langlois, D. Shental-Bechor, H. M. Greenblatt, B. K. Pandey, M. S. Smith, R. Paxman, C. D. Torgerson, J. P. Merrell, C. C. Ritz, M. B. Prigozhin, Y. Levy and J. L. Price, *J Am Chem Soc*, 2014, **136**, 17547-17560.
3. M. S. Smith, W. M. Billings, F. G. Whitby, M. B. Miller and J. L. Price, *Org. Biomol. Chem.*, 2017, **15**, 5882–5886.
4. D. Y. Jackson, D. S. King, J. Chmielewski, S. Singh and P. G. Schultz, *Journal of the American Chemical Society*, 1991, **113**, 9391-9392.
5. A. M. Leduc, J. O. Trent, J. L. Wittliff, K. S. Bramlett, S. L. Briggs, N. Y. Chirgadze, Y. Wang, T. P. Burris and A. F. Spatola, *P Natl Acad Sci USA*, 2003, **100**, 11273-11278.
6. C. E. Schafmeister, J. Po and G. L. Verdine, *Journal of the American Chemical Society*, 2000, **122**, 5891-5892.
7. L. D. Walensky, A. L. Kung, I. Escher, T. J. Malia, S. Barbuto, R. D. Wright, G. Wagner, G. L. Verdine and S. J. Korsmeyer, *Science*, 2004, **305**, 1466-1470.